# MULTI-SCALE OPTIMIZATION-BASED ENERGY TRANSITION STRATEGIES FOR MODELING, DESIGN, AND OPERATION OF PROCESS SYSTEMS

A Dissertation

by

COSAR DOGA DEMIRHAN

Submitted to the Office of Graduate and Professional Studies of
Texas A&M University
in partial fulfillment of the requirements for the degree of

DOCTOR OF PHILOSOPHY

| | |
|---|---|
| Chair of Committee, | Efstratios N. Pistikopoulos |
| Committee Members, | Mahmoud El-Halwagi |
| | M. M. Faruque Hasan |
| | Ivan Damnjanovic |
| Head of Department, | Arul Jayaraman |

August 2020

Major Subject: Chemical Engineering

# ABSTRACT

21st century energy production, conversion, and delivery systems are expected to succeed in multiple goals such as meeting the increasing energy demand, being economically feasible, being less carbon-intensive, increasing resource utilization efficiency. This requires a transition in technologies, operation strategies, and use of energy in our everyday life. Such a transition necessitates a better understanding and analysis of both the existing and futuristic technologies, pathways, and scenarios.

The aim of my dissertation is to use process systems engineering methods to develop generic frameworks to arrive at realistic integrated solutions to complex energy and environmental problems. Mathematical optimization is at the heart of these systematic and quantitative analysis methods. The systems under investigation range from mesoscale to megascale levels over time horizons from hours to days or years handling chemical engineering problems like modeling, design, planning, and scheduling. The common vision throughout every study is to gain insight on the challenges awaiting the energy transition and provide promising solutions.

This dissertation comprises various studies focusing on both improving the current practices like in the petroleum industry operations or chemical process design and analyzing feasibility of long-range energy transition scenarios that put an emphasis on integrating renewables like solar and wind in power, fuels, and chemicals production. The studies include (i) development of an integrated data-driven modeling and global optimization framework for improving short-term production planning operations in petroleum refineries, (ii) use of a process synthesis and global optimization approach to design optimal ammonia production processes from various pathways including natural gas reforming, biomass gasification, and renewable-powered electrolysis, (iii) development of a novel simultaneous design, scheduling, and supply chain strategy to optimize renewable power generation, storage, and transportation systems, and (iv) an extension of this latter strategy to integrate renewable energy systems with fossil energy systems for multi-product process networks to produce power, fuels, and chemicals in integrated facilities.

# DEDICATION

To my parents Nihal and Namik.

# ACKNOWLEDGMENTS

This PhD journey has not been an easy one. I received a lot of support from a great number of people during the last five years and I think they deserve an acknowledgment here.

My biggest gratitude goes to Professor Efstratios Pistikopoulos. I originally started my PhD studies with late Professor Christodoulos Floudas who unfortunately passed away on August 14, 2016. This was a huge shock not only to his students and but to the whole chemical engineering academic community. In addition to all the financial and bureaucratic hardships amidst dealing with the personal loss of a dear friend, Professor Pistikopoulos accepted me and the rest of the Floudas group members in his research group. He provided us with funding and many interesting research questions. He honored Professor Floudas' legacy by supporting his students and complementing his research ideas. Thank you Professor Pistikopoulos for your guidance and support in my research pursuits. Thank you Maria Pistikopoulos for hosting me and the rest of the research group at your residence for many times. I was away from my parents, but I always felt that I was with my family.

I also want to acknowledge the help and guidance by Professor Floudas. His vision made the work presented in Chapter 2 possible. While I only had the chance to work with him for about ten months, I was utterly inspired by his genius, passion, and his complete devotion to this work. Even after your passing, your family, Fotini and Ismini always checked on us to make sure that all his students were doing okay and following their passions. Professor Floudas's influence and wisdom will always be remembered and deeply missed. His memory and legacy will go on thanks to both his students' and Professor Pistikopoulos' efforts. I hope, this dissertation will stand as a testimony to my respect to both of these great mentors and their visions.

The work in this dissertation has been examined and advised by a valuable thesis committee including Professors Mahmoud El-Halwagi, Faruque Hasan, and Ivan Damnjanovic, whose suggestions and precious time spent on this dissertation are kindly appreciated. I deeply enjoyed my conversations with Professor Phanourios Tamamis and valued his advice.

I express my deep gratitude to Dr. Joseph Powell from Royal Dutch Shell for supporting my research efforts in the last 3.5 years of my PhD studies. He provided our research team with thought provoking research directions and suggested me to consider a career opportunity at Shell that I enthusiastically followed. His advices and vision were the key promoters that galvanized my motivation to work on renewable energy technologies. I also want to thank my former collaborators (and now colleagues) from Shell New Energies team: Dr. Clara Heuberger, Dr. Mark Klokkenburg, and Nort Thijjsen. The last few years of my research were heavily inspired by our discussions over numerous teleconferences we had. I am thankful for your trust in my work and I am looking forward to keep on working with you.

As most of my friends know, moving to College Station after living in Istanbul for all my life has been a difficult transition for me. I met amazing people in the last five years who made my life more than bearable and helped me fill it up with many cherishable memories. The biggest credit goes to the "Turkish Gang", who provided me with a second family in the United States since 2015. Many thanks goes to my dear friends and colleagues Dr. Emre Demirel, Dr. Burcu Beykal, Dr. Melis Onel, Dr. Onur Onel, and Dr. Baris Burnak. Thank you for being with me and supporting me during some of the most stressful periods of my life.

In the last few years, I received a great support from senior group members of both Floudas and Pistikopoulos research groups: Prof. Fani Boukouvala, Prof. Chris Kieslich, Dr. Yannis Guzman, Dr. Alexander Niziolek, Dr. Logan Matthews, Dr. Nikos Diangelakis, Dr. Maria Papathanasiou, Dr. Ioana Nascu, Dr. Richard Oberdieck, Dr. Styliana Avraamidou, Dr. Mario Villaneuva, Dr. Hari Ganesh, and Dr. Gerald Ogumerem. I need to express my gratitude to Fani, for her great hospitality in Atlanta during my visit and her amazing support to finish the work that we started during her post-doctoral time in College Station.

I thank my classmates, cohorts, and fellow group members: Dr. William Tso, Dr. Justin Katz, Dr. Arora Vargas, Yuhe Tian, Iosif Pappas, Dr. Yoojung Choi, Xiao Yu, Haneol Song, Lina Lee, and Hyeju Song for their warm friendships. My research partner William deserves a special mention. We were together during the transition to a new group and we have worked on the same

project since the last 3.5 years, where I thoroughly enjoyed his company and our thought provoking discussions. I wish my fellow group members and friends: Cory Allen, Stefanos Baratsas, Marcello Di Martino, Chris Gordon, Rahul Kakodkar, Dustin Kenefake, Vaishnav Meduri, and Shivam Vedant the best luck with their graduate studies. Another round of thanks goes to my dear friends and fellow members of our tennis club: Dr. Ishan Bajaj, Dr. Chen Ling, Dr. Abhinav Narasingam, Spyridon Tsolas, Patrick Lathrop, and Ian Echols; as well as the fellow officers and volunteers of the Texas A&M Energy Research Society: Dr. Shachit Iyer, Akhil Arora, Kasturi Sarang, Dr. Prashanth Siddhamshetty, Anne Le, Denis Su-Feher, Dr. Bassel Daher, Dr. Kevin Topolski, Bingyu Wang and Dr. Pankaj Goel. A great special thanks goes to Yoon Joo Jo, who has supported me from the beginning till the end of the writing of this dissertation during the days of COVID-19. Dear Yoon, I am deeply grateful for your company.

Finally, my heartfelt appreciation goes to my parents Nihal and Namik Demirhan for their never ending moral support. I know it has not been easy being separated from your only child for this long. It has been difficult enough for me. Thank you for always sharing your guidance. This degree is dedicated to you.

CONTRIBUTORS AND FUNDING SOURCES

## Contributors

This dissertation was supported by a thesis committee consisting of Professors Efstratios N. Pistikopoulos, Mahmoud El-Halwagi, and M. M. Faruque Hasan of the Artie McFerrin Department of Chemical Engineering, and Professor Ivan Damnjanovic of the Zachry Department of Civil & Environmental Engineering.

The raw plant data used in Chapter 2 was provided by Kyungwon Kim of Hyundai Oilbank Company. Hyeju Song provided help with data grouping. The implementation of the single-period production planning model and the initial data-driven modeling work for Chapter 2 were jointly conducted with Dr. Fani Boukouvala. The work in Sections 3, 4, and 5 were a part of the ongoing collaboration between the Pistikopoulos Research Group and Royal Dutch Shell. The conceptualization stage of the projects were supported by Dr. Joseph Powell, Dr. Clara Heuberger, and Dr. Mark Klokkenburg from Royal Dutch Shell. The ammonia production process models used in Section 3 were jointly developed with William Tso. The design and scheduling model first presented in Section 4 was developed in collaboration with William Tso. The clustered data used in Sections 4 and 5 were prepared by a methodology jointly developed with William Tso.

All other work conducted for the dissertation was completed by the author independently.

## Funding Sources

This graduate study was funded by financial support from Texas A&M Energy Institute, Hyundai Oilbank Company (Section 2), Royal Dutch Shell (Sections 3, 4, and 5), and a Texas A&M Graduate Assistant Teaching (GAT) fellowship.

# NOMENCLATURE

| | |
|---|---|
| ac | Alternating Current |
| AHC | Agglomerative Hierarchical Clustering |
| AIC | Akaike Information Criteria |
| aMDEA | Activated Methyl Diethanolamine |
| ASU | Air Separation Unit |
| ATR | Autothermal Reformer |
| BEP | Breakeven Price |
| BES | Battery Electric Storage |
| BGS | Biomass Gasifier |
| BIC | Bayesian Information Criteria |
| BTL | Biomass-to-Liquids |
| CAES | Compressed Air Energy Storage |
| CAPEX | Capital Expenses |
| CBGTL | Coal-Biomass-Gas-to-Liquids |
| CDU | Crude Distillation Unit |
| CEPCI | Chemical Engineering Plant Cost Index |
| CV | Cross-Validation |
| DAC | Direct Air Capture |
| dc | Direct Current |
| DCU | Delayed Coker Unit |
| DEC | Dense Energy Carrier |
| DNI | Direct Normal Irradiation |

| | |
|---|---|
| DOE | Department of Energy |
| EIA | Energy Information Administration |
| EV | Electric Vehicles |
| FAO | Food and Agriculture Organization |
| FBBT | Feasibility-Based Bounds Tightening |
| FTS | Fischer-Tropsch Synthesis |
| GAMS | General Algebraic Modeling System |
| GHG | Greenhouse Gas |
| GHGI | Greenhouse Gas Index |
| GHGAE | GHG Avoided by Electricity |
| GHGAN | GHG Avoided by Ammonia Production |
| GHT | Gasoil Hydrotreating Unit |
| GTL | Gas-to-Liquids |
| HBR | Haber-Bosch Reactor |
| HCR | Hydrocracker Unit |
| HDI | Human Development Index |
| HPC | High-Performance Computing |
| HPRC | Texas A&M High-Performance Research Computing |
| IA | Iterative Algorithm |
| IDCF | Interest During Construction Factor |
| IEA | International Energy Agency |
| IPCC | Intergovernmental Panel on Climate Change |
| k-NN | $k^{th}$ Nearest Neighbor |
| kbpd | Kilo (Thousand) Barrel per Day |
| KDR | Known Data Regression |

| | |
|---|---|
| KMX | Kerosene Mercaptan Oxidation Unit |
| LBO | Lubrication Base Oils Unit |
| LCCR | Levelized Capital Charge Cost |
| LCOC | Levelized Cost of Chemicals |
| LCOE | Levelized Cost of Electricity |
| LCOF | Levelized Cost of Fuels |
| LER | Light Ends Recovery Unit |
| LIM | Linear Plus Interaction Terms Model |
| LIQM | Linear Plus Interaction and Quadratic Terms Model |
| LM | Linear Terms Model |
| LQM | Linear Plus Quadratic Terms Model |
| LP | Linear Program |
| MDI | Missing Data Imputation |
| MILP | Mixed-Integer Linear Program |
| MINLP | Mixed-Integer Nonlinear Program |
| MOGD | Methanol-to-Olefins-Gasoline-Distillate |
| MSCF | Million Standard Cubic Feet |
| MSW | Municipal Solid Waste |
| MTG | Methanol-to-Gasoline |
| NaS | Sodium Sulfur |
| NHT | Naphtha Hydrotreating Unit |
| NIPALS | Nonlinear Iterative Partial Least Squares Regression |
| NLP | Nonlinear Program |
| NREL | National Renewable Energy Laboratory |
| NRMSE | Normalized Root Mean Squared Error |

| | |
|---|---|
| NSRDB | National Solar Radiation Database |
| NY | New York |
| OBBT | Optimality-Based Bounds Tightening |
| OGAPS | Office of Graduate and Professional Studies at Texas A&M University |
| OLS | Ordinary Least Squares |
| OM | Operations and Maintenance |
| OPEX | Operational Expense |
| PCS | Power Conversion System |
| PEM | Protonn Exchange Membrane |
| PPA | Power Purchase Agreement |
| PPCA | Probabilistic Principal Component Analysis |
| PR | Primary Reformer |
| PSA | Pressure Swing Adsorption |
| PSE | Process Systems Engineering |
| PSH | Pumped Storage Hydro |
| PV | Photovoltaics |
| RDF | Refuse Derived Fuel |
| RE | Renewable Energy |
| RMSE | Root Mean Squared Error |
| RSM | Response Surface Model |
| RTN | Resource-Task Network |
| R-WGS | Reverse Water-Gas Shift |
| SA | Surface Area |
| SE | Squared Error |
| SLP | Sequential Linear Programming |

| | |
|---|---|
| SMR | Steam Methane Reformer |
| SOL | Structure Oriented Lumping |
| SR | Secondary Reformer |
| SVM | Support Vector Machine |
| Syngas | Synthesis Gas |
| TOC | Total Overnight Cost |
| tpd | Ton per Day |
| TSCF | Trillion Standard Cubic Feet |
| TSR | Trimmed Scores Regression |
| TX | Texas |
| VDU | Vacuum Distillation Unit |
| WGS | Water-Gas Shift |

TABLE OF CONTENTS

Page

LIST OF FIGURES

FIGURE Page

LIST OF TABLES

TABLE Page

# 1. INTRODUCTION AND LITERATURE SURVEY

## 1.1 A Snapshot of the Energy Landscape: Yesterday, Today, and Tomorrow

The prehistoric human evolution and the course of history and have been characterized by a quest for controlling the storage and flow of concentrated and versatile forms of energy and their conversion into heat, light, and motion [1]. The development of human societies result in larger populations with growing complexity of social and productive institutions to provide a higher quality of life for a growing number of people. United Nations Development Programme reports and academic research suggest a strong correlation between increasing per capita energy use and Human Development Index (HDI) especially at low to moderate energy use levels [2, 3].

The world population is expected to reach ten billion by 2070 [4] and the world gross domestic product (GDP) is expected to double from 2020 till 2040 largely due to the emerging economies and the expanding middle classes in the Asia Pacific countries like China and India [5]. With this growth, the global energy demand is projected to rise from 570 exajoules in 2015 to 1000 exajoules by 2070 [6, 7]. This trend urges us to answer the question of whether there is enough energy resources to meet the future demand.

Since the industrial revolution in the $17^{th}$ century, the productivity and the resulting economic growth has been fueled predominantly by fossil hydrocarbons like coal, petroleum (oil), and natural gas. Fossil fuels are chemical mixtures formed by anaerobic decomposition of buried dead organism that are fossilized during a period of millions of years. As the fossils are exposed to heat and pressure over a long time, the dilute solar energy harvested originally via photosynthesis is concentrated and stored in the chemical bonds between mainly carbon and hydrogen atoms. When burned (combusted), this stored energy is released along with the by products of oxidized carbon and hydrogen, carbon dioxide and water, respectively. Easy and affordable access to fossil fuels provided the utmost impetus to countries like the United States to reach great wealth and, as of 2019, there is still a strong reliance on fossil fuels in energy consumption on a global scale, such

that fossil fuels comprise the 85% of the global energy consumption [7]. Although there have been debates on the availability of fossil resources, there appears to be enough to supply the global demand in the near future for another 50 years for petroleum and natural gas and 150 years for coal. However, the stone age didn't end for lack of stone and the fossil fuel age is likely to end before the world runs out of them. An existential risk to the quality of life on Earth might lead to the eventual decline of the fossil fuels.

There is a high environmental cost that comes with using fossil fuels, that is the release of carbon dioxide to the atmosphere during combustion. While contributing only to the 20% of the greenhouse gas (GHG) emissions, carbon dioxide is responsible for 80% of the radiative forcing that sustains the Earth's greenhouse effect resulting in the global warming, since it is the predominant non-condensing gas in the atmosphere [8, 9]. Global carbon dioxide emissions have been on the rise since the last 250 years and annual emissions reached 36.8 billion tons (Gt) in 2018 [10]. According to the Fifth Assessment Report by the Intergovernmental Panel on Climate Change (IPCC), if the emissions continue to increase at the current rate, the global warming is likely to reach 1.5 °C between 2030 and 2052 causing a climate change [11]. The impacts of this change can include more frequent and longer heat waves, extreme precipitation events, and warming & acidification of the ocean along with an increase in general mean sea levels. These risks will be unevenly distributed, affecting the disadvantaged people and communities in countries of all levels of development. Projected disasters include increased cases of floods and wildfires, more frequent water shortages or restrictions, problems in food production, and rise in heat-related human mortality [11].

For sustaining the quality of human life on Earth, the energy landscape needs to be adjusted, modified, and made fit to a new standard where carbon emissions are more tightly accounted and reduced while meeting the growing demand for energy. "Business as usual" attitude with current high dependency on fossil fuels is a pathway to many problems. What can be done then? Are there more suitable energy sources that can be chosen to fight the effects of climate change and put us on a more sustainable trajectory? Should the societies invest in improving the existing technologies

or take a risk and go for promising sustainable technologies that are not tested at commercial scale yet? If societies decide that a "transition" to a more sustainable energy landscape is needed, what would it look like? It is important to imagine what kind of energy systems are going to be needed to decide on which pathways to take and what technologies to invest in.

## 1.2 Energy Transition: Challenges and Opportunities

21st century energy production, conversion, and delivery systems are expected to achieve multiple objectives. They should meet the increasing energy demand, be economically feasible, be less carbon-intensive, and increase resource utilization efficiency [12, 13, 14]. This requires a transition in technology, operation strategies, and possibly a philosophy in how energy is generated and stored.

Figure 1.1 is prepared, to better understand (i) the development of the modern energy landscape, (ii) the interplay between the shares of primary energy sources, and (iii) the possible future evolution of the energy mixture in the example of an industrialized country: the United States. The data are taken from Energy Information Administration's (EIA) Monthly Energy Review [15] and the figures show the total primary energy consumption and the breakdown of energy source usage in electric power, transportation, industrial, commercial, and residential sectors. According to the data, 80% of the United States primary energy consumption still relies on fossil fuels like coal, petroleum, and natural gas as of 2019. Especially, the transportation sector is heavily dependent on petroleum products which have a 91% share. Looking at the historical trends in how the primary source shares in the mix have evolved, it appears very likely that fossil fuels will be around in the near and even far future. The numbers show a few important trends that will be more prominent in the future. The share of coal is on a historic downfall. Natural gas, a cleaner and more energy-dense fossil fuel, has become the more preferred energy source in sectors like industrial, commercial, and residential. Similarly, electric power has increased its share in commercial and residential sector. Electric power is not a primary source and electrification is powered by growing shares of natural gas and renewables along with significant contribution by nuclear energy, and some decreasing contribution by coal.

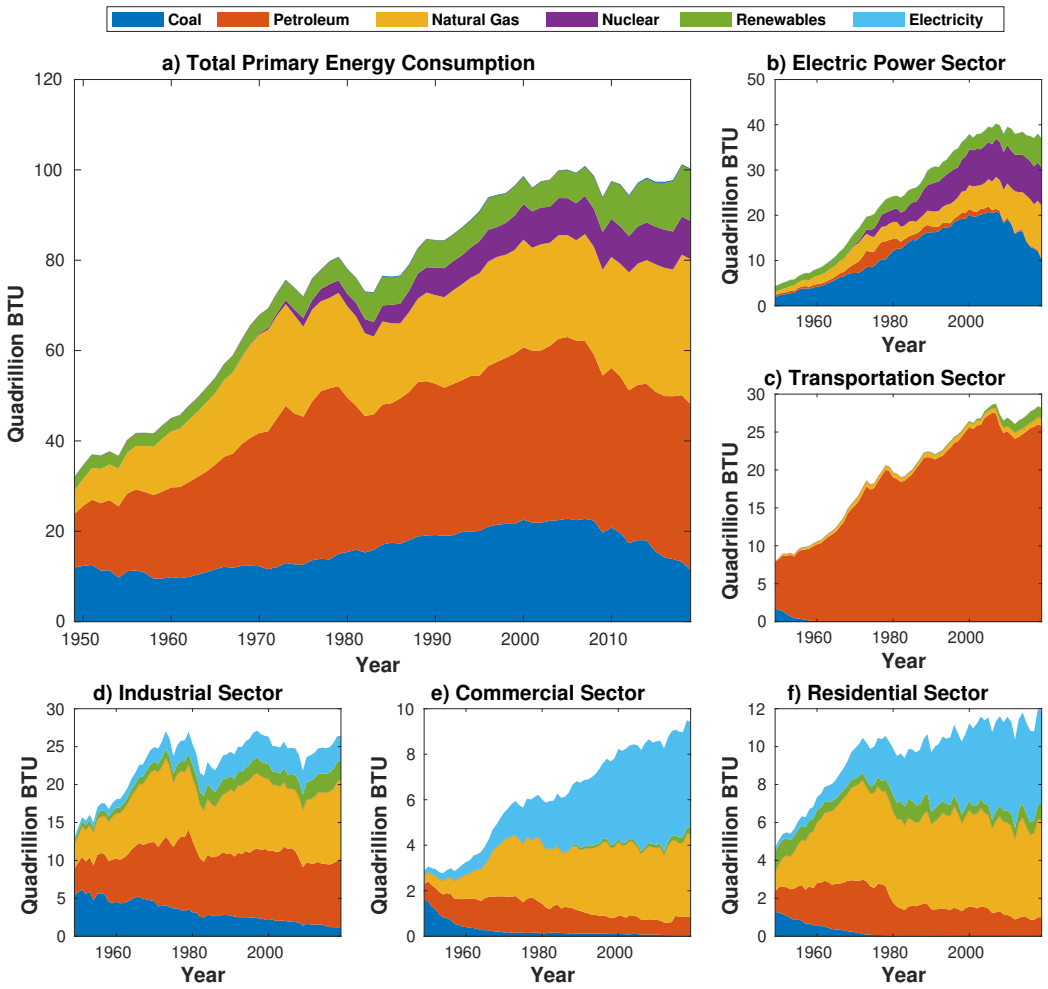


Figure 1.1: The breakdown of (a) the total primary energy consumption and analyses of the (b) electric power, (c) transportation, (d) industrial, (e) commercial, and (f) residential sectors in the United States show that as of 2019, 80% of the United States primary energy consumption relies on fossil fuels like coal, petroleum, and natural gas. The changing trends show that the use of natural gas and increasing electrification powered by growing shares of renewables might play a key role in the energy transition.

The current evolution of the primary energy source utilization indicates that the dependency on fossil fuels is not likely to end in the near future. Obviously, this is a complex problem and with energy systems at global scale, there really is no silver bullet than can solve all the problems at all locations. One way to reduce or mitigate the effects of burning fossil fuels is to modify the existing infrastructure. This includes using (i) better control, operation, and supply chain decision-making strategies, (ii) retrofitting the existing energy conversion facilities with carbon

capture technologies, and (iii) investing in newer and cleaner energy conversion technologies with a shift from carbon-intensive fuels like coal to less carbon-intensive and cleaner fuels such as natural gas. These strategies can lessen the harms of the current pathways used. Apart from option (i), options (ii) and (iii) will arguably bring down the economic attractiveness of using fossil fuels if the carbon dioxide released during conversion is captured. Carbon capture and storage technologies are energy-intensive, and using any fossil fuel technology can be at best carbon neutral, making sustainability still a significant concern.

A second alternative is nuclear energy that had promised a bright and clean future to replace fossil fuels. Nuclear energy via fission reaction can provide emission-free power, however, requires paramount safety consideration since its byprodut, the radiation contamination poses a great threat to all living beings and the environment if not prevented or sealed properly. Also, flexible power production causes many stability issues in the current nuclear reactor technology. On top of these, nuclear energy lost the public interest it once had after two catastrophic incidents in Chernobyl, Ukraine and Fukushima Daiichi, Japan in 1986 and 2011, respectively, that prevented its further penetration above its current 10% share in the global energy mix. The next generation nuclear is likely to make a return, however, investment costs and safety requirements will not make it easily compete with cheap fossil fuel energy prices.

A more promising way to reduce humanity's dependency on fossil fuels is to increase the penetration of renewable resources such as geothermal, hydro, biomass, solar, and wind in the power sector via electrification and production of valuable chemicals production [14]. This is an efficient decarbonization strategy that is already underway thanks to the the variety and abundance of the renewables and decline in renewable investment costs. By the end of 2018, renewable technologies constitute roughly one-third of the overall global capacity, with biggest portion of the recent capacity increase coming from solar and wind technologies [16]. Solar and wind energy are promising pathways to enable electrification. However, both resources suffer from intermittency and seasonal variability, resulting in low capacity utilization in the absence of energy storage technologies [17, 14]. Biomass has been a candidate replacement for fossil fuels and its

application in power, fuels, and chemicals sectors have been studied extensively by national labs and academia. Crop residues like corn stover and forest residues like hardwood type of biomass can be economically feasible with gasification technology if provided at a steady supply.

In addition to intermittency and variability in supply, renewable resources also suffer from uneven geographical distribution. Figure 1.2 illustrates the availability of solar, wind, and biomass resources for the United States using the online resources of the National Renewable Energy Laboratory (NREL) [18, 19, 20]. When superimposed on each other, it is seen that each renewable resource is stranded at a different part of the country. Additionally, they are often isolated and far from strong demand locations like metropolitan areas and industrial zones. As a result, the optimal renewable utilization strategies should be location specific and consider the value chain aspect of the products.

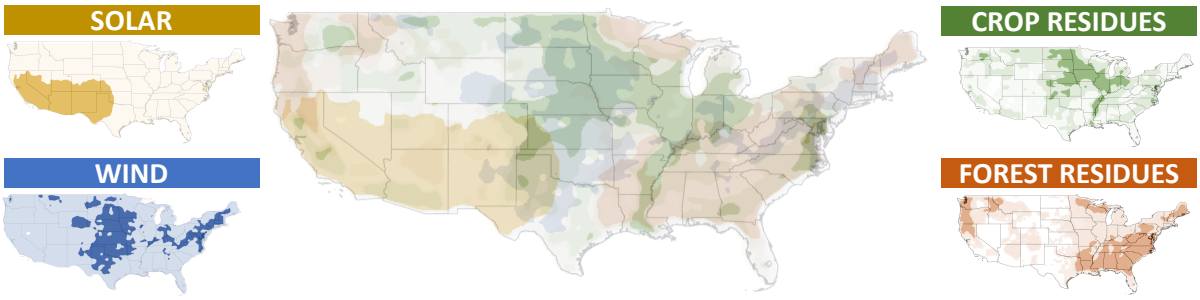


Figure 1.2: The availability of renewable energy sources across the United States show an uneven geographical distribution. Solar energy is located in the Southwest, whereas wind is strong in the Midwest. Crop residues and forest residues are spread to the Midwest and Southeast regions, respectively.

It is very likely that at least in the near future, the energy systems will comprise multiple competing pathways and combinations of various technologies that rely on hybrid feedstocks. Informed decision-making strategies will be needed in areas like process modeling, design, control, scheduling, planning, and supply chain management. These are time- and space-dependent functions requiring decision-making strategies across all different scales. This brings the question

of how to make such informed decisions?

### 1.3 Process Systems Engineering: Its Philosophy, Role, and Tools

The existence of multiple pathways, competing technologies, and numerous alternatives make decision-making difficult. As the integrated systems grow in complexity, a traditional method for energy systems design such as using heuristics that rely on rules of thumb become less useful to a decision-maker. While heuristics combined with experience can generate quick solutions that are often reasonably good, it does not provide a way to establish the quality of the solution. Furthermore, conflicting objectives or comparison of alternatives in a problem might require arbitrary decisions. As an alternative, high-efficiency targeting approaches that focus on reaching thermodynamic limits can reduce energy consumption, but most of the time ignore capital cost considerations. They might also require considerable insight and trial & error [21, 22]. Experimentally testing all the options in commercial scale is practically impossible and risky.

Mathematical optimization-based methods that rely on rigorous algorithms and simultaneous consideration of physics, chemistry, biology, and economics in a system have proven themselves as promising tools to help decision-makers generate design and operational strategies for integrated systems [21]. Optimization approach aims to find the best possible solution to the problem by quantifying the "goodness" of solutions. Optimization methods thrive when tackling systems with high degrees of freedom. Since integration means an increase in the degrees of the freedom, this translates into bigger room for improvement for energy systems. Rigorous optimization methods rely on systematic solution strategies, rather than exhaustive trial & error [23, 24].

Process systems engineering (PSE) [25] methods have mathematical optimization at their core and they aim to provide a generic framework to arrive at realistic integrated solutions to complex energy and environmental problems. The energy systems of interest range from nanoscale to megascale levels over time horizons that range from milliseconds to months or years [26, 27]. The applications range from design decisions like modeling and process synthesis to operational decisions such as scheduling, planning, and control [28].

The most commonly used tools of PSE include (i) mathematical modeling via first-principles,

data-driven, or hybrid approaches [29, 30, 31, 32, 33, 34, 35], (ii) superstructure optimization for modeling all possible alternatives in an process system design including different system configurations, process integration, pathway interactions, operating conditions, and other important design parameters in problems like process heat integration, or supply chain management [36, 37, 38, 39, 40, 41], and (iii) mixed-integer linear and nonlinear programming for modeling with continuous and binary decision variables to model mass and energy balances as well as logical conditions between discrete events in a superstructure [42, 43, 21, 44, 45, 46, 47]. These tools provide powerful aid in achieving the objectives of this dissertation.

## 1.4 Dissertation Objectives

The proposed works aim to address the aforementioned challenges by using a variety of process systems engineering tools such as data-driven modeling, superstructure optimization with mixed integer linear and nonlinear modeling, nonlinear multi-period planning, process synthesis for optimal design, global optimization, simultaneous design-scheduling-supply chain strategies.

### 1.4.1 Improving Production Planning in Petroleum Industry via Refinery Data

Production planning operations in the refining industry focus on both the long-term strategic decisions like purchasing the best crude oil mixture for future plans that cover a few months to a year and the short-term scheduling decisions like allocating streams or deciding on distillation cutpoints that cover the span of several days [48, 49]. Production planning problems are often large-scale optimization problems and the modeling efforts have traditionally relied on linear programming (LP) or mixed-integer linear programming (MILP) principles by using fixed-yield planning models and swing-cut models due to tractability concerns [50, 51].

Linear models have low computational cost, however they often fail to capture the inherent nonlinearities in the refinery operations [52]. Therefore, there has been significant efforts in the industry and academia to develop nonlinear models for refinery processes since the 1980s [53]. Commercially available planning software tools like Aspen PIMS (AspenTech) and GRTMPS (Haverly Systems) rely mostly on linear models. Even though they can handle nonlinear equations

and large-scale problems, the use of nonlinear terms in the such software is restricted [53], since nonlinear optimization formulations are often nonconvex problems and solution algorithm return local solution. Although the computational power has increased tremendously in the last decade and powerful commercial global optimization solvers such as BARON [54] and ANTIGONE [55] are now available, the use of high-fidelity and nonconvex models in planning optimization is still limited due to the arising computational complexity [52]. Surveys on the use of planning and scheduling software indicate that such tools are inherently challenging to master for the engineers and the economists without proper optimization background [56]. For this reason, stream allocation in chemical industries is, more often than not, made based on company experts' experience and manual calculations [57].

**My contribution** here is to develop a framework that combines data-driven modeling with nonlinear multi-period planning formulation that is used for optimizing refinery production plans using real plant data. The developed framework is applied to the Daesan Refinery by Hyundai Oilbank Company in South Korea. Nonlinear input-output models for all processing units are created using real plant data. The multi-period production plan allows for inventory management to improve the economic performance of the refinery.

### 1.4.2 Sustainable Ammonia Production from Renewable Feedstocks

Ammonia is one of the most widely produced chemicals in the world. Global ammonia production in 2015 was reported to be over 140 million tons [58]. Currently, more than 80% of the produced ammonia is used for fertilizer production and the remaining is used as raw material in the production of urea, ammonium nitrate and other nitrogen-based chemicals [59]. According to Food and Agriculture Organization (FAO), overall demand for agricultural products is expected to grow at 1.1% per annum from 2007 to 2050 as a result of the increasing world population [60]. Growing agricultural production necessitates the need for fertilizers; thus, demand for ammonia-based for agricultural fertilizer alone is expected to dramatically increase in the future.

Besides its use as a commodity chemical, ammonia stands out as a hydrogen-based dense energy carrier to store renewable energy. This has two reason: (i) it has a high hydrogen content

(17.8 wt%) and (ii) when produced from renewable energy and feedstocks, it does not produce any GHG emissions upon conversion back to energy. Ammonia can be stored as a liquid under relatively low pressure (0.87 MPa) and ambient temperature (20 °C) or atmospheric pressure and mild cryogenic temperature (-20 °C). It has a hydrogen volume density of 105.0 kg/m$^3$, which is about 45% higher than that of liquid hydrogen (71.2 kg/m$^3$). There is a vast pipeline infrastructure in the United States for distributing liquid ammonia. Once produced, ammonia can be stored and transported out with relative ease using the existing infrastructure [61]. Stored energy can be recovered back since ammonia can also be used as a synthetic fuel in diesel engines, internal combustion engines, and gas turbines with little modification [62]. Conversion of ammonia to hydrogen in a fuel cell can also be a feasible technology to be used in mobile vehicles in the future [63]. Early mentions of ammonia as an energy vector date back to 1982, where the suggested way to power ammonia production is to use the rejected heat from nuclear energy plants [64]; however, more recent works are focused on using renewables in ammonia production [65, 66, 67, 68].

Due to this dual opportunity to be used as both a fertilizer and an energy carrier, demand for ammonia in the future is expected only to grow. The modern ammonia production method, the famous Haber-Bosch process, is often considered among the most important inventions of the 20$^{th}$ century [69]; however, it emits an average value of 2.8 tons of $CO_2$/ton of ammonia produced, contributing to more than 1% of global greenhouse gas (GHG) emissions [70, 71]. Although, state-of-the-art processes have brought down the energy requirements from 60 GJ/ton of ammonia produced to 28-30 GJ/ton [72], ammonia production is still highly energy intensive, using about 3-5% of the world's natural gas resources [59]. If ammonia will continue to be produced in even greater amounts, the production needs to become more sustainable.

**My contribution** here is an implementation of process synthesis and global optimization methods to synthesize sustainable ammonia production processes with significant GHG reductions. Aim of this study is to compare biomass-, wind-, and solar-based ammonia production routes with natural gas-based reference case study via having all process options in the same process superstructure. Case studies are done for different geographical locations, where feedstock and

electricity prices and availability vary greatly.

### 1.4.3 Efficient Generation, Storage, and Transportation of Renewable Energy

Global renewable energy generation capacity reached 2,351 GW at the end of 2018, constituting roughly one-third of the overall global capacity [16]. The actual amount of the generated renewable energy, however, makes up for only about 11% of the global total primary energy consumption, signaling that the capacity utilization is low for renewable technologies [73]. Intermittency and temporally asynchronous renewable energy supply and power demand are the sources of this problem [17, 14]. Solar photovoltaics and wind turbines have been undergoing a fast growth in deployment. In 2018, 54 and 29% of the total global renewable capacity increase were attributed to solar and wind technologies, respectively. These technologies are also the ones that are plagued most seriously by low capacity utilization [74].

Energy storage at grid-scale (GWh-scale) is one way to ensure the balance between the renewable power supply and demand and therefore improve the capacity utilization [75]. Energy storage in vectors, that are also called as dense energy carriers (DECs) offer the possibility of transporting stored energy from one location to another [26]. Hydrogen ($H_2$) and hydrogen-based DECs like, ammonia ($NH_3$), or methanol ($CH_3OH$) have orders of magnitude higher volumetric energy density compared to stationary storage options such as pumped storage-hydro (PSH), compressed air energy storage (CAES), or battery electric storage (BES) [76]. The variety of the storage options necessitate quantitatively exploration of the trade-offs between competing technologies under various scenarios.

Optimal integration of hydrocarbon-based renewable resources into fuels and chemicals production has been traditionally tackled with the multi-scale approach with the steady-state assumption, where unit design [77, 78], process flow sheet optimization [79], and supply chain analysis [80] problems are solved independently using different mathematical models for each scale [81]. However, optimization of design and operation of energy systems with time-varying resources like solar and wind is more challenging. It is impossible to directly integrate wind and solar resources into steady process systems due to renewable resource intermittency causing some

units to remain idle or partially idle for certain periods of time, where steady-state assumption is not valid [22]. The temporal variability in short-term scheduling and spatial variability in supply chain optimization need to be considered as a part of optimal design strategy.

**My contribution** here is to develop a multi-scale modeling and optimization strategy relying on mixed-integer linear programming techniques to find the optimal design and operational decisions of multi-location GWh-scale energy generation and storage systems. The strategy uses multi-period formulation to address the intermittency in the resource availability. The multi-location aspect allows for the production and transportation of DECs between high- and low-potential regions to account for the supply chain problems. The overall approach is multi-scale by nature since it deals with problems of various time and length scales (i.e. design, scheduling, and supply chain) simultaneously.

### 1.4.4 Multi-product Process Network Optimization for Energy Sectors Integration

Decarbonization via shifting the primary energy sources from carbon-intensive fossil-fuels to renewable- and sustainable-resources is a significant pillar of the energy transition. The aforementioned challenges related to this transition prevail in various energy sectors such as power generation and distribution systems, transportation fuels production, chemicals & heavy industrial production, and residential & commercial buildings [6, 7, 82]. Historically, each of the aforementioned energy system has been treated separately by its own technical community [83]. However, operation of one sector affects the others since all these energy systems become more and more interconnected over the time.

It is highly important to determine what sectors and sources of energy can play key roles in enabling sectors integration for decarbonization. Increasing renewable penetration is a promising action, however, the intermittency aspect of solar and wind resources makes it rather capital intense. Therefore, it is essential to get the biggest return for the investment made. This makes systems analysis and understanding the energy landscape crucial. The interconnectivity of multiple systems makes conventional or heuristics-based decision-making across multi-sectors more difficult. However, systems modeling and optimization approach can analyze the individual

elements of the each system; investigate the trade-offs in systems integration and exploit the synergies between various system elements [26, 28].

Recalling Figure 1.1, improving the natural gas utilization and increasing renewable energy penetration in the electric power sector can lead to decarbonization in industrial, commercial, and residential sectors as well. For decarbonizing the transportation sector, low-emission electric power can play a role to decrease the share of petroleum-based liquid fuels (e.g. gasoline, diesel, kerosene, etc.) via increased use of electric vehicles (EVs). Alternatively, liquid fuels produced synthetically via gas-to-liquids (GTL) processes from hydrogen and captured carbon dioxide that are produced via renewable or low-emission routes can have a significant impact on emission reductions. Also, dense energy carriers (DECs), like hydrogen, ammonia, and methanol, can play a dual role in storing renewable energy and providing heat & power in all the aforementioned energy sectors and fuel for the transportation sector.

**My contribution** here is to extend the multi-scale modeling and optimization strategy developed for optimizing the renewable energy generation, storage, and transportation systems to fuels and chemicals production to optimally design and operate multi-product process networks. Using multi-period formulation the intermittent renewable resources are integrated with fossil fuel technologies. Multi-product process networks allow for analysis of optimal primary energy source mixture to produce sustainable products.

# 2. INTEGRATED DATA-DRIVEN MODELING AND GLOBAL OPTIMIZATION APPROACH FOR MULTI-PERIOD NONLINEAR PRODUCTION PLANNING

## 2.1 Production Planning Operations in the Refinery Industry

Many refinery operations such as crude distillation, hydrocracking, or hydrotreating are complex processes that display strong nonlinear relationships between process inputs and output [52]. As a result, there has been significant efforts in the industry and academia to develop nonlinear models for refinery processes since the 1980s [53]. For this purpose, Mobil has developed a proprietary lumping technique called structure-oriented lumping (SOL) in early 1990s to predict physical properties using group contribution methods [84]. SOL models have been used to model the reaction networks in vacuum residua conversion [85] and heavy oil hydroprocessing [86].

Commonly investigated topics by the academia include blending [87, 88, 89], crude distillation, and fluid catalytic cracking processes[90, 91, 92]. Nonlinear models can be first principle-based or empirical [92]. First principle models consist of mass and energy balance equations as well as phase equilibrium conditions along an entire column. Such rigorous models also include flow rates and compositions of all internal and external streams as well as operating conditions such as tray temperatures and pressures. Optimization formulations of such systems present inherently nonlinear and nonconvex problems. Although the computational power has increased tremendously in the last decade and powerful commercial global optimization solvers such as BARON [54] and ANTIGONE [55] are now available, the use of such high-fidelity models in planning optimization is restricted due to the arising computational complexity [52].

Aspen PIMS (AspenTech) and GRTMPS (Haverly Systems), two commercially available inverntory managment tools, use sequential linear programming (SLP) techniques to solve nonlinear programming (NLP) models, where NLP models are linearly approximated around a reference operating point. While SLP is a well-established method in the industry to solve

large-scale nonlinear problems, it suffers from yielding locally optimum solutions when handling nonconvex NLP models [50]. Therefore, academic literature conducts studies to efficiently incorporate accurate nonlinear models in optimization of the refinery process operations [93, 94]. Studies focusing on nonlinear and mixed integer nonlinear programming (MINLP) problems often also examine necessary global optimization strategies to solve the resulting problems [89, 95, 96].

A promising way to model nonlinearity in complex processes with low computational cost is to use data-driven models. Data-driven models are used in a plethora of disciplines such as chemical engineering, financial management, mechanical engineering, geosciences, etc. [97, 98, 99]. The analytical form of data-driven models are known and they are especially useful if the rigorous model of a process is computationally expensive or the finding an analytical expression for the required input-output relationship is nontrivial [33]. Data-driven models can be trained with simulation or operational data.

Despite all the interest in improving planning operations in both academia and the petrochemical industries, collaborations are quite rarely published [14]. This limited research is often due to the confidentiality restrictions [100, 101]. In their work, Li et al. [52] use a data-driven approach to optimize the production plan of an existing petrochemical complex in China owned by PetroChina Company Ltd. They use the operational plant data provided by the company to train nonlinear process models. Their work highlights that if companies are willing to share their data with academia, state-of-the-art modeling and optimization techniques can help the industry to improve their operations.

## 2.2 Integrated Modeling and Optimization Framework

With this study, an integrated data-driven and global optimization approach for nonlinear multi-period production planning is proposed that significantly extends the previously proposed framework by Li et al. [52], featuring: (i) automatic generation of nonlinear and sparse data-driven process models where yields and properties of the process models are based on input properties and compositions, (ii) estimation of model parameters using real-plant data, and (iii) a global optimization solution strategy of the large-scale nonlinear and multi-period production planning

model using ANTIGONE. The automated model selection aims to achieve a certain degree of sparsity in the models. Sufficiently sparse models can improve the computational efficiency in multi-period planning formulations and allow for the use of commercial global optimization software. This integrated modeling and planning approach is first described and later applied to optimize the production planning problem of Hyundai Oilbank Company Ltd.'s Daesan Refinery in South Korea, where the processing units are modeled using the historical operational data provided by the company. Various data processing, model training, and single- and multi-period formulations are analyzed and the optimal production plans for selected days of operation are compared with the actual plan to show the effectiveness of the current approach.

The framework is best described in four major steps as illustrated in Figure 2.1. **Step 1** comprises collection, grouping, and processing of the raw data provided by the industrial partner. In **Step 2**, data-driven yield and property prediction models for all the processing units are developed. Lasso and elastic net regularization methods are compared to obtain sparse prediction models. In **Step 3**, a process superstructure is generated with all possible connections and available operating modes in the refinery. With the addition of mass balance, capacity, inventory, and demand constraints, lower and upper bound values on all decision variables, and the objective function to the processing models, a discrete-time multi-period planning problem is obtained. Finally, **Step 4** is when the resulting optimization problem, that is a large-scale nonconvex, constrained NLP, is solved to $\varepsilon$-global optimality using commercial global optimization solvers. The details of each step are elaborated in the following sections of this chapter.

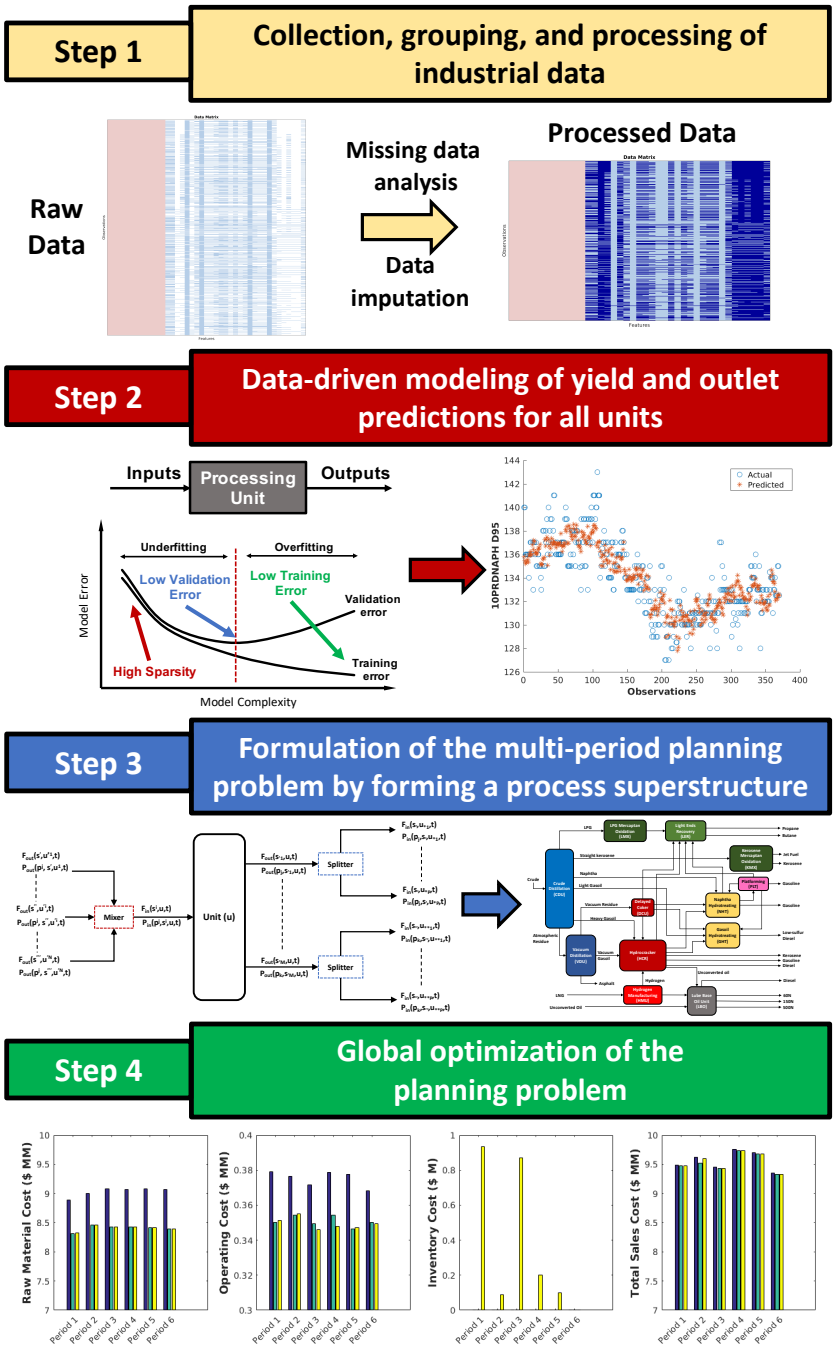


Figure 2.1: Integrated data-driven modeling and global optimization approach for production planning.

### 2.2.1 Data Processing

Data collection, grouping, and processing is an most important step in this framework. Since modeling is purely data-driven, the raw data taken from a plant often need to be checked for consistency and reliability prior to any modeling efforts. The data sets for each processing unit are formed as matrices where each column consists of either flow rates or properties (features) and each row consists of the corresponding measurements made at each operating day (observations).

The original raw data set consists of various property measurements for every stream in the plant. While using all the stream flow rates is essential to model all the possible connections, reducing the number of property measurements down to the smallest essential amount of features is important in reducing the size of the optimization problem. The initial list of predicted properties for each processing unit are decided by the company experts. Additional properties that do not belong the initial list are also included to the properties to be predicted, since they need to be later used as input variables to the connected processing units. Once formed, the mass balances and the measurements in the data set are checked for consistency by the company experts. However, this alone is not sufficient to declare the data set as reliable.

The raw data consist of noise and occasional missing points. There are potential reasons listed in the literature for sources of noise in actual data such as variability in operating personnel, data acquisition devices of the processing units, and random error [52]. Missing data are commonly caused by sensor breakdown, data acquisition system malfunction, data recording errors [102], and often by decisions and/or mistakes by the operation personnel [103]. While the stream flow rates and yields are measured every day, some property measurements are only taken on a weekly basis, often after crude oil change. While removing a mostly empty row (or a column) is one way to get rid of the missing data problem [104], more often than not, the missing data points are isolated cells in a big data matrix. Removing an entire row can mean losing precious information on other useful features.

Missing data imputation is a way to regain some of the information missing in the original data set [105]. Previous work by Li et al. uses k-nearest neighbor (k-NN) algorithm to replace

the missing data point with the corresponding value from the nearest-column, where the nearest column is the closest column in Euclidean distance. For this purpose, they use MATLAB's $knnimpute$ function. In this study, in addition to the k-NN algorithm, available imputation techniques available in MATLAB are tested to find the best performing technique for this data set. The alternative methods are the probabilistic principal component analysis (PPCA) using MATLAB's $ppca$ function, the iterative algorithm (IA), the nonlinear iterative partial least squares regression algorithm (NIPALS), the known data regression (KDR), and the trimmed scores regression (TSR) methods. The latter four methods are available in MATLAB through the Missing Data Imputation (MDI) Toolbox that is described in the works of Folch-Fortuny et al. [103, 106]. After the missing data are imputed, the data set is normalized and then ready for the data-driven modeling.

### 2.2.2 Data-Driven Modeling and Feature Selection

#### *2.2.2.1 Model Training*

The aim in data-driven modeling is to establish relationships between several explanatory input variables and the response variables that are to be predicted using the available data [107]. All refinery units have significant variety in the outputs with respect to changing input conditions, often showing nonlinear relationships. To capture the relationships the prediction models are allowed to include linear, quadratic, and bilinear interaction terms. Such models are referred to as quadratic models or polynomial response surface models (RSM). For this purpose, individual parameter estimation problems are solved for each yield and property prediction model. The inputs are tested for correlation by checking Pearson correlation coefficients. A cutoff value of 0.7 is used for elimination inputs and no significant correlations in the data set are observed.

There are important challenges related to using data-driven models, which need to be addressed in any study. Two important decisions in data-driven modeling are the input-output relationships and the adequate model complexity. There are trade-offs between finding (i) a model that best fits the training data set, (ii) a model that makes the best predictions when tested with data outside

the training set, and (iii) a sparse model that ensures computational efficiency when used in an optimization application. In order to use nonlinear models in multi-period optimization problems, it is beneficial to have a model that simultaneously satisfies all the three points to a degree. While objectives (i) and (ii) can often be achieved by k-fold cross-validation (CV) approach, addressing objective (iii) requires a somewhat different approach. Sparsity in models is often obtained by selecting a subset of inputs and omitting a set of predictors in the model. Since the size of multi-period optimization problems scales linearly with the number of periods, sparsity in models becomes crucial to reduce the size of a problem.

There are various variable selection methods in the literature such as Akaike Information Criteria (AIC), Bayesian Information Criteria (BIC), lasso, ridge, or elastic net types of regularization [33], or nonlinear methods such as support vector regression (SVM) [108, 109]. Regularization methods use a nonnegative hyperparameter, the regularization coefficient $\lambda$, to penalize the coefficients of the predictors. Lasso regularization penalizes the $L^1$-norm of the coefficients, whereas ridge regularization penalizes the $L^2$-norm. Lasso method pushes the coefficients to be zero, effectively eliminating predictors, if they are not relevant. While ridge method penalizes large values of coefficients, it does not necessarily push them to be zero. Elastic net is a mixture of both methods, having both $L^1$- and $L^2$-norm in its objective function to be minimized [110]. Regularization is a fast method and easy to implement. The objective of the regularization problem is given in Equation 2.1:

$$\min_{\beta,\beta_0} \quad \left( \frac{1}{2N} \sum_{k=1}^{N} (y_k - \beta_0 - x_k^T \beta)^2 + \lambda \left( \frac{(1-\alpha)}{2} \|\beta\|^2 + \alpha \|\beta\| \right) \right) \tag{2.1}$$

Equation 2.1 becomes the lasso regularization problem for $\alpha = 1$ and ridge for $\alpha = 0$. In elastic net regularization, $\alpha$ can take any value between 0 and 1. In any case, a larger $\lambda$ penalizes more terms, resulting in a sparser model.

In this study, two regularization methods are used to obtain sparse models: (1) lasso- and (2) elastic net- regularization. For elastic net $\alpha = 0.5$ is used. For both methods, MATLAB's $lasso$ function is used with 5-fold cross-validation. The function solves a parameter estimation problem

with the objective of minimizing the cross-validated mean square error (MSE), that is shown in Equation 2.2, where $y_k$ is the observed value and $\hat{y}_k$ is the predicted value.

$$MSE = \frac{\sum_{k=1}^{N}(\hat{y}_k - y_k)^2}{N} \tag{2.2}$$

The $lasso$ function performs regularization using a geometric sequence of $\lambda$'s, resulting in 100 discrete values of $\lambda$ and 100 parameter estimation problems solved. The function reduces the number of non-zero regression coefficients gradually by using a larger values of $\lambda$ in each step. This results in 100 sets of parameters for each prediction model. Among those 100 sets, two are highlighted by MATLAB: the one with the minimum cross-validation MSE (minMSE) and the one with minimum MSE plus one standard error (minMSE+1SE), a sparser model due to larger regularization coefficient in expense of a larger cross-validation MSE.

Depending on the scale of the variables $y_k$ the range of MSE can be very different. While this does not affect the optimal solution of the parameter estimation problem, normalizing MSE for all the models can be useful is comparing the relative accuracy of different models (e.g. yield vs. property predictions). Taking the square root of MSE and then dividing it by the range of the measured data is commonly used to normalize MSE as shown in Equation 2.3 and the obtained quantity is called normalized root mean squared error (NRMSE).

$$NRMSE = \frac{\sqrt{MSE}}{y^{max} - y^{min}} \tag{2.3}$$

#### *2.2.2.2 Yield and Property Prediction Models*

In this section, the generic expressions for the prediction models are presented. The full list of all the variables and parameters used in the notation is given in the Nomenclature chapter. The outlet flow rate of a stream from a unit, $F_{out}(s, u, t)$, is calculated from its yield and the total input

flow rate to that unit using Equation 2.4.

$$F_{out}(s,u,t) = \frac{Yield(s,u,t)}{100}\sum_{s'} F_{in}(s',u,t) \qquad \forall u \in U^{pro}, s \in S_u^{out}, s' \in S_u^{in} \tag{2.4}$$

The yields are predicted from inlet flow rates and inlet properties. Equations 2.5 and 2.6 show the mapping between the inputs variables and the output yields, and the general form of the yield prediction equations, respectively.

$$Yield(s,u,t) = f[F_{in}(s',u,t), P_{in}(p',s',u,t)] \qquad \forall u \in U^{pro}, s \in S_u^{out}, s' \in S_u^{in}, p' \in P_{s',u}^{in}, t \tag{2.5}$$

$$Yield(s,u,t) = C_{yield}(s,u)\{\beta_{yield,0}(s,u) + \sum_{i=1}^{I_{yield,u}} \beta_{yield,i}(s,u)x_{yield,i}(u,t) + \sum_{i=1}^{I_{yield,u}}\sum_{j=1,j\geq i}^{I_{yield,u}} \beta_{yield,i,j}(s,u)x_{yield,i}(u,t)x_{yield,j}(u,t)\} \qquad \forall u \in U^{pro}, s \in S_u^{out}, s' \in S_u^{in}, p' \in P_{s,u}^{in}, t \tag{2.6}$$

where $x_{yield,i}(u,t)$ and $x_{yield,j}(u,t)$ can either be $F_{in}(s',u,t)$ or $P_{in}(p',s',u,t)$ and $C_{yield}(s,u)$ is the factor used to scale the value of $Yield(s,u,t)$. $I_{yield,u}$ is the set of inputs for yield predictions for unit u, respectively that are associated with the unit $u$. $\beta_{yield,0}(s,u)$, $\beta_{yield,i}(s,u)$, and $\beta_{yield,i,j}(s,u)$ are the parameters of the model.

Outlet properties are predicted from inlet flow rates, inlet properties, and outlet flow rates. Equations 2.7 and 2.8 describe the mappings between the input variables and the output properties or outlet yields for each unit.

$$P_{out}(p,s,u,t) = f[F_{in}(s',u,t), F_{out}(s,u,t), P_{in}(p',s',u,t)] \qquad \forall u \in U^{pro}, s \in S_u^{out}, s' \in S_u^{in}, p \in P_{s,u}^{out}, p' \in P_{s',u}^{in}, t \tag{2.7}$$

Equation 2.8 shows the form of property prediction equations:

$$P_{out}(p,s,u,t) = C_{Pout}(p,s,u)\{\beta_{prop,0}(p,s,u) + \sum_{i=1}^{I_{prop,u}} \beta_{prop,i}(p,s,u)x_{prop,i}(u,t) + \sum_{i=1}^{I_{prop,u}} \sum_{j=1,j\geq i}^{I_{prop,u}} \beta_{prop,i,j}(p,s,u)x_{prop,i}(u,t)x_{prop,j}(u,t)\} \quad \forall u \in U^{pro}, s \in S_u^{out}, s' \in S_u^{in}, p \in P_{s,u}^{out}, p' \in P_{s',u}^{in}, t \tag{2.8}$$

where $x_{prop,i}(u,t)$ and $x_{prop,i}(u,t)$ can either be $F_{in}(s',u,t)$, $F_{out}(s,u,t)$, or $P_{in}(p',s',u,t)$ and $C_{Pout}(p,s,u)$ is the factor used to scale the value of $P_{out}(p,s,u,t)$. $b_{prop,0}(s,u)$, $b_{prop,i}(s,u)$, and $b_{prop,i,j}(s,u)$ are the parameters of the yield prediction equation for stream $s$ leaving unit $u$. $I_{prop,u}$ is the set of inputs for yield predictions for unit u, respectively that are associated with the unit $u$.

#### *2.2.2.3 Feature Selection*

A feature selection approach to reduce the number of terms in the regression models, in other words increasing the model sparsity, serves a multitude of goals. Sparsity in this work is defined in Equation 2.9:

$$Sparsity = \frac{Number\ of\ nonzero\ parameters}{Number\ of\ all\ possible\ parameters} \tag{2.9}$$

MATLAB's $lasso$ function is called for four different type of models: (a) linear terms only (LM), (b) linear plus interaction terms (LIM), (c) linear plus quadratic terms (LQM), (d) linear plus interaction and quadratic terms (LIQM). For each type of model, two versions are obtained: the minMSE and minMSE+1SE, with different sparsity and CV errors. The procedure for feature selection to generate sparse data-driven models is presented in Table 2.1.

This procedure aims to create a subset of relevant features first by comparing the cross validation MSE (CV-MSE) of the regularized LM models (Steps 1 and 2). Later on, interaction and quadratic terms of the selected features are also included in the model to see if performance of the model is improved (Steps 3 and 4). Overfitting is a significant concern that is possible to

Table 2.1: Feature selection procedure.

| **Procedure** Feature selection to obtain sparse models | |
|---|---|
| Step 1 | Initialize the model sparsity cutoff criteria (CC) for yields and properties as 85% and 90%, respectively |
| Step 2 | Train regularized LM using 5-fold CV |
| Step 3 | Pick the best regularized model |
| Step 4 | Use the subset of variables selected by LM and train regulzarized LIM, LQM, and LIQM using 5-fold CV |
| Step 5 | Eliminate any model where: # possible terms $\geq$ 0.1(# observations) to prevent overfitting |
| Step 6 | Pick the model with the minimum CV-MSE that obeys: Model sparsity $\geq$ CC |
| Step 7 | If no model is selected, then relax the CC by 5% and go to Step 6; else continue |
| Step 8 | If the linear terms of all the features do not appear in the model, retrain the model including the linear terms; else continue |
| Step 9 | Print the model and continue to Step 1 for the next prediction model |

run into if the number of observations are not large enough. A rule of thumb is to use at least an order of magnitude more observations than the number of terms. Models that do not obey this conditions are eliminated (Step 5). Then, the model with the minimum CV-MSE that obeys the sparsity criterion is selected (Step 6). If no model obeys the initial sparsity cutoff criterion, the criterion is relaxed by 5% (Step 7). The models including the nonlinear terms are also regularized to eliminate insignificant nonlinear terms. This can potentially give models that include nonlinear combinations of a feature while its linear terms are eliminated (Step 4). As per convention for the surface response model training [107], the linear term of any feature that appears in any nonlinear form is forced to be included in the final (Step 8).

### 2.2.3 Multi-Period Planning Problem Formulation

Multi-period formulation allows the production facility to produce and store products over a planning horizon and inventory constraints tie the production plans of adjacent periods to each other. The additional degrees of freedom coming from inventory management provides room for improvement in the objective function value. Since the planning problem is solved for all periods simultaneously, the problem grows large in size compared to singe-period formulation where each period is solved individually. While single-period models are easier to solve due to smaller problem

size, they are subjected to a few limitations: one such limitation is observed when the minimum demand exceeds the refinery production capacity, resulting in a violation of demand satisfaction constraints [87, 93]. Single-period plans also provide less flexibility to the schedulers by ignoring the inventory levels, resulting in possible infeasibility when considering in scheduling operations. Multi-period formulation is a way to overcome this problem and to have more flexible production plans. The optimal solution of a multi-period problem is at least as good as the single-period problem. However, since the number of decision variables and constraints are scaled linearly with respect to the number of periods, finding a global solution to a nonlinear and nonconvex multi-period problem can be difficult. For this reason, multi-period planning models are mostly reported to use linear equations for the processing units [111].

This work uses a discrete-time model with each time period represented uniformly by a single-day. This choice is made in accordance with the way the industrial partner makes their planning decisions, however, the duration of a period in the model can be nonuniform. The multi-period planning problem is formulated by including mass balance equations, capacity constraints, inventory constraints, operational restrictions, demand constraints, and the objective function along with the process models. These constraints provide the necessary physical restrictions to the process. The full list and definition of variables, sets, and parameters are presented in the Nomenclature section.

#### *2.2.3.1 Connections and Unit Mass Balances*

A typical refinery operation is summarized in Figure 2.2. The refinery process under investigation begins with the blending of various crude oil feeds and Daesan Refinery blends up to seven different crudes to obtain their crude oil mixture. The blended crude oil is fed to the crude distillation unit (CDU) to be separated into fractions of different products. The rest of process can be summarized as further separation and upgrading of the crude oil distillates. In this study, crude oil blending is not included in the model, since a different branch of the refinery experts is working on finding the optimum blend. Hence the main input to the refinery is blended crude oil.

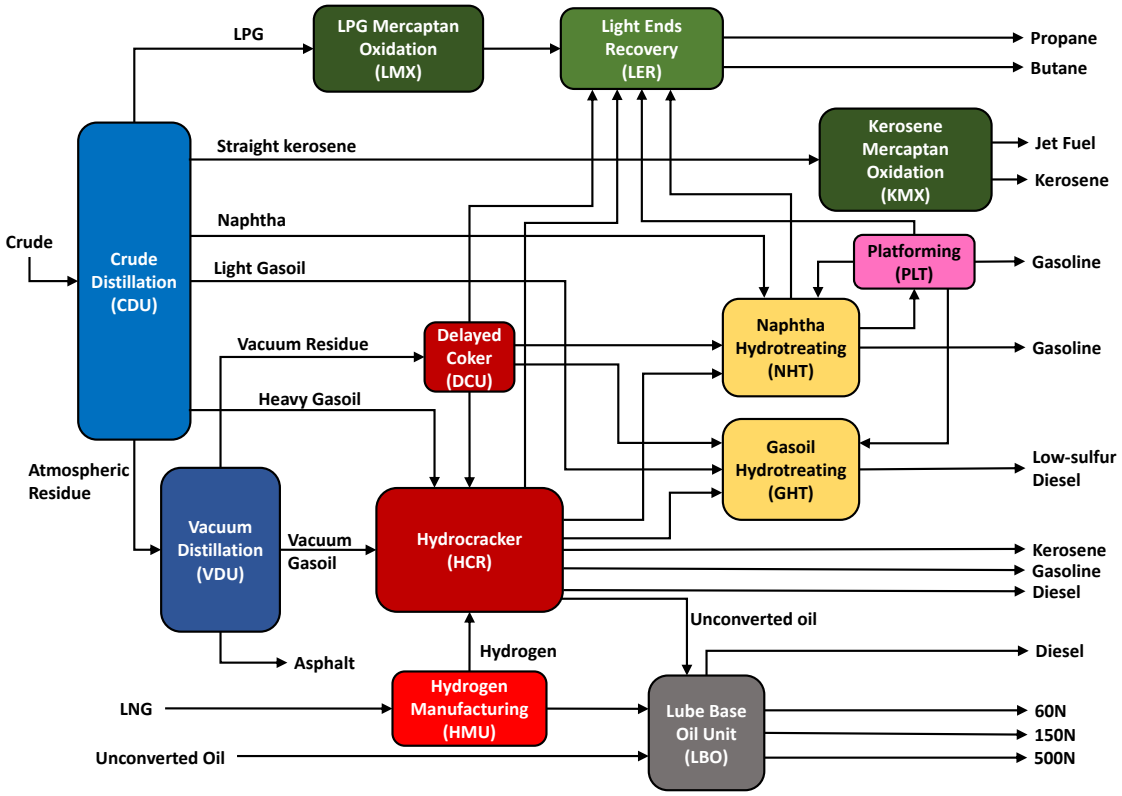


Figure 2.2: Simplified flowsheet of the refinery processes in Plant #1.

The plant topology with all possible stream connections is represented by a process superstructure. The stream connections are formulated as shown in Equations 2.10 and 2.11. Only allowable connections are made possible by constraining the equations using the stream connections subset $UC$. A pictorial representation of the inputs and outputs to unit u is shown in Figure 2.3.

$$\sum_{u^*}\sum_{s^*} F(s^*,u^*,s',u,t) \geq F_{in}(s',u,t)$$
$$\forall (u,u^*) \in U^{pro}, s^* \in S^{out}_{u^*}, s' \in S^{in}_{u}, (s^*,u^*,s,u) \in UC, t \tag{2.10}$$

$$F_{out}(s,u,t) \geq \sum_{(s',u')} F(s,u,s'',u'',t)$$
$$\forall (u,u'') \in U^{pro}, s \in S^{out}_{u}, s'' \in S^{in}_{u''}, (s,u,s'',u'') \in UC, t \tag{2.11}$$

where the $F_{out}(s,u,t)$ is calculated using Equation 2.12. Equations 2.10 and 2.11 are not strict

equality constraints, hence the flow of streams entering the unit can be adjusted if needed.

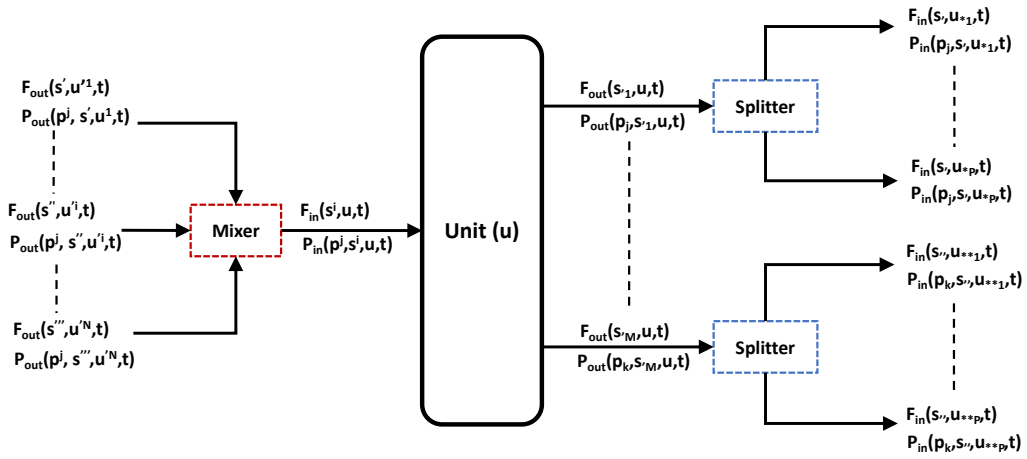


Figure 2.3: Schematic diagram showing how inputs and outputs are related from different units.

$$F_{out}(s,u,t) = \left[\sum_{s' \in sin(s',u)} F_{in}(s',u,t)\right] Yield(s,u,t)/100 \qquad \forall u \in U^{pro}, s \in S_u^{out}, s' \in S_u^{in}, t \tag{2.12}$$

The property information is also transferred using the connections subsets $UC(s,u,s',u')$, $P_{s,u}^{in}$, and $P_{s,u}^{out}$ as shown in Equation 2.13:

$$\begin{aligned} P_{in}(p,s',u',t) &= P_{out}(p,s,u,t) \\ \forall (u,u') \in U^{pro}, s \in S_u^{out}, s' \in S_u^{in}, \\ p \in (P_{s,u}^{in} \cup P_{s,u}^{out}), (s,u,s',u') \in UC, t \end{aligned} \tag{2.13}$$

The yield and property prediction Equations (2.5 and 2.7) are modified with slack variables and they take the form of Equations 2.14 and 2.15.

$$Yield(s,u,t) = f[F_{in}(s',u,t), P_{in}(p',s',u,t)] \pm YieldSlacks(s,u,t) \qquad \forall u \in U^{pro}, s \in S_u^{out}, s' \in S_u^{in}, p' \in P_{s,u}^{in}, t \tag{2.14}$$

$$P_{out}(p,s,u,t) = f[F_{in}(s',u,t), F_{out}(s,u,t), P_{in}(p',s',u,t)] \pm PropSlacks(p,s,u,t)$$
$$\forall u \in U^{pro}, s \in S_u^{out}, s' \in S_u^{in}, p \in P_{s,u}^{out}, p' \in P_{s,u}^{in}, t \tag{2.15}$$

By the addition of slack variables, slight violations of the upper or lower bounds of the predicted quantities are allowed. Since yield and property prediction constraints are in forms of equalities, adding slack variables to these equations relaxes the problem. Note that the slack variables are constrained to be no more than $5\%$ of the upper bound of the predicted variable. To give an example, if the upper bound of a yield prediction is $40\%$ and the model predicts the yield as $40.8\%$, then the negative slack will have the value $0.8\%$ and the level value of the prediction will be $40\%$. Since nonzero slacks are essentially not desired, the sum of all the slacks is later added to the objective function to be minimized.

The throughput of the unit is the total flow rate leaving and it must not exceed the unit capacity. Equation 2.16 ensures that condition.

$$CAPmin(u) \leq \sum_s F_{out}(s,u,t) \leq CAPmax(u)$$
$$\forall u \in U^{pro}, s \in S_u^{out}, t \tag{2.16}$$

#### *2.2.3.2 Variable Bounds*

For each variable there are upper and lower bounds coming from two years of operational data. Equations 2.17 to 2.21 show the upper and lower bounds on the decision variables.

$$F_{in}^{low}(s,u) \leq F_{in}(s,u,t) \leq F_{in}^{up}(s,u)$$
$$\forall u \in (U^{pro} \cup U^{hyp}), s \in S_u^{in}, t \tag{2.17}$$

$$F_{out}^{low}(s,u) \leq F_{out}(s,u,t) \leq F_{out}^{up}(s,u)$$
$$\forall u \in (U^{pro} \cup U^{hyp}), s \in S_u^{out}, t \tag{2.18}$$

$$Yield^{low}(s,u) \leq Yield(s,u,t) \leq Yield^{up}(s,u) \quad \forall u \in U^{pro}, s \in S_u^{out}, t \tag{2.19}$$

$$P_{in}^{low}(p,s,u) \leq P_{in}(p,s,u,t) \leq P_{in}^{up}(p,s,u) \quad \forall u \in (U^{pro} \cup U^{hyp}), s \in S_u^{in}, p \in P_{s,u}^{in}, t \tag{2.20}$$

$$P_{out}^{low}(p,s,u) \leq P_{out}(p,s,u,t) \leq P_{out}^{up}(p,s,u) \quad \forall u \in (U^{pro} \cup U^{hyp}), s \in S_u^{in}, p \in P_{s,u}^{out}, t \tag{2.21}$$

#### *2.2.3.3 Demand Constraints*

For each final product there is a different demand during the planning horizon. Upper and lower bounds on the demand for a product is addressed in Equation 2.22. All products are sent to the hypothetical $SALES$ unit.

$$MinDemand(s,t) \leq F_{in}(s,SALES,t) \leq MaxDemand(s,t) \quad \forall s \in S_{SALES}^{in}, t \tag{2.22}$$

#### *2.2.3.4 Inventory Balance Constraints*

The inventory variables $Inv(s,t)$ and $Inv^0(s,t)$ are used to connect the production variables to the sales variables. Equations 2.23 and 2.24 allow some of the refinery products to be stored in inventory.

$$Inv(s,t) = Inv^0(s,t-1) + \sum_u \sum_{s'} F(s',u,s,SALES,t) \quad \forall u \in U^{pro}, s \in S_{SALES}^{in}, s' \in S_u^{out}, (s',u,s,SALES) \in UC, t \tag{2.23}$$

$$Inv^0(s,t) = Inv(s,t) - F_{in}(s,SALES,t) - W(s,t) \quad \forall s \in S_{SALES}^{in}, t \tag{2.24}$$

$Inv(s,t)$ and $Inv^0(s,t)$ show the inventory level at the beginning of a period and at the end after the demands are satisfied, respectively. The inventory constraints and increased time horizon of

the model allow products to be stored when either the demand or the crude prices are low. The excess production can later be used to meet the product demands when they are higher than refinery capacity. Alternatively, some excess products can be discarded if $W(s,t)$ variable is nonzero.

#### *2.2.3.5 Objective Function*

The objective of this project is to maximize the gross profit of the refinery, that is presented in Equation 2.25.

$$\begin{aligned} Profit = \sum_{t} \Big\{ & \sum_{s} Price(s, SALES, t) F_{in}(s, SALES, t) \\ & - \sum_{s'} Cost(s', PURC, t) F_{out}(s', PURC, t) \\ & - \sum_{u} OperatingCost(u) \sum_{s''} F_{out}(s'', u, t) \\ & - \sum_{s} InvCost(s) Inv^{0}(s,t) \Big\} \end{aligned} \tag{2.25}$$

$$\forall u \in U^{pro}, s \in S^{in}_{SALES}, s' \in S^{out}_{PURC}, s'' \in S^{out}_{u}, t$$

where the cost of all raw materials that are purchased at the hypothetical $PURC$ unit and the operating costs of all processing units are subtracted from the total gross sales, which is the total revenue gained by sold products that are sent to the hypothetical $SALES$ unit. Total profit is calculated in $\$MM/day$ (millions of \$/day) basis.

The objective function for the main optimization problem is the sum of negative profit and slack variables. The addition of slack variables and minimizing the sum ensures that while maximizing the profit, the slack variables (thus the small violations of hard bounds) are forced to be as small as possible. The objective function is shown in Equation 2.26.

$$
\begin{aligned}
Objective\ Function = -Profit \\
+\gamma \sum_{t} \Big\{ \sum_{u} \sum_{s} \sum_{p} PropSlacks(p,s,u,t) \\
+ \sum_{u} \sum_{s} YieldSlacks(s,u,t) \Big\} \\
\forall u \in U^{pro}, s \in S_{u}^{out}, p \in P_{s,u}^{out}, t
\end{aligned}
\tag{2.26}
$$

The coefficient $\gamma$ is found by a process of trial. Different values for $\gamma$ are tested, and the largest value that is ensuring that while the sums of slacks have a weight in the objective function they are not dominating the profit maximization objective. The optimization problem is presented in Equation 2.27:

$$
\begin{aligned}
\min \quad & Objective\ Function \quad (Equation \quad 2.26) \\
\text{s.t.} \quad & Equations \quad 2.6, 2.8 \\
& Equations \quad 2.10 - 2.24
\end{aligned}
\tag{2.27}
$$

### 2.2.4 Global Optimization

Here, the global optimization software and algorithms are briefly explained. For more information, the readers are encouraged to read the work of Misener and Floudas [55] which describes the novel components of the commercial solver ANTIGONE. The discrete-time, multi-period, planning model is a nonconvex, constrained NLP model where the nonlinearity comes from the quadratic and bilinear terms and the nonconvexity is caused by the bilinear interaction terms coming from property and yield prediction models.

The planning problem is modeled in GAMS and solved with the solver ANTIGONE to $\varepsilon$-global optimality. ANTIGONE takes the user defined NLP, detects the special structures, and reformulates the problem. It uses term-based underestimators to create tight convex lower bound problems (underestimations) in the form of a mixed integer linear optimization (MILP) program. Then, the MILP is combined with the upper bound (original problem) NLP in a

branch-and-cut algorithm to find the global optimum solution. The algorithm generates tight convex underestimators, dynamically generates separating hyperplanes, bounds the variables, branches on the search space, and finds feasible solutions. As time progresses the lower and upper bounds converge to a global optimum solutions.

## 2.3 Computational Studies

### 2.3.1 Data Processing Results

The data set consists of daily averaged stream flow rates for all unit inputs and outputs, connections between units, daily/weekly/biweekly property measurements, product demands, raw material costs, as well as unit operating costs. Additionally, unit capacities, allowable lower and upper limits on product qualities, and detailed descriptions of the refinery flow sheet are given. The Daesan Refinery consists of three subplants within their refinery complex. Among the three plants, Plant #1 is chosen for this study. After grouping the data for each unit and having it approved by the company experts, the imputation analysis is done.

The performance of the data imputation techniques can depend on the missingness mechanism and the ratio of observations to features. [105] lists some of the mechanism as (i) random missingness, (ii) missingness that is correlated in time which can often be due to sensor failure, (iii) missingness with a patter that can be caused by multi-rate data, and (iv) censorship. The data set consists of columns with various missingness mechanisms, mainly suffering from types (i) and (iii). In order to compare the six imputation techniques listed above, test sets are generated with varying degrees of missing data by removing cells randomly to form matrices with missingness fraction ranging from 0.1 to 0.5. Afterwards, the squared error (SE) between imputed values and the actual values are compared.

Figure 2.4 shows the performance of these methods on data sets taken from six refinery units, i.e. CDU, DCU, GHT, HCR, LER, and NHT. Note that the results obtained from NIPALS algorithm are not included in the figures because for many cases NIPALS performed significantly worse than the other five. An analysis of the results showed that in 56.7% of the total cases of 30,

k-NN algorithm is the best, followed by TSR, which performs best in 33.3% of the cases, and KDR, which is the best in only 10% of the cases. In these studies, PPCA and IA give much larger SE, especially with increasing fraction of missing data. Since k-NN algorithm consistently performs well with high fractions of missing data (e.g. 0.4-0.5), it is chosen over the other methods.

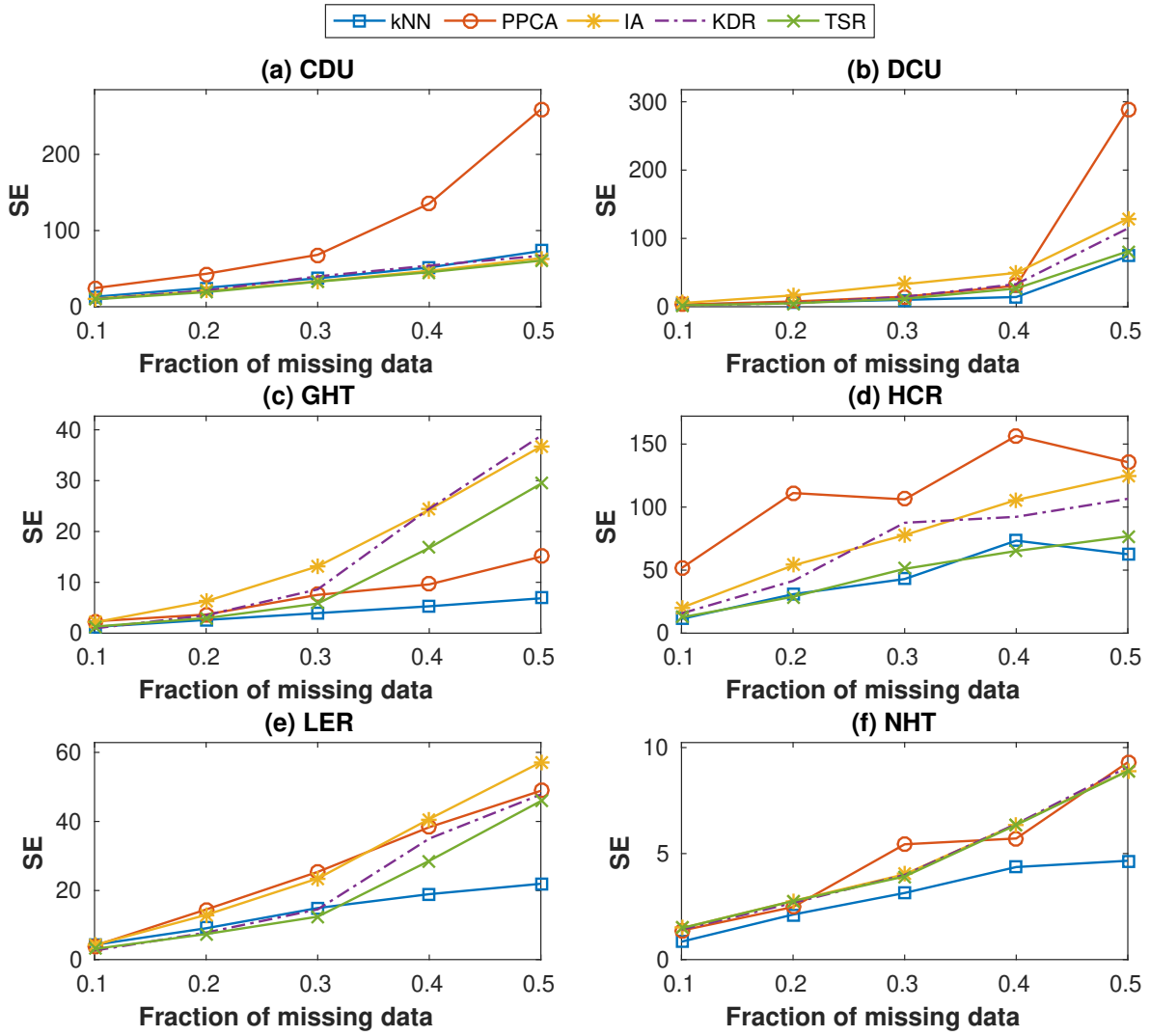


Figure 2.4: Imputation performance of k-NN, PPCA, IA, KDR, and TSR methods show that k-NN performs consistently well in all six process unit data sets.

In order to restrict the degree of imputations, the amount of missing data on a row is limited to a cutoff value of 50% for yield inputs and 50% for property inputs. If a row (i.e. a day of

observations) has more missing data that these cutoff values, it is removed completely from the data set. The overall missing data percentages before imputation ranged between 9 and 42% for all the units. The number of rows after removals ranged between 177 and 688. Additional reasons for row removal included larger than 10% mass balance error, a plant-wide shutdown, and maintenance shutdowns for individual units.

### 2.3.2 Parameter Estimation and Feature Selection Results

73 product yield and 181 outlet property prediction models are trained with the plant data. Regression analyses are done with lasso- and elastic net-regularization techniques using 5-fold cross validation. Sparse models are obtained with the feature selection procedure described earlier. 10% of the data is spared from the training data in order to be used for testing the models. The cross-validation NRMSE (CV-NRMSE) distributions of the lasso- and elastic net-regularized models are shown with box plots in Figure 2.5.

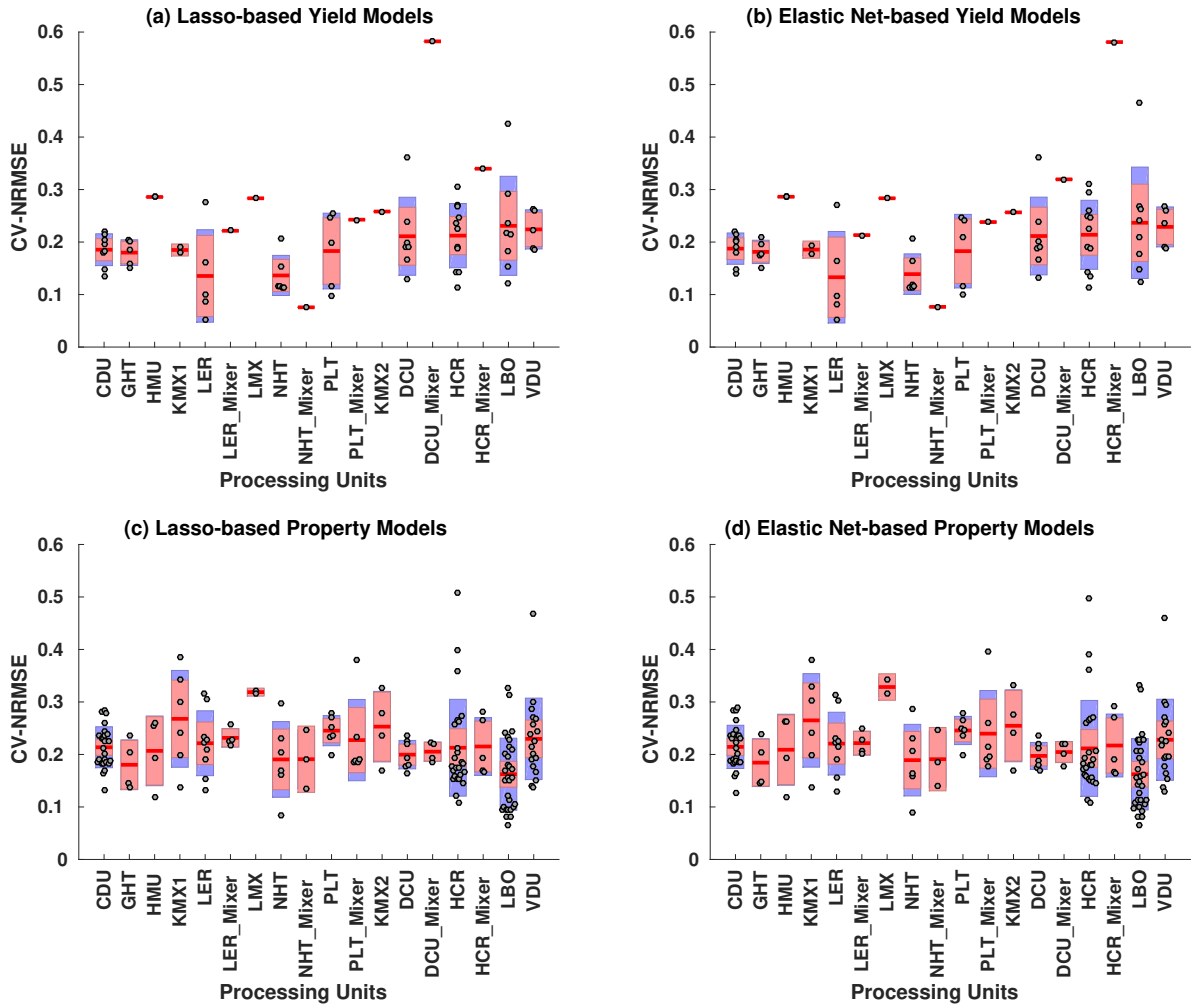


Figure 2.5: CV-NRMSE for property and yield prediction models (Red boxes show the 25$^{th}$ and 75$^{th}$ percentiles, blue whiskers show the 5$^{th}$ and 95$^{th}$ percentiles, grey dots show the CV-NRMSE of all individual prediction models associated with each unit).

The results show that there is no big difference between the CV-NRMSE of the lasso- and elastic net-regularization models. Figure 2.6 shows the histogram of % model sparsity in prediction models.

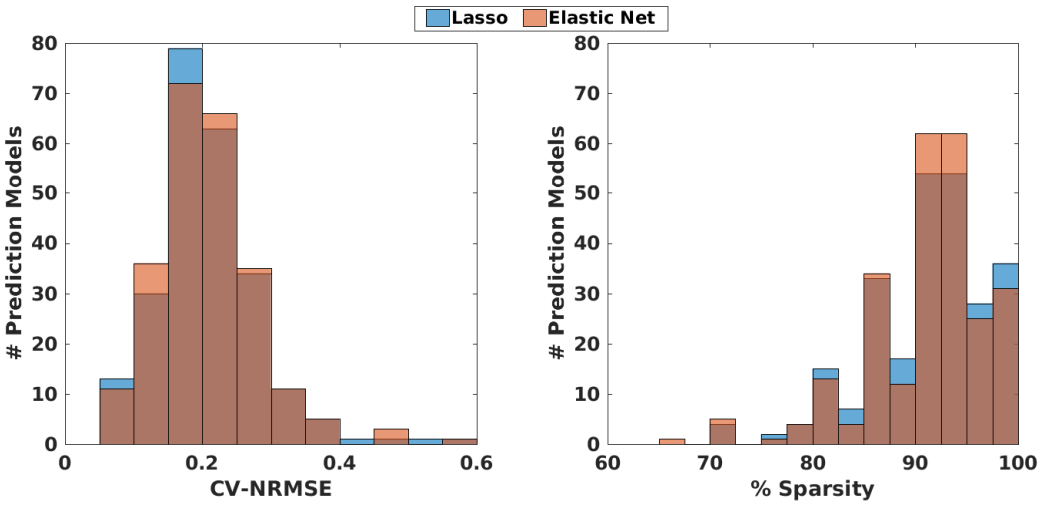


Figure 2.6: Histograms of CV-NRMSE and % sparsity of the data-driven prediction models.

Table 2.2: The list of the regularization model selected with respect to the yield and property prediction models.

| Unit | # Yield Models | Selected Models | # Property Models | Selected Models |
|---|---|---|---|---|
| CDU | 8 | Elastic Net | 25 | Elastic Net |
| GHT | 5 | Lasso | 4 | Elastic Net |
| HMU | 4 | Elastic Net | 4 | Lasso |
| KMX1 | 2 | Elastic Net | 6 | Elastic Net |
| LER | 5 | Lasso | 9 | Lasso |
| LER Mixer | 1 | Lasso | 4 | Lasso |
| LMX | 1 | Elastic Net | 2 | Elastic Net |
| NHT | 6 | Lasso | 6 | Elastic Net |
| NHT Mixer | 1 | Elastic Net | 3 | Elastic Net |
| PLT | 5 | Elastic Net | 6 | Lasso |
| PLT Mixer | 1 | Elastic Net | 6 | Lasso |
| KMX2 | 1 | Elastic Net | 4 | Elastic Net |
| DCU | 7 | Lasso | 7 | Lasso |
| DCU Mixer | 1 | Lasso | 4 | Elastic Net |
| HCR | 11 | Lasso | 27 | Elastic Net |
| HCR Mixer | 1 | Elastic Net | 6 | Elastic Net |
| LBO | 8 | Elastic Net | 32 | Elastic Net |
| VDU | 5 | Lasso | 26 | Lasso |

Results indicate that both regularization methods give the intended sparsity to the models. More than 87% of models have a sparsity greater than 85%. For deciding on which regularization model to use, 10% of the original data that is previously spared is used for testing. After comparing the testing NRMSE the list of selected models for each unit is presented in Table 2.2.

### 2.3.3 Production Planning Case Studies

#### *2.3.3.1 Global Optimization*

The planning problem is solved for selected days of October 2015. Both the single- and multi-period planning models are NLP. The problem is solved using ANTIGONE's advanced branch-and-bound algorithm, while CPLEX and CONOPT are selected as MILP and NLP solvers, respectively. All case studies are solved on a high-performance computing machine at Texas A&M High-Performance Research Computing (HPRC) facility using Ada IBM/Lenovo x86 HPC Cluster operated with Linux (CentOS 6) using 1 node (20 cores per node with 64 GB RAM). ANTIGONE 1.1 is used with GAMS 26.1.0 as the default solver. The solution time is limited to one hour and optimality criterion is set as 0.0001. Statistics of the single-period (SP) and multi-period (MP) optimization problems are given in Table 2.3. For problem size comparison, SP solution for period 1 is presented (SP-1) along with 2-, 4-, 6-, and 8-period MP solutions, that are MP-2, MP-4, MP-6, and MP-8, respectively.

Using ANTIGONE's options, piecewise linear underestimators with logarithmic partitioning scheme are selected to relax the nonconvex bilinear terms. Using default McCormick type convex envelopes can give results much faster, but the solution algorithm takes considerably more time to close the optimality gap within the vicinity of the global optimum. The rate of closing the gap also slows down with time. On the other hand, the solution algorithm with tighter piecewise linear underestimators can take more time to obtain the result, but it can close the optimality gap much faster by the end of the solution time. The optimal solutions obtained with ANTIGONE are later compared with the ones obtained using BARON 19.7.13 and IPOPT 3.11 and they are given in Table 2.3. The difference between optimal solutions of different solvers are found to be within

Table 2.3: Single- and multi-period planning formulation statistics

| Model Statistics | | SP-1 | MP-2 | MP-4 | MP-6 | MP-8 |
|---|---|---|---|---|---|---|
| Total continuous variables | | 1,349 | 2,718 | 5,434 | 8,150 | 10,866 |
| Total equations | | 859 | 1,716 | 3,430 | 5,144 | 6,858 |
| Total nonlinear terms | | 442 | 884 | 1,768 | 2,652 | 3,536 |
| Solver Statistics | | SP-1 | MP-2 | MP-4 | MP-6 | MP-8 |
| ANTIGONE | Profit ($ MM) | 0.356 | 0.742 | 1.677 | 2.152 | 2.334 |
| | Solution time (s) | 1,566 | 3,600 | 3,600 | 3,600 | 3,600 |
| | Relative gap | 0.00 | 0.52 | N/A | N/A | 0.98 |
| BARON | Profit ($ MM) | 0.356 | 0.742 | 1.677 | 2.154 | 2.330 |
| | Solution time (s) | 3,600 | 3,600 | 3,600 | 3,600 | 3,600 |
| | Relative gap | 0.59 | 0.66 | N/A | N/A | N/A |
| IPOPT | Profit ($ MM) | 0.356 | 0.743 | 1.674 | 2.154 | 2.333 |
| | Solution time (s) | 0.5 | 1.3 | 4.1 | 22.5 | 6.6 |
| | Relative gap | N/A | N/A | N/A | N/A | N/A |

0.2%. IPOPT is much faster than the other two solver to find a solution, however, it does not provide a gap of optimality since it is a local solver. Among the two global solvers, BARON is found to be faster to locate a solution than ANTIGONE but was slower to close the gap in SP and MP studies, this is due to BARON being used with default options, whereas with ANTIGONE piecewise underestimators are used. ANTIGONE is the solver to bound the lower and upper bound solutions more consistently as well as finding the best optimal solution within the one hour time, even though the MP problem can leave an optimality gap. The size of a 8-period problem shown in Table 2.3 shows that large-scale nonconvex NLPs still pose a challenge to the state-of-the-art global solvers. While, no solver used in this study has a significant advantage over others, since ANTIGONE gives the best results, its results are presented in the following section.

The problem of computational complexity is a common concern with multi-period models. In this study, an 8-period plans considers 8 days of operation horizon, since each period is as long as day. While multi-period planning presents improvements over single-period planning even when the optimality gap is not closed, computational limitations prevent the maximum number of periods that the planning problem can be solved for. For plans that cover longer time horizons, use of representative time periods with varying weights assigned to each time period can be useful.

Some clustering methods such as k-means [112, 113] and hierarchical clustering [114] are already used in planning and scheduling problems like capacity expansion. Future work should focus on reducing the number of representative time periods and the current planning model can be easily modified work with representative periods.

#### *2.3.3.2 Optimal Plans*

The multi-period (MP) problem has been solved for 2-, 4-, 6-, and 8-periods. Here the results obtained with 8-period problems (MP-8) are shown. Single-period (SP) problem is solved for each of the 8 periods separately. Crude oil is the primary input to the refinery process. In the optimization problem, crude oil properties are fixed to those of the actual operation, however inlet crude oil flow rate is left free as a decision variable. Availability of the crude oil is limited by the use of crude oil in the actual plan for that period. For the case studies, the demand profiles for all refinery products, product prices, raw material costs, and product quality specifications are set to values identical to the actual plant operation. Due to confidentiality restrictions, the full details of the actual or optimal plans are not disclosed. Instead a breakdown of the major gross profit contributors is presented in Figure 2.7.

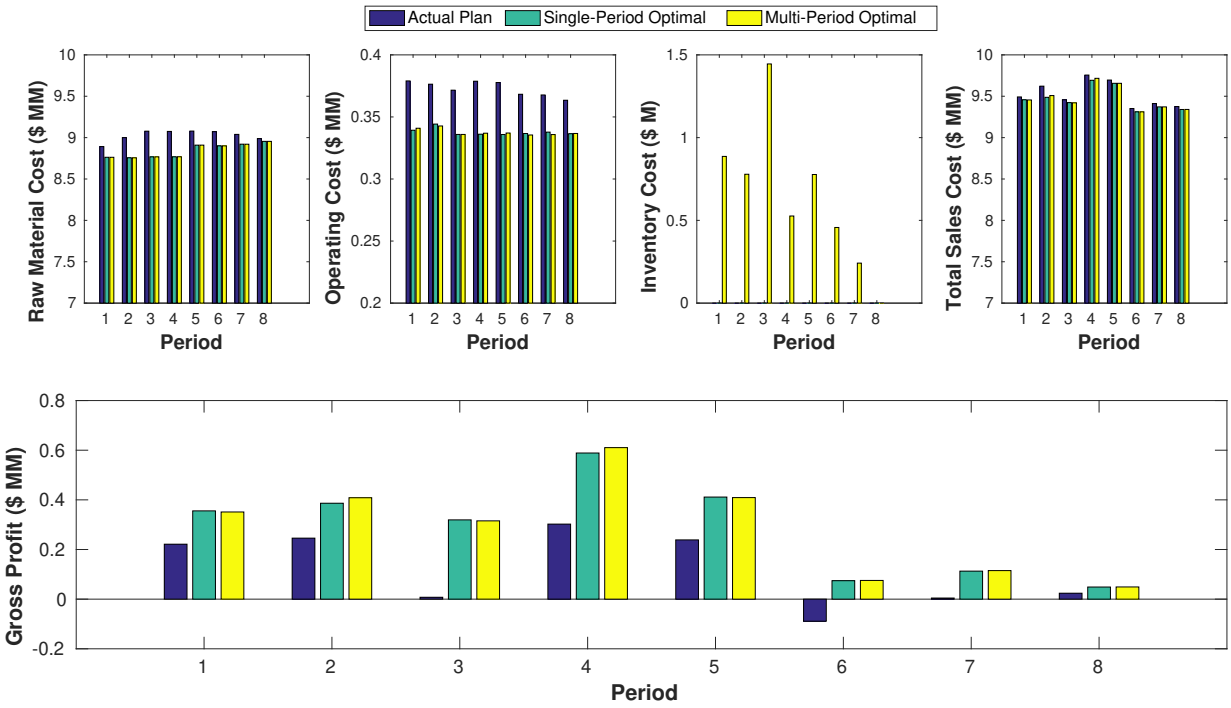


Figure 2.7: Comparison of actual, single-period, and multi-period optimization results indicate that both the single- and multi-period plans are superior over the actual plan.

Results indicate that both SP and MP optimal plans outperform the actual plan in every period. Optimal plans reduce the operating costs and the amount of raw material purchased while producing the same output as the actual plan by using the full advantage of the mathematical models for the processing units and optimal stream allocation. When MP-8 is compared with actual daily plans, the biggest reductions are observed in the operating costs that come from the changes in the operation crude distillation (CDU), vacuum distillation (VDU), delayed coker (DCU) and hydrocracker (HCR) units. In the MP optimal plan, CDU operation increases kerosene production slightly while decreasing the light and heavy gasoil production. VDU unit increases the vacuum gasoil production to be sent to HCR, while decreasing the vacuum residue that is sent to the DCU. DCU produces more lighter products, while HCR produces more kerosene and less diesel. This decrease in diesel production is compensated by the increased production of the lube base oil plants (LBO). LBO increases diesel production by using the available unconverted oil. Naphtha (NHT) and gasoil hydrotreating (GHT) units' throughputs do not change significantly, while kerosene

mercaptan oxidation units (KMX1 and KMX2) slightly increase their production. Overall, some portion of the diesel production shift from HCR to LBO. This makes sense, since HCR is more costly to operate for this refinery.

In periods 1, 2, 4, 5 and 8 the optimal plans result in 57-94% improvement in gross profit. Periods 3, 6, and 7 are operational days where actual plan is vastly inferior to optimal plans. MP plan brings the operational costs further down compared to SP plans since some of the products can be produced and stored in the earlier periods when the resources are cheaper that are later sold to satisfy the demand. Total gross profit for the eight periods considered is $955,300 for the actual plan. SP plan gives $2,297,500 whereas MP plan gives $2,334,200. Improvements in gross profit are 140.5% and 144.3% for SP and MP plans, respectively. Although, the aforementioned changes in operation in the MP plan are similar to the ones in SP plans, MP plan also has the advantage of the inventory management, that results in the additional 3.8% improvement in gross profit.

## 2.4 Conclusions

With this work, an integrated data-driven modeling and global optimization approach in developed to solve multi-period production planning problems. This work achieves (i) automatic generation of nonlinear and sparse data-driven process models where yields and properties of the process models are based on input properties and compositions, (ii) estimation of model parameters using real-plant data, and (iii) global optimization solution strategy of the large-scale nonlinear and multi-period production planning model using commercial solvers. Given operational data, accurate nonlinear data-driven input-output models for refinery processing and mixing units can be obtained. Lasso- and elastic net-regularization methods are used to obtain the process models. Obtained models have enough sparsity to be efficiently used in large-scale multi-period nonlinear optimization problems. Optimal production plans can improve the actual operation by allocating the streams more efficiently between units to reduce raw material and operating costs. Multi-period planning approach provides further improvement over single-period planning. While this work specifically focuses on production planning in refinery operations, the proposed integrated modeling and optimization approach can be applied to any production facility.

# 3. PROCESS SYNTHESIS AND GLOBAL OPTIMIZATION FOR NOVEL SUSTAINABLE AMMONIA PRODUCTION ROUTES *

## 3.1 Ammonia Production from Fossil and Renewable Feedstocks

Ammonia ($NH_3$) is synthesized at industrial scale by the Haber-Bosch process where nitrogen ($N_2$), that is coming from the air, is combined with hydrogen ($H_2$), that is traditionally extracted from a fossil feedstock. $N_2$ is highly unreactive and it is converted to $NH_3$ ( Eq. 3.1) only in the presence of a catalyst. Due to exothermicity, thermodynamic limitations, and reaction stoichiometry, high $NH_3$ yield requires lowering the temperature and increasing the pressure. However, while thermodynamically feasible, the reaction is kinetically limited at low temperatures; hence, a trade-off between reaction rate and conversion is made, and the reactor is operated under high pressure (usually between 150-300 bar) and high temperature (above 400 °C), where only $\sim$20-35% of the reactants are converted in each pass. Haber-Bosch process reaches high overall conversions by using multiple large recycle streams and removing the products and inerts from the reactor effluent stream [59]. Alternative methods to produce ammonia are electrochemical synthesis, membrane reactor system, and biological processes. While these methods might become feasible in the future, as of today, they are still immature for industrial scale production [115, 116, 117]. Most analyses done on future technologies suggest that the Haber-Bosch process will continue to be used to produce ammonia in large-scale in the near future, with an open possibility of significant changes in the hydrogen generation part. Therefore, this work focuses only on state-of-the-art configurations of the Haber-Bosch process [59, 118].

$$N_2(g) + 3H_2(g) \rightleftharpoons 2NH_3(g), \quad \Delta H^\circ = -91.4\ kJ/mol \tag{3.1}$$

*Reprinted from "Sustainable ammonia production through process synthesis and global optimization" by Demirhan, C.D. and Tso, W.W. and Powell, J.B. and Pistikopoulos, E.N., 2019, AIChE Journal, 2019, Vol. 67, No. 7, Copyright 2020 by John Wiley and Sons and Copyright Clearance Center.

While most of the ammonia production process stayed somewhat the same throughout more than 100 years of industrial practice, hydrogen generation technologies have significantly evolved. Both sustainability and economics of ammonia production can be significantly affected by the choice of hydrogen source. A global report from 2007 showed that, natural gas reforming-based ammonia production (the preference in the U.S.) had a huge 67% share, which was followed by coal gasification-based production with 27% (mostly from China). The remaining was shared by naphtha, fuel oil, and other feedstocks [119]. Although natural gas is the most efficient fossil feedstock in terms of energy economics and greenhouse gas emission savings [120], it still has a significant carbon footprint of 1.60-1.90 ton $CO_2$/ton $NH_3$ produced, which includes both fuel and feedstock use. The emissions can go up to 3.8 ton $CO_2$/ton $NH_3$ produced if coal is used as fuel and feedstock [121].

Producing ammonia from biomass gasification has been studied by several researchers over the last few years. Gilbert et al. [122] state that 65% reduction of GHG emissions is achieved for a biomass gasification-based ammonia production system, and Tock et al. [123] compare biomass-based production with natural gas-based production and points out that next to reduced emissions, the former can be economically competitive depending on the resource price and introduction of a carbon tax. Andersson and Lundgren [124] investigated integrating biomass gasification in an existing pulp and paper mill. Arora et al. [72] studied small-scale ammonia production by combining biomass gasification with steam reformers in a techno-economic perspective in one study. Another work of Arora et al. [125] examined performance of various biomass types in a similar framework. SynGest Inc. has a patent on producing ammonia from biomass gasification [126] and constructed world's first biomass-to-ammonia plant in Menlo, Iowa.

As of 2018, hydrogen production from water electrolysis is the least common technique, taking about 0.5% share of global ammonia production. Alkaline and proton exchange membrane (PEM) are two of the most common types of electrolyzers. Alkaline electrolysis systems are suitable for large-scale industrial applications due to their low capital cost, whereas less mature and more expensive PEM technology is more adept to dynamic operation. Water electrolysis is less efficient

than reforming, but it can be used in conjunction with inexpensive electricity that comes from a renewable energy source [61]. For instance, researchers are working to combine water electrolysis with onshore and offshore wind energy. Among the groups that study onshore wind energy studies, Morgan et al. [62] have a techno-economic analysis of the wind-ammonia system, and Allman et al. [127] point out the overlap of wind resources and ammonia demand locations in a supply chain optimization problem for wind powered ammonia production. A further work of Morgan et al. [61] focuses on offshore wind, and Allman and Daoutidis [128] study optimal scheduling of wind-powered ammonia production. Using solar energy to power ammonia synthesis concept is investigated by works of Du et al. [129], a feasibility analysis of solar PV-to-ammonia route, and Sanchez and Martin [130], performing an optimization based production design of ammonia from solar and wind energy.

Despite the increasing interest in studying sustainable ammonia production in the literature, there is no work focusing on global optimization-based process synthesis approach with simultaneous heat, power, and water integration applied to a variety of feedstocks. This work aims to contribute a study on the production of ammonia from a wide selection renewable resources such as hardwood or corn stover type of biomass, municipal solid waste, solar power, and wind power. Renewable-based ammonia production is later compared with the natural gas-based reference case. In order to account for the effects of variability in renewable energy availability and prices, case studies are done for states of Texas, California, and Iowa. Break-even prices for producing ammonia and report optimal process topologies, overall cost breakdown, investment costs breakdown, and GHG emission balances are calculated in the following sections.

### 3.2 Process Synthesis and Process Superstructure

This section describes the major components of the ammonia production process. Ammonia production process consists of the following sections: (i) synthesis gas generation, (ii) water electrolysis (iii) synthesis gas cleaning, (iv) ammonia synthesis loop, (v) air separation, (vi) waste water treatment, and (vii) heat & power integration. The conceptual design of the process synthesis with simultaneous heat, power, and water integration is illustrated in Figure 3.1. The

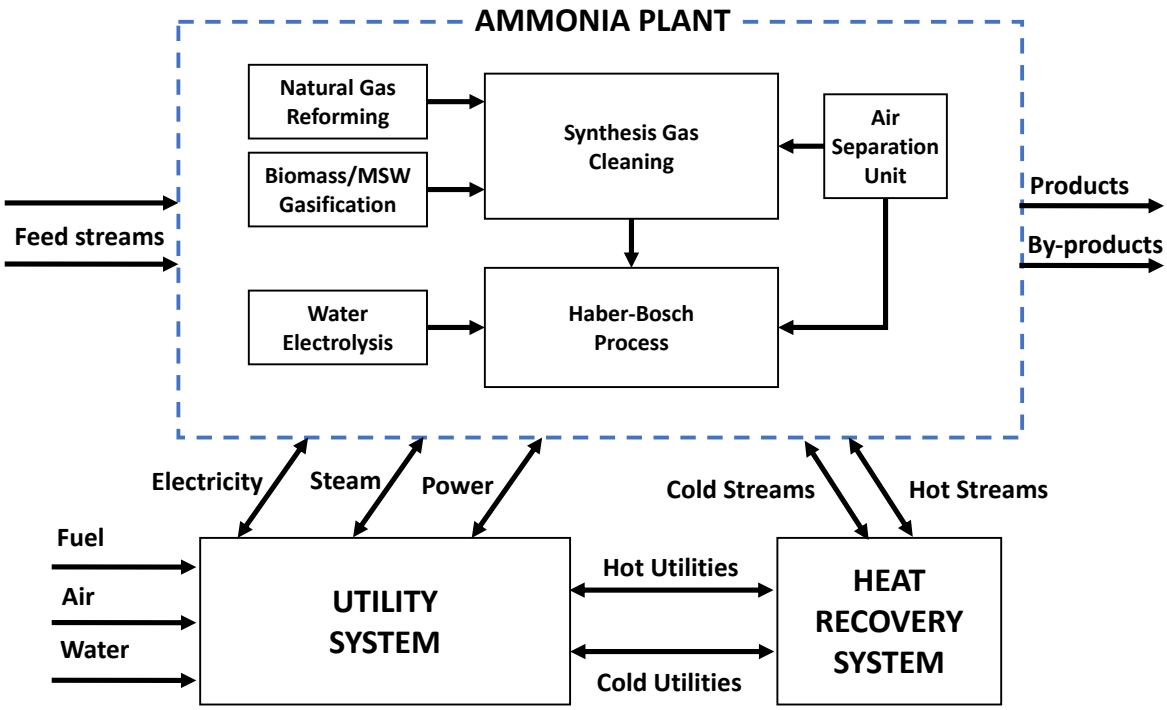


Figure 3.1: Conceptual design of the ammonia process consists of (a) the ammonia plant including sections (i)-(v), (b) the utility system that exchanges electricity, steam, power, with the plant, and (c) the heat recovery system that interacts with both (a) and (b) to provide heating and cooling duties to the plant.

superstructures for process sections (i), (ii), (iii), and (iv) are shown in the following subsections. Sections (v), (vi), and (vii) are described in the previous works of Floudas and coworkers in the publications of Elia at al. [131] and Baliban et al. [132, 133]. The complete mathematical model of the process synthesis superstructure is given in Appendix B. Mass and energy balance equations are solved around each processing unit. All physical properties and the thermodynamic relationships are calculated using Peng-Robinson equation of state with Boston-Mathias alpha function (PR-BM) method.

For sake of simplicity in illustration of the flowsheet, the heat exchangers, compressors, pumps, and expanders are omitted in the figure, however they are present where needed before and after each processing unit in the superstructure. Rectangular boxes represent units consisting of multiple

steps of processes that are modeled as input-output units (e.g. Rectisol unit, aMDEA unit, etc.). The input output relations of such units are found from company reports or studies by other groups. More information on model parameters of such units with the references can be found in Appendix B.

### 3.2.1 Synthesis Gas Generation

Figure 3.2 shows the superstructures of the synthesis gas generation and water electrolysis sections. Syngas generation section includes natural gas reforming-based and biomass gasification-based production trains. The following sections describe each train in detail. The objective of this step is to produce $H_2$ and $N_2$ in the desired ratio for ammonia synthesis.

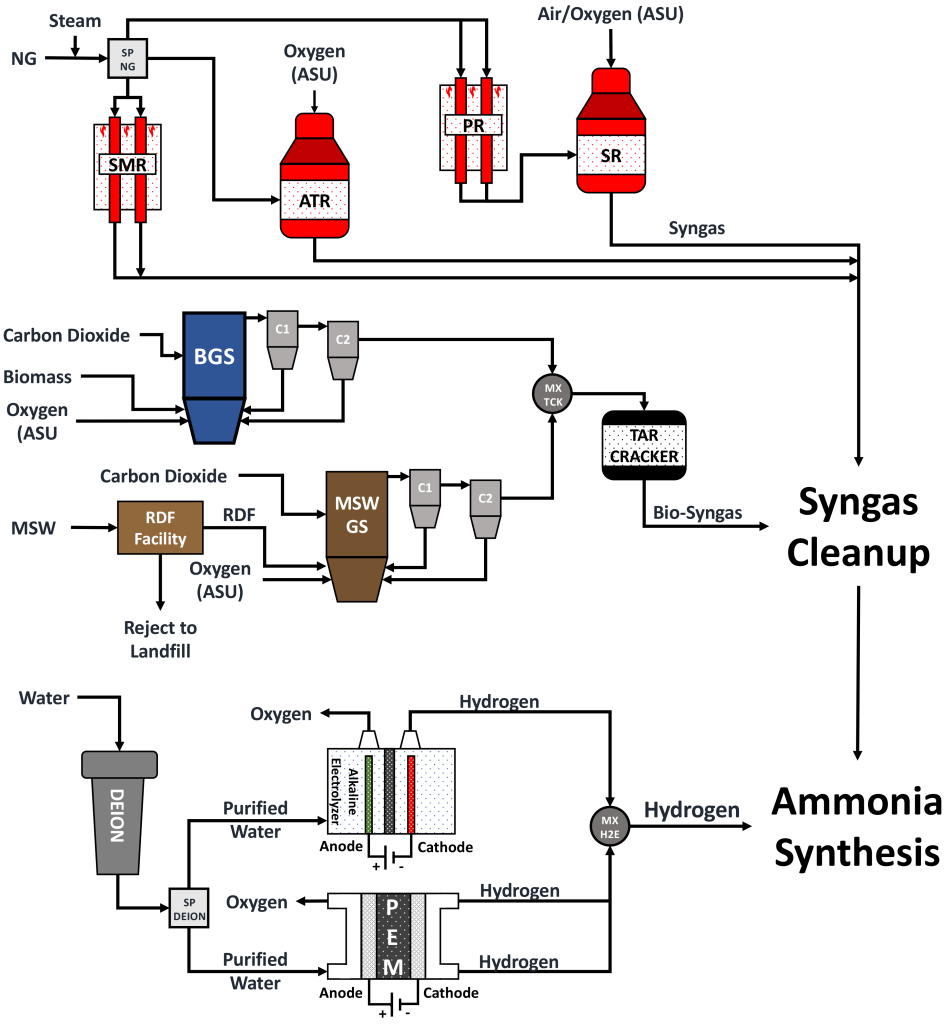


Figure 3.2: Hybrid feedstock synthesis gas generation and water electrolysis sections.

### *3.2.1.1 Natural Gas Conversion*

Natural gas from the pipeline, removed of sulfur species, is compressed to 31 bar and can be sent to three different reforming reactors, that are (1) steam reforming (SMR), (2) autothermal reforming (ATR), or (3) the choice of traditional ammonia production plants: primary reformer (PR) and secondary reformer (SR) in series, that are essentially an SMR followed up by an ATR. In option (1), SMR operates at 30 bar with a reaction temperature of either 800, 850, or 900 °C.

It partially converts $CH_4$ to synthesis gas over a nickel catalyst. SMR is modeled using steam reforming and water-gas shift equilibria (Eqs. 3.2 and 3.3, respectively), the effluent is sent to synthesis gas cleanup section. Option (2) uses an ATR that operates at 30 bar with a reaction temperature of 900 °C. It also uses a nickel catalyst. Autothermal reformer uses high purity oxygen coming from the air separation unit (ASU) to combust some of the $CH_4$ to supply heat to the endothermic steam reforming reaction. Steam reforming and water-gas shift reactions are accompanied by methane combustion (Eq. 3.4) in the reformer.

$$CH_4(g) + H_2O(g) \rightleftharpoons CO(g) + 3H_2(g), \quad \Delta H^\circ = 206.0\ kJ/mol \tag{3.2}$$

$$CO(g) + H_2O(g) \rightleftharpoons CO_2(g) + H_2(g), \quad \Delta H^\circ = -41.0\ kJ/mol \tag{3.3}$$

$$CH_4(g) + 2O_2(g) \rightleftharpoons CO_2(g) + 2H_2O(g), \quad \Delta H^\circ = -802.3\ kJ/mol \tag{3.4}$$

Option (3), is the approach used in traditional single-train ammonia production plants and it consists of two parts. In the first part, PR is modeled after the SMR and it operates at 800 °C and 31 bar. After partial conversion of $CH_4$, the reformer effluent is mixed with large amounts of air. In this configuration, $N_2$ can be added to the system at SR. The $O_2$ in the air is combusted in SR, that is modeled similar to ATR unit. SR operates at 1000 °C and 30 bar and methane combustion, water-gas shift, and steam reforming reactions (Eqs. 3.2-3.4) take place in it. In traditional ammonia plants PR and SR configuration does not necessitate an ASU unit for pure $N_2$ generation, however it requires a larger cleanup section due to early introduction of $N_2$ to the synthesis gas (syngas). The effluents from all the options are sent to synthesis gas cleanup section, to remove the carbon oxide species ($CO_x$) and inerts, before they are sent to the ammonia synthesis loop.

#### *3.2.1.2 Biomass Gasification*

As an alternative to natural gas, various type of biomass such as forest residue (hardwood), agricultural crops (corn stover), and municipal solid waste (MSW) can also be used as renewable sources of hydrogen. A gasification unit is used for thermochemical conversion of biomass into a

syngas mixture. The detailed models of the hardwood, corn stover, and MSW gasifiers used in this work can be found in papers of Baliban et al. [77] and Onel et al. [78], respectively. This section will briefly describe the processes involving biomass gasification.

The hardwood- or corn stover-type biomass is delivered to the refinery as pellets with a moisture content of 45 wt.%. Biomass is dried and lockhopped with compressed $CO_2$ at 31 bar. The mixture is fed to a circulating gasifier (BGS) operating at either 900, 1000, or 1100 °C and 30 bar. Pure oxygen, produced in ASU, and steam are sent to the gasifier to facilitate char gasification. The biomass gasifier is modeled stoichiometrically and simulates pyrolysis of biomass. The gasifier effluent is cooled down to 883 °C and sent to two cyclones (C1 and C2) in series to remove ash from the system, while unreacted char is recycled back to the gasifier. The vapor products are sent to a tar cracker operating at 925 °C to decompose some of the residual hydrocarbons. The effluent from the tar cracker is referred to as bio-syngas. The biomass gasification section is outlined in Figure 3.2.

While hardwood or corn stover can be processes using available pellets, MSW type of biomass requires a more intricate handling process. Since MSW contains undesired components such as glass, metals, etc., it needs to be processed to produce refuse derived fuel (RDF) [134, 135]. An RDF facility removes the non-combustible material from MSW and condenses RDF into pellets that are later sent to a drier to remove its high moisture content. Dried and lockhopped RDF is sent to an MSW gasifier (MSW-GS) that operate at either 800, 850, or 900 °C and 30 bar in the presence of calcium dolomite catalyst. The gasifier effluent is sent to two ash cyclones (C1 and C2) that are followed up by a tar cracker to decompose the remaining hydrocarbons. Syngas from biomass gasification require a cleanup section to remove any sulfur and carbon oxide species.

#### *3.2.1.3 Water Electrolysis*

Another hydrogen production method is water electrolysis. For water electrolysis, alkaline (AL-EYZ) and proton electrolyte membrane (PEM) type of electrolyzers (PEM-EYZ) are considered. Both technologies require water purification and a deionizer (DEION) unit to generate purified water. The output of the DEION can either be sent to AL-EYZ or PEM-EYZ. AL-EYZ

is modeled after NEL alkaline electrolyzers and it operates at 80 °C and 1 bar. With an electrochemical reaction $H_2$ and $O_2$ are produced from $H_2O$ in stoichiometric amounts as shown in Eq. 3.5. The $H_2$ output is compressed to 30 bar. PEM-EYZ is modeled after ProtonOnSite PEM electrolyzer and it is producing a pure $H_2$ stream available at 30 bar and 40 °C. The hydrogen streams from both electrolyzers are mixed and sent to the electrolyzer splitter. Since the product of water electrolysis is pure hydrogen and it does not require any cleaning. The electrolyzer splitter sends hydrogen at 30 bar and 25 °C directly to the ammonia synthesis loop.

$$2H_2O(l) \rightleftharpoons 2H_2(g) + O_2(g) \tag{3.5}$$

### 3.2.2 Synthesis Gas Cleanup

The purpose of the synthesis gas cleanup section is to reduce the amount of undesired species and adjust the ratio $H_2$ and $N_2$ in the ammonia synthesis gas. Synthesis gas from a hydrocarbon source includes poisonous species (e.g. CO, $CO_2$, NO, $N_2O$, COS, HCN) and inerts (e.g.Ar, $CH_4$) for the iron ammonia synthesis catalyst. The synthesis gas coming from reforming of natural gas (will be referred to as syngas from this point on) contains $H_2$, $H_2O$, $CO_2$, CO, $CH_4$, $N_2$, NO, $N_2O$, and Ar. The synthesis gas coming from the gasifier (will be referred to as bio-syngas) contains $NH_3$, HCN, COS, $H_2S$, $C_2H_2$, $C_2H_4$, and $C_2H_6$ in addition to all the species present in syngas. Therefore both of these streams need to be cleaned before being sent to the ammonia synthesis section. While the poisonous species need to be completely removed, the inerts can be sent to the Haber-Bosch reactor. If inerts are present in the ammonia synthesis loop, the equipment will be larger in size, and additional separation steps might be required to remove them, so that they are not accumulated in the recycle stream. Traditional single-train ammonia production methods do not shy away from having inerts in the ammonia synthesis loops, whereas more modern methods prefer having an inert-free ammonia synthesis gas [59].

The synthesis gas cleanup section can be viewed in three subsections: first part is characterized by increasing/adjusting the $H_2$ yield using water-gas shift reaction, the second part by bulk $CO_2$

removal, and the third part by final purification to completely remove all the poisonous and/or inert species. The superstructure of the entire cleanup section is shown in Figure 3.3.

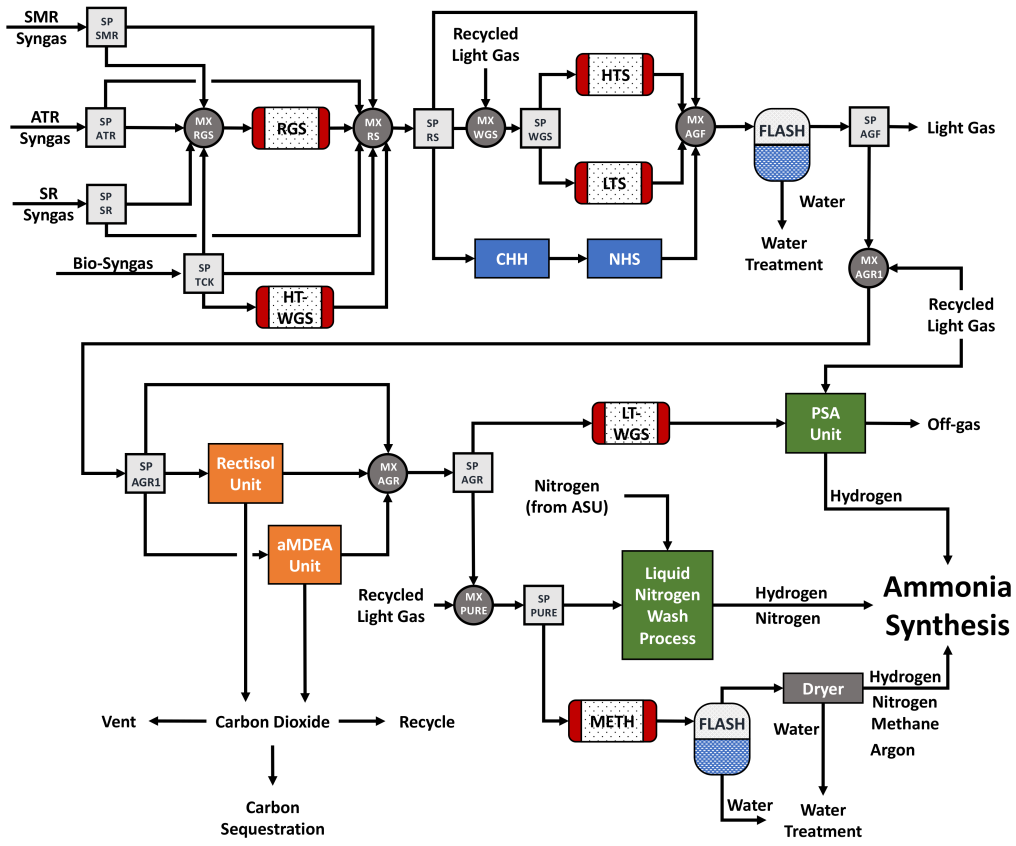


Figure 3.3: Hybrid feedstock synthesis gas cleanup section.

Syngas from steam reforming can be sent to a the mixer, MX-RGS, to be directed to a forward/reverse water-gas shift reactor (RGS) that operates at 29 bar and either 400, 500, or 600 °C. Alternatively syngas can bypass RGS and head straight for the raw syngas mixer MX-RS. Bio-syngas can be mixed with syngas at MX-RGS or sent to a forward water-gas shift reactor (HT-WGS). Syngas collected at MX-RS is called raw syngas. It is split at SP-RS and can be sent to a high- (HTS) or low-temperature water-gas shift (LTS) unit, where CO is shifted with $H_2O$

to $CO_2$. In this way, not only is CO converted to readily removable $CO_2$, but additional $H_2$ is also produced in the process. The high-temperature shift is carried out at 350 °C and 28.5 bar over an iron-chromium catalyst, while the low-temperature shift is operated at 250 °C and 28.5 bar over a copper-zinc catalyst. Both shift reactors are modeled using equilibrium model (Eq. 3.3). Alternatively, raw syngas can be sent through a COS-HCN hydrolyzer, that is followed up by a $NH_3$-HCl stripper, where the residual tar, particulates, and $NH_3$ in the stream are removed. In another alternative, raw syngas at SP-RS can bypass all these options and sent directly to the acid gas flash (AGF) unit. AGF is modeled using liquid-vapor phase equilibrium calculations. It operates at 24.5 bar and 35 °C, and flashes out about 95% of the water. The vapor effluent of AGF is sent to SP-AGF where it is directed to either downstream $CO_2$ removal units or to the light gas header. This mostly water-free syngas can either be sent to $CO_2$ process or bypass it. There are two process options for bulk $CO_2$ and possible sulfur removal, either a Linde Rectisol unit [136], or an BASF aMDEA (activated methyldiethanolamine) process [137]. Removed $CO_2$ can be recycled to be used elsewhere (e.g. in the gasifier), sent for sequestration, or vented. $CO_x$-lean syngas streams are mixed at MX-AGR and compressed to 34 bars before the final purification step.

There are three alternatives for the final purification before the ammonia synthesis loop. First option is sending the $CO_x$-lean syngas to a methanator (METH) where all the poisonous carbon oxide species are completely hydrogenated to inert $CH_4$ over a nickel catalyst (Eqs. 3.6 and 3.7). METH is modeled as a stoichiometric reactor and operates at 300 °C and 33 bar. The outlet stream is sent to another flash unit and through molecular sieve drying (Dryer) using Sylobeads to remove any remaining $H_2O$. The effluent of Dryer consists of $H_2$, $N_2$, $CH_4$, and Ar.

$$CO(g) + 3H_2(g) \rightleftharpoons CH_4(g) + H_2O(g), \quad \Delta H^\circ = -206.0\ kJ/mol \tag{3.6}$$

$$CO_2(g) + 3H_2(g) \rightleftharpoons CH_4(g) + 2H_2O(g), \quad \Delta H^\circ = -165.0\ kJ/mol \tag{3.7}$$

The second option is a liquid nitrogen wash unit, that is modeled after Air Liquide's process and operates at 30 °C and 31 bar. The unit washes the syngas stream with liquid nitrogen coming

from the ASU to remove hydrocarbons, carbon oxide species, and inert gases and produces a pure ammonia synthesis gas mixture of hydrogen and nitrogen. Liquid nitrogen wash unit utilizes 0.02 tons of liquid nitrogen per ton of syngas treated and it is able to recover 99.6% of the $H_2$ that is present in the synthesis gas stream and can adjust the required $H_2/N_2$ ratio.

The third option is using a pressure swing adsorption (PSA) unit that accepts hydrogen-rich streams and increases their the hydrogen concentration by selectively adsorbing impurities. Unit specifications are taken from UOP's Polybed PSA systems. PSA unit is capable of processing streams with hydrogen compositions as low as 80 %, and produces a 99.999 % pure hydrogen stream. The off-gases from PSA and other units are sent to light gas header, which can either be vented or sent to the fuel combustor. The optimization algorithm decides whether to recycle the gases back to process units to increase overall yield or send them to fuel combustor (FCM) to generate heat and/or power.

### 3.2.3 Ammonia Synthesis Loop

Due to low single-pass conversion at the Haber-Bosch reactor, unreacted ammonia synthesis gases need to be recycled back after removing the product and inerts. The process superstructure allows for various synthesis loop configurations and recycle options that are illustrated in Figure 3.4.

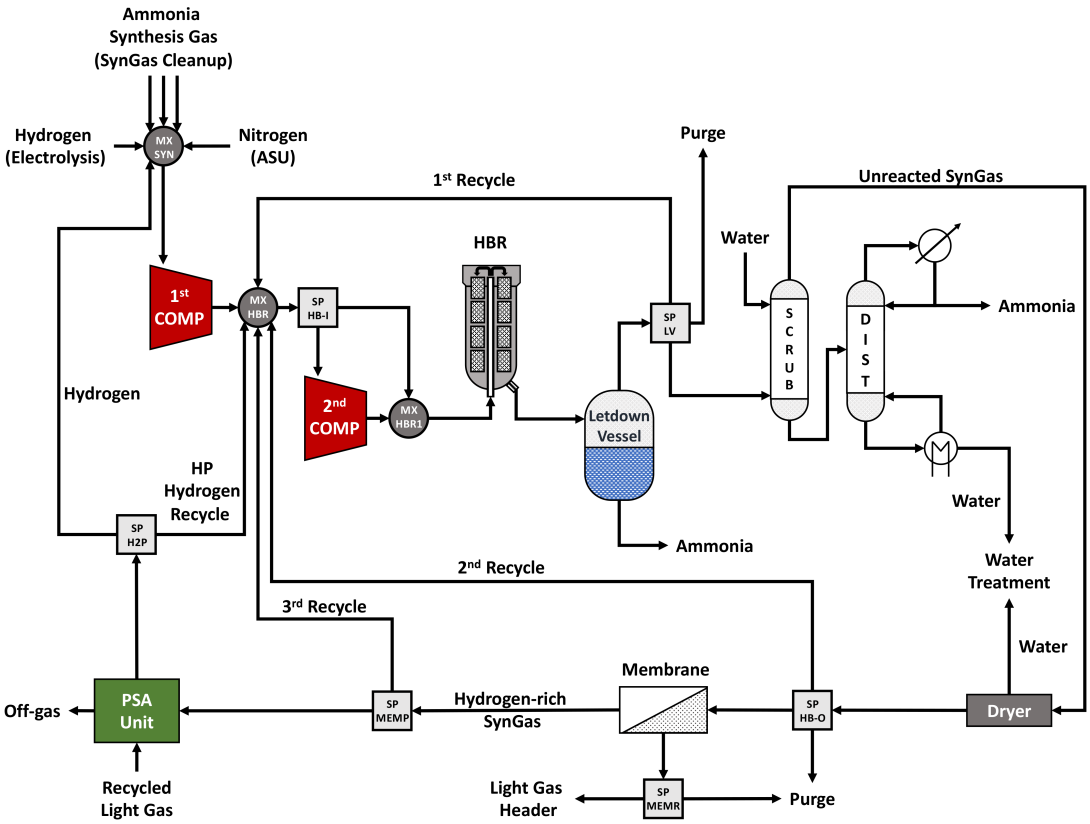


Figure 3.4: Ammonia synthesis loop section.

### *3.2.3.1 Haber-Bosch Reactor*

The ammonia synthesis gases coming from synthesis gas cleanup section, water electrolysis, ASU, and $H_2$ coming from PSA unit are mixed at MX-SYN at 30 °C and 31 bar and sent to the first compression step where the pressure of the stream is increased up to 85.5 bar. The fresh feed is mixed with four different recycle streams at MX-HBR. Ammonia synthesis gas stream can be split at SP-HB-I to five separate compression trains leading to five different Haber-Bosch reactors (HBR) operating at distinct pressures of 85.5, 130, 170, 210, or 250 bar. A second compression stage is required for all reactor options except the one operating at 85.5 bar. The streams are connected at five different mixers and sent to HBR. Pressure has a larger effect on the conversion (∼20-35%) than temperature does. Moreover, downstream product separation and transportation

options for ammonia are also highly dependent on pressure. Hence, the only variable here is the reactor pressure. Inlet and outlet temperatures of HBR are set at 400 °C and 440 °C, respectively. Ammonia synthesis reaction (Eq. 3.1) is the only reaction taking place at HBR.

Ammonia synthesis is an exothermic reaction. Industrial Haber-Bosch reactors are operated adiabatically and they consist of multiple reaction stages with interstage cooling to capture the heat of reaction. This heat is later used to preheat the reactor inlet stream. Due to trade-offs between thermodynamic and kinetic limitations, even when multiple stages are used, the Haber-Bosch reactors often do not reach equilibrium conversion. Hence, HBR is not modeled as an equilibrium reactor. Instead, a data-driven approach is used to model conversion of HBR by using a dataset of 25 industrial (Imperial Chemical Industries, Kellogg Brown & Root, Haldor Topsøe, Uhde GmbH, Casale) [138, 139, 140, 59, 141, 142, 143, 144, 145, 146, 147, 148, 149] and experimental practices [150, 151, 152, 153, 154]. Reactor pressure, outlet temperature, and inlet compositions are inputs to the model and predict the conversion of the limiting reactant (either $H_2$ or $N_2$, depending on the $H_2/N_2$ ratio). Models with linear, quadratic, and cubic terms of the input variables are compared using cross-validation method and as a result the fully linear model is selected. Conversion of HBR, $X_r$, is calculated using Eq. 3.8, where A-G are fitted parameters determined from the solution of the parameter estimation problem.

$$X_r(T, P, y_i) = A + B \cdot T + C \cdot P + D \cdot y_{H_2} + E \cdot y_{N_2} + F \cdot y_{NH_3} + G \cdot y_{Inert} \tag{3.8}$$

Details of the data-driven modeling approach are presented in Appendix B of the supplementary material. Interested readers can read works of Boukouvala et al. [155], Onel et al. [156], and Beykal et al. [156] to learn more about data-driven modeling techniques and their applications.

#### *3.2.3.2 Synthesis Loop Configurations for Product Separation*

HBR effluent contains product $NH_3$, unreacted $H_2$ and $N_2$, and possible inerts. Before being recycled back to the HBR, products and some inerts need to be removed from the recycle stream to prevent accumulation. The effluent is cooled to ambient conditions before being refrigerated

down to -20 °C to condense $NH_3$. Next, a letdown vessel flashes out the liquid $NH_3$ product at 25 bar. The letdown vessel is modeled using liquid-vapor phase equilibrium. The vapor from the vessel is splitted at SP-LV to either be purged, or compressed to 85.5 bar to be recycled back to MX-HBR (1st Recycle), or sent to scrubber-distillation system (SCRUB-DIST) for further ammonia recovery. SCRUB unit removes ammonia from the recycle stream by scrubbing the vapors with $H_2O$. The water scrubber is modeled after an example from an industrial patent [157]. The resulting $NH_3/H_2O$ mixture is sent to DIST unit, that is a distillation column modeled using data from a RadFrac model built in Aspen Plus with thermodynamic calculations based on PR-BM method. Distillation product purities are found to be in good agreement with the values reported in literature [59]. $NH_3$ product is either stored at pressurized conditions (20 °C and 25 bar) or cooled further and stored at ambient pressure (-33.33 °C and 1.01 bar). The vapor leaving from the top of SCRUB contains unreacted ammonia synthesis gas with some $H_2O$, that is removed in a molecular sieve Dryer unit. The Dryer effluent still contains some of the product $NH_3$, it can either be pressurized and recycled back to MX-HBR (2nd Recycle) or to a membrane separation unit for further purification. The membrane is modeled after an Air Products design and operates at 60 °C and 25 bar. The permeate of the membrane is a $H_2$-rich gas that can either be pressurized and recycled back to MX-HBR (3rd Recycle) or sent to PSA unit. PSA unit takes all the $H_2$-rich streams and produces a 99.999% pure $H_2$ stream. That can either be sent to low pressure mixer MX-SYN at 31 bar or to high pressure mixer MX-HBR at 85.5 bar after being compressed in a separate compressor (HP Hydrogen Recycle). While each recycle stream comes with the requirement of additional separation units, $NH_3$ content of the streams decrease at each successive recycle option.

Light gases from the ammonia synthesis loop are sent to the light gas header and from there they can either be recycled directly to various mixing point in the process, sent to PSA for $H_2$ recovery, or sent to FCM for heat and power generation.

### 3.2.4 Investment Costs

Cost estimations for the process units are collected from several literature sources. Total overnight costs ($TOC_u$) are calculated by sum of direct and indirect costs, using Eq. 3.9.

$$TOC_u = (1 + IC)(1 + BOP)C_o\left(\frac{S}{S_o}\right)^{sf} \tag{3.9}$$

BOP is the balance of plant (assumed to be 0.20 and includes site preparation, civil works, etc.), IC is the indirect costs (assumed to be 0.32 and include engineering, startup, spare parts, royalties, fees, and contingencies), $C_o$ is the base cost in MM$, S is the cost flow, $S_o$ is the base case flow, and sf is the scaling factor. $S_{max}$ is the maximum flow for a process unit, when it is reacted multiple trains are used and the cost for each train is scaled with a factor of 0.9. The list of cost parameters are given in Table 3.1 with the references. All costs are converted to 2016 prices using the Chemical Engineering Plant Cost Index (CEPCI).

$TOC_u$ needs to be annualized in order for us to compare it with the annual feedstock, utility, and operations & maintenance (OM) costs. $TOC_u$ is annualized following the approach used by Kreutz et al. [136], where investments costs are multiplied by levelized capital charge cost (LCCR) and interest during costruction factor (IDCF) as shown in Eq. 3.10. The values for LCCR and IDCF are taken as 14.38%/year and 1.0716, respectively.

$$CC_u = LCCR \cdot IDCF \cdot TOC_u \tag{3.10}$$

Annual operating and maintenance costs (OM) are assumed to be 4.5% of the total overnight costs and the plant is assumed to operate for 330 day/year (CAP) similar to industrial ammonia production plants. PROD is the production capacity of the plant (e.g. 1,000 tons/day of $NH_3$). Using these values, investment and OM are levelized as shown in Eqs. 3.11 and 3.12, respectively.

$$Cost_u^{Inv} = \left(\frac{CC_u}{CAP \cdot PROD}\right) \tag{3.11}$$

Table 3.1: Investment Cost Parameters and Scaling Factors (Given in 2016 $).

| Unit Name | $C_o$ (MM$) | $sf$ | $S_o$ | $S_{max}$ | Cost Flow Basis | Ref. |
|---|---|---|---|---|---|---|
| Biomass Handling (forest) | 4.31 | 0.77 | 17.94 | 33.33 | kg/s of as received biomass | [136] |
| Biomass Handling (nonforest) | 13.76 | 0.77 | 17.94 | 33.33 | kg/s of as received biomass | [136] |
| Biomass Gasifier | 51.2 | 0.7 | 17.94 | 33.33 | kg/s of dry biomass | [158] |
| MSW Handling and RDF Facility | 135.98 | 0.77 | 45.2 | 33.33 | kg/s of RDF | [134] |
| MSW Gasifier | 51.2 | 0.7 | 17.94 | 33.33 | kg/s of dry biomass | [158] |
| SMR/Primary Reformer | 28.49 | 0.67 | 12.2 | 35 | kg/s of feed | [159] |
| ATR/Secondary Reformer | 20.37 | 0.67 | 12.2 | 24 | kg/s of feed | [159] |
| PEM Electrolyzer | 50.05 | 0.85 | 50 | 1000 | MW of electricity | [159] |
| Alkaline Electrolyzer | 5.92 | 0.95 | 10 | 1000 | MW of electricity | [160] |
| Air Compressor | 5.59 | 0.67 | 10 | 30 | MW of electricity | [158] |
| Air Separation Unit (ASU) | 230.77 | 0.5 | 145 | 41.67 | kg/s of $O_2$ feed | [159] |
| Forward Shift Reactor (WGS, HTS, LTS) | 3.47 | 0.67 | 150 | 250 | kg/s of feed | [161] |
| Reverse Shift Reactor (RGS) | 3.47 | 0.67 | 107.9 | 250 | kg/s of feed | [161] |
| COS-HCN Hydrolyzer | 4.82 | 0.88 | 56.98 | 250 | kg/s of feed | [136] |
| Rectisol $CO_2$ Removal Unit | 29.77 | 0.63 | 2.51 | 8.78 | kmol/s of feed | [136] |
| aMDEA $CO_2$ Removal Unit | 10.11 | 0.63 | 41.9 | 500 | kg/s of feed | [137] |
| Methanator | 35.01 | 0.72 | 10 | 50 | kg/s of feed | [162] |
| Liquid Nitrogen Wash | 29.77 | 0.63 | 2.51 | 8.78 | kmol/s of feed | [136] |
| Pressure Swing Adsorption (PSA) | 7.38 | 0.65 | 0.29 | 1.78 | kmol/s of purge gas | [158] |
| Sylobead Dryer | 4.76 | 0.6 | 6.3 | 67.2 | kg/s of feed | [163] |
| Flash Separator | 0.16 | 0.59 | 10 | 220 | m3/s of feed | [164] |
| Ammonia Converter (85.5 bar) | 18.32 | 0.67 | 3.56 | 7.13 | kmol/s of feed | [162] |
| Ammonia Converter (130 bar) | 19.92 | 0.67 | 3.56 | 7.13 | kmol/s of feed | [162] |
| Ammonia Converter (170 bar) | 22.3 | 0.67 | 3.56 | 7.13 | kmol/s of feed | [162] |
| Ammonia Converter (210 bar) | 25.49 | 0.67 | 3.56 | 7.13 | kmol/s of feed | [162] |
| Ammonia Converter (250 bar) | 30.27 | 0.67 | 3.56 | 7.13 | kmol/s of feed | [162] |
| Refrigerator | 1.19 | 0.7 | 0.7 | 10.55 | MW of heat removed | [164] |
| Letdown Tank | 0.28 | 0.56 | 10 | 220 | m3/s of feed | [164] |
| Ammonia-Water Scrubber | 0.16 | 0.67 | 1 | 125 | m3/s of feed | [157] |
| Ammonia-Water Distillation | 1.88 | 0.68 | 1 | 150 | kg/s of feed | [165] |
| Hydrogen Separation Membrane | 4.61 | 0.67 | 1 | 3.6 | kg/s of hydrogen removed | [166] |
| Compressors | 6.93 | 0.67 | 10 | 20 | MW of electricity | [165] |
| $CO_2$ Sequestration | 22.42 | 0.6 | 24.4 | 30 | MW of electricity | [165] |
| Gas Turbine | 75.66 | 0.75 | 226 | 334 | MW of electricity | [158] |
| Steam Turbine | 61.47 | 0.67 | 136 | 500 | MW of electricity | [158] |
| Sour Stripper | 3.93 | 0.53 | 11.52 | - | kg/s of feed | [167] |
| Biological Digestor | 4.68 | 0.71 | 115.74 | - | kg/s of feed | [168] |
| Reverse Osmosis | 0.32 | 0.85 | 4.63 | - | kg/s of feed | [168] |
| Cooling Tower | 57.85 | 0.65 | 1.75 | - | GW of heating deficit | [167] |

$$Cost_u^{OM} = \left( \frac{TOC_u \cdot OM}{365\ days/year \cdot PROD} \right) \tag{3.12}$$

Levelized unit cost $Cost^U_u$ is the sum of levelized investment and OM costs and it is calculated by

Eq. 3.13.

$$Cost_u^U = Cost_u^{Inv} + Cost_u^{OM} \tag{3.13}$$

### 3.2.5 Utility Requirements

Simultaneous heat, power, and water integration framework determines the total minimum utility cost for the process. The utility requirements of several units such as Rectisol, aMDEA, or electrolyzers are known they are shown in Appendix B. Remaining units such as heat exchangers, compressors, etc. are calculated using energy conservation and total heat balance equations that are presented in Appendix B.

### 3.2.6 Greenhouse Gas Emissions

Improving the sustainability of ammonia production requires reducing greenhouse gas emissions. $CO_2$ is considered as the only greenhouse gas (GHG) in this work and ammonia production from natural gas has a significant carbon footprint. Total GHG (TGHG) emissions (in $CO_2$ equivalent/s) include (a) feedstock acquisition and transportation ($GHG_{feedstock}$), (b) process emissions ($GHG_{process}$), and (c) product end use and $CO_2$ transportation for sequestration ($GHG_{product}$). These values are calculated from the Argonne GREET Model for well-to-wheel emissions [169] and assuming transportation distances for feedstocks (50 miles), products (100 miles), and $CO_2$ (50 miles). Table 3.2 shows the GHG emissions from the feedstocks used in this work [79]. The TGHG emissions from the process are compared with the avoided GHG emissions

Table 3.2: GHG emissions of feedstocks in g/kg flow.

| Feedstock | GHG Emission |
|---|---|
| Natural gas | 391.38 |
| Corn stover | -1472.76 |
| Hardwood | -896.87 |
| MSW | -1252.66 |

from a typical natural gas-based ammonia production plant. GHG emission index (GHGI) is calculated to compare the sustainability of the plant to the reference plant as shown in Eq. 3.14.

$$GHGI = \left( \frac{GHG_{feedstock} + GHG_{process} + GHG_{product}}{GHGAE + GHGAN} \right) \tag{3.14}$$

Carbon footprint of the ammonia plant (GHGAN) is assumed to be 1.694 ton $CO_2$/ton $NH_3$ produced [121]. There are larger numbers reported in the literature. In this work a smaller process emission number is selected to restrict the emissions more strictly. An additional source of GHG emissions is heat and power generation. The plant can buy electricity from the grid to supply the utility need of the processes. Buying electricity from the grid contributes to the GHG emissions. The GHG emissions avoided by electricity (GHGAE) is calculated by using a typical natural gas-based emissions value of 101.3 kg $CO_2$ eq/GJ. GHGAE takes a negative value if electricity is bought from the grid; as a result, this puts a restriction on the process emissions ($GHG_{process}$) according Eq 3.14. The process superstructure includes simultaneous heat and power integration, therefore the plant can produce its own electricity and heating utilities by combusting fuel or recycled light gases in the fuel combustor unit and using a steam turbine. The plant can also sell the electricity to the grid to improve process economics. By doing that plant produces more process emissions, however, the emissions from grid electricity generation are avoided; hence, GHGAE takes positive value. GHGAE can have an effect on the BEP and it is affected by GHG emission restrictions, as well as natural gas and electricity prices.

The parameter $GHG_{red}$ is used to dictate how much GHG reduction is to be imposed on the plant as shown in Eq. 3.15. For this work, at least 75% reduction of GHG emissions are enforced to increase the sustainability of ammonia production, thus $GHG_{red}$ is set equal to 0.25.

$$GHGI \leq GHG_{red} \tag{3.15}$$

### 3.2.7 Objective Function

The objective function of the sustainable ammonia production is to minimize the levelized annual cost of ammonia production. Eq. 3.16 shows all the contributions to the objective function.

$$min \sum_{f \in Feed} Cost^{f} + Cost^{El} + Cost^{Seq} + \sum_{u \in U_{Inv}} Cost_{u}^{U} \tag{3.16}$$

Feedstock cost ($Cost^{f}$) contributors are natural gas, biomass, water, etc. Electricity costs ($Cost^{El}$) can be negative if the plant outputs electricity as a byproduct, otherwise it is positive. $CO_2$ sequestration costs ($Cost^{Seq}$) can be paid to meet GHG emission constraints by sequestering $CO_2$ instead of venting it. There are no byproducts of ammonia production in this process.

## 3.3 Deterministic Global Optimization

The process synthesis superstructure described in the preceding sections and presented in Appendix B form a large-scale nonconvex, mixed-integer, nonlinear optimization (MINLP) problem. The optimization model consists of 18,573 continuous, 38 binary variables, and 18,924 constraints. Nonlinearity and nonconvexity come from the bilinear, trilinear, and quadrilinear terms that are used in modeling the splitters, equilibrium reactors/separators, data-driven models, as well as concave power functions that describe the unit investment costs. The optimization model is formulated in GAMS environment.

In order to solve this model to global optimality, a tailored branch-and-bound algorithm is implemeted. The MINLP model is decomposed into lower and upper bound problems. The lower bound problem is a mixed-integer linear optimization (MILP) model that is obtained by replacing the nonlinear terms with linearized ones. Trilinear and quadrilinear terms are recursively formulated into bilinear expressions and then together with the concave cost functions relaxed with piecewise linear underestimators using logarithmic partitioning scheme where every piece is represented with a binary variable. While piecewise linear underestimators increase the number of binary variables in the MILP problem they provide much tighter relaxations compared to

McCormick type convex envelopes [170]. When the MILP is solved using GAMS/CPLEX [171] the obtained solution is a valid lower bound on the original MINLP problem. By generating a solution pool, several starting points are generated. When the binary variables in the original MINLP are fixed at these starting points, multiple nonlinear optimization (NLP) problems are created as the upper bound problems. The NLPs are solved using GAMS/CONOPT [172], and the best solution is an upper bound on the original MINLP problem. The branch-and-bound algorithm is used to close the gap between lower and upper bound problems and converge toward the global optimum.

At every node of the branch-and-bound tree, before the MILP relaxation, an optimality-based bounds tightening (OBBT) routine is performed to tighthen the bounds on the total molar flow rates and investment costs. Also, at the root node, a feasibility-based bounds tightening (FBBT) routine is performed to tighten the bounds on molar species flow rates. When a node in the tree is branched, two children nodes are formed. Branching is done on the continuous variables, that participate in a nonlinear expression, that has the largest relaxation error. The upper bound is updated if the NLP objective function at a given node is lower than the current upper bound value. Nodes with a lower bound objective function that is greater than the current upper bound are fathomed. Since this is a large-scale problem, the branch-and-bound algorithm is run until 100 CPU hours have passed or all the nodes in the tree have been explored. The optimal solution to the MINLP problem is the best reported NLP solution. For a more detailed discussion about global optimization theory and algorithms, interested readers are directed to textbooks by Floudas [173, 174].

### 3.4 Computational Studies

Using the described methodology, the benefits of using different renewable feedstocks in ammonia production are compared. These results are compared with natural gas-based production with reduced GHG emissions via using $CO_2$ sequestration technology.

Ammonia break-even prices are calculated for three different states: (a) Texas, (b) California, and (c) Iowa. These states are selected because they are both producers of ammonia in the United States [175, 176] and they are particularly rich in renewable resources that are considered in this

work, namely biomass (hardwood, corn stover, MSW), wind, and solar. Each state considered in this study has a different portfolio of resources. Texas is rich with pretty much all renewable resources such as biomass (hardwood, MSW), wind, and solar energy. Texas is the leader in the United States in terms of energy production from wind. Also the prices of natural gas and grid electricity are relatively cheaper. California has good biomass (hardwood, MSW) and wind resources, and it is the leading state in solar energy. Natural gas and grid electricity prices are more expensive in California compared to those in Texas. Iowa has biomass (corn stover, MSW) and a strong wind energy potential, however it does not have a significant solar potential, hence it is not considered for solar powered ammonia production in this study. Availability of the renewables have been investigated from online databases or publications of NREL [20, 177], DOE [178, 179], and Niziolek et al. [80] to make sure that suggested production rates are feasible with the existing resources. In addition to various renewable feedstock options, different plant scales are tested to observe the effects economies of scale on the process performance.

Modeling and costing of wind turbines and solar PV modules are not done explicitly in this work. The levelized cost of electricity (LCOE) coming from wind and solar energy are used that are based on the Reports by DOE [179] and NREL [177], respectively. By using LCOE, the installed cost and performance of the corresponding technology are captured as a part of electricity costs. However, it is important to out point out that both wind- and solar-based electricity prices used in this study are assumed to obey power purchase agreements (PPA), where the energy producers are incentivized to compete with grid electricity. That is the reason why renewable LCOE are lower than the grid electricity prices. Since these contract prices are set arbitrarily and intentionally low via taxpayer subsidies, they might not reflect the true cost of production of electricity using that resource. It should be mentioned that electricity coming from wind or solar is assumed not to have a carbon footprint as opposed to the fossil fueled grid electricity. This work also assumes continuous production and uninterrupted availability of wind and solar electricity, which is not a reality as of today. Obtaining uninterrupted renewable power is still a topic of ongoing academic and industrial research. This intermittency problem of the wind and solar resources is a very

important challenge that is addressed in Sections 4 and 5 of this thesis. In this section, the focus is instead on a comparison of price competitiveness of various renewable technologies in the same process superstructure and global optimization framework. However, in order to observe the effect of addition of energy storage technology to make uninterrupted renewable power supply possible, a sensitivity analysis on renewable LCOE in included in the upcoming subsections. The nominal cost parameters for biomass (i.e. corn stover, hardwood, MSW), RDF operation, grid electricity, wind/solar LCOE, natural gas, water, and $CO_2$ transportation, storage, and monitoring ($CO_2$ TS&M) are presented in Table 3.3.

Table 3.3: Nominal cost parameters for the ammonia production for each state.

| Commodity | Texas | California | Iowa |
|---|---|---|---|
| Corn stover [180] | - | - | \$120/dry metric ton |
| Hardwood [180] | \$70/dry metric ton | \$70/dry metric ton | - |
| MSW [79] | \$0/dry metric ton | \$0/dry metric ton | \$0/dry metric ton |
| RDF operation [79] | \$66.67/dry metric ton | \$66.67/dry metric ton | \$66.67/dry metric ton |
| Grid electricity [181] | \$0.0533/kWh | \$0.1192/kWh | \$0.0605/kWh |
| Wind LCOE [179] | \$0.044/kWh | \$0.060/kWh | \$0.044/kWh |
| Solar PV LCOE [177] | \$0.0512/kWh | \$0.0450/kWh | - |
| Natural gas [182] | \$3.28/TSCF | \$7.00/TSCF | \$5.24/TSCF |
| Water [180] | \$0.5/metric ton | \$0.5/metric ton | \$0.5/metric ton |
| $CO_2$ TS&M [180] | \$5/metric ton | \$5/metric ton | \$5/metric ton |

Five case studies are performed for each state at each of the reported scales. GHG emissions from renewable-based plants are restricted to be less than 25% of that of a typical ammonia plant (i.e. 75% reduction of GHG emissions) as described in the previous sections. Case studies will be denoted as S-F-C, where S represents the state, F represents the feedstock type and C denotes the plant capacity in metric tons per day. Feedstock type are (i) natural gas (N), (ii) hardwood (H) (iii) corn stover (C), (iv) MSW (M), (v) onshore wind energy (W), and (vi) solar PV (S). 3 plant capacities are tested: 250, 500, and 1,000 metric tons of ammonia/day. To give an example, TX-H-500 denotes a plant built in Texas using hardwood as feedstock and producing 500 metric tons of ammonia/day. While industrial ammonia plant capacities can reach up to 2,400 tons/day,

the largest plants are limited with 1,000 metric tons/day of production, in order not to put a big strain on availability of renewable resources. N cases only use natural gas and grid electricity, H/C/M cases only use biomass and grid electricity, whereas W and S cases only use renewable wind and solar electricity, respectively.

All case studies are solved on a High-Performance Computing (HPC) machine at Texas A&M High-Performance Research Computing facility using Ada IBM/Lenovo x86 HPC Cluster operated with Linux (CentOS 6) using 1 node (20 cores per node with 64 GB RAM). CPLEX 12 and CONOPT 3.16 solvers are used with GAMS 24.4.5.

Following sections will show the optimal process topologies, investment and overall cost breakdown, and GHG emissions analysis results. Overall mass, energy, and carbon balances for all the case studies plus the detailed flowsheet of a sample case study that includes the stream temperature, pressure, phase, and component flow rates are included in Appendix B.

### 3.4.1 Optimal Process Topologies

Key topological decisions include: (i) natural gas conversion method and operating conditions, (ii) biomass gasifier temperature, (iii) electrolyzer type selection, (iv) configuration of the forward/reverse-water gas shift reactors, (v) bulk $CO_2$ removal technology, (vi) ammonia synthesis gas purification technology, (vii) ammonia synthesis reactor operating pressure, (viii) ammonia synthesis loop configurations, (ix) natural gas utilization for process heat and electricity, (x) light gas and/or fuel gas combustion, (xi) $CO_2$ sequestration. Optimal process topologies are shown in three parts in Tables 3.4, 3.5, and 3.6.

The syngas generation sections are different depending on the type of feedstock used and the state the plant is located in. Most natural gas-based cases rely on ATR technology. For Texas, a parallel (but smaller in capacity) train of PR and SR trains are selected next to ATR technology. Selection of ATR and SR technologies use high purity oxygen coming from ASU to reduce energy requirements of the steam reforming process. For Texas case studies, two stages of water-gas shift reactors are used, whereas California and Iowa cases mostly prefer single stage water-gas shift reactors. Texas and Iowa cases also use small alkaline electrolyzers to generate some of

their hydrogen. This is likely to be a result of the tight 75% GHG emission reduction constraint that are imposed. Although electrolyzers consume lots of electricity, they produce less emissions compared to steam reforming. The reason for selecting electrolyzers can be attributed to the lower grid electricity to natural gas price ratio. In California, a higher grid electricity to natural gas price ratio causes electrolyzers not to be selected.

For all hardwood and corn stover-type of biomass gasification cases, the lowest gasifier operating temperature option of 900 °C is selected. Texas and Iowa cases use single water-gas shift reactors; however California case does not utilize a water-gas shift reactor. MSW gasification uses a different gasifier and its operating temperature is selected as 800 °C for small-scale production for all states. As the plant scale gets larger, 850 °C becomes the preferred operating temperature for all case studies.

Rectisol unit is preferred for bulk $CO_2$ removal in natural gas-based production, whereas aMDEA unit is selected for all biomass-based processes. PSA unit is preferred over methanation or liquid nitrogen wash processes options due to its more efficient performance for final ammonia synthesis purification. $CO_2$ sequestration is used in all natural gas and hardwood cases to reduce the GHG emissions. It is not selected when corn stover or MSW is chosen as the feedstock. Since wind and solar powered ammonia production do no use any hydrocarbon feedstock, syngas generation/cleanup sections are not used in their case studies. Alkaline electrolyzers are selected over PEM for all cases, due to their lower capital costs. Larger scale processes often use a combustion unit to generate additional heat by utilizing some of the produced hydrogen.

In all the case studies, lowest pressure (85.5 bar) Haber-Bosch reactors are selected. As a result, the single-pass conversion is low ($\sim$ 20%), but there is only one compression step. Therefore, the power requirements of the ammonia synthesis loop are minimized. Loop configurations are very similar for almost all case studies. The 1$^{st}$ and 2$^{nd}$ recycle options are selected for all feedstock types and capacities. Therefore, the scrubbers-distillation system and dryer units are all used. A 3$^{rd}$ recycle option consisting of a membrane separator is only selected in larger scale natural gas based production to further increase production. With each successive recycle option, more ammonia

product or hydrogen is separated out. Hence, a recycle stream of reactants with higher purity is fed to the reactor at the expense of increasing investment and OM costs. In most cases, two recycle streams are enough to economically achieve a high overall ammonia yield.

Table 3.4: Optimal topologies of the ammonia plants for each case study - Part I.

| | **Texas** | | | **California** | | | **Iowa** | | |
|---|---|---|---|---|---|---|---|---|---|
| Technology | TX-N-250 | TX-N-500 | TX-N-1000 | CA-N-250 | CA-N-500 | CA-N-1000 | IA-N-250 | IA-N-500 | IA-N-1000 |
| SMR Temp. | - | - | - | - | - | - | - | - | - |
| ATR | Y | Y | Y | Y | Y | Y | Y | Y | Y |
| PR and SR | Y | Y | Y | - | - | - | - | - | - |
| Gasifier Temp. | - | - | - | - | - | - | - | - | - |
| Alkaline EYZ | Y | - | - | - | - | - | Y | Y | Y |
| PEM EYZ | - | - | - | - | - | - | - | - | - |
| ASU | Y | Y | Y | Y | Y | Y | Y | Y | Y |
| HT-WGS | - | - | - | - | - | - | - | - | - |
| RGS Temp. | 400 °C | 400 °C | 400 °C | - | - | - | - | - | - |
| HTS | - | Y | - | - | - | - | - | - | - |
| LTS | Y | - | Y | Y | Y | Y | Y | Y | Y |
| CHH-NHS | - | - | - | - | - | - | - | - | - |
| Rectisol | Y | Y | Y | Y | Y | Y | Y | Y | Y |
| aMDEA | - | - | - | - | - | - | - | - | - |
| Liquid $N_2$ Wash | - | - | - | - | - | - | - | - | - |
| METH | - | - | - | - | - | - | - | - | - |
| LT-WGS | Y | Y | Y | Y | Y | Y | Y | Y | Y |
| PSA | Y | Y | Y | Y | Y | Y | Y | Y | Y |
| HBR Pres. | 85.5 bar | 85.5 bar | 85.5 bar | 85.5 bar | 85.5 bar | 85.5 bar | 85.5 bar | 85.5 bar | 85.5 bar |
| 1st Recycle | Y | Y | Y | Y | Y | Y | Y | Y | Y |
| 2nd Recycle | Y | Y | Y | Y | Y | Y | Y | Y | Y |
| 3rd Recycle | - | Y | Y | - | Y | - | - | Y | Y |
| HP $H_2$ Recycle | - | - | - | - | - | - | - | - | - |
| FCM | Y | Y | Y | Y | Y | Y | Y | Y | Y |
| $CO_2$ Seq. | Y | Y | Y | Y | Y | Y | Y | Y | Y |
| Technology | TX-H-250 | TX-H-500 | TX-H-1000 | CA-H-250 | CA-H-500 | CA-H-1000 | IA-C-250 | IA-C-500 | IA-C-1000 |
| SMR Temp. | - | - | - | - | - | - | - | - | - |
| ATR | - | - | - | - | - | - | - | - | - |
| PR and SR | - | - | - | - | - | - | - | - | - |
| Gasifier Temp. | 900 °C | 900 °C | 900 °C | 900 °C | 900 °C | 900 °C | 900 °C | 900 °C | 900 °C |
| Alkaline EYZ | - | - | - | - | - | - | - | - | - |
| PEM EYZ | - | - | - | - | - | - | - | - | - |
| ASU | Y | Y | Y | Y | Y | Y | Y | Y | Y |
| HT-WGS | - | - | - | - | - | - | Y | Y | Y |
| RGS Temp. | - | - | - | - | - | - | - | - | - |
| HTS | Y | Y | Y | - | - | - | - | - | - |
| LTS | - | - | - | - | - | - | - | - | - |
| CHH-NHS | - | - | - | - | - | - | Y | Y | Y |
| Rectisol | - | - | - | - | - | - | - | - | - |
| aMDEA | Y | Y | Y | Y | Y | Y | Y | Y | Y |
| Liquid $N_2$ Wash | - | - | - | - | - | - | - | - | - |
| METH | - | - | - | - | - | - | - | - | - |
| LT-WGS | Y | Y | Y | Y | Y | Y | Y | Y | Y |
| PSA | Y | Y | Y | Y | Y | Y | Y | Y | Y |
| HBR Pres. | 85.5 bar | 85.5 bar | 85.5 bar | 85.5 bar | 85.5 bar | 85.5 bar | 85.5 bar | 85.5 bar | 85.5 bar |
| 1st Recycle | Y | Y | Y | Y | Y | Y | Y | Y | Y |
| 2nd Recycle | Y | Y | Y | Y | Y | Y | Y | Y | Y |
| 3rd Recycle | - | - | - | - | - | - | - | - | - |
| HP $H_2$ Recycle | - | - | - | - | - | - | - | - | - |
| FCM | Y | Y | Y | Y | Y | Y | Y | Y | Y |
| $CO_2$ Seq. | Y | Y | Y | Y | Y | Y | - | - | - |

Table 3.5: Optimal topologies of the ammonia plants for each case study - Part II.

| | **Texas** | | | **California** | | | **Iowa** | | |
|---|---|---|---|---|---|---|---|---|---|
| Technology | TX-M-250 | TX-M-500 | TX-M-1000 | CA-M-250 | CA-M-500 | CA-M-1000 | IA-M-250 | IA-M-500 | IA-M-1000 |
| SMR Temp. | - | - | - | - | - | - | - | - | - |
| ATR | - | - | - | - | - | - | - | - | - |
| PR and SR | - | - | - | - | - | - | - | - | - |
| Gasifier Temp. | 800 °C | 850 °C | 850 °C | 800 °C | 800 C ° | 850 C ° | 800 °C | 800 °C | 850 °C |
| Alkaline EYZ | - | - | - | - | - | - | - | - | - |
| PEM EYZ | - | - | - | - | - | - | - | - | - |
| ASU | Y | Y | Y | Y | Y | Y | Y | Y | Y |
| HT-WGS | - | Y | - | - | - | - | - | - | Y |
| RGS Temp. | - | - | - | - | - | - | - | - | - |
| HTS | - | - | Y | - | - | Y | - | - | - |
| LTS | Y | - | - | - | - | - | Y | Y | - |
| CHH-NHS | - | - | - | - | - | - | - | - | - |
| Rectisol | - | - | - | - | - | - | - | - | - |
| aMDEA | Y | Y | Y | Y | Y | Y | Y | Y | Y |
| Liquid $N_2$ Wash | - | - | - | - | - | - | - | - | - |
| METH | - | - | - | - | - | - | - | - | - |
| LT-WGS | Y | Y | Y | Y | Y | Y | Y | Y | Y |
| PSA | Y | Y | Y | Y | Y | Y | Y | Y | Y |
| HBR Pres. | 85.5 bar | 85.5 bar | 85.5 bar | 85.5 bar | 85.5 bar | 85.5 bar | 85.5 bar | 85.5 bar | 85.5 bar |
| 1st Recycle | Y | Y | Y | Y | Y | Y | Y | Y | Y |
| 2nd Recycle | Y | Y | Y | Y | Y | Y | Y | Y | Y |
| 3rd Recycle | - | - | - | - | - | - | - | - | - |
| HP $H_2$ Recycle | - | - | - | - | - | - | - | - | - |
| FCM | Y | Y | Y | Y | Y | Y | Y | Y | Y |
| $CO_2$ Seq. | - | - | - | - | - | - | - | - | - |
| Technology | TX-W-250 | TX-W-500 | TX-W-1000 | CA-W-250 | CA-W-500 | CA-W-1000 | IA-W-250 | IA-W-500 | IA-W-1000 |
| SMR Temp. | - | - | - | - | - | - | - | - | - |
| ATR | - | - | - | - | - | - | - | - | - |
| PR and SR | - | - | - | - | - | - | - | - | - |
| Gasifier Temp. | - | - | - | - | - | - | - | - | - |
| Alkaline EYZ | Y | Y | Y | Y | Y | Y | Y | Y | Y |
| PEM EYZ | - | - | - | - | - | - | - | - | - |
| ASU | Y | Y | Y | Y | Y | Y | Y | Y | Y |
| HT-WGS | - | - | - | - | - | - | - | - | - |
| RGS Temp. | - | - | - | - | - | - | - | - | - |
| HTS | - | - | - | - | - | - | - | - | - |
| LTS | - | - | - | - | - | - | - | - | - |
| CHH-NHS | - | - | - | - | - | - | - | - | - |
| Rectisol | - | - | - | - | - | - | - | - | - |
| aMDEA | - | - | - | - | - | - | - | - | - |
| Liquid $N_2$ Wash | - | - | - | - | - | - | - | - | - |
| METH | - | - | - | - | - | - | - | - | - |
| LT-WGS | - | - | - | - | - | - | - | - | - |
| PSA | - | - | Y | Y | Y | Y | - | - | Y |
| HBR Pres. | 85.5 bar | 85.5 bar | 85.5 bar | 85.5 bar | 85.5 bar | 85.5 bar | 85.5 bar | 85.5 bar | 85.5 bar |
| 1st Recycle | Y | Y | Y | Y | Y | Y | Y | Y | Y |
| 2nd Recycle | Y | Y | Y | Y | Y | Y | Y | Y | Y |
| 3rd Recycle | - | - | - | - | - | - | - | - | - |
| HP $H_2$ Recycle | - | - | - | - | - | - | - | - | - |
| FCM | - | - | Y | Y | Y | Y | - | - | Y |
| $CO_2$ Seq. | - | - | - | - | - | - | - | - | - |

### 3.4.2 Overall Cost Breakdown

The overall cost of the ammonia plants are minimized in the optimization problem. Break-even ammonia prices (BEP) are measured in \$/ton of $NH_3$, and they indicate the profitability of the plant.

Table 3.6: Optimal topologies of the ammonia plants for each case study - Part III.

| | **Texas** | | | **California** | | |
|---|---|---|---|---|---|---|
| Technology | TX-S-250 | TX-S-500 | TX-S-1000 | CA-S-250 | CA-S-500 | CA-S-1000 |
| SMR Temp. | - | - | - | - | - | - |
| ATR | - | - | - | - | - | - |
| PR and SR | - | - | - | - | - | - |
| Gasifier Temp. | - | - | - | - | - | - |
| Alkaline EYZ | Y | Y | Y | Y | Y | Y |
| PEM EYZ | - | - | - | - | - | - |
| ASU | Y | Y | Y | Y | Y | Y |
| HT-WGS | - | - | - | - | - | - |
| RGS Temp. | - | - | - | - | - | - |
| HTS | - | - | - | - | - | - |
| LTS | - | - | - | - | - | - |
| CHH-NHS | - | - | - | - | - | - |
| Rectisol | - | - | - | - | - | - |
| aMDEA | - | - | - | - | - | - |
| Liquid $N_2$ Wash | - | - | - | - | - | - |
| METH | - | - | - | - | - | - |
| LT-WGS | - | - | - | - | - | - |
| PSA | - | Y | Y | - | - | Y |
| HBR Pres. | 85.5 bar | 85.5 bar | 85.5 bar | 85.5 bar | 85.5 bar | 85.5 bar |
| 1$^{st}$ Recycle | Y | Y | Y | Y | Y | Y |
| 2$^{nd}$ Recycle | Y | Y | Y | Y | Y | Y |
| 3$^{rd}$ Recycle | - | - | - | - | - | - |
| HP $H_2$ Recycle | - | - | - | - | - | - |
| FCM | - | Y | Y | - | - | Y |
| $CO_2$ Seq. | - | - | - | - | - | - |

The lower BEP value, the more profitable the plant is. Ammonia BEP values for Texas, California, and Iowa case studies are presented in Table 3.7. Results show that plant size and electricity prices has an effect on the selection of the source of power in ammonia production. Especially in Texas, producing power from biomass is more favorable than buying electricity from the grid at smaller plant scales as shown in TX-H-250. As the plant size gets larger, some of the biomass is sent to the fuel combustor in the H&P integration section to generate power, since power generation section benefits from economies of scale. In California, due to high electricity prices, the ammonia plants do not buy electricity from the grid; instead they produce their own electricity by combusting biomass.

A graphical comparison of the BEP for all Texas based ammonia plants is illustrated in Figure 3.5. Results indicate that ammonia BEP values are highly dependent on the state's resources. In Texas, natural gas and grid electricity prices are lower than those in California and Iowa. For this reason, natural gas, hardwood, or MSW-based processes are more profitable in Texas. In general, natural gas and biomass-based ammonia processes have lower BEP values than wind or

Table 3.7: Overall cost breakdown for ammonia plants for each case study.

| | **Texas** | | | **California** | | | **Iowa** | | |
|---|---|---|---|---|---|---|---|---|---|
| Cost Contributions | TX-N-250 | TX-N-500 | TX-N-1000 | CA-N-250 | CA-N-500 | CA-N-1000 | IA-N-250 | IA-N-500 | IA-N-1000 |
| Biomass | 0.00 | 0.00 | 0.00 | 0.00 | 0.00 | 0.00 | 0.00 | 0.00 | 0.00 |
| Natural Gas | 79.03 | 85.34 | 84.98 | 219.11 | 207.53 | 232.87 | 122.73 | 136.52 | 136.40 |
| Water | 0.71 | 0.69 | 0.66 | 1.01 | 0.92 | 1.10 | 0.96 | 0.91 | 0.89 |
| Investment | 285.16 | 229.52 | 181.18 | 338.82 | 259.38 | 207.41 | 283.49 | 237.31 | 185.33 |
| $CO_2$ TS&M | 6.78 | 7.26 | 7.17 | 8.61 | 8.11 | 9.20 | 6.62 | 7.23 | 7.21 |
| OM | 75.29 | 60.60 | 47.83 | 89.45 | 68.48 | 54.76 | 74.84 | 62.64 | 48.93 |
| Electricity | 106.59 | 88.66 | 82.46 | 92.38 | 105.29 | 72.66 | 129.74 | 92.92 | 91.39 |
| BEP ($/ton $NH_3$) | 553.56 | 472.05 | 404.29 | 749.41 | 649.71 | 578.01 | 618.40 | 537.50 | 470.15 |
| Cost Contributions | TX-H-250 | TX-H-500 | TX-H-1000 | CA-H-250 | CA-H-500 | CA-H-1000 | IA-C-250 | IA-C-500 | IA-C-1000 |
| Biomass | 114.28 | 120.21 | 138.09 | 144.00 | 144.06 | 144.05 | 217.80 | 217.79 | 217.79 |
| Natural Gas | 0.00 | 0.00 | 0.00 | 0.00 | 0.00 | 0.00 | 0.00 | 0.00 | 0.00 |
| Water | 0.96 | 0.99 | 1.19 | 1.28 | 1.30 | 1.30 | 1.24 | 1.24 | 1.24 |
| Investment | 245.55 | 211.77 | 180.91 | 298.10 | 233.40 | 183.38 | 271.06 | 212.06 | 166.37 |
| $CO_2$ TS&M | 0.39 | 0.07 | 0.02 | 0.05 | 0.05 | 0.05 | 0.00 | 0.00 | 0.00 |
| OM | 64.83 | 55.91 | 47.76 | 78.71 | 61.61 | 48.42 | 71.57 | 55.98 | 43.93 |
| Electricity | 86.70 | 45.53 | 7.44 | 0.00 | 0.00 | 0.00 | 63.39 | 63.39 | 63.39 |
| BEP ($/ton $NH_3$) | 512.69 | 434.48 | 375.41 | 522.16 | 440.40 | 377.19 | 625.06 | 550.48 | 492.73 |
| Cost Contributions | TX-M-250 | TX-M-500 | TX-M-1000 | CA-M-250 | CA-M-500 | CA-M-1000 | IA-M-250 | IA-M-500 | IA-M-1000 |
| Biomass | 104.32 | 107.44 | 108.49 | 138.99 | 138.83 | 138.00 | 107.55 | 107.33 | 107.44 |
| Natural Gas | 0.00 | 0.00 | 0.00 | 0.00 | 0.00 | 0.00 | 0.00 | 0.00 | 0.00 |
| Water | 1.03 | 0.99 | 0.99 | 1.40 | 1.40 | 1.38 | 0.99 | 0.99 | 0.99 |
| Investment | 325.22 | 277.02 | 233.49 | 403.13 | 322.50 | 270.03 | 348.30 | 277.22 | 231.47 |
| $CO_2$ TS&M | 0.00 | 0.00 | 0.00 | 0.00 | 0.00 | 0.00 | 0.00 | 0.00 | 0.00 |
| OM | 85.87 | 73.14 | 61.65 | 106.43 | 85.14 | 71.29 | 91.96 | 73.19 | 61.12 |
| Electricity | 84.89 | 56.75 | 52.54 | 0.00 | 0.00 | 0.00 | 62.27 | 62.34 | 64.40 |
| BEP ($/ton $NH_3$) | 601.31 | 515.36 | 457.16 | 649.97 | 547.87 | 480.71 | 611.08 | 521.08 | 465.42 |
| Cost Contributions | TX-W-250 | TX-W-500 | TX-W-1000 | CA-W-250 | CA-W-500 | CA-W-1000 | IA-W-250 | IA-W-500 | IA-W-1000 |
| Biomass | 0.00 | 0.00 | 0.00 | 0.00 | 0.00 | 0.00 | 0.00 | 0.00 | 0.00 |
| Natural Gas | 0.00 | 0.00 | 0.00 | 0.00 | 0.00 | 0.00 | 0.00 | 0.00 | 0.00 |
| Water | 2.41 | 2.41 | 2.38 | 2.38 | 2.38 | 2.38 | 2.41 | 2.41 | 2.38 |
| Investment | 276.51 | 233.46 | 205.31 | 284.86 | 240.09 | 207.05 | 276.51 | 233.46 | 205.31 |
| $CO_2$ TS&M | 0.00 | 0.00 | 0.00 | 0.00 | 0.00 | 0.00 | 0.00 | 0.00 | 0.00 |
| OM | 73.01 | 61.63 | 54.21 | 75.21 | 63.39 | 54.67 | 73.01 | 61.63 | 54.21 |
| Electricity | 532.42 | 532.43 | 524.63 | 715.40 | 715.40 | 715.58 | 532.42 | 532.43 | 524.63 |
| BEP ($/ton $NH_3$) | 884.36 | 829.93 | 786.53 | 1077.84 | 1021.26 | 979.66 | 884.36 | 829.93 | 786.53 |
| Cost Contributions | TX-S-250 | TX-S-500 | TX-S-1000 | CA-S-250 | CA-S-500 | CA-S-1000 | - | - | - |
| Biomass | 0.00 | 0.00 | 0.00 | 0.00 | 0.00 | 0.00 | - | - | - |
| Natural Gas | 0.00 | 0.00 | 0.00 | 0.00 | 0.00 | 0.00 | - | - | - |
| Water | 2.41 | 2.38 | 2.38 | 2.41 | 2.41 | 2.38 | - | - | - |
| Investment | 276.51 | 240.10 | 205.65 | 276.51 | 233.45 | 205.31 | - | - | - |
| $CO_2$ TS&M | 0.00 | 0.00 | 0.00 | 0.00 | 0.00 | 0.00 | - | - | - |
| OM | 73.01 | 63.39 | 54.30 | 73.01 | 61.63 | 54.21 | - | - | - |
| Electricity | 619.56 | 610.49 | 610.72 | 544.54 | 544.53 | 536.55 | - | - | - |
| BEP ($/ton $NH_3$) | 971.48 | 916.33 | 873.02 | 896.46 | 842.03 | 798.45 | - | - | - |

solar powered processes. In terms of economies of scale, natural-gas based processes are the most favorable and non-biomass renewable processes are the least. This can be observed from the cost functions for reforming, gasification, and electrolysis, the technologies for producing hydrogen, which is the most expensive part of the plant as described in the next section.

For Texas, TX-H processes are the most profitable options, offering 7-8% decrease in BEP across three different plant scales when compared to TX-N ones. Even though hardwood feedstock

costs are larger than natural gas costs, TX-N processes use more electricity for both electrolyzers and $CO_2$ sequestration. Almost half of the BEP comes from annualized investment costs, with biomass and electricity costs following it. With increasing plant scale, the share of electricity prices go down, and the process starts generating some of its own electricity by biomass combustion. TX-N is the second most profitable option, and the TX-M case is the third. TX-M BEP values are 9-13% higher than those of TX-N. The share of investment costs in TX-M is significantly greater due to RDF facilities used to pre-process the municipal waste. Likewise, extra RDF facilities also increase its OM costs. TX-M becomes less competitive against TX-N at larger plant capacities.

TX-W and TX-S results are much less competitive than natural gas and biomass ones. Investments costs of TX-W and TX-S do not benefit as much from economies of scale due to increasing electrolyzer stack size. Moreover, electricity costs are the biggest contribution to the high BEP values. Electrolysis consumes lots of electricity and is less energy efficient than steam reforming or biomass gasification. The BEP of TX-W-250 is 60% more expensive than TX-N-250, and this difference goes up to 95% for the largest scale. The BEP of TX-S-250 is 76% more expensive than TX-N-250, and it goes up to 116% for TX-S-1000.

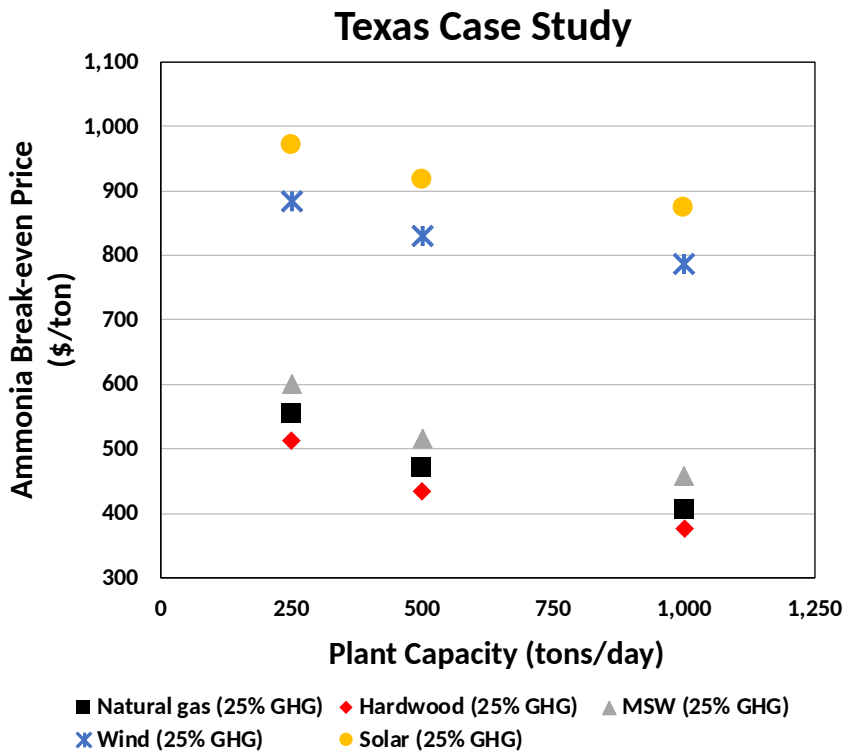


Figure 3.5: Ammonia break-even prices vs. plant capacity for Texas Case Study.

Figure 3.6 shows the BEP prices for California based ammonia plants. Because of the more expensive natural gas and grid electricity prices in California, CA-N cases have 35-42% higher BEPs compared to TX-N ones. CA-H is 30-34% more profitable than CA-N, which makes hardwood a very attractive feedstock in California. Since the biomass price is assumed to be the same for both states, the difference in biomass costs comes from increased consumption of hardwood in California. The zero cost of electricity shows that the ammonia plant produces its own electricity through biomass combustion. The resulting BEP of all CA-H cases are very similar to those of TX-H. CA-M cases are less competitive than CA-H ones, but still 13-17% more profitable than those for CA-N. CA-M process also produces its own electricity since it is cheaper to do so than purchasing grid electricity. CA-W and CA-S cases are less competitive than CA-N, CA-H, and CA-M. Solar LCOE is cheaper than wind LCOE in California, so CA-S has a lower

BEP. CA-S cases have 20-38% higher BEPs compared to CA-N cases, whereas CA-W cases have 44-69% higher BEPs.

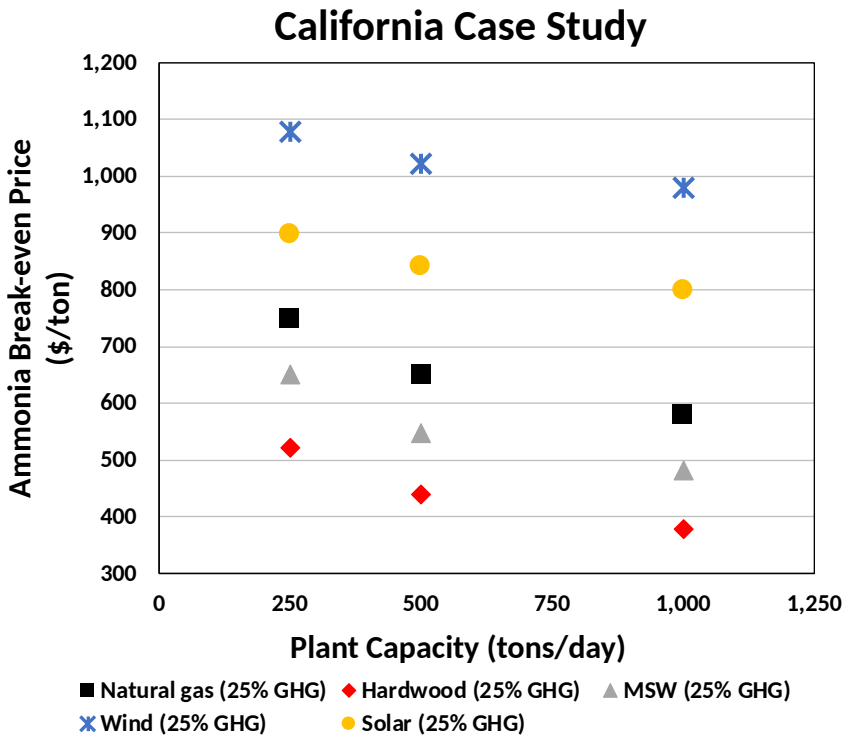


Figure 3.6: Ammonia break-even prices vs. plant capacity for California Case Study.

Figure 3.7 shows the BEP prices for Iowa based ammonia plants. Natural gas and grid electricity prices in Iowa are between those in Texas and California. As such, the BEP of IA-N cases are higher than those of TX-N and lower than those of CA-N. Iowa is rich in corn stover type of biomass, but corn stover has a higher unit price than hardwood. Consequently, biomass costs are a larger share of the IA-C BEP than for the other biomass studies. For Iowa, IA-N, IA-C, and IA-M have very similar cost results. IA-M processes are slightly more profitable, and IA-C are slightly less profitable. IA-W has the same characteristic of TX-W, since the reported wind LCOE is the same for both states.

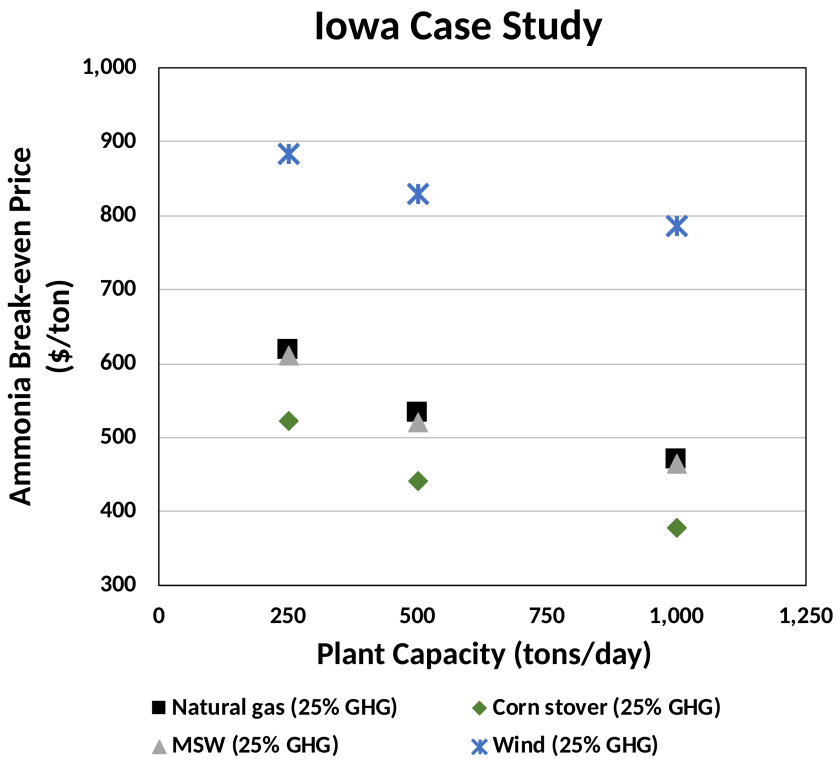


Figure 3.7: Ammonia break-even prices vs. plant capacity for Iowa Case Study.

### 3.4.3 Investment Cost Breakdown

The investment cost analysis of ammonia production is divided into 7 sections: (i) syngas generation, (ii) syngas cleanup, (iii) ammonia synthesis loop, (iv) water electrolysis, (v) air separation, (vi) H&P integration, and (vii) wastewater treatment. Table 3.8 shows the investment costs of each section in an ammonia plant for all case studies.

Ammonia synthesis gas generation includes hydrogen and nitrogen production, and this the most significant portion of the total investment costs. For natural gas-based cases, the syngas generation/cleanup, water electrolysis, and air separation sections constitute on average 60% of the total investment costs. Ammonia synthesis loop takes a 25% share. The difference in states mainly come from H&P integration. This section is used to improve the energy economics of the ammonia production by optimally recovering waste process heat and using fuel to generate power

Table 3.8: Investment cost breakdown for ammonia plants for each case study.

| | **Texas** | | | **California** | | | **Iowa** | | |
|---|---|---|---|---|---|---|---|---|---|
| Sections | TX-N-250 | TX-N-500 | TX-N-1000 | CA-N-250 | CA-N-500 | CA-N-1000 | IA-N-250 | IA-N-500 | IA-N-1000 |
| Syngas Generation | 31.90 | 51.72 | 83.08 | 19.93 | 31.40 | 51.62 | 17.69 | 28.30 | 46.72 |
| Syngas Cleanup | 30.45 | 49.71 | 77.58 | 40.01 | 52.79 | 99.30 | 29.00 | 48.51 | 75.87 |
| Ammonia Syn. Loop | 38.90 | 67.98 | 107.61 | 38.82 | 72.41 | 97.54 | 38.90 | 68.90 | 109.92 |
| Water Electrolysis | 4.25 | 0.00 | 0.00 | 0.00 | 0.00 | 0.00 | 9.53 | 8.77 | 15.37 |
| Air Separation | 28.88 | 50.14 | 71.50 | 44.37 | 62.14 | 91.14 | 28.88 | 52.15 | 76.13 |
| H&P Integration | 11.20 | 15.31 | 32.19 | 28.47 | 44.72 | 79.50 | 18.36 | 33.63 | 51.34 |
| Wastewater Treat. | 7.10 | 10.89 | 16.04 | 9.80 | 14.27 | 25.06 | 9.41 | 13.84 | 21.53 |
| Total (MM$) | 152.66 | 245.75 | 387.99 | 181.40 | 277.72 | 444.17 | 151.77 | 254.09 | 396.88 |
| Sections | TX-H-250 | TX-H-500 | TX-H-1000 | CA-H-250 | CA-H-500 | CA-H-1000 | IA-C-250 | IA-C-500 | IA-C-1000 |
| Syngas Generation | 35.74 | 60.50 | 109.40 | 42.09 | 68.77 | 112.81 | 37.36 | 61.03 | 99.72 |
| Syngas Cleanup | 18.68 | 28.65 | 46.69 | 17.95 | 28.09 | 43.97 | 19.34 | 30.67 | 48.71 |
| Ammonia Syn. Loop | 38.90 | 61.64 | 97.72 | 38.90 | 61.64 | 97.72 | 38.90 | 61.64 | 97.72 |
| Water Electrolysis | 0.00 | 0.00 | 0.00 | 0.00 | 0.00 | 0.00 | 0.00 | 0.00 | 0.00 |
| Air Separation | 28.88 | 41.31 | 59.18 | 28.88 | 41.31 | 59.18 | 28.88 | 41.31 | 59.18 |
| H&P Integration | 0.00 | 20.76 | 50.68 | 21.22 | 33.77 | 53.73 | 11.07 | 17.61 | 28.02 |
| Wastewater Treat. | 9.05 | 13.53 | 23.21 | 10.32 | 15.93 | 24.67 | 9.23 | 14.26 | 22.05 |
| Total (MM$) | 131.46 | 226.75 | 387.43 | 159.60 | 249.91 | 392.72 | 145.12 | 227.07 | 356.29 |
| Sections | TX-M-250 | TX-M-500 | TX-M-1000 | CA-M-250 | CA-M-500 | CA-M-1000 | IA-M-250 | IA-M-500 | IA-M-1000 |
| Syngas Generation | 77.02 | 131.72 | 200.91 | 95.31 | 159.37 | 240.27 | 78.78 | 131.64 | 199.46 |
| Syngas Cleanup | 20.07 | 31.95 | 45.58 | 20.63 | 32.33 | 48.25 | 20.20 | 31.70 | 45.91 |
| Ammonia Syn. Loop | 38.90 | 61.64 | 89.30 | 38.90 | 61.64 | 89.30 | 38.99 | 61.64 | 89.30 |
| Water Electrolysis | 0.00 | 0.00 | 0.00 | 0.00 | 0.00 | 0.00 | 0.00 | 0.00 | 0.00 |
| Air Separation | 28.88 | 41.31 | 55.17 | 28.88 | 41.31 | 55.17 | 28.88 | 41.31 | 55.17 |
| H&P Integration | 0.00 | 16.06 | 25.80 | 21.02 | 33.44 | 48.55 | 10.63 | 16.88 | 23.35 |
| Wastewater Treat. | 9.13 | 13.82 | 19.88 | 11.06 | 17.17 | 23.57 | 8.89 | 13.51 | 19.67 |
| Total (MM$) | 174.11 | 296.63 | 436.82 | 215.83 | 345.31 | 505.20 | 186.47 | 296.83 | 433.05 |
| Sections | TX-W-250 | TX-W-500 | TX-W-1000 | CA-W-250 | CA-W-500 | CA-W-1000 | IA-W-250 | IA-W-500 | IA-W-1000 |
| Syngas Generation | 0.00 | 0.00 | 0.00 | 0.00 | 0.00 | 0.00 | 0.00 | 0.00 | 0.00 |
| Syngas Cleanup | 0.00 | 0.00 | 0.00 | 0.00 | 0.00 | 0.00 | 0.00 | 0.00 | 0.00 |
| Ammonia Syn. Loop | 38.90 | 61.64 | 97.72 | 38.90 | 61.64 | 97.76 | 38.90 | 61.64 | 97.72 |
| Water Electrolysis | 63.99 | 121.75 | 232.20 | 63.99 | 121.75 | 232.24 | 63.99 | 121.75 | 232.20 |
| Air Separation | 28.88 | 41.31 | 59.18 | 28.88 | 41.31 | 59.19 | 28.88 | 41.31 | 59.18 |
| H&P Integration | 0.00 | 0.00 | 11.77 | 4.65 | 7.40 | 11.79 | 0.00 | 0.00 | 11.77 |
| Wastewater Treat. | 16.08 | 24.97 | 38.32 | 15.90 | 24.67 | 38.47 | 16.08 | 24.97 | 38.32 |
| Total (MM$) | 148.04 | 249.97 | 439.68 | 152.50 | 257.08 | 443.38 | 148.04 | 249.97 | 439.68 |
| Sections | TX-S-250 | TX-S-500 | TX-S-1000 | CA-S-250 | CA-S-500 | CA-S-1000 | - | - | - |
| Syngas Generation | 0.00 | 0.00 | 0.00 | 0.00 | 0.00 | 0.00 | - | - | - |
| Syngas Cleanup | 0.00 | 0.00 | 0.00 | 0.00 | 0.00 | 0.00 | - | - | - |
| Ammonia Syn. Loop | 38.90 | 61.64 | 97.72 | 38.90 | 61.64 | 97.72 | - | - | - |
| Water Electrolysis | 63.99 | 121.75 | 232.20 | 63.99 | 121.75 | 232.20 | - | - | - |
| Air Separation | 28.88 | 41.31 | 59.18 | 28.88 | 41.31 | 59.18 | - | - | - |
| H&P Integration | 0.00 | 7.40 | 11.94 | 0.00 | 0.00 | 11.77 | - | - | - |
| Wastewater Treat. | 16.08 | 24.67 | 38.33 | 16.08 | 24.97 | 38.32 | - | - | - |
| Total (MM$) | 148.04 | 257.08 | 440.38 | 148.04 | 249.97 | 439.68 | - | - | - |

for the plant. In California, to combat higher feedstock and electricity prices, H&P integration costs more than that in Texas. Therefore, California ammonia plants have higher investment costs.

Hardwood and corn stover-based processes are slightly less expensive than natural gas-based processes. The biggest difference comes from smaller syngas cleanup sections in the biomass plants. Biomass plants use aMDEA process, whereas natural gas plants use Rectisol unit plus additional water-gas shift reactors and sequestration units for reducing GHG emissions.

MSW-based processes are more expensive than other biomass plants due to an extra RDF facility used to pre-process the waste. The addition of a RDF facility can be observed in the larger costs of syngas generation.

Wind and solar powered ammonia production plants have similar investment cost breakdowns due to alike process topologies. Ammonia plants using electrolyzers are more capital intensive, compared to steam reforming or biomass gasification. As expected, water electrolysis and water treatment sections have the largest share in the plant. Their total share is between 54% and 62%, whereas shares of ammonia synthesis loop and air separation sections decrease with increasing plant scale. This is due to the almost linear scale-up characteristics of the alkaline electrolyzers.

### 3.4.4 Greenhouse Gas Emission Balances

All the case studies have a GHG Index less than or equal to 0.25, so that the proposed ammonia production processes do not emit more than 25% of a typical natural gas-based ammonia plant. All case studies manage to achieve this goal, and infeasibility is not observed due to emission restrictions. Table 3.9 summarizes the GHG balances for all the case studies.

Results indicate that natural gas- and hardwood- based processes operate at the GHG emissions limit. $CO_2$ sequestration is only used for natural gas-based processes. The negative GHG contribution attributed to biomass is due to its carbon sink property. Since biomass absorbs the $CO_2$ from the atmosphere, biomass intake negatively contributes to $CO_2$ emissions. When biomass is decomposed into synthesis gas, the captured $CO_2$ is released back to the atmosphere thus positively contributing to the emissions. There are also additional GHG emissions due to acquisition, processing, and delivery of biomass feedstock, as well as its use in the fuel combuster to generate power for the plant. As a result, the net $CO_2$ emissions of the biomass-based processes are positive. Wind or solar electricty is assumed not to produce any GHG. Negative GHGAE values show the cases, when the plant uses electricity from the grid. If GHGAE is zero, this means in that case study, the plant is either generating its own electricity (in case of using biomass feedstock) or using renewable electricity (in case of wind or solar power).

To conclude these case studies, average energy consumption values for each feedstock type are

Table 3.9: GHG balances (given in kg $CO_2$ equivalent/s) of the ammonia plants for each case study.

| | **Texas** | | | **California** | | | **Iowa** | | |
|---|---|---|---|---|---|---|---|---|---|
| GHG Contributions | TX-N-250 | TX-N-500 | TX-N-1000 | CA-N-250 | CA-N-500 | CA-N-1000 | IA-N-250 | IA-N-500 | IA-N-1000 |
| Biomass | 0.000 | 0.000 | 0.000 | 0.000 | 0.000 | 0.000 | 0.000 | 0.000 | 0.000 |
| Natural Gas | 0.594 | 1.283 | 2.556 | 0.772 | 1.462 | 3.281 | 0.578 | 1.285 | 2.568 |
| Vented $CO_2$ | 0.097 | 0.276 | 0.685 | 0.241 | 0.507 | 0.940 | 0.076 | 0.341 | 0.711 |
| Seq. $CO_2$ | 0.007 | 0.014 | 0.028 | 0.008 | 0.016 | 0.036 | 0.007 | 0.014 | 0.028 |
| TGHG | 0.698 | 1.573 | 3.269 | 1.021 | 1.985 | 4.259 | 0.660 | 1.641 | 3.308 |
| GHGAE | -2.110 | -3.510 | -6.530 | -0.818 | -1.864 | -2.573 | -2.263 | -3.241 | -6.376 |
| GHGAN | 4.902 | 9.804 | 19.607 | 4.902 | 9.804 | 19.607 | 4.902 | 9.804 | 19.607 |
| GHG Index | 0.25 | 0.25 | 0.25 | 0.25 | 0.25 | 0.25 | 0.25 | 0.25 | 0.25 |
| GHG Contributions | TX-H-250 | TX-H-500 | TX-H-1000 | CA-H-250 | CA-H-500 | CA-H-1000 | IA-C-250 | IA-C-500 | IA-C-1000 |
| Biomass | -7.702 | -16.205 | -37.230 | -9.707 | -19.420 | -38.841 | -7.843 | -15.686 | -31.372 |
| Natural Gas | 0.000 | 0.000 | 0.000 | 0.000 | 0.000 | 0.000 | 0.000 | 0.000 | 0.000 |
| Vented $CO_2$ | 8.498 | 18.206 | 41.985 | 10.932 | 21.871 | 43.742 | 8.583 | 17.167 | 34.334 |
| Seq. $CO_2$ | 0.000 | 0.000 | 0.000 | 0.000 | 0.000 | 0.000 | 0.000 | 0.000 | 0.000 |
| TGHG | 0.796 | 2.000 | 4.754 | 1.225 | 2.451 | 4.902 | 0.740 | 1.481 | 2.962 |
| GHGAE | -1.716 | -1.803 | -0.589 | 0.000 | 0.000 | 0.000 | -1.106 | -2.211 | -4.422 |
| GHGAN | 4.902 | 9.804 | 19.607 | 4.902 | 9.804 | 19.607 | 4.902 | 9.804 | 19.607 |
| GHG Index | 0.25 | 0.25 | 0.25 | 0.25 | 0.25 | 0.25 | 0.20 | 0.20 | 0.20 |
| GHG Contributions | TX-M-250 | TX-M-500 | TX-M-1000 | CA-M-250 | CA-M-500 | CA-M-1000 | IA-M-250 | IA-M-500 | IA-M-1000 |
| Biomass | -7.730 | -15.922 | -28.095 | -10.300 | -20.575 | -35.734 | -7.970 | -15.908 | -27.822 |
| Natural Gas | 0.000 | 0.000 | 0.000 | 0.000 | 0.000 | 0.000 | 0.000 | 0.000 | 0.000 |
| Vented $CO_2$ | 8.450 | 17.389 | 30.687 | 11.258 | 22.483 | 39.049 | 8.706 | 17.377 | 30.385 |
| Seq. $CO_2$ | 0.000 | 0.000 | 0.000 | 0.000 | 0.000 | 0.000 | 0.000 | 0.000 | 0.000 |
| TGHG | 0.720 | 1.467 | 2.593 | 0.957 | 1.908 | 3.314 | 0.736 | 1.469 | 2.563 |
| GHGAE | -1.681 | -2.247 | -3.635 | 0.000 | 0.000 | 0.000 | -1.086 | -2.175 | -3.925 |
| GHGAN | 4.902 | 9.804 | 17.129 | 4.902 | 9.804 | 17.129 | 4.902 | 9.804 | 17.129 |
| GHG Index | 0.22 | 0.19 | 0.19 | 0.20 | 0.19 | 0.19 | 0.19 | 0.19 | 0.19 |
| GHG Contributions | TX-W-250 | TX-W-500 | TX-W-1000 | CA-W-250 | CA-W-500 | CA-W-1000 | IA-W-250 | IA-W-500 | IA-W-1000 |
| Biomass | 0.000 | 0.000 | 0.000 | 0.000 | 0.000 | 0.000 | 0.000 | 0.000 | 0.000 |
| Natural Gas | 0.000 | 0.000 | 0.000 | 0.000 | 0.000 | 0.000 | 0.000 | 0.000 | 0.000 |
| Vented $CO_2$ | 0.000 | 0.000 | 0.000 | 0.000 | 0.000 | 0.000 | 0.000 | 0.000 | 0.000 |
| Seq. $CO_2$ | 0.000 | 0.000 | 0.000 | 0.000 | 0.000 | 0.000 | 0.000 | 0.000 | 0.000 |
| TGHG | 0.000 | 0.000 | 0.000 | 0.000 | 0.000 | 0.000 | 0.000 | 0.000 | 0.000 |
| GHGAE | 0.000 | 0.000 | 0.000 | 0.000 | 0.000 | 0.000 | 0.000 | 0.000 | 0.000 |
| GHGAN | 4.902 | 9.804 | 19.607 | 4.902 | 9.804 | 19.607 | 4.902 | 9.804 | 19.607 |
| GHG Index | 0.00 | 0.00 | 0.00 | 0.00 | 0.00 | 0.00 | 0.00 | 0.00 | 0.00 |
| GHG Contributions | TX-S-250 | TX-S-500 | TX-S-1000 | CA-S-250 | CA-S-500 | CA-S-1000 | - | - | - |
| Biomass | 0.000 | 0.000 | 0.000 | 0.000 | 0.000 | 0.000 | - | - | - |
| Natural Gas | 0.000 | 0.000 | 0.000 | 0.000 | 0.000 | 0.000 | - | - | - |
| Vented $CO_2$ | 0.000 | 0.000 | 0.000 | 0.000 | 0.000 | 0.000 | - | - | - |
| Seq. $CO_2$ | 0.000 | 0.000 | 0.000 | 0.000 | 0.000 | 0.000 | - | - | - |
| TGHG | 0.000 | 0.000 | 0.000 | 0.000 | 0.000 | 0.000 | - | - | - |
| GHGAE | 0.000 | 0.000 | 0.000 | 0.000 | 0.000 | 0.000 | - | - | - |
| GHGAN | 4.902 | 9.804 | 19.607 | 4.902 | 9.804 | 19.607 | - | - | - |
| GHG Index | 0.00 | 0.00 | 0.00 | 0.00 | 0.00 | 0.00 | - | - | - |

given in Figure 3.8. Natural gas-based process consumes about 32 GJ/ton and it is more efficient than biomass, wind, and solar energy based processes. While reported energy consumption of industrial ammonia plants using natural gas can go down to 28 GJ/ton, the optimization objective in this work is to minimize the overall costs of ammonia production, that also includes investment cost considerations.

The preliminary studies show that the energy efficiency of the process can go below 30

GJ/ton if the objective is minimizing total energy consumption. Also, it is worth mentioning that $CO_2$ sequestration is an energy consuming process. Corn stover-based process has decent energy efficiency of 33 GJ/ton. Hardwood- and MSW-based processes are less efficient with 36 and 38 GJ/ton values, respectively. Wind- or solar-powered electrolyzers are not as efficient as steam reforming or biomass gasification, the average energy consumption of electrolyzer-based process is 43 GJ/ton, that is 34% greater than natural gas-based process. This low efficiency of electrolyzer-based production is one the key reasons of high ammonia BEP for wind or solar powered processes.

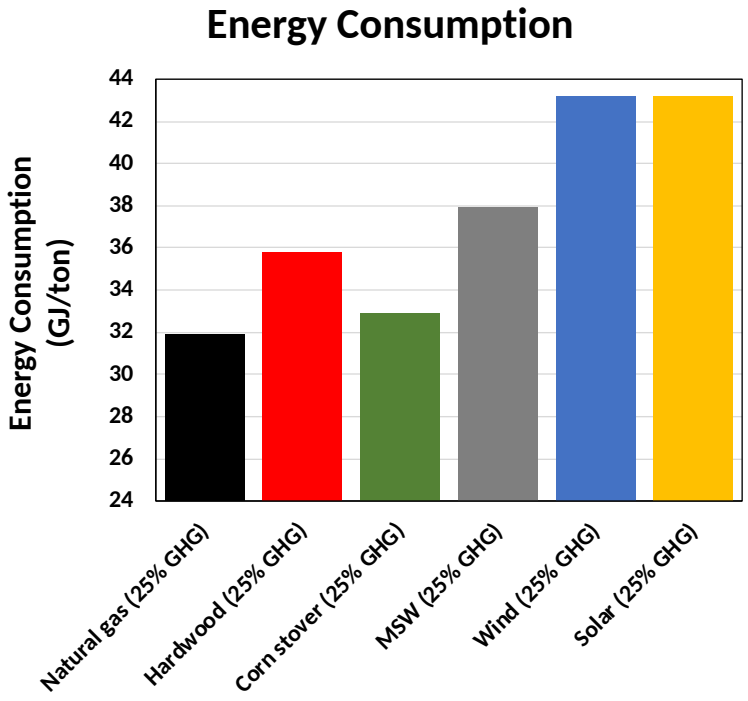


Figure 3.8: Energy consumption (given in GJ/ton $NH_3$) for all feedstock types.

### 3.4.5 Sensitivity Analysis

As shown in the previous cases, ammonia BEP is sensitive to feedstock and electricity prices. While sensitivity to natural gas and electricity prices are investigated to some degree by doing case studies on different states, there are also a few interesting cases that might require some attention. In this section, the effects of GHG emission restrictions on the natural gas-based reference case and the price sensitivity of hardwood gasification-based ammonia production are investigated. The sensitivity analyses are done for Texas.

Table 3.10 shows the overall cost and investment cost breakdowns, and GHG balances for cases where GHG emissions are set to be less or equation to 50, 75, and 100% of those of a typical ammonia plant. By relaxing the GHG emission limitations, the effect of $CO_2$ capture on the economic performance of the natural gas-based ammonia process is investigated.

Table 3.10: Sensitivity analysis for GHG emission reductions.

| | **Texas (50% GHG emissions)** | | | **Texas (75% GHG emissions)** | | | **Texas (100% GHG emissions)** | | |
|---|---|---|---|---|---|---|---|---|---|
| Overall Cost Break. | TX-N-250 | TX-N-500 | TX-N-1000 | TX-N-250 | TX-N-500 | TX-N-1000 | TX-N-250 | TX-N-500 | TX-N-1000 |
| Biomass | 0.00 | 0.00 | 0.00 | 0.00 | 0.00 | 0.00 | 0.00 | 0.00 | 0.00 |
| Natural Gas | 78.77 | 103.02 | 101.03 | 80.15 | 104.57 | 104.56 | 83.03 | 104.55 | 106.34 |
| Water | 0.98 | 0.94 | 0.91 | 0.94 | 0.94 | 0.94 | 0.96 | 0.94 | 0.96 |
| Investment | 231.55 | 212.68 | 163.74 | 237.42 | 212.03 | 163.58 | 238.20 | 213.16 | 166.02 |
| $CO_2$ TS&M | 6.14 | 7.24 | 7.07 | 4.85 | 5.63 | 5.63 | 3.71 | 3.91 | 4.00 |
| OM | 61.13 | 56.14 | 43.23 | 62.68 | 55.99 | 43.18 | 62.89 | 56.29 | 43.84 |
| Electricity | 141.35 | 61.91 | 63.83 | 120.58 | 55.13 | 55.04 | 111.14 | 52.73 | 50.02 |
| BEP ($/ton $NH_3$) | 519.93 | 441.93 | 379.83 | 506.61 | 434.28 | 372.96 | 499.92 | 431.55 | 371.15 |
| Inv. Cost Break. | TX-N-250 | TX-N-500 | TX-N-1000 | TX-N-250 | TX-N-500 | TX-N-1000 | TX-N-250 | TX-N-500 | TX-N-1000 |
| Syngas Generation | 17.65 | 31.28 | 48.87 | 15.74 | 29.95 | 47.66 | 15.058 | 31.17 | 48.78 |
| Syngas Cleanup | 18.61 | 41.56 | 60.24 | 17.37 | 40.29 | 64.32 | 16.808 | 39.42 | 63.39 |
| Ammonia Syn. Loop | 39.08 | 61.53 | 106.28 | 38.90 | 61.98 | 98.10 | 38.897 | 61.68 | 99.50 |
| Water Electrolysis | 8.90 | 0.00 | 0.00 | 9.17 | 0.00 | 0.00 | 9.041 | 0.00 | 0.00 |
| Air Separation | 30.15 | 63.46 | 89.48 | 28.88 | 63.13 | 90.58 | 28.875 | 63.76 | 91.67 |
| H&P Integration | 0.00 | 15.76 | 24.25 | 8.27 | 17.56 | 27.97 | 10.011 | 18.04 | 30.10 |
| Wastewater Treat. | 9.59 | 14.14 | 21.56 | 8.78 | 14.13 | 21.68 | 8.831 | 14.38 | 22.08 |
| Total (MM$) | 123.97 | 227.73 | 350.67 | 127.10 | 227.03 | 350.30 | 127.522 | 228.24 | 355.53 |
| GHG Balances | TX-N-250 | TX-N-500 | TX-N-1000 | TX-N-250 | TX-N-500 | TX-N-1000 | TX-N-250 | TX-N-500 | TX-N-1000 |
| Biomass | 0.000 | 0.000 | 0.000 | 0.000 | 0.000 | 0.000 | 0.000 | 0.000 | 0.000 |
| Natural Gas | 0.592 | 1.549 | 3.038 | 0.603 | 1.572 | 3.145 | 0.624 | 1.572 | 3.198 |
| Vented $CO_2$ | 0.453 | 2.113 | 4.210 | 1.278 | 4.132 | 8.269 | 2.074 | 6.136 | 12.432 |
| Seq. $CO_2$ | 0.006 | 0.014 | 0.028 | 0.005 | 0.011 | 0.022 | 0.004 | 0.008 | 0.016 |
| LGHG | 1.052 | 3.676 | 7.276 | 1.886 | 5.716 | 11.436 | 2.701 | 7.716 | 15.646 |
| GHGAE | -2.799 | -2.451 | -5.055 | -2.387 | -2.183 | -4.359 | -2.200 | -2.088 | -3.961 |
| GHGAN | 4.902 | 9.804 | 19.607 | 4.902 | 9.804 | 19.607 | 4.902 | 9.804 | 19.607 |
| GHG Index | 0.50 | 0.50 | 0.50 | 0.75 | 0.75 | 0.75 | 1.00 | 1.00 | 1.00 |

The decrease in overall costs and BEP of ammonia prove that relaxing GHG emission limitations improve the profitability of natural gas-based production. 50% GHG level results in an average of 6.2% lower BEP for each scale, whereas 75% GHG level brings BEP down by an average of 8.1%, and 100% GHG level brings BEP down by an average of 8.8%. As a result, 50% GHG level case become on par with hardwood-based production, and 75 and 100% GHG level cases give slightly lower ammonia BEP. While the total investment costs are larger with less GHG restrictions, the contribution of investments costs in overall costs decreases. Meanwhile, natural gas consumption increases with less strict GHG emission restrictions, since natural is used as a fuel in H&P integration section to generate power. Electricity contribution is larger for small scale production due to existence of electrolyzers, however it drops sharply for medium and large scale production where electrolyzers are no longer selected. Total investment costs decrease by 17% on average for small scale production, the decrease is less sharp in medium and large scale production as shown by an average of 8% decrease. Syngas generation and cleanup sections become smaller compared to the 25% GHG level case, and H&P integration section has a much larger share in 50, 75, and 100% GHG level cases. GHG balances show that the plants still operate at the limiting conditions. This is reasonable since plants use every bit of natural gas in the H&P integration to improve the economics of ammonia production. When GHG emission restrictions are becoming tighter, the $CO_2$ TS&M costs increase as expected. The decreasing $CO_2$ emissions from the natural gas-based process can be lowered from 100% to 25% without increasing the overall process costs by more than 9%. After $CO_2$ is removed from the ammonia synthesis gas, the additional cost of lowering process emissions is mostly coming from its handling and sequestration. Since removed $CO_2$ is already at very high purity, no further purification is needed; hence, there are no extra investment costs coming with that. Figure 3.9 can also be seen to visually observe the change in ammonia BEP.

To see the effect of hardwood selling prices, the nominal selling price ($70/dry metric ton) was perturbed about 20% to obtain low ($55/dry metric ton) and high ($85/dry metric ton) selling prices. The resulting analyses are illustrated in Table 3.11.

Table 3.11: Sensitivity analysis for hardwood selling prices.

| | **Texas ($55/dry metric ton)** | | | **Texas ($85/dry metric ton)** | | |
|---|---|---|---|---|---|---|
| Overall Cost Breakdown | TX-H-250 | TX-H-500 | TX-H-1000 | TX-H-250 | TX-H-500 | TX-H-1000 |
| Biomass | 110.65 | 111.59 | 113.19 | 148.49 | 170.28 | 145.93 |
| Natural Gas | 0.00 | 0.00 | 0.00 | 0.00 | 0.00 | 0.00 |
| Water | 1.24 | 1.28 | 1.30 | 0.96 | 1.24 | 0.99 |
| Investment | 294.13 | 231.57 | 183.38 | 271.19 | 229.92 | 166.58 |
| $CO_2$ TS&M | 0.07 | 0.05 | 0.05 | 0.16 | 0.05 | 0.07 |
| OM | 77.65 | 61.13 | 48.42 | 71.59 | 60.71 | 43.98 |
| Electricity | 6.50 | 3.69 | 0.00 | 47.60 | 7.56 | 45.60 |
| BEP ($/ton $NH_3$) | 490.24 | 409.30 | 346.32 | 539.99 | 469.79 | 403.16 |
| Investment Cost Breakdown | TX-H-250 | TX-H-500 | TX-H-1000 | TX-H-250 | TX-H-500 | TX-H-1000 |
| Syngas Generation | 41.43 | 68.08 | 112.81 | 37.49 | 67.47 | 98.94 |
| Syngas Cleanup | 17.90 | 28.01 | 43.97 | 18.64 | 27.94 | 44.93 |
| Ammonia Syn. Loop | 38.90 | 61.64 | 97.72 | 38.90 | 61.64 | 99.05 |
| Water Electrolysis | 0.00 | 0.00 | 0.00 | 0.00 | 0.00 | 0.00 |
| Air Separation | 28.88 | 41.31 | 59.18 | 28.88 | 41.31 | 59.18 |
| H&P Integration | 20.15 | 32.79 | 53.73 | 12.46 | 31.77 | 33.08 |
| Wastewater Treat. | 9.96 | 15.74 | 24.67 | 8.71 | 15.68 | 20.99 |
| Total (MM$) | 157.47 | 247.95 | 392.72 | 145.19 | 246.19 | 356.76 |
| GHG Balances | TX-H-250 | TX-H-500 | TX-H-1000 | TX-H-250 | TX-H-500 | TX-H-1000 |
| Biomass | -9.493 | -19.148 | -38.841 | -8.243 | -18.904 | -32.403 |
| Natural Gas | 0.000 | 0.000 | 0.000 | 0.000 | 0.000 | 0.000 |
| Vented $CO_2$ | 10.686 | 21.562 | 43.742 | 9.233 | 21.280 | 36.402 |
| Seq. $CO_2$ | 0.000 | 0.000 | 0.000 | 0.000 | 0.000 | 0.000 |
| TGHG | 1.193 | 2.414 | 4.902 | 0.990 | 2.376 | 3.999 |
| GHGAE | -0.129 | -0.146 | 0.000 | -0.943 | -0.300 | -3.611 |
| GHGAN | 4.902 | 9.804 | 19.607 | 4.902 | 9.804 | 19.607 |
| GHG Index | 0.25 | 0.25 | 0.25 | 0.25 | 0.25 | 0.25 |

As expected, changing the selling price of hardwood, affects BEP of ammonia. 20% decrease of hardwood price, results in an average 6% decrease in BEP. The advantage of using cheaper feedstock becomes more articulate in larger scales, where the contribution of biomass to overall cost decrease while the remaining sections stay somewhat the same. Investment costs have large share in the overall cost in small scale plant, which decrease as the plants become larger. Electricity costs decrease with cheaper feedstock, since the plant generates its own power by combusting the biomass. Using biomass for generating power results in larger investment costs as evidenced by more expensive syngas generation section. This effect is further observed by an increase in vented $CO_2$ in GHG balances, and a decrease in GHGAE. When the selling price of hardwood is increased by 20%, ammonia BEP increase by an average of 7%. Total investment costs increase at small and medium capacities, but decrease in large capacity plant. This is caused by using electricity instead of biomass for power generation. This is also evidenced by the decreasing vented $CO_2$ amounts and increased GHGAE in the GHG balances. Figure 3.10 is used to illustrate

the effect of hardwood price explained in this section. A final sensitivity analysis is done for the

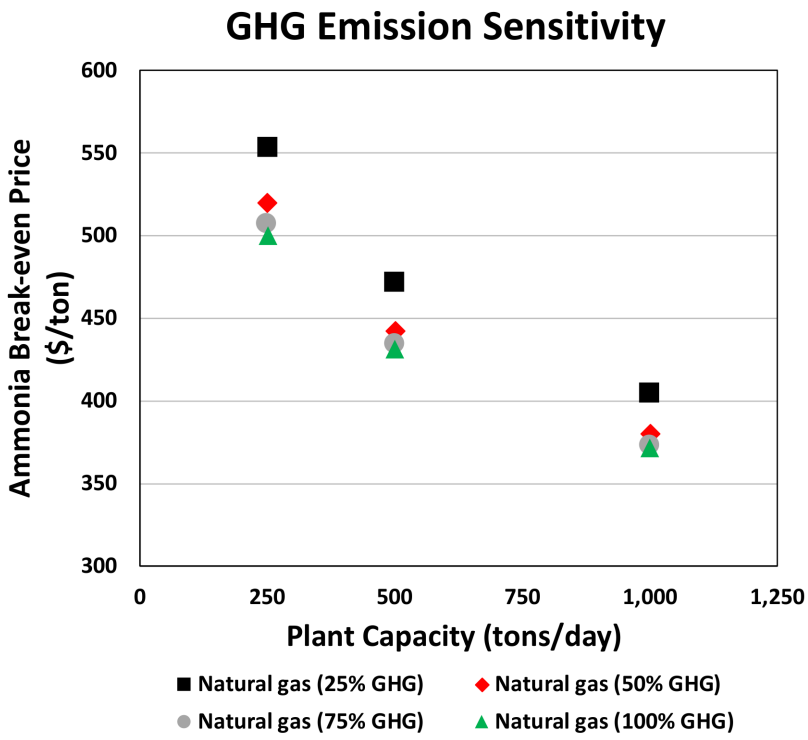


Figure 3.9: Effect of GHG emission limitations on break-even price of natural gas-based processes.

renewable levelized cost of electricity (LCOE). Earlier results show that economic performance of the wind- or solar-based ammonia production heavily depends the renewable LCOE. Table 3.12 shows how ammonia BEPs are affected by changes in renewable wind electricity prices. Tested values of renewable LCOE are between \$0.020/kWh and \$0.120/kWh. As the LCOE goes down to \$0.020/kWh, ammonia BEP prices become much more lower than previous values. However, electrolysis-based ammonia production is still more expensive than steam reforming of natural gas- or thermochemical conversion of biomass-based production for the state of Texas. While ammonia BEP becomes favorable with lower LCOE, such low LCOE might not be possible to achieve. In fact, due to intermittency problems with renewable resources; wind and solar power production

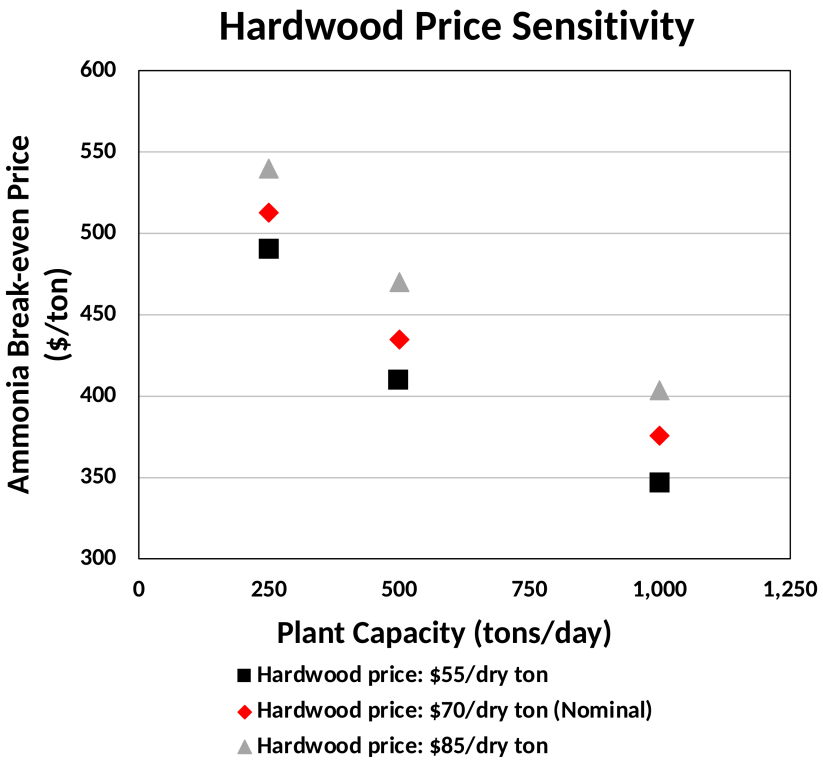


Figure 3.10: Effect of hardwood selling prices on break-even price of natural gas-based processes.

facilities should be coupled with storage technologies, if uninterrupted electricity supply is to be provided. Such storage technologies will undoubtedly increase the LCOE of renewable resources in the near future and make electrolysis-based production even more unfavorable, as shown by the sensitivity analysis.

## 3.5 Conclusions

This work investigates the effects of feedstock type, price, and availability on the sustainable ammonia production processes through a process synthesis and global optimization framework. The process superstructure contains multiple competing technologies for syngas generation, syngas cleanup, water electrolysis, and ammonia synthesis loop configurations to accommodate different fossil and renewable feedstocks. Investigated renewables include hardwood, corn stover, MSW, and water with wind and solar energy powering its electrolysis. Case studies are conducted for

Table 3.12: Sensitivity analysis for renewable LCOE.

| | **BEP ($/ton $NH_3$)** | | |
|---|---|---|---|
| Wind LCOE ($/kWh) | TX-W-250 | TX-W-500 | TX-W-1000 |
| 0.020 | 593.73 | 539.30 | 500.08 |
| 0.040 | 835.53 | 781.10 | 738.26 |
| 0.060 | 1077.33 | 1022.90 | 976.44 |
| 0.080 | 1319.13 | 1264.70 | 1214.62 |
| 0.100 | 1560.93 | 1506.50 | 1452.80 |
| 0.120 | 1802.73 | 1748.30 | 1690.98 |

feedstock availabilities and prices in Texas, California, and Iowa. The optimal process topology, total cost and investment costs breakdown, and GHG emission analyses for all the case studies are reported.

The results indicate that for bringing down the emissions from ammonia plants to 25% of the current level, biomass gasification is a more attractive choice over steam reforming of natural gas. In Texas, hardwood is up to 8% more profitable than natural gas. In California, due to expensive natural gas and electricity, using hardwood is 32% and MSW is 15% more profitable than using natural gas. In Iowa, natural gas, corn stover, and MSW-based productions do not have a significant advantage over each other. In general, hardwood type of biomass performed better than corn stover and MSW. For all the states under investigation, high wind and solar powered ammonia production costs indicate that wind and solar technologies need to further mature to become more competitive over other alternatives. Unless very strict GHG emission limitations or economic incentives are imposed, it is hard for these technologies to compete with other feedstocks. Biggest factor for this result is the low efficiency of water electrolysis as evidenced by its high energy consumption. In that respect, the authors would like to suggest that combining wind and solar resources with alternative ammonia production methods, such as electrochemical ammonia production, can be an interesting topic for future studies. One topic that has not been addressed in this work is the by-product water electrolysis, that is high-purity oxygen. While hydrogen is directly used in the ammonia synthesis section, oxygen, the other product of electrolysis, is not sold or even costed. If enough demand for this high-purity oxygen is available, this can positively affect the economic

performance of the electrolysis-based ammonia production.

The sensitivity analyses show that GHG emission limitations are key factors in performance of natural gas-based production. It is possible to bring the emission levels from 100% to 25%, with 9% increase in BEP. As expected, when the limitations are relaxed natural gas-based production gives lower ammonia BEP compared to nominal cases, especially in the state of Texas, where natural gas prices are lowest. Changing the selling price of hardwood biomass by 20% results in 6-7% increase or decrease in ammonia BEP. If the renewable LCOE goes down, ammonia BEP becomes more attractive. This might not be possible in the near future though; since uninterrupted renewable electricity supply requires currently not-existing storage units, which will cause the LCOE to be greater than the current prices.

The economic performance of ammonia production is very sensitive to both feedstock prices, electricity prices, and GHG emission restrictions. An increase natural gas price in the future, decrease in cost of renewable technologies, or implementation of carbon emission caps can open the door to significant penetration of renewables into the ammonia market.

# 4. MULTI-SCALE ENERGY SYSTEMS ENGINEERING APPROACH FOR RENEWABLE POWER GENERATION AND STORAGE OPTIMIZATION [1]

## 4.1 Energy Storage Technologies and Energy Vectors

Energy storage at grid-scale (GWh-scale) is one way to ensure the balance between the renewable power supply and demand and therefore improve the capacity utilization [75]. Energy storage in vectors, that are also called as dense energy carriers (DECs) offer the possibility of transporting stored energy from one location to another [183]. Hydrogen ($H_2$) and hydrogen-based DECs like, ammonia ($NH_3$), or methanol ($CH_3OH$) have orders of magnitude higher volumetric energy density compared to stationary storage options such as pumped storage-hydro (PSH), compressed air energy storage (CAES), or battery elecric storage (BES). The attributes of various technologies are shown in Table 4.1 for a more quantitative comparison [76].

Table 4.1: Energy storage technology comparison.

| Attribute | PSH | CAES | BES (Li-ion) | BES (NaS) | $H_2$ (l) | $H_2$ (g) | $NH_3$ (l) | $CH_3OH$ (l) |
|---|---|---|---|---|---|---|---|---|
| Energy density (kWh/L) | 0.001 | 0.005 | 0.2-0.7 | 0.3 | 2.5 | 1.0 | 4.3 | 4.6 |
| $H_2$ Content (wt.%) | - | - | - | - | 100.0 | 100.0 | 17.8 | 12.6 |
| $H_2$ Density (kg/m$^3$) | - | - | - | - | 71.2 | 24 - 40 | 105 | 99.8 |
| Storage T (°C) | 20 | 20 | -10-20 | 300-350 | -253 | 20 | -33 / 20 | 20 |
| Storage P (atm) | 1 | 300 | 1 | 1 | 1 | 350 / 700 | 1 / 10 | 1 |
| Storage range (GWh) | 1-100 | 0.01-10 | <0.01 | <0.01 | <10 | <10 | scalable | scalable |
| Power range (GW) | 1 | 0.3 | 0.01 | 0.01 | 0.01 | 0.01 | scalable | scalable |
| Storage duration | Months | Months | Hours | Hours | Weeks | Months | Months | Months |

Among the DEC, hydrogen stands out due to its high gravimetric energy density (33 kWh/kg) [184]. Hydrogen can make way for a low-carbon economy and research on the move to a hydrogen-economy has been the focus of discussions since the 1970s [185]. Japan recently became the first country to take a step towards hydrogen economy [186] and for stranded countries

[1] Reprinted with permission from "A Multiscale Energy Systems Engineering Approach for Renewable Power Generation and Storage Optimization" by Demirhan, C.D. and Tso, W.W. and Powell, J.B. and Heuberger, C.F. and Pistikopoulos, E.N., 2020, Industrial & Engineering Chemistry Research, Vol. 59, No. 16, pp. 7706–7721, Copyright 2020 by American Chemical Society.

with scarce resources and little available land, such as Japan, import of renewable DEC will be important [187]. However, hydrogen's low volumetric energy density under ambient conditions (0.003 kWh/L) is a drawback and extreme pressures or cryogenic temperatures are required for its large-scale storage and transportation [183]. Ammonia and methanol can be promising alternatives since they have higher volumetric energy density and more favorable storage conditions. They are readily produced in large amounts as commodities and they have their own distribution network [188]. Using ammonia and methanol as DEC can benefit from economies of scale if deployed in GWh-scale energy storage. An earlier supply chain optimization study by Tso et al. [189] on replacing Texas' partial power demand with renewable DEC shows that ammonia and methanol can be more attractive than hydrogen when seasonal and long-term storage is considered.

Optimization of design and operation of energy systems with time-varying resources is challenging. The previous work of Tso et al. [189] assumed performance coefficients for the dynamically operated units to approximate their aggregate output over a time horizon. While this approach is one way to consider the effect of intermittency, it tends to overestimate the process costs while underestimating the process efficiency. Furthermore, solving the process synthesis problem with the steady-state assumption and then solving the scheduling problem for that fixed design can at best result in suboptimal, if not infeasible, operation.

Thus, there is a need for simultaneous consideration of design and operation. This topic of optimization-based design and scheduling or planning and scheduling has been receiving increasing attention in the last few years in the process systems engineering community [190, 22]. Investigated topics include design and operation of power systems [191, 192], industrial demand-side management [193, 194], hydrogen networks [195], EV vehicle deployment strategies [196], ammonia production [127, 197, 198], solar power generation and storage systems [199, 200, 201, 202, 203], and power & fuels production [204, 205].

## 4.2 Modeling and Optimization of Renewable-based Energy Systems

### 4.2.1 Problem Definition

In order to analyze different scenarios involving renewable-based energy system networks, the temporal and spatial variability of renewable supply and power demand need to be explicitly considered in the optimization formulation. For this purpose, a multi-period and multi-location simultaneous design, operation, and supply chain strategy is developed. The multi-period formulation addresses the intermittency in the resource availability, whereas multi-location aspect allows for the production and transportation of DECs between high- and low-potential regions. The overall approach is multi-scale by nature since it deals with problems of multiple time and length scales that are design, scheduling, and supply chain. The pictorial representation of the such a framework is shown in Figure 4.1.

This design, operation, and supply chain strategy should take the following as inputs:

- the time-dependent solar and wind resource availability at each location,
- the time-dependent profile of the power load demand at each location,
- the detailed process input-output and costing information for power generation, storage, and DEC production technologies,
- the operational limitations such as maximum production rate changes and operating mode switches,
- the available transportation and storage infrastructure.

And return the optimal solution that includes:

- the process and storage unit capacities,
- the time-dependent production rates in each process,
- the material and energy flow rates between processes in the process network,
- the unit commitment and operating mode selections for power production, storage, and DEC production technologies,
- the inventory management for storage of resources,

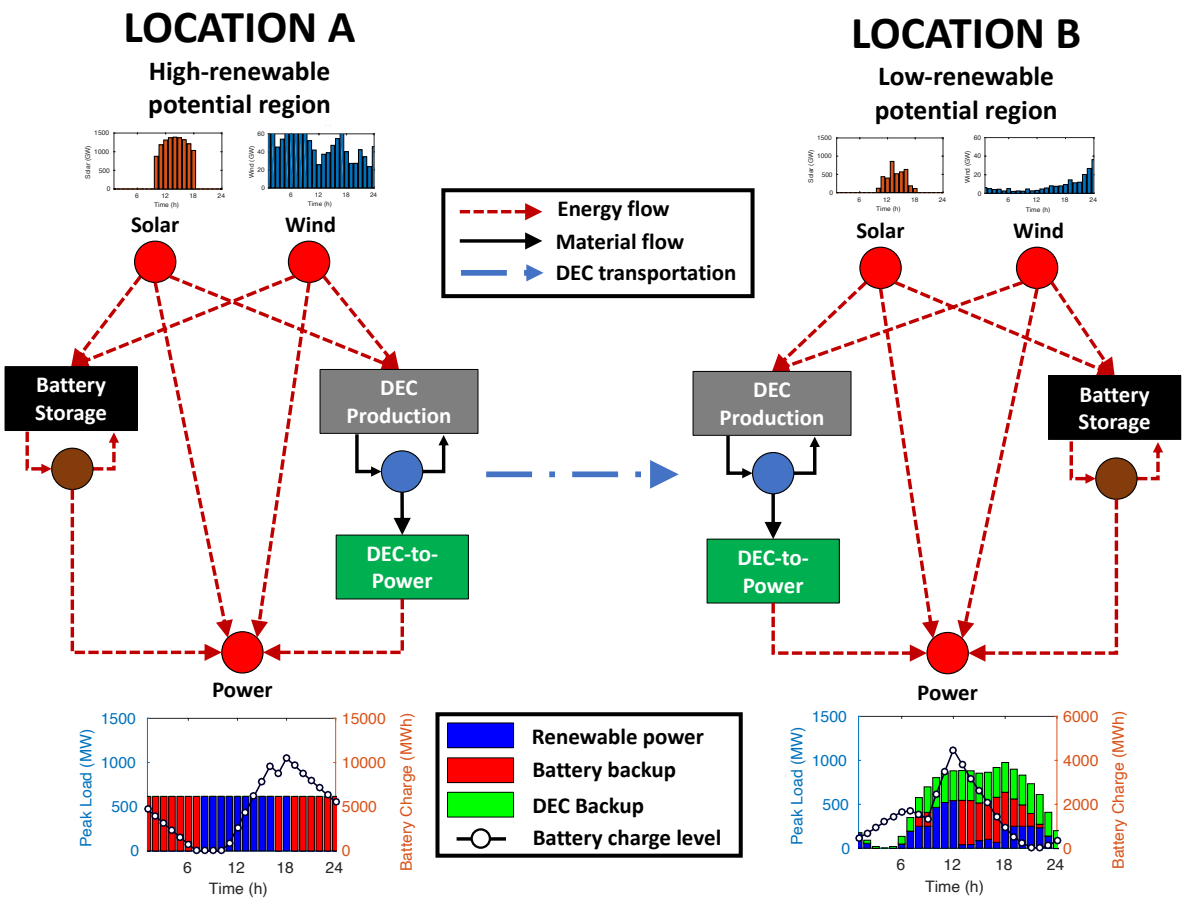


Figure 4.1: Conceptual depiction of novel power generation and storage networks.

- the transportation flows of DEC.

In the following sections, the details of the modeling and optimization formulation will be described.

### 4.2.2 Resource-Task Network Representation

This work uses a resource-task network (RTN) formulation [206], where the resources can be purchased, consumed, generated, sold, stored, or transported to a different location and the processes can convert material and/or energy resources to other resources. The renewable resource availability changes during the day so the temporal space is discretized for multi-period operational decisions. Inventory constraints keep track of all the resources entering and leaving the process network in one location and connect the consecutive time periods. All the input-output

relationships are linearly correlated.

### 4.2.3 Process Network Superstructure

Figure 4.2 shows the superstructure for the renewable-based energy generation and storage process network. The resources are represented by circles and the processes by rectangles. Although all the resources and the processes are modeled in the same way and can be represented with a few generic constraints, a color code is used to help the readers better visualize interaction between different resource and process types. Dark blue and light blue circles represent material resources that can be stored and cannot be stored, respectively. Similarly, brown and red circles represent the energy resources that can be stored and cannot be stored, respectively. The solid black lines with arrows show the unidirectional material flows (in kg/h) between the processes and the energy flows (in MW) are shown by dashed red lines. Grey rectangles show the conversion processes that are converting mainly material resources to other materials, that can consume or generate power or heat. Black colored rectangles show the energy storage processes that convert electrical power that cannot be stored by itself to a form that can be stored such as battery charge or elevated water. Green rectangles are indicating back-to-power processes, that convert fuels or energy carriers to power that is used to meet the power load demand.

In the process network, the sources of renewable power are solar and wind. The modeled processes include power generation from solar PV and wind farms and stationary energy storage (SES) options like sodium-sulfur (NaS) BES, PSH, and CAES, that can store power in battery charge, elevated water, and compressed air, respectively. SES technologies consist of storage and power conversion systems (PCS) to store and convert stored resources back to power, respectively. Hydrogen is produced from water using electrolyzers. Hydrogen can be stored either as a cryogenic liquid or a pressurized gas in liquefaction or compression processes, respectively. Haber-Bosch process is used for ammonia synthesis from high-purity hydrogen coming from the electrolyzers and nitrogen coming from the air separation unit (ASU). Carbon dioxide is captured from air with the direct air capture (DAC) unit. Hydrogen and carbon dioxide are sent to a reverse water-gas shift (R-WGS) unit to produce syngas that is later sent to a methanol synthesis unit to produce methanol.

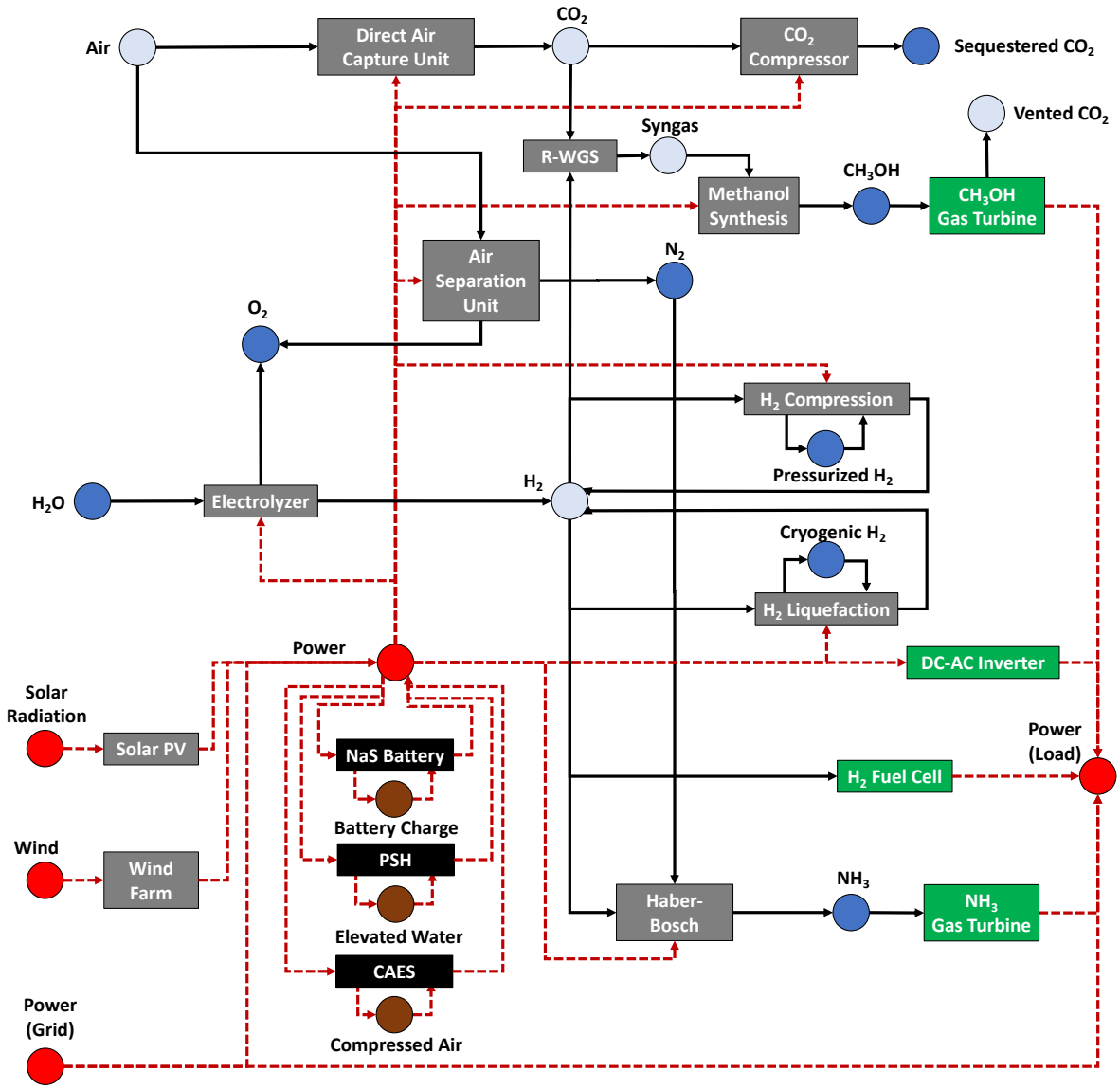


Figure 4.2: Process network superstructure for renewable power generation and storage pathways and technologies.

The stored DECs can be transported to a different location by railroad or trucks. Hydrogen, ammonia, and methanol can be converted back to power using $H_2$ fuel cell, $NH_3$ gas turbine, or $CH_3OH$ gas turbine, respectively. Power outputs of solar PV and wind farm, and many other processes are in dc form, which need to be converted to ac with an inverter unit in order to be sent to the power grid. The outputs of fuel cell and gas turbines are in AC. Additionally, electricity

from the local grid can be purchased at a price for backup power.

The input-output parameters for all the processes are taken from previously studied MINLP-based design problems as described in Chapter 3. The full process models are given in Appendix C.

### 4.2.4 Time Representation and Data Clustering

The availability of wind and solar resources exhibits both daily and seasonal variation. Hence, the temporal space needs to be discretized. Daily solar irradiation can be approximated with a handful of discrete regimes, while wind speed fluctuates almost all the time. In order to successfully integrate wind and solar energy with the energy storage and DEC production processes, hourly resolution is used for discretization. This means, the RTN model has continuous and discrete decision variables for every time step of the horizon. Modeling the optimization problem for an entire year (8760 time steps/periods) can capture a lot of variability, however, it makes the problem intractable, as the size of multi-period problems scales linearly with the total number of periods considered [207].

In order to reduce the computational burden of solving a simultaneous design and operation problem while considering a significant portion of the resource variability, a small subset of time periods is used that capture the characteristics of variability in a few representative periods similar to the works of Heuberger et al. [208], Lara et al. [209], and Zhang et al. [205]. With this time representation (depicted in Figure 4.3), weights are assigned to characteristic time periods to indicate their overall contribution to the annual operation. Each characteristic time period is named a season. For this study, the length of a season is selected as a day (i.e. 24 hours). The weight of a season corresponds to the number of times that a representative season is observed in a year. By the concept of cycling a season as many times as its weight, a year can be simulated without increasing the problem size.

For computational efficiency, the largest variability in resources should be captured with the least number of representative seasons. K-means clustering is a popular approach in the literature to reduce large data sets into a small number of clusters. It is easy to implement, however,

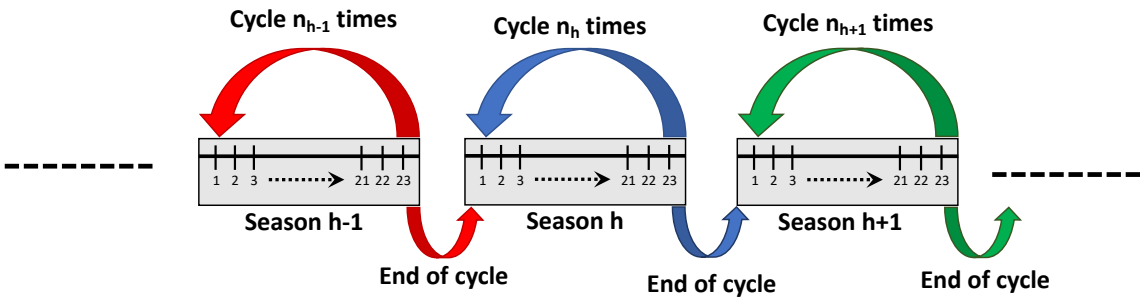


Figure 4.3: An illustration of the representative seasons. Each representative season is cycled (repeated) according to its cluster size obtained from the AHC analysis before moving the next one. This approach assigns a weight to each season without growing the size of the optimization problem.

the quality of the clusters is initialization dependent. Also, k-means clustering approach alone does not preserve the time chronology while constructing representative days. As an alternative, hierarchical clustering techniques offer some advantages [112, 113]. In their recent work, Pineda and Morales [114] used agglomerative hierarchical clustering (AHC) to find representative weeks, days, and hours in a capacity expansion planning problem. They use a bottom-up approach that identifies clusters that are closest to each other and merge them using a distance matrix. In this work, their strategy is applied to cluster hourly data consisting of wind speed, solar irradiation, electricity prices, and power load. A cutoff criteria of 1% within cluster variation is used to choose the number of clusters. The details of the AHC implementation is explained in the work of Tso et al. [210].

### 4.2.5 Mathematical Model

The complete mixed-integer linear programming (MILP) model consists of: (i) the network design constraints for production and storage facilities, (ii) the operating mode selection with ramp up/down constraints, (iii) the resource balance constraints, (iv) the seasonal continuity constraints, (v) the investment and operational cost functions, and (vi) the objective function. The complete mathematical model with the nomenclature and the modeling parameters are presented in Appendices A and B, respectively. The full optimization model is presented below.

#### 4.2.5.1 Network Design Constraints

Equations for network design, that allow for processes i and storage vessels for resources j to be selected or not are shown in Equations 4.1 and 4.2:

$$CAP^{P}_{a,i} \leq CAP^{P-max}_{i} x^{P}_{a,i} \quad \forall a, i \tag{4.1}$$

$$CAP^{S}_{a,j} \leq CAP^{S-max}_{j} x^{S}_{a,j} \quad \forall a, j \tag{4.2}$$

#### 4.2.5.2 Operating Mode Selection and Ramp Up and Down Constraints

Each process i can have multiple modes m among which only one can be selected at a time t. Equations for mode selection are shown in Equations 4.3 to 4.8:

$$\sum_{m \in Modes_{i,m}} y_{a,i,m,h,t} = x^{P}_{a,i} \quad \forall a, i, h \in Season_h, t \in Time_{h,t} \tag{4.3}$$

$$P_{a,i,h,t} = \sum_{m \in Modes_{i,m}} P^{m}_{a,i,m,h,t} \quad \forall a, i, h \in Season_h, t \in Time_{h,t} \tag{4.4}$$

$$P^{m}_{a,i,m,h,t} \geq CAP^{Pm-min}_{i,m} Cap^{P}_{a,i} \quad \forall i, m \in Modes_{i,m}, h, t \in Time_{h,t} \tag{4.5}$$

$$P^{m}_{a,i,m,h,t} \leq CAP^{Pm-max}_{i,m} Cap^{P}_{a,i} \quad \forall a, i, m \in Modes_{i,m}, h, t \in Time_{h,t} \tag{4.6}$$

$$P^{m}_{a,i,m,h,t} \geq CAP^{Mode-min}_{i,m} y_{a,i,m,h,t} \quad \forall a, i, m \in Modes_{i,m}, h, t \in Time_{h,t} \tag{4.7}$$

$$P^{m}_{a,i,m,h,t} \leq CAP^{Mode-max}_{i,m} y_{a,i,m,h,t} \quad \forall a, i, m \in Modes_{i,m}, h, t \in Time_{h,t} \tag{4.8}$$

Equations 4.5 and 4.6 set the lower and upper bounds of the production range of mode m of process i. During dynamic operation, a processing unit might change its throughput in a fixed mode or switch to a different mode. Below are the equations used to represent mode switch. Equations 4.9 and 4.10 bound the up ramping and down ramping rates of throughput of a unit by using a big-M

parameter to bound change of $P^m_{i,m,h,t}$ between consecutive time periods t-1 and t.

$$P^m_{a,i,m,h,t} - P^m_{a,i,m,h,t-1} \geq -\Delta Rate^{max}_{i,m} - M(2 - y_{a,i,m,h,t} - y_{a,i,m,h,t-1}) \quad \forall a, i, m \in Modes_{i,m}, h, t \in Time_{h,t} \tag{4.9}$$

$$P^m_{a,i,m,h,t} - P^m_{a,i,m,h,t-1} \leq \Delta Rate^{max}_{i,m} + M(2 - y_{a,i,m,h,t} - y_{a,i,m,h,t-1}) \quad \forall a, i, m \in Modes_{i,m}, h, t \in Time_{h,t} \tag{4.10}$$

Equation 4.11 is used to designate mode switch. The binary variable $z_{i,m',m,h,t-1}$ is equal to 1 process i switches from mode m to m' at time t of season h:

$$\sum_{m' \in Trans_{i,m,m'}} z_{a,i,m',m,h,t-1} - \sum_{m \in Trans_{i,m',m}} z_{a,i,m,m',h,t-1} = y_{a,i,m,h,t} - y_{a,i,m,h,t-1} \quad \forall a, i, m \in Modes_{i,m}, h, t \in Time_{h,t} \tag{4.11}$$

Equations 4.12 and 4.13 put restrictions on the minimum time required to switch between modes and a sequence that needs to be followed in case it is required, respectively.

$$y_{a,i,m',h,t} \geq \sum_{k=1}^{\theta_{i,m,m'}} z_{a,i,m,m',h,t-k} \quad \forall i, (m, m') \in TransModes_{i,m,m'}, a, h, t \in Time_{h,t} \tag{4.12}$$

$$z_{a,i,m,m',h,t-\bar{\theta}_{i,m,m',m''}} = z_{a,i,m',m'',h,t} \quad \forall a, i, (m, m', m'') \in Seq_{i,m,m',m''}, h, t \in Time_{h,t} \tag{4.13}$$

#### *4.2.5.3 General Resource Balance Constraints*

The mass balance for each resource is written in terms of inventory balances in the network. Equation 4.14 is a total mass balance for resource j at any time t in season h.

$$
\begin{aligned}
Inv_{a,j,h,t} = (1 - Loss_{j,h}) Inv_{a,j,h,t-1} + \sum_{i} \sum_{m \in Modes_{i,m}} Conversion_{i,m,j,t} P^{m}_{a,i,m,h,t} \\
+ B_{a,j,h,t} - S_{a,j,h,t} \\
+ \sum_{a',q} (1 - Loss^{trans}_{a,a',j,q}) Trans_{a',a,j,q,h,t} - Trans_{a,a',j,q,h,t} \\
\forall a, j, h, t \in Time_{h,t}
\end{aligned}
\tag{4.14}
$$

$Conversion_{i,m,j,t}$ is a parameter that sets the input-output relationships for each process that are written with respect to the reference resource j for each mode m of process i. The full list of inputs and outputs to processes are given in Appendix C. Equations 4.15 and 4.16 sets upper bounds for nameplate process and inventory storage capacities, respectively:

$$P_{a,i,h,t} \leq Cap^{P}_{a,i} \quad \forall a, i, h, t \in Time_{h,t} \tag{4.15}$$

$$Inv_{a,j,h,t} \leq Cap^{S}_{a,j} \quad \forall a, j, h, t \in Time_{h,t} \tag{4.16}$$

Supply and demand constraints are written for each resource j in forms of Equations 4.17 to 4.19:

$$B_{a,j,h,t} \leq B^{max}_{a,j,h,t} \quad \forall a, j, h, t \in Time_{h,t} \tag{4.17}$$

$$S_{a,j,h,t} \leq D_{a,j,h,t} \quad \forall a, j \in Demand_{j}, h, t \in Time_{h,t} \tag{4.18}$$

$$S_{a,j,h,t} = 0 \quad \forall a, j \in NoDischarge_{j}, h, t \in Time_{h,t} \tag{4.19}$$

#### *4.2.5.4 Seasonal Continuity Constraints*

Equations ranging from 4.20 to 4.26 show the connection between subsequent seasons, where $n_h$ is the number of times a season is cycled. The continuity condition shows that inventory needs to be accumulated over the course of a season and carried over to the next one. These constraints

are adapted from [205].

$$y_{a,i,m,h,0} = y_{a,i,m,h,|Time_{h,t}|} \quad \forall a, i, m \in Modes_{i,m}, h \tag{4.20}$$

$$z_{a,i,m,m',h,t} = z_{a,i,m,m',h,t+|Time_{h,t}|} \quad \forall a, i, (m, m') \in TransModes_{i,m,m'}, h, -\theta_i^{max} - 1 \leq t \leq -1 \tag{4.21}$$

$$y_{a,i,m,h,|Time_{h,t}|} = y_{a,i,m,h+1,0} \quad \forall a, i, m \in Modes_{i,m}, h \in Season_h \setminus |Season_h| \tag{4.22}$$

$$z_{a,i,m,m',h,t+|Time_{h,t}|} = z_{a,i,m,m',h+1,t} \quad \forall a, i, (m, m') \in TransModes_{i,m,m'}, h \in Season_h \setminus |Season_h|, -\theta_i^{max} - 1 \leq t \leq -1 \tag{4.23}$$

$$Inv_{a,j,h}^{excess} = Inv_{a,j,h,|Time_{h,t}|} - Inv_{a,j,h,0} \quad \forall a, j, h \tag{4.24}$$

$$Inv_{a,j,h,0} + n_h Inv_{a,j,h}^{excess} = Inv_{a,j,h+1,0} \quad \forall a, j, h \in Season_h \setminus |Season_h| \tag{4.25}$$

$$Inv_{a,j,|Season_h|,0} + n_{|Season_h|} Inv_{a,j,|Season_h|}^{excess} = Inv_{a,j,1,0} \quad \forall a, j \tag{4.26}$$

#### *4.2.5.5 Investment and Operational Cost Functions*

Capital investment cost are approximated by piecewise linear functions of the processing plant capacities as shown in Equations 4.27 to 4.30:

$$Cap_{a,i}^{P} = \sum_{l \in PL_{i,l}} \left[ \lambda_{a,i,j} (CAP_{i,l-1}^{segment} - CAP_{i,l}^{segment}) + CAP_{i,l}^{segment} w_{a,i,l} \right] \quad \forall a, i \tag{4.27}$$

$$Capex_{a,i} = \sum_{l \in PL_{i,l}} \left[\lambda_{a,i,j}(CAPEX^{segment}_{i,l-1} - CAPEX^{segment}_{i,l}) + CAPEX^{segment}_{i,l} w_{a,i,l}\right] \quad \forall a, i \tag{4.28}$$

$$\lambda_{a,i,l} \leq w_{a,i,l} \quad \forall a, (i,l) \in PL_{i,l} \tag{4.29}$$

$$\sum_{l \in PL_{i,l}} w_{a,i,l} = x^{P}_{a,i} \quad \forall i \tag{4.30}$$

Total capital expenses consist of sum of unit investment costs, storage costs, and the land purchase costs as given in Equation 4.31:

$$\begin{aligned} Capex^{total}_{a} = &\sum_{i} \left[Capex_{a,i} + Cost^{land}_{a,i} Cap^{P}_{a,i}\right] \\ &+ \sum_{j} \left[Cost^{S-fixed}_{j} x^{S}_{a,j} + Cost^{S-var}_{j} Cap^{S}_{a,j}\right] \end{aligned} \tag{4.31}$$

Operational expenses as shown in Equation 4.32 are the sum of unit processing costs, resource purchase and discharge costs:

$$\begin{aligned} Opex_a = \sum_{h} \sum_{t \in Time_{h,t}} n_h \Bigg[ &\sum_{i} \sum_{m \in Modes_{i,m}} (Cost^{P-fixed}_{i,m,h} y_{a,i,m,h,t} + Cost^{P-var}_{i,m,h} P^{m}_{a,i,m,h,t}) \\ &+ \sum_{j} Cost^{Purchase}_{a,j,h,t} B_{a,j,h,t}/\rho_j + Cost^{Discharge}_{a,j,h,t} S_{a,j,h,t}/\rho_j \Bigg] \end{aligned} \tag{4.32}$$

Transportation costs are calculated using Equation 4.33:

$$\begin{aligned} Trans^{total}_{j,q} = \sum_{h} \sum_{t \in Time_{h,t}} n_h \Bigg[ &\sum_{a} \sum_{a'} Cost^{trans-fix}_{j,q} \\ &+ Cost^{trans-var}_{j,q} Distance_{a,a'} Trans_{a,a',j,q,h,t} \Bigg] \\ &\forall (j,q) \in TPModes_{j,q} \end{aligned} \tag{4.33}$$

#### *4.2.5.6 Objective Function*

The model is solved to minimize the annualized production cost of meeting the power demand. This is also called the levelized cost of electricity (LCOE). For this purpose, total capital investment is annualized using 8% annual discount rate. Sum of annualized capital cost and operational costs gives the objective function value $TotalCost$ as shown in Equation 4.34:

$$TotalCost = \sum_{a} \Big[ (0.08) Capex_a^{total} + Opex_a \Big] + \sum_{j,q \in TPModes_{j,q}} Trans_{j,q}^{total} \tag{4.34}$$

The resulting optimization problem is:

$$\begin{aligned} \min \quad & (Equation \quad 4.34) \\ \text{s.t.} \quad & Equations \quad 4.1 - 4.33 \end{aligned} \tag{4.35}$$

## 4.3 Computational Studies

### 4.3.1 Case Studies

The simultaneous design and operation strategy is used to investigate the impact of DEC production in a high renewable energy potential region in Amarillo, Texas to reduce the cost of renewable energy penetration in a low renewable energy potential region in New York City, New York. For simplicity the locations are referred to as TX and NY, from this point on. The problem is illustrated in Figure 4.4.

With the computational studies, the following questions are aimed to be answered: (a) Can the high renewable potential in Texas be used to partially power a city in a low renewable potential region in the Northeast (e.g. New York City)? (b) Can DECs be used to transport the renewable energy in Texas to the Northeast? (c) How would this compare against using the local renewable potential and battery storage in the Northeast? (d) What should be the targeted energy demand (e.g. base load or peak matching)? (e) What renewable energy penetration would give the best economic return?

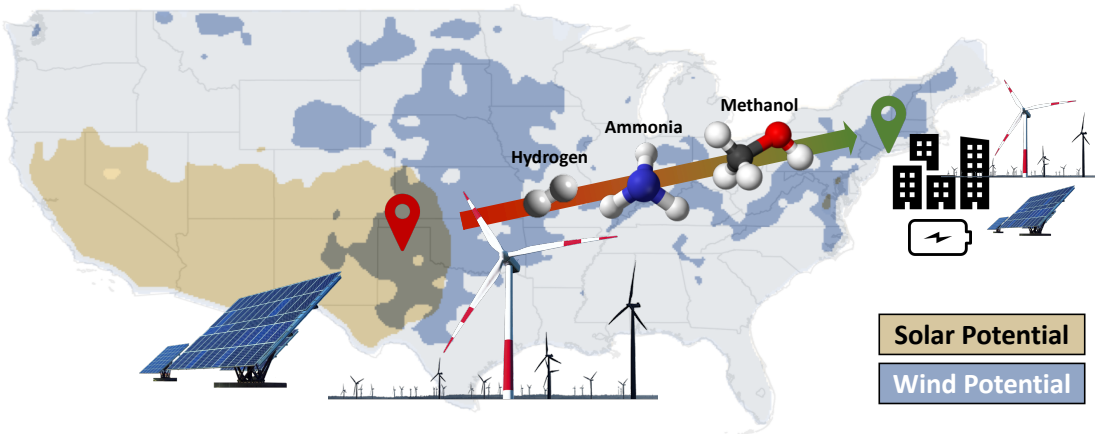


Figure 4.4: Illustration of the DEC supply chain problem.

The objective of the optimization problem is to minimize the levelized cost of electricity (LCOE) of meeting the power demand. Case studies are investigated for (i) base load matching (BL) and (ii) peak demand matching (PM) relying only on solar and wind resources in TX or NY. The total annual power demand replaced by renewables in both studies is the same and it accounts for 10% of NY's annual power demand, that is 5,430 GWh. For both case studies, three scenarios are investigated. Scenario 1 focuses on local power production and battery storage in NY. The base case for all comparisons is solar PV and BES-based renewable power generation and storage. In scenario 2, renewable energy is produced and stored in DECs in TX using both solar and wind energy. DECs are later transported to NY where they are converted to power with power conversion technologies. Scenario 3 investigates production of DEC in TX together with local power production and battery storage in NY. In scenarios 2 and 3, by considering multiple sites, design, scheduling, and supply chain decisions are optimized at the same time.

Each case investigated is referred to with a unique case ID that has with four indicators: [Demand Profile]-[Scenario]-[DEC in TX]-[Renewable Energy (RE) in NY]. To give an example: BL-1-x-SW indicates a case where the demand profile is base load, the scenario under investigation is 1, there is no DEC production (its non-existence is showed with "x"), and solar (S) and wind (W) resources in NY are used. PM-3-HA-S indicates peak matching (PM) profile with scenario 3,

with hydrogen (H) and ammonia (A) production in TX along with local solar (S) energy use in NY. In scenarios 2 and 3, where DECs are produced in TX, both solar and wind resources are allowed to be used for power production. The full list of the investigated cases in this work is presented in Table 4.2.

Table 4.2: List of the investigated cases.

| Case ID | Demand Profile | DEC in TX | RE in NY | Case ID | Demand Profile | DEC in TX | RE in NY |
|---|---|---|---|---|---|---|---|
| BL-1-x-S | Base load | - | S | PM-1-x-S | Peak matching | - | S |
| BL-1-x-SW | Base load | - | S, W | PM-1-x-SW | Peak matching | - | S, W |
| BL-2-H-x | Base load | H | - | PM-2-H-x | Peak matching | H | - |
| BL-2-HA-x | Base load | H, A | - | PM-2-HA-x | Peak matching | H, A | - |
| BL-2-HM-x | Base load | H, M | - | PM-2-HM-x | Peak matching | H, M | - |
| BL-3-H-S | Base load | H | S | PM-3-H-S | Peak matching | H | S |
| BL-3-HA-S | Base load | H, A | S | PM-3-HA-S | Peak matching | H, A | S |
| BL-3-HM-S | Base load | H, M | S | PM-3-HM-S | Peak matching | H, M | S |
| BL-3-H-SW | Base load | H | S, W | PM-3-H-SW | Peak matching | H | S, W |
| BL-3-HA-SW | Base load | H, A | S, W | PM-3-HA-SW | Peak matching | H, A | S, W |
| BL-3-HM-SW | Base load | H, M | S, W | PM-3-HM-SW | Peak matching | H, M | S, W |

All case studies are solved on a high-performance computing (HPC) machine at Texas A&M High-Performance Research Computing facility using Ada IBM/Lenovo x86 HPC Cluster operated with Linux (CentOS 6) using 1 node (20 cores per node with 64 GB RAM). CPLEX 12.8 solver is used with GAMS 26.1.0. The solution time is limited to 24 hours.

### 4.3.2 Modeling Assumptions

Below are given the modeling assumptions and some of the modeling parameters used for the computational studies. The full list of modeling parameters are presented in Appendix C.

- The only sources of power are solar and wind resources.
- Grid electricity purchase is not allowed for any case study.
- Location dependent solar direct normal irradiation (DNI) and wind speed are taken from NSRDB [18] and Wind Toolkit [19]. Wind speed is taken at 80 m.
- Available land for solar energy in Texas and New York are 1,459 and 839 $km^2$, respectively [211].

- Available land for wind farms in Amarillo, Texas and New York City, New York are 1,700 and 164 $km^2$ [211].
- Renewable electricity provided to the grid is not sold at a price.
- Water purchase cost is \$0.4/ton. Water availability does not have an upper bound.
- Electricity prices from Texas are taken from Ercot resources [212], whereas the electricity prices and load demand information for NY are taken from LCG Consulting's website [213].
- Solar DNI, wind speed, load demand, and electricity prices are clustered together using AHC method.
- 12 representative seasons are used.
- Investment cost parameters are location independent.
- Investment costs are annualized such that 8% of the total overnight cost is paid annually.
- Hydrogen can be stored as compressed gas at 700 bar and 20°C or a cryogenic liquid at 1 atm and -259°C.
- Available transportation modes are railroad and truck.
- Time lag in transportation is not considered. Instead, 20% of cryogenic hydrogen and 3% of ammonia are assumed boil-off during transportation. Boil-off of methanol and compressed hydrogen are assumed to be negligible.
- All processing units have ramping constraints.
- PSH and CAES technologies are not considered in the process network for the case studies.
- NaS-type baterries are considered for the case studies. Battery storage self-discharge rate is 8%/day.

Available technologies for each location are listed in Table 4.3:

### 4.3.3 Clustered Data for the Case Studies

Solar and wind resource potentials given in $W/m^2$ and m/s, respectively are converted to their MW-equivalent resource availabilities using Equations 4.36 and 4.37:

$$B^{max}_{a,Solar,h,t} = (Solar\ DNI)(Land^{max}_{a,Solar}) \tag{4.36}$$

Table 4.3: List of available technologies for each location.

| Technology | Texas | New York |
|---|---|---|
| Solar PV | Y | Y |
| Wind Farm | Y | Y |
| Electrolyzer | Y | - |
| Air Separation Unit | Y | - |
| Haber-Bosch Process | Y | - |
| $CH_3OH$ Synthesis | Y | - |
| Direct Air Capture | Y | - |
| $H_2$ Compression | Y | Y |
| $H_2$ Liquefaction | Y | Y |
| NaS BES/PCS | Y | Y |
| $H_2$ Fuel Cell | - | Y |
| $NH_3$ Gas Turbine | - | Y |
| $CH_3OH$ Gas Turbine | - | Y |
| dc-ac Inverter | - | Y |

$$B^{max}_{a,Wind,h,t} = \frac{1}{2}\rho_{air}\pi(SA)^2(Wind\ Speed)^3(Land^{max}_{a,Wind})(10^{-6}) \tag{4.37}$$

Where $B^{max}_{a,Solar,h,t}$ and $B^{max}_{a,Solar,h,t}$ are solar and wind resource availability in MW, $\rho_{air}$ is the density of air given in kg/m$^3$, $SA$ is the swept area by the rotor blades (where rotor blade diameter is 108 m), wit $Land^{max}_{a,Solar}$ and $Land^{max}_{a,Wind}$ are the maximum land available for solar and wind energy, respectively.

Solar and wind availabilities in TX and NY for all representative seasons along the weights of the seasons are shown in Figures 4.5 and 4.6. The same scale on solar and wind energy potential is used in both figures to quantitatively compare renewable potentials in two locations. From Figures 4.5 and 4.6 it is observed that TX has a significant advantage over NY in both solar and wind energy potential. This is not surprising, since TX is the nation's leading wind energy producer. Solar energy potential in TX is also extremely promising due to availability of land and consistent solar irradiation profiles. It is interesting to note from Figure 4.5, that most of the time the peak solar and wind energy in TX are asynchronous. Solar energy has a consistent presence from morning to early evening, whereas wind energy potential more often than not peaks from night to early morning. This creates a potential for synergy in integrating solar and wind, since one resource can take over the power load when the other fades. Figure 4.6 indicates that while NY has some potential for solar energy production, even though the solar availability is less consistent compared to that in

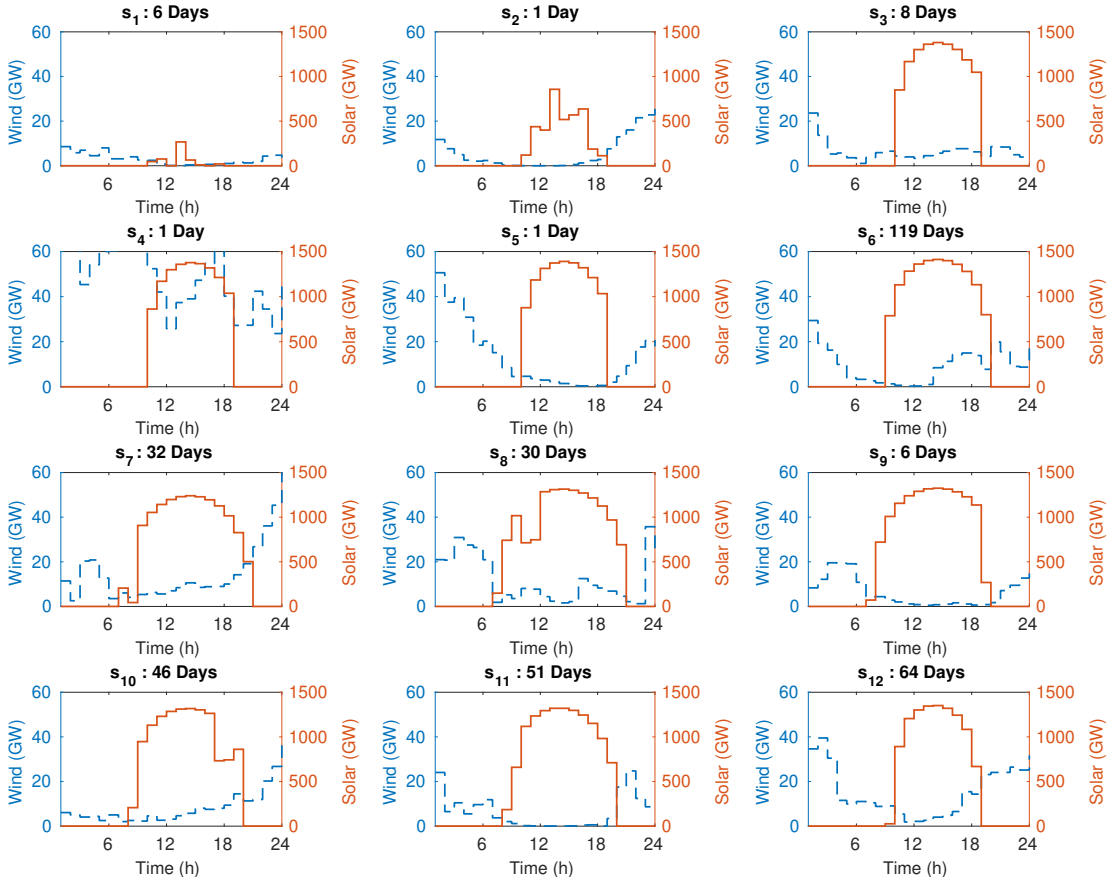


Figure 4.5: Solar (straight lines) and wind (dashed lines) potential of representative seasons in TX.

TX. Although high wind speeds are observed in NY, the available land for wind energy production is significantly small. As a result, the wind potential is orders of magnitude lower compared to that in TX. NY's solar energy has a much higher potential than its wind energy.

Figure 4.7 shows the power load demand profiles for base load and peak matching cases. Peak matching requires significant ramp up and down requirements as the power demand increases towards the evening, whereas base load requires a constant output of renewable power. A close inspection of Figures 4.5, 4.6, and 4.7 reveals that there is enough solar or wind potential in TX to meet the chosen power demand in NY. Although NY's wind potential is low, the local solar potential is strong enough to meet the the power demand in many seasons.

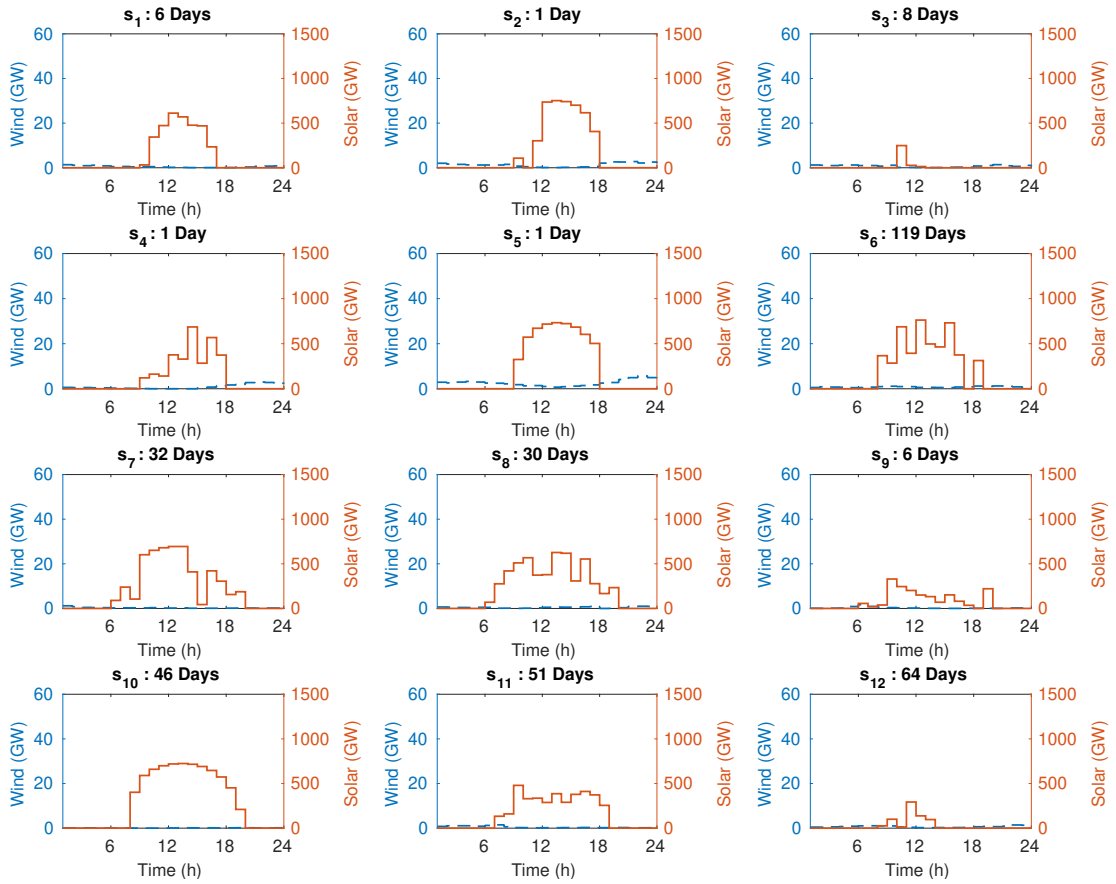


Figure 4.6: Solar (straight lines) and wind (dashed lines) potential of representative seasons in NY.

## 4.4 Results and Discussion

10% of NYC's power load demand is equivalent to 5,430 GWh per year. Base load and peak matching examples are investigated in case studies I and II, respectively. In this section, a total of six examples will be investigated in detail. Table 4.4 presents the location-dependent generation and storage capacity, power and DEC production, whereas Table 4.5 presents the location-dependent CAPEX and OPEX for selected examples. Figure 4.8 shows the total annual cost breakdown of capital and operating costs. The full set of results for all the cases that are previously described in Table 4.2 can be found in Tables D.1 to D.4 of Appendix D.

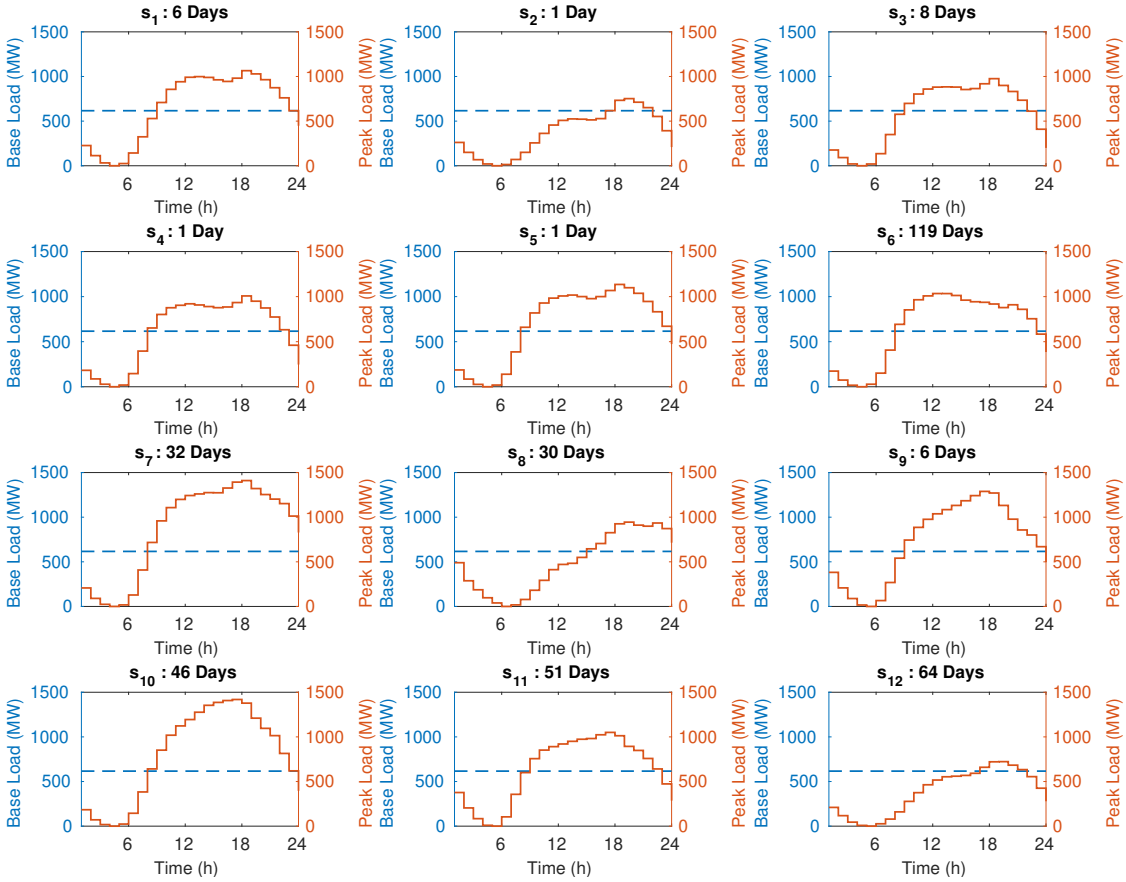


Figure 4.7: NY Power load demand profiles of base load (dashed lines) and peak load (straight lines) matching cases.

### 4.4.1 Case Study I: Base Load Matching

The first case study investigates the cost of meeting a constant base load for the entire year. To illustrate how DECs can improve local renewable energy generation and storage, the following examples are compared: BL-1-x-S, BL-2-H-x, and BL-3-H-S. Top three entries in Tables 4.4 and 4.5 show the details of these example cases.

BL-1-x-S case shows that, solar potential in NY is strong enough to penetrate 10% of the power demand. However, due to intermittency both the solar PV and the battery storage capacity need to be oversized to meet the power demand feasibility conditions. 17.49 GWh of BES capacity to provide 10% solar-based continuous power is the main drawback in relying solely on local solar energy potential. Due to the losses during storage, the total renewable energy that needs to be

Table 4.4: Renewable energy generation and storage capacity and DEC production targets for selected case studies.

| Case ID | LCOE ($/kWh) | TX-RE Cap. (GW) | TX-NaS (GWh) | TX-RE Gen. (GWh/a) | NY-RE Cap. (GW) | NY-NaS (GWh) | NY-RE Gen. (GWh/a) | Hydrogen (ton/a) |
|---|---|---|---|---|---|---|---|---|
| BL-1-x-S | 0.284 | 0 | 0 | 0 | 10.51 | 17.42 | 6,493 | 0 |
| BL-2-H-x | 0.341 | 4.94 | 0 | 22,962 | 0 | 0 | 0 | 330,921 |
| BL-3-H-S | 0.157 | 0.38 | 0 | 1,796 | 2.43 | 10.49 | 6,164 | 26,199 |
| PM-1-x-SW | 0.142 | 0 | 0 | 0 | 3.7 | 8.29 | 6,255 | 0 |
| PM-2-H-x | 0.371 | 5.15 | 0 | 23,048 | 0 | 0 | 0 | 333,034 |
| PM-3-H-SW | 0.109 | 0.09 | 0 | 640 | 1.95 | 5.19 | 6,025 | 9,166 |

Table 4.5: CAPEX and OPEX for selected case studies.

| Case ID | LCOE ($/kWh) | Tot. Cost ($ MM/a) | Tot. CAPEX ($ MM) | TX-CAPEX/a ($ MM/a) | TX-OPEX/a ($ MM/a) | NY-CAPEX/a ($ MM/a) | NY-OPEX/a ($ MM/a) | Transport. ($ MM/a) |
|---|---|---|---|---|---|---|---|---|
| BL-1-x-S | 0.284 | 1,533.21 | 18,535.07 | 0.00 | 0.00 | 1,482.81 | 50.41 | 0.00 |
| BL-2-H-x | 0.341 | 1,839.96 | 10,696.19 | 848.05 | 448.66 | 95.57 | 120.48 | 327.20 |
| BL-3-H-S | 0.157 | 848.55 | 9,070.79 | 95.33 | 42.96 | 630.33 | 53.02 | 26.91 |
| PM-1-x-SW | 0.142 | 777.58 | 9,158.34 | 0.00 | 0.00 | 732.67 | 44.91 | 0.00 |
| PM-2-H-x | 0.371 | 2,026.97 | 17,129.99 | 933.72 | 413.88 | 208.98 | 119.80 | 350.59 |
| PM-3-H-SW | 0.109 | 594.79 | 6,540.24 | 20.58 | 16.03 | 502.64 | 48.56 | 6.98 |

generated in NY is 6,493 GWh/a, that is 20% larger than the total annual power load demand (5,430 GWh/a). The LCOE is $0.284/kWh. BL-2-H-x case meets the same power demand by relying on hydrogen produced in TX. Due to the low round trip efficiency of the hydrogen route, the total renewable energy that needs to be generated in TX is 16,115 GWh/a, that is 420% larger than the annual power load demand. Due to high potential of solar and wind energy in TX and their integration, renewable energy production in TX is much cheaper than that in NY. It has a much higher capacity utilization, evidenced by 53% smaller total renewable energy generation capacity. The LCOE of BL-2-H-x is $0.341/kWh, 20% more expensive than that of BL-1-x-S. While producing DECs in TX and sending them to NY is less capital intensive, its operating costs are significantly high due to increasing transportation costs and OPEX of hydrogen storage and electrolysis processes. The resulting process networks for BL-1-x-S and BL-2-H-x can be found in Appendix D in Figures D.1 and D.2, respectively.

BL-3-H-S is the case that highlights the synergy of using DECs together with local renewable resources. Renewable energy generation in TX and NY are 1,796 and 6,164 GWh/a, respectively.

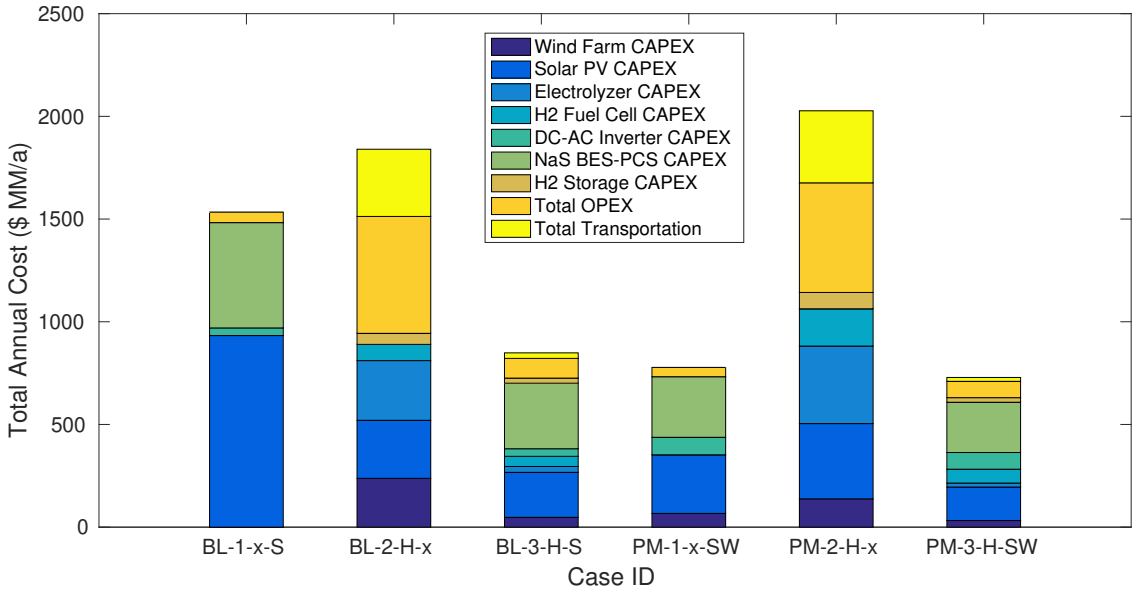


Figure 4.8: Total annual cost breakdown of selected cases for base and peak load matching.

The main portion of the renewable power production is coming from local NY resources. It is interesting to note that, the renewable energy generated in this case is only 5% smaller than that in BL-1-x-S with a 40% smaller battery storage and 77% smaller solar PV capacity. Availability of DEC backup prevents the need for oversizing to make up for the additional power requirements. Thus, capacity utilization is increased. Due to this increase, BL-3-H-S has a LCOE of $0.157/kWh, 45% lower than that of BL-1-x-S. The process network for BL-3-H-S is presented in Figure 4.9.

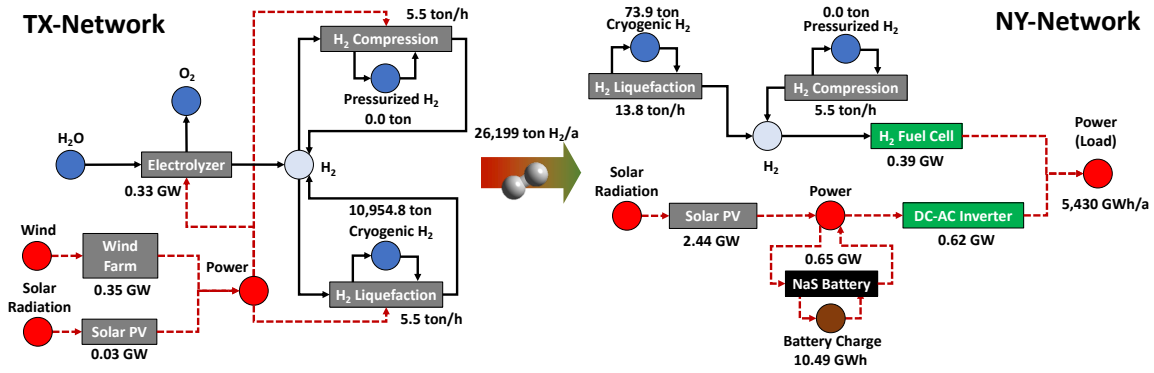


Figure 4.9: Process network for BL-3-H-S.

The contributions of annualized CAPEX, OPEX, and transportation costs to the total annual cost for these three cases are given in Figure 4.8. The results show that BL-1-x-S costs are heavily dominated by the solar PV and BES units. BL-1-x-S suffers from power generation and storage capacity oversizing and the resulting low capacity utilization. BL-2-H-x has smaller solar PV and wind farm costs, even though the generated renewable energy is almost 3.5 times as much as that by BL-1-x-S as mentioned earlier. However, the electrolyzer costs in TX for BL-2-H-x are high. Hydrogen is stored and transported mainly as a cryogenic liquid, hence transportation costs and liquefaction OPEX are significantly contributing to the total cost. The sum of the largescale hydrogen storage, operation, and transportation costs make the total cost 20% more than that of BL-1-x-S. BL-3-H-S cost has a significant share coming from battery storage, however, total transportation and renewable power generation costs are much smaller compared to BL-2-H-x.

Finally, the power scheduling results from BL-3-H-S case are presented to explain how and when DECs help the local power generation and battery storage systems. Figure 4.10 shows that for most of the seasons, local solar PV and NaS battery power conversion system (PCS) are capable of meeting the power load. Hydrogen as a DEC is used mainly as a backup fuel. Especially on the days with low renewable availability such as are $s_1$, $s_3$, $s_4$, or $s_{12}$. While case BL-1-x-S shows that NY resources are strong enough to be self-sufficient, the low renewable days are causing power generation and energy storage units to be overdesigned by 77% and 40% over the best case BL-3-H-S in order to ensure the feasibility condition throughout the entire year.

For sake of simplicity, the detailed results are presented for the cases where hydrogen is the only DEC and the wind power in NY not available. It can be seen from Tables D.1 and D.2, that the cases where ammonia or methanol are considered alongside hydrogen can provide improvements in OPEX and transportation costs. In most cases, ammonia and methanol are sent as DEC together with cryogenic hydrogen. Another source of improvement is integration of wind power in NY to the process network. By using combined solar and wind power, BL-1-x-SW case has the LCOE of \$0.147/kWh, 48% lower than BL-1-x-S. The advantage of solar and wind integration is improved capacity utilization as evidenced by smaller solar PV and wind farm units as well as smaller battery

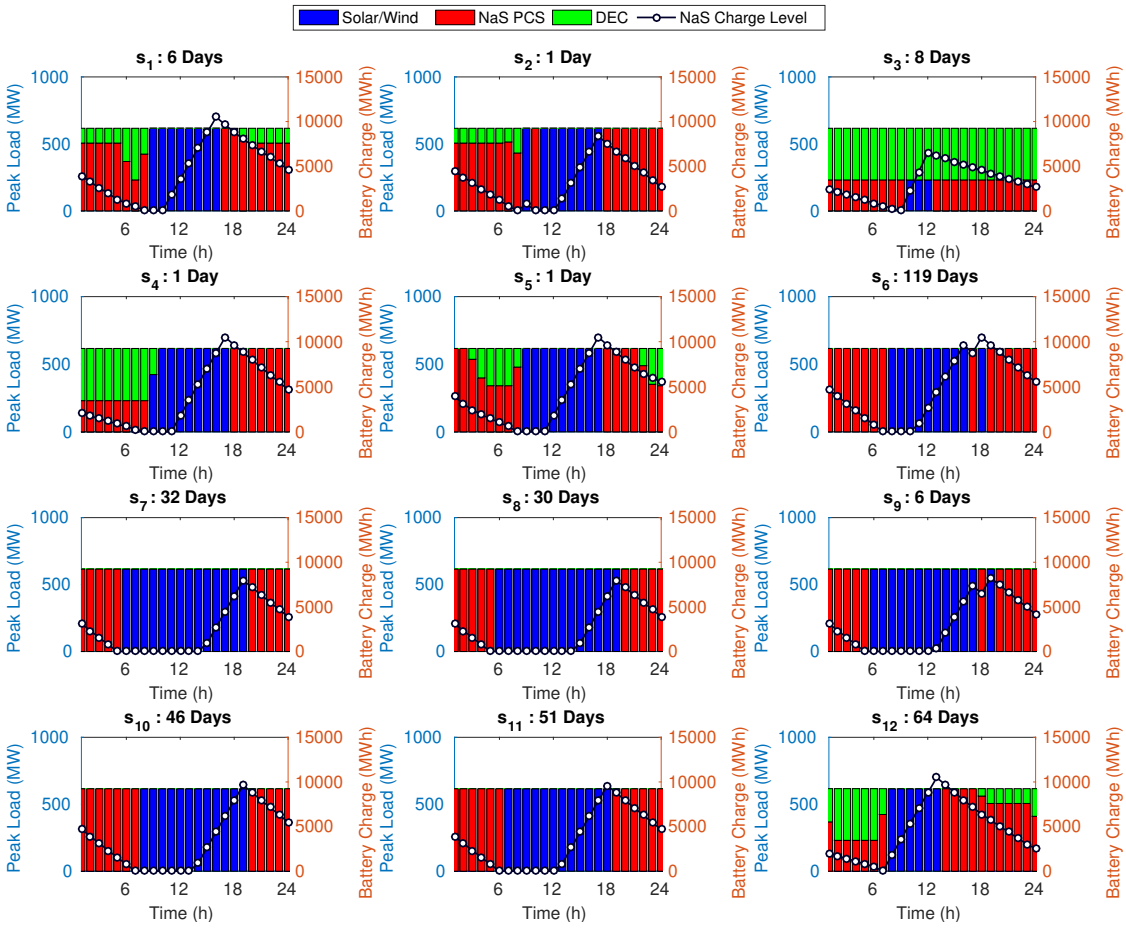


Figure 4.10: Power scheduling results for BL-3-H-S case.

storage requirement. The lack of synchronicity between solar and wind power provides a more balanced supply of renewable power to the process network. When solar and wind power in NY is combined with DEC coming from TX, LCOE can be as low as \$0.116/kWh-\$0.104/kWh for the cases of BL-3-H-SW, BL-3-HA-SW, and BL-3-HM-SW.

### 4.4.2 Case Study II: Peak Load Matching

In this case study, the power output of the system in NY is not constant at base load throughout the year, but increasing and decreasing according to the actual power demand. The results for scenarios 1, 2, and 3 indicate similar trends between base load matching cases. In order to highlight the benefits of using both solar and wind in NY, detailed results are shown for the examples of PM-1-x-SW, PM-2-H-x, and PM-3-H-SW.

PM-1-x-SW case shows that integration of solar and wind power brings the total renewable power generation capacity and battery storage requirements down. Due to asynchronous availability of solar and wind power, the need the battery storage is 43% less than that in PM-1-x-S (see Table 4.4). The resulting LCOE is \$0.142/kWh. PM-2-H-x is found to be plagued by high CAPEX for electrolyzer and fuel cell along with storage and transportation costs as shown in Figure 4.8. Since the peaking power demand requires high nameplate capacity for electrolyzer and fuel cell units, the capacity utilization is low and the installed capacity is not used for most of the time. The LCOE for replacing the peaking power demand with hydrogen is found to be \$0.371/kWh. The process networks for PM-1-x-SW and PM-2-H-x can be found in Appendix D in Figures D.3 and D.4, respectively.

PM-3-H-SW finds a good balance between using the local resources in NY and DEC coming from TX as evidenced by the low LCOE of \$0.109/kWh. Most of the renewable energy used is generated in NY (6,025 GWh/a) and only a small backup power is provided by DEC, hence the renewable energy generated in TX is much smaller (640 GWh/a). The battery storage requirement in NY is 37% less than that in PM-1-x-SW and 64% less than that in PM-1-x-S. The power scheduling for PM-3-H-SW is shown in Figure 4.12. The contribution of DEC to total power supplied is small and only used in days when either the local renewable power is low or the power demand is very high as in $s_1$, $s_3$, $s_7$, or $s_{10}$. The process network for PM-3-H-SW is presented in Figure 4.11.

Similar to base load matching studies, integration of local solar and wind power in NY to be very beneficial to reduce the costs. Also, use of ammonia and methanol along with hydrogen offers further improvements in process economics as in the cases of PM-3-HA-SW and PM-3-HM-SW as shown in Tables D.3 and D.4.

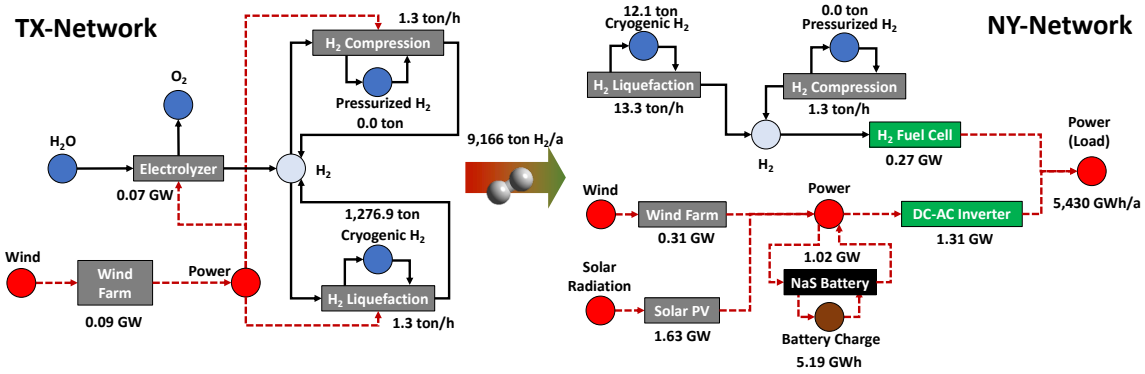


Figure 4.11: Process network for PM-3-H-SW.

### 4.4.3 Sensitivity of Results

#### *4.4.3.1 Effects on Energy Storage on the Cost of Electricity*

Using this design and operation strategy, the cost of renewable electricity without storage is calculated. For this purpose, the model is set to meet the aggregate annual energy demand instead meeting hourly commitments by changing Equation 4.18 with Equation 4.38. The optimizer minimizes the cost by eliminating the storage facilities and the process network provides the output power to the grid whenever renewable energy is available. Table 4.6 shows the LCOE for each technology for each location.

$$\sum_{h} \sum_{t \in Time_{h,t}} n_h S_{a,j,h,t} \geq \sum_{h} \sum_{t \in Time_{h,t}} n_h D_{a,j,h,t} \quad \forall a, j \in Demand_j \tag{4.38}$$

Table 4.6: LCOE for solar- and wind-based technologies in TX and NY.

| Technology | LCOE ($/kWh) | CAPEX ($ MM/a) | CAPEX/a ($ MM/a) | OPEX/a ($ MM/a) | Capacity (GW) | Demand Load (GWh/a) |
|---|---|---|---|---|---|---|
| TX-Solar PV | 0.042 | 2,479.50 | 198.36 | 30.14 | 1.36 | 5,401 |
| TX-Wind Farm | 0.041 | 1,737.06 | 138.96 | 83.04 | 0.72 | 5,401 |
| TX-Grid Electricity [212] | 0.117 | N/A | N/A | N/A | N/A | N/A |
| NY-Solar PV | 0.046 | 2,749.61 | 219.97 | 30.14 | 1.50 | 5,401 |
| NY-Wind Farm | 0.053[2] | 755.78 | 60.46 | 24.91 | 0.31 | 1,620 |
| NY-Grid Electricity [213] | 0.210 | N/A | N/A | N/A | N/A | N/A |

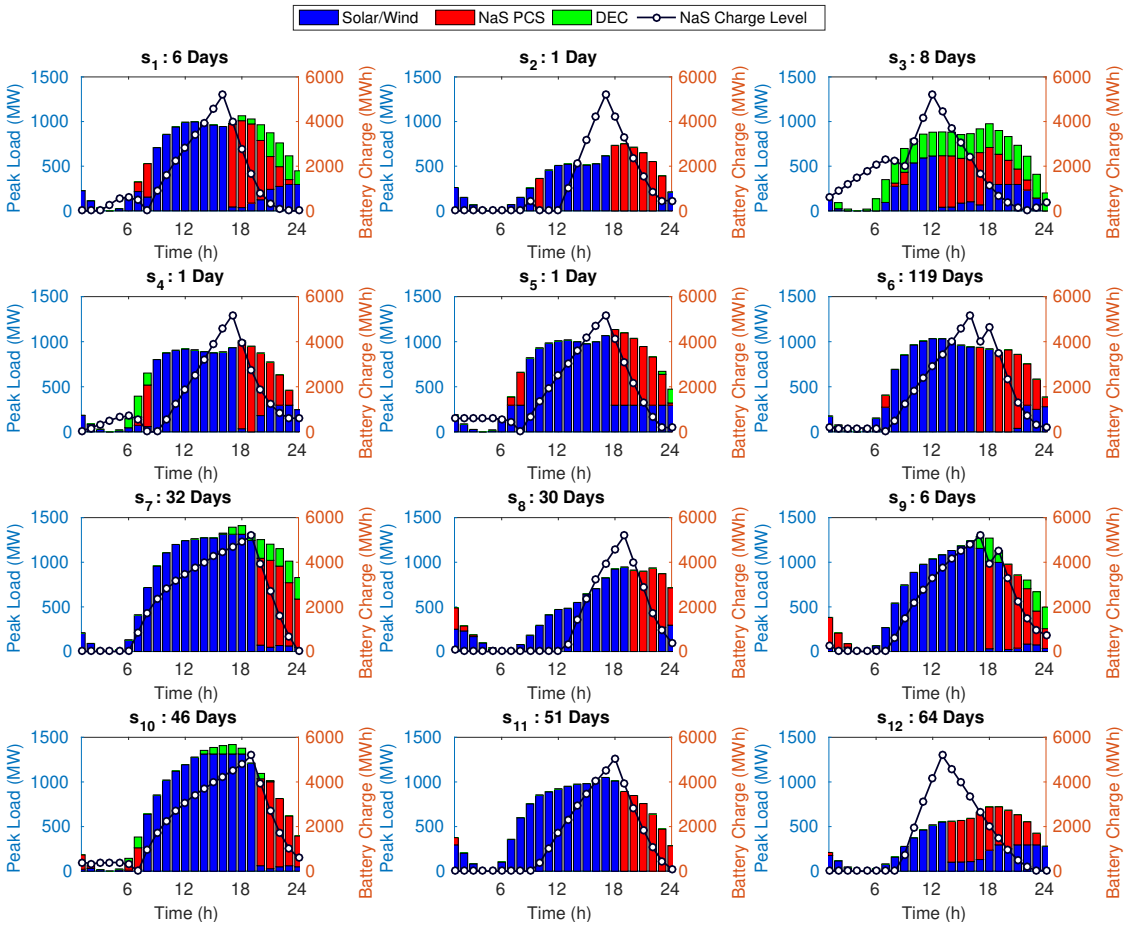


Figure 4.12: Power scheduling results for PM-3-H-SW case.

In Chapter 3, solar PV and wind-based levelized cost of electricity values reported by NREL [177] and DOE [179] are used in TX case studies to produce ammonia from renewable hydrogen. The base case studies used solar PV-based and wind-based power at the price of $0.051/kWh and $0.044/kWh, respectively. While these values are lower than mostly fossil-based grid electricity due to PPA, energy storage in the power generation systems is not considered. The optimal LCOEs calculated from the model to be very similar to the values reported by DOE and NREL.

The addition of local energy storage methods in NY increases the cost of renewable electricity roughly six times (see BL-1-x-S and PM-1-x-S). With the use of DECs, the cost of electricity can potentially be only three times more expensive. With DECs as back-up fuel, the cost of

[2]Wind potential in NY is not strong enough to meet 10% of NY power demand. The reported value is only for meeting 3% total demand.

zero-emission renewable energy can be cost competitive with fossil-based grid electricity.

#### *4.4.3.2 Renewable Energy Penetration Level*

The case study results shown thus far are aiming to meet 10% of total NY power load. In this section, a sensitivity analysis is done to see how the renewable penetration level affects the LCOE. Results for three scenarios comparing batteries, hydrogen, and their combined use are presented for levels of 5, 10, 15, and 20% renewable penetration in NY in Table 4.7.

Table 4.7: LCOE various levels of renewable energy penetration in NY.

| Case ID | 5% Load LCOE ($/kWh) | 10% Load LCOE ($/kWh) | 15% Load LCOE ($/kWh) | 20% Load LCOE ($/kWh) | Case ID | 5% Load LCOE ($/kWh) | 10% Load LCOE ($/kWh) | 15% Load LCOE ($/kWh) | 20% Load LCOE ($/kWh) |
|---|---|---|---|---|---|---|---|---|---|
| BL-1-x-S | 0.222 | 0.284 | 0.334 | infeas. | PM-1-x-S | 0.205 | 0.247 | 0.297 | 0.322 |
| BL-2-H-x | 0.333 | 0.341 | 0.344 | 0.349 | PM-2-H-x | 0.368 | 0.371 | 0.373 | 0.378 |
| BL-3-H-S | 0.157 | 0.157 | 0.160 | 0.162 | PM-3-H-S | 0.133 | 0.134 | 0.134 | 0.134 |

The LCOE is highly sensitive to renewable penetration level if the system only relies on local solar energy and battery storage in NY. In Case Studies I and II, in the absence of a backup fuel or wind energy, both solar PV and battery storage capacities are oversized to ensure feasibility on days with low solar irradiation. Due to low renewable energy potential in NY, the LCOE goes up roughly 50% for both BL-1-x-S and PM-1-x-S cases as the penetration level increases. Larger solar penetration in NY indicates even lower capacity utilization.

With the presence of DEC as a backup fuel and local battery storage, the LCOE of the energy systems to be more stable in the face of varying penetration level. Cases BL-3-H-S and PM-3-H-S indicate the LCOE does not change significantly as the renewable penetration changes from 5 to 20%. As described earlier, DECs prevent oversizing the power generation and storage capacity. The share of DEC in power mixture increase slightly versus the shares of the local power generation and storage. For the cases relying solely on DEC coming from TX for power, BL-2-H-x and PM-2-H-x, the cost of electricity to increase with the level of penetration. However, this increase is not as much as that of BL-1-x-S or PM-1-x-S. The results indicate that for renewable energy to

penetrate easier, both local resources and backup options in the form of DECs are important.

#### *4.4.3.3 Number of Representative Seasons*

The design and operation decisions are dependent on the renewable resource availability. The focus of this study is not on how to select the most appropriate number of representative seasons. Also, the size of the multi-location scheduling problem is too large to be solved for an entire year (365 clusters), even when the design decisions are fixed. This section aims to highlight the effects of time clustering on the design and operation by showing results obtained when different number of representative seasons are used. For this analysis, optimal results obtained from 4, 12 (base case), and 16 clusters are compared with each other. The MILP with 4 clusters is easily solved. At 16 clusters, some case studies fail to find a solution within the solution time limitations when more than one DEC is considered. This is due to the increasing problem size with more time periods considered.

Table 4.8: LCOE for solar- and wind-based technologies in TX and NY.

| Case ID | 4 Seasons LCOE ($/kWh) | 12 Seasons LCOE ($/kWh) | 16 Seasons LCOE ($/kWh) | Case ID | 4 Seasons LCOE ($/kWh) | 12 Seasons LCOE ($/kWh) | 16 Seasons LCOE ($/kWh) |
|---|---|---|---|---|---|---|---|
| BL-1-x-S | 0.287 | 0.284 | 0.368 | PM-1-x-S | 0.230 | 0.247 | 0.327 |
| BL-1-x-SW | 0.146 | 0.147 | 0.148 | PM-1-x-SW | 0.129 | 0.142 | 0.143 |
| BL-2-H-x | 0.345 | 0.341 | 0.341 | PM-2-H-x | 0.357 | 0.371 | 0.372 |
| BL-2-HA-x | 0.345 | 0.341 | 0.341 | PM-2-HA-x | 0.357 | 0.370 | 0.371 |
| BL-2-HM-x | 0.323 | 0.321 | 0.330 | PM-2-HM-x | 0.331 | 0.335 | 0.344 |
| BL-3-H-S | 0.157 | 0.157 | 0.163 | PM-3-H-S | 0.147 | 0.134 | 0.139 |
| BL-3-HA-S | 0.146 | 0.151 | 0.150 | PM-3-HA-S | 0.135 | 0.121 | 0.129 |
| BL-3-HM-S | 0.134 | 0.135 | 0.139 | PM-3-HM-S | 0.123 | 0.117 | 0.117 |
| BL-3-H-SW | 0.107 | 0.116 | 0.116 | PM-3-H-SW | 0.104 | 0.109 | 0.110 |
| BL-3-HA-SW | 0.103 | 0.111 | 0.112 | PM-3-HA-SW | 0.099 | 0.106 | no sol. |
| BL-3-HM-SW | 0.103 | 0.104 | 0.105 | PM-3-HM-SW | 0.099 | 0.103 | 0.104 |

Table 4.8 shows the LCOE obtained for some of the cases shown earlier. As the number of representative seasons increase, days with higher and lower renewable potential are added to the inputs. The combined effect is a potential increase in the variability in the input space. As a result, the network design needs to be feasible and optimal on potentially resource-scarce seasons. This

leads the way to overdesign and low capacity utilization. In the case of using solely local resources (i.e. Scenario 1) optimal decisions hedge against variability by designing larger energy storage units so that feasibility is ensured. When DECs are introduced to the problem (i.e. Scenarios 2 and 3), the design decisions of both energy production and storage units to be less sensitive to input variability.

An interesting conclusion can be made here: Optimizing the design of a renewable power-based energy system with battery storage as only option can suggest overdesign of battery storage for strict feasibility constraints. On the other hand, relying on DECs for zero-emission backup fuel, can improve the reliability of the power systems. While a comprehensive analysis of representative season selection and their effects on the design and operation are beyond the scope of this particular work, future studies should focus on decomposition algorithms to make the most reliable and flexible design and operation decisions.

## 4.5 Conclusions

In this study, an optimization-based multi-scale design and operation strategy is introduced to analyze the techno-economic feasibility of renewable power generation and storage systems. A process network is formulated with renewable power generation and storage options, DEC production processes, and back-to-power conversion units. The dynamic changes in renewable resource availability and power demand are explicitly handled by hourly scheduling decisions that are a part of the design phase.

The strategy is tested to integrate wind and solar energy in TX to produce DECs and send them to NY to compare feasibility of using DECs alongside local renewable energy generation and storage. Various scenarios are compared where (i) local renewable power generation and storage in NY, (ii) fully replacing the energy demand via DECs produced in TX, and (iii) combined use of DECs and local power generation and storage technologies are considered.

Case study results show that when used together with local battery storage, hydrogen-based DECs can offer up to 50% cost reductions for solar PV and BES in both base load and peak matching scenarios. The main advantage of using DECs is providing a clean backup fuel for times

when local intermittent renewable resources are scarce. DECs can improve capacity utilization of renewable power networks by preventing power generation and storage capacity oversizing. Fully replacing the energy demand via DECs produced at a high renewable energy potential region like TX offer less promising economics due to increased transportation and storage costs. The DEC-local resource synergy is found to be more valuable to exploit. The cost of local power generation and storage, if available, is highly sensitive to renewable penetration levels. Availability of a clean backup power source helps to stabilize it. Also, integration of solar and wind power to be highly beneficial since these two resources generally peak at different times. Integration of solar and wind mitigates the intermittency effects of a single resource.

Three type of DECs are investigated within this work: hydrogen, ammonia, and methanol. All DEC options showed promising potential. Hydrogen production from water electrolysis is useful to handle intermittent power supply from solar and wind resources. In many case studies, both ammonia and methanol offer slightly lower overall costs due to cheaper storage and transportation costs over hydrogen, even though production CAPEX and OPEX increase slightly.

# 5. INTEGRATED MULTI-PRODUCT PROCESS NETWORK OPTIMIZATION FOR RENEWABLE AND FOSSIL ENERGY SYSTEMS

## 5.1 Integrated Renewable and Fossil Energy Systems

Natural gas (or methane) conversion is a versatile route for not only power and heat generation but also chemical feedstocks like synthesis gas (syngas) and hydrogen production. Natural gas can be used as a feedstock for liquid transportation fuels production via gas-to-liquids (GTL) processes like Fischer-Tropsch synthesis (FTS), Methanol-to-Gasoline (MTG) and Metanol-to-Olefins-Gasoline-Distillate (MOGD). The US has a nation-wide pipeline infrastructure that enables strong logistics for natural gas distribution. Natural gas conversion technologies are cleaner than those of petroleum or coal. Nevertheless, if no carbon capture technology is used, both (i) combustion to produce heat & power and (ii) traditional steam reforming to produce syngas or hydrogen still have significant carbon footprints. To meet low-emission conversion of methane, direct decomposition of methane via pyrolysis technology can offer a solution. Methane pyrolysis produces elemental carbon and hydrogen, a very high quality and emission-free fuel for both power and heat generation. If done in the absence of an oxidizing environment and some of the product hydrogen is used to provide the required heat supply for the reaction, pyrolysis can be an emission-free hydrogen and power production technology. While promising, methane pyrolysis technology is still in the early phase of development with limited data available in the literature.

As a lower-emission alternative, renewable sources of power like solar and wind energy are also promising to enable sector integration via electrification. However, both resources suffer from intermittency and seasonal variability, resulting in low capacity utilization in the absence of energy storage technologies [17, 14, 214]. Biomass has been a candidate replacement for fossil fuels and its application in power, fuels, and chemicals sectors have been studied extensively by national labs and academia. Crop residues like corn stover and forest residues like hardwood type of biomass can be economically feasible with gasification technology if provided at a steady supply. For the

transportation sector, there has been significant work on design and supply chain optimization of systems of biomass-to-liquids (BTL) and hybrid mixtures of coal-biomass-gas-to-liquids (CBGTL) [215, 216, 78, 79, 217].

While many renewable resources provide promising alternatives to fossil fuels, they suffer heavily from intermittency and uneven geographical distribution. Recall from Figure 1.2 the geographical distribution of solar, wind, and biomass resources for the United States. Each renewable resource is stranded at a different part of the country. Additionally, they are often isolated and far from strong demand locations like metropolitan areas and industrial zones. As a result, the optimal renewable utilization strategies should be location specific and consider the value chain aspect of the products [183].

In order to analyze different scenarios involving energy system networks that include both fossil and renewable resource, the temporal and spatial variability of renewable supply and power demand need to be considered explicitly in the optimization formulation. For this purpose, the multi-period and multi-location simultaneous design, operation, and supply chain strategy developed in Chapter 4 is used.

## 5.2 Modeling and Optimization of Integrated Energy Systems

### 5.2.1 Problem Definition

The conceptual depiction of the multi-scale modeling and optimization approach is given in Figure 5.1. This approach allows for simultaneous optimization of both process synthesis at each location and the supply chain of multiple locations. A single-location integrated multi-product process network is illustrated in Figure 5.1(a). A multi-product process network takes a variety of feedstocks as inputs to produce different products via different process blocks. At the center of the network lies the hydrogen generation and storage processes. Hydrogen is generated from either reformation of natural gas or water electrolysis. Produced hydrogen can be stored as energy carrier or used as a feedstock for hydrogen-based energy carrier, chemicals, and fuels production. Other feedstocks such as nitrogen, oxygen, and carbon oxide species are obtained via air separation,

methane conversion, and carbon capture processes. The demand for products like power, fuels, and chemicals is unevenly distributed. Furthermore, many metropolitan and industrial areas might demand more than one type of product. Hence, there is the supply chain aspect of the problem that needs to be addressed where transportation alongside production needs to be optimized as illustrated in 5.1(b).

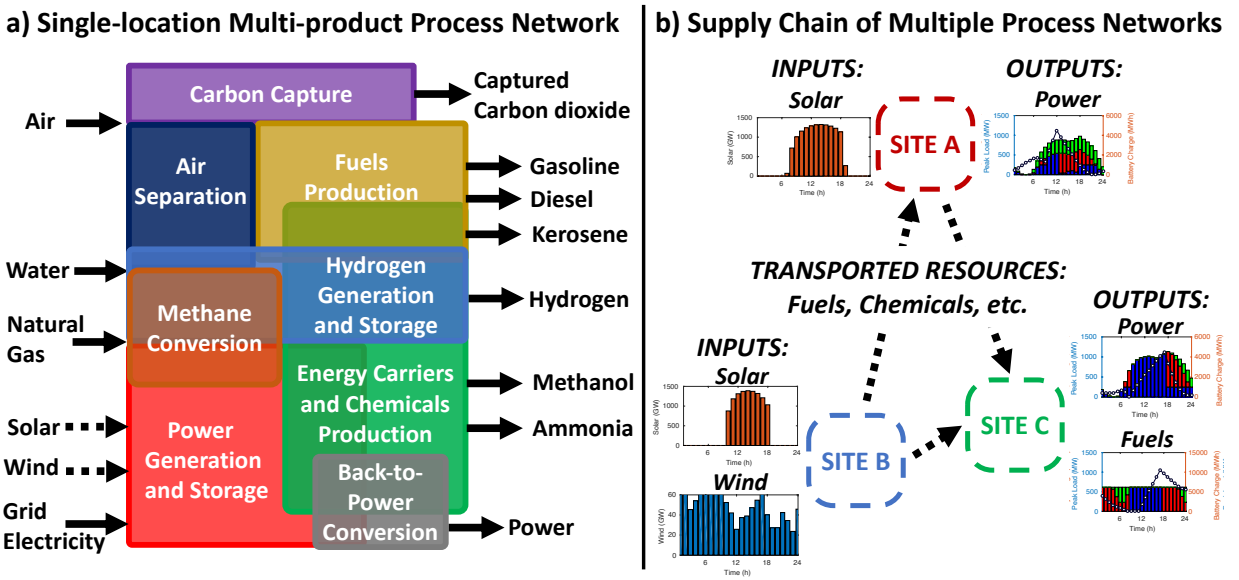


Figure 5.1: Conceptual depiction of novel power generation and storage networks.

The design, operation, and supply chain strategy should take the following as inputs:

- the time-dependent resource availability at each location,
- the time-dependent profile of the resource demand at each location,
- the detailed process input-output and costing information for all available process technologies,
- the operational limitations such as maximum production rate changes and operating mode switches,
- the available transportation and storage infrastructure.

And returns the optimal solution that comprises:

- the process and storage unit capacities,
- the time-dependent production rates in each process,
- the material and energy flow rates between processes in the process network,
- the unit commitment and operating mode selections for all process technologies,
- the inventory management for storage of resources,
- the transportation flows of products.

In the following section, the details of the modeling and optimization formulation are described.

### 5.2.2 Network and Time Representation

The resource-task network (RTN) formulation [206] used in study work has previously been described in Chapter 4. With the RTN formulation, the resources can be purchased, consumed, generated, sold, stored, or transported to a different location and the processes can convert material and/or energy resources to other resources. The renewable resource availability changes during the day so the temporal space is discretized for multi-period operational decisions. Inventory constraints keep track of all the resources entering and leaving the process network in one location and connect the consecutive time periods. All the input-output relationships are linearly correlated. The time representation used in this study has previously been introduced in Chapter 4 and illustrated in Figure 4.3.

### 5.2.3 Process Superstructure

The work in this chapter further extends the process superstructure by including fossil-based technologies for methane conversion and fuels production via two different pathways. The extended process superstructure is shown in Figure 5.2 for the renewable- and fossil-based processes in the RTN representation. As before, the resources are represented by circles and the processes by rectangles. The specifics of the color codes are the same as in Chapter 4 and will not be repeated here for sake of brevity.

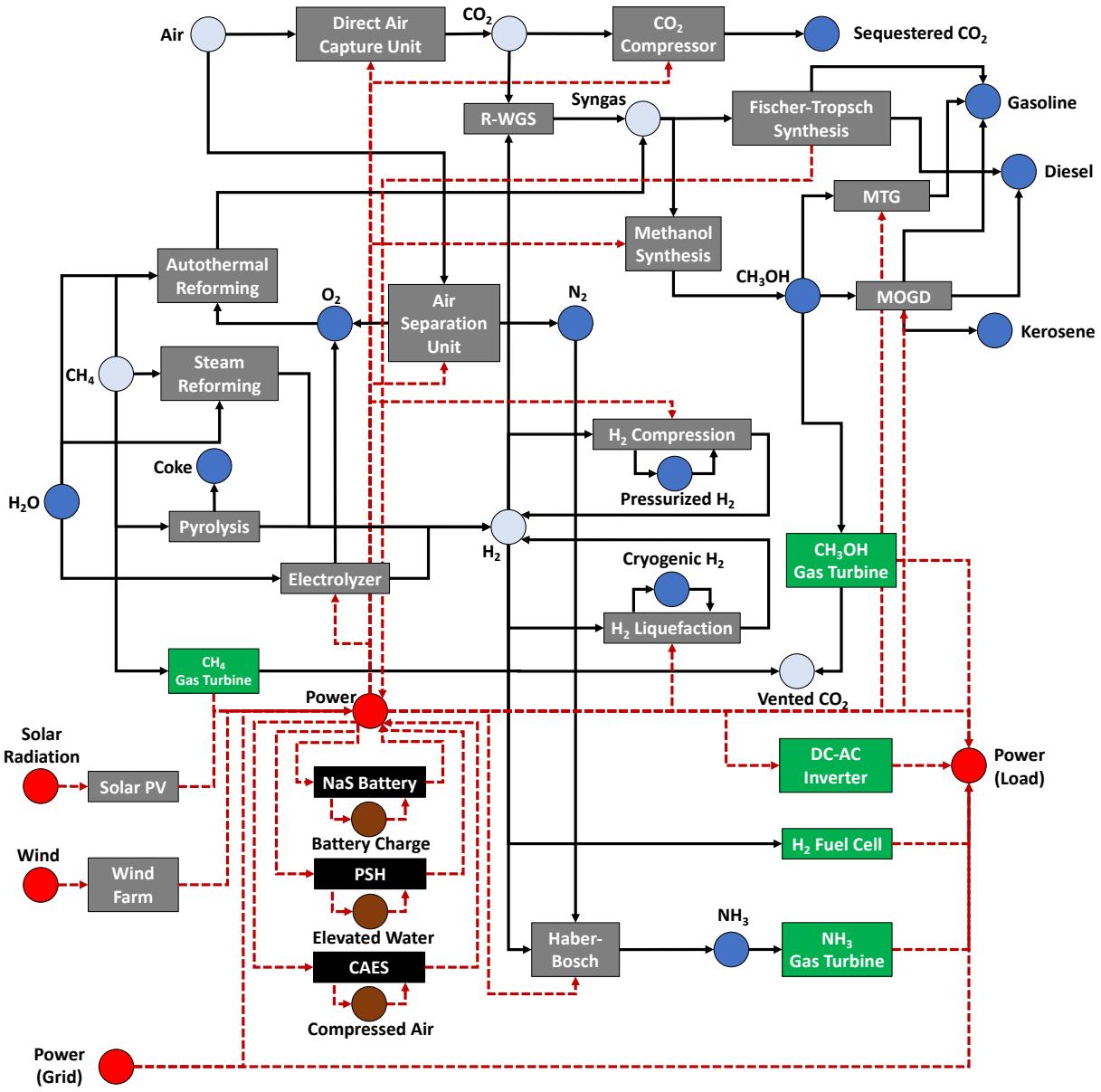


Figure 5.2: Process network superstructure for integrated multi-product facilities.

In the process network, the primary sources of power can either renewable (i.e. solar and wind) or fossil fuels (i.e. methane ($CH_4$)). Alternatively, the network can purchase power from grid that is assumed to be generated from fossil fuels. Power generation processes include solar PV, wind farms, and $CH_4$ gas turbine. Power cannot be stored unless an energy storage technology is used such as sodium-sulfur (NaS) battery electric storage (BES), pumped-storage hydro (PSH),

and compressed air energy storage (CAES), that can store power in battery charge, elevated water, and compressed air, respectively. These processes consist of storage and power conversion systems (PCS) to store and convert stored resources back to power, respectively. Hydrogen can be produced from water using electrolysis or from methane conversion technologies such as steam reforming (SMR) or pyrolysis (MP). Hydrogen can be stored either as a cryogenic liquid or a pressurized gas in liquefaction or compression processes, respectively. Hydrogen can be used as (i) DEC to store and transport power, (ii) precursor to transportation fuels production, or (iii) precursor to chemicals production. For fuels production, hydrogen is mixed with carbon dioxide and sent to a reverse-water-gas shift (R-WGS) process to obtain a syngas mixture with $H_2$:CO ratio of 2.2:1. Carbon dioxide is captured from air with the direct air capture (DAC) unit. Alternatively the syngas can be obtained from autothermal reforming of methane (ATR). Syngas can be converted to transportation fuels via GTL technologies such as (i) FTS and (ii) MTG/MOGD processes. FTS produces gasoline and diesel, whereas MTG/MOGD can produce gasoline, diesel, and kerosene. FTS can produce liquid fuels from syngas, however, MTG/MOGD route requires an additional step for methanol synthesis. For chemicals production, current options include ammonia synthesis via Haber-Bosch process or methanol synthesis. The high-purity nitrogen and oxygen used in fuels or chemicals production are generated via an air separation unit (ASU). The stored fuels, chemicals, and DECs can be transported to a different location by railroad or trucks. Hydrogen, ammonia, and methanol can be converted back to power using $H_2$ fuel cell, $NH_3$ gas turbine, or $CH_3OH$ gas turbine, respectively to produce renewable power. Power outputs of solar PV and wind farm, and many other processes are in direct current (dc), which need to be converted to alternative current (ac) with dc-ac inverter unit in order to be sent to the power grid. The outputs of fuel cell and gas turbines are in ac.

The input-output parameters for all the processes are taken from previously studied MINLP-based design problems as described in Chapter 3. The full process models are given in Appendix C.

### 5.2.4 Mathematical Model

The complete mixed-integer linear programming (MILP) model consists of: (i) the network design constraints for production and storage facilities, (ii) the operating mode selection with ramp up/down constraints, (iii) the general resource balance constraints, (iv) the specific resource balance constraints mainly for carbon accounting and fuels productions section, (v) the seasonal continuity constraints, (vi) the investment and operational cost functions, and (vii) the objective function. Most of the mathematical model is presented in Chapter 4. Here, only the new constraints added to the formulation are presented.

#### *5.2.4.1 Resource Specific Balance Constraints*

In addition to the more general resource balance constraints, more specific balance constraints are added for certain resources. Fuel production ratios are imposed with Equations 5.1 and 5.2.

$$S_{a,j,h,t} \geq (FuelsRatio_j^{US} - 0.05) \sum_{j \in LiquidFuels_j} S(a,j,h,t) \quad \forall a, j \in LiquidFuels_j, h, t \in Time_{h,t} \tag{5.1}$$

$$S_{a,j,h,t} \leq (FuelsRatio_j^{US} + 0.05) \sum_{j \in LiquidFuels_j} S(a,j,h,t) \quad \forall a, j \in LiquidFuels_j, h, t \in Time_{h,t} \tag{5.2}$$

Equations 5.3 and 5.4 present the demand constraints that are specific for liquid transportation fuels written in barrel and energy equivalency. Equation 5.3 imposes the fuel ratios on the liquid transportation fuels.

$$S_{a,j,h,t} \geq D_{Fuels}^{total} FuelsRatio_j^{US} \rho_j \quad \forall a, j \in LiquidFuels_j, h, t \in Time_{h,t} \tag{5.3}$$

Equation 5.4 calculates the total energy content of a fuels plant with the fuel ratios given with a specific plant scale by $D_{Fuels}^{total}$ and makes sure that the produced fuels have the fuel products with

equivalent higher heating value (HHV).

$$\sum_{j \in LiquidFuels_j} S_{a,j,h,t} HHV_j \geq \sum_{j \in LiquidFuels_j} D^{total}_{Fuels} FuelsRatio^{US}_{a,j} \rho_j HHV_j \quad \forall a, h, t \in Time_{h,t} \tag{5.4}$$

#### *5.2.4.2 Process Emission Constraints*

The process GHG emissions are accounted with Equation 5.5. The only GHG considered in the process network is carbon dioxide. For the accounting purposes, the carbon dioxide entering or leaving the network is accounted in each unit it appears. Equation 5.6 calculates the total net process emissions.

$$LocalGHG_a = \sum_h \sum_{t \in Time_{h,t}} n_h \big[ - P_{a,DAC,h,t} + S_{a,VentedCO_2,h,t} - S_{a,SeqCO_2,h,t} \big] \quad \forall a \tag{5.5}$$

$$TotalGHG = \sum_a LocalGHG_a \tag{5.6}$$

#### *5.2.4.3 Objective Function*

The model is solved to minimize the annualized production cost of meeting the power demand. This is also called the levelized cost of electricity (LCOE). For this purpose, total overnight capital investment, $Capex^{total}_a$, is annualized using 8% annual discount rate. Sum of annualized capital cost and operational costs, $Opex_a$ and $Trans^{total}_{j,q}$ along with the carbon tax penalty or gain gives the objective function value $TotalCost$ as shown in Equation 5.7:

$$TotalCost = \sum_a \Big[ (0.08) Capex^{total}_a + Opex_a \Big] + \sum_{j,q \in TPModes_{j,q}} Trans^{total}_{j,q} + (CarbonTax) TotalGHG \tag{5.7}$$

The resulting optimization problem is:

$$\begin{aligned} \min \quad & TotalCost \quad (Equation \quad 5.7) \\ \text{s.t.} \quad & Equations \quad 4.1 - 4.33 \\ & Equations \quad 5.1 - 5.6 \end{aligned} \tag{5.8}$$

## 5.3 Computational Studies

The multi-scale strategy for optimal design and operation of multi-product process networks is applied to examples from three different sectors: (i) synthetic fuels production, (ii) chemicals (i.e. hydrogen, ammonia, and methanol) production, and (iii) renewable power generation and storage. Technologies for these sectors are included in the process superstructure. First, these three examples are optimized as three separate energy systems. Later, they are integrated in a multi-product process network.

### 5.3.1 Synthetic Fuels Production

The transport sector, including road, air, and waterborne transport, contributes to slightly more than 20% of the global GHG emissions. In 2018, about 92% of the total U.S. transportation sector needs were accounted by petroleum products [218]. According to 2018 data, the U.S. consumed an average of value of 20.5 million barrels of petroleum per day [219]. With growing concerns over expensive crude oil prices and increased scrutiny over high levels of GHG emissions, the U.S. transportation sector faces major challenges that must be addressed through the investigation of novel processes to produce liquid fuels. While governments all over the world aim to reduce the GHG emissions from transport drastically by mid century, in the absence of vital measures, emissions are expected to continue increasing due to the increasing demand for transport [220].

One way to bring down the GHG emissions without totally replacing the transportation infrastructure is to produce low-emission fuels require using renewable energy sources such as biomass, solar, and wind energy, as well as captured carbon. Previous multi-scale engineering work by Floudas and coworkers focused on process synthesis of transportation fuels production

from hybrid feedstock routes including coal, biomass, and municipal solid waste gasification, and natural gas reforming; their efforts mainly focused on optimal steady-state designs [215, 216, 78, 79, 217]. Product facilities are optimized for production scales between 1-100 kbpd of liquid transportation fuels. Levelized cost of fuels for GTL, BTL, and CBGTL pathways are found between \$8.2-\$24.5/GJ, \$13.6-\$25.8/GJ, and \$16.1-\$18.8/GJ respectively. This chapter focuses on synthetic fuels production from novel methane pyrolysis pathway and water electrolysis powered by renewable solar and wind.

### 5.3.2 Chemicals Production

Hydrogen, ammonia, and methanol provide dual opportunities for both chemicals and DEC use. Production of hydrogen and ammonia have been studied in detail in Chapter 3. In Chapter 3, costs of ammonia production for 250-1000 tpd scale in Texas for natural gas, hardwood biomass, municipal solid waste, solar, and wind pathways are found between \$404-\$553/ton, \$375-\$521/ton, \$457-\$601/ton, \$873-\$971/ton, and \$786-\$884/ton, respectively. These numbers provide 50% GHG emission reduction compared to a typical ammonia plant and continuous supply of renewable solar and wind energy is costed based on current PPA, which does not include any energy storage technology. In Chapter 4, all three chemicals are produced as DECs and used in the context of energy transportation from Texas to New York. Individual production is not studied. In this chapter, the levelized costs of chemicals are investigated for zero-emission hydrogen, ammonia, and methanol production.

### 5.3.3 Renewable Power Generation and Storage

Energy storage at grid-scale (GWh-scale) is one way to ensure the balance between the renewable power supply and demand and therefore improve the capacity utilization [75]. Energy storage in vectors, that are also called as dense energy carriers (DECs) offer the possibility of transporting stored energy from one location to another. For strict stationary storage applications the available technologies also include pumped storage-hydro (PSH), compressed air energy storage (CAES), or battery electric storage (BES). In Table 4.6 from Chapter 4, the cost of solar

and wind power in Texas the absence of any storage is shown as $0.042/kWh and $0.041/kWh, respectively. This power output is not steady. In this chapter, the cost of steady renewable power using BES and DEC is investigated.

### 5.3.4 Case Studies

Below are given a list of case studies in Table 5.1 that can complete the picture of hybrid feedstock to fuels, chemicals, and power production by incorporating renewables like solar and wind into the picture along with methane conversion technologies like reforming and pyrolysis.

### 5.3.5 Modeling Assumptions

Below are given the modeling assumptions and some of the modeling parameters used for the computational studies. The full list of modeling parameters are presented in Appendix C.

- The primary sources of energy are methane, solar and wind.
- Cost of methane is assumed to be $2.80/TSCF for Texas as an average value for 2019 [15].
- Grid electricity purchase is not allowed for any case study.
- Location dependent solar direct normal irradiation (DNI) and wind speed are taken from NSRDB [18] and Wind Toolkit [19]. Wind speed is taken at 80 m.
- Available land for solar energy in Texas is 1,459 $km^2$ [211].
- Available land for wind farms in Amarillo, Texas is 1,700 $km^2$ [211].
- Renewable electricity provided to the grid is not sold at a price.
- Water purchase cost is $0.4/ton. Water availability does not have an upper bound.
- Electricity prices from Texas are taken from Ercot resources [212].
- Solar DNI, wind speed, load demand, and electricity prices are clustered together using AHC method.
- 12 representative seasons are used.
- Investment costs are annualized such that 8% of the total overnight cost is paid annually.
- Hydrogen can be stored as compressed gas at 700 bar and 20°C or a cryogenic liquid at 1 atm and -259°C.

Table 5.1: List of case studies for fuels production investigate fuels production with United States ratio (U) and its energy equivalent without any fuel ratio restrictions (E). Energy content of 5 kbpd transportation fuels with Unites States ratio is equal to 2868 GWh/day. For chemicals production hydrogen (H), ammonia (A), and methanol (M) are studied at 50, 500, and 500 tpd scales, respectively. Power production (P) cases focus on 500 MW steady ac output. Primary energy source and technologies considered are methane autothermal reforming (ATR), methane pyrolysis (MP), solar PV (S), and wind farms (W). Integrated multi-product plant integrates (NT) fuels, chemicals, and power production from all available energy sources and technologies.

| Case ID | Products | Production Scale | Primary Energy Source | Primary Energy Conversion Technology |
|---|---|---|---|---|
| *Fuels Production* | | | | |
| U-ATR | Fuels (US Ratio) | 5 kbpd | Methane | Autothermal Reforming |
| U-MP | Fuels (US Ratio) | 5 kbpd | Methane | Pyrolysis |
| U-S | Fuels (US Ratio) | 5 kbpd | Solar | Solar PV |
| U-W | Fuels (US Ratio) | 5 kbpd | Wind | Wind Farm |
| U-SW | Fuels (US Ratio) | 5 kbpd | Solar, Wind | Solar PV, Wind Farm |
| E-ATR | Fuels (n/r) | 2,868 GWh/a | Methane | Autothermal Reforming |
| E-MP | Fuels (n/r) | 2,868 GWh/a | Methane | Pyrolysis |
| E-S | Fuels (n/r) | 2,868 GWh/a | Solar | Solar PV |
| E-SW | Fuels (n/r) | 2,868 GWh/a | Wind | Wind Farm |
| E-SW | Fuels (n/r) | 2,868 GWh/a | Solar, Wind | Solar PV, Wind Farm |
| *Chemicals Production* | | | | |
| H-MP | Hydrogen | 50 tpd | Methane | Pyrolysis |
| H-S | Hydrogen | 50 tpd | Solar | Solar PV |
| H-W | Hydrogen | 50 tpd | Wind | Wind Farm |
| H-SW | Hydrogen | 50 tpd | Solar, Wind | Solar PV, Wind Farm |
| A-MP | Ammonia | 500 tpd | Methane | Pyrolysis |
| A-S | Ammonia | 500 tpd | Solar | Solar PV |
| A-W | Ammonia | 500 tpd | Wind | Wind Farm |
| A-SW | Ammonia | 500 tpd | Solar, Wind | Solar PV, Wind Farm |
| M-MP | Methanol | 500 tpd | Methane | Pyrolysis |
| M-S | Methanol | 500 tpd | Solar | Solar PV |
| M-W | Methanol | 500 tpd | Wind | Wind Farm |
| M-SW | Methanol | 500 tpd | Solar, Wind | Solar PV, Wind Farm |
| *Power Generation and Storage* | | | | |
| P500-S | Power | 500 MW | Solar | Solar PV |
| P500-W | Power | 500 MW | Wind | Wind Farm |
| P500-SW | Power | 500 MW | Solar, Wind | Solar PV, Wind Farm |
| *Integrated Fuels, Chemicals, and Power Production* | | | | |
| | Fuels (n/r) | 2868 GWh/a | | |
| | Hydrogen | 50 tpd | | |
| INT-NT | Ammonia | 500 tpd | Methane, Solar, Wind | No restrictions |
| | Methanol | 500 tpd | | |
| | Power | 500 MW | | |

- Carbon tax can be \$0, \$50, or \$100/ton of net carbon dioxide emissions.
- Process emissions are restricted to be less than or equal to 0 t $CO_2$/a. Negative emissions, results in receiving carbon tax credits.
- Gasoline, diesel, and kerosene are the transportation fuels considered.
- United States fuel ratios for gasoline, diesel, and kerosene are 66.6, 21.5, and 11.9 vol%, respectively.
- All processing units have ramping constraints.
- PSH and CAES technologies are not considered in the process network for the case studies.
- NaS-type baterries are considered for the case studies. Battery storage self-discharge rate is 8%/day.

All case studies are solved on a high-performance computing (HPC) machine at Texas A&M High-Performance Research Computing facility using Ada IBM/Lenovo x86 HPC Cluster operated with Linux (CentOS 6) using 1 node (20 cores per node with 64 GB RAM). CPLEX 12.8 solver is used with GAMS 26.1.0. The solution time is limited to 24 hours.

### 5.3.6 Input Clustered Data for Time-dependent Resources

Solar and wind resource potentials given in W/m$^2$ and m/s, respectively are converted to their MW-equivalent resource availabilities using Equations 4.36 and 4.37 as described in Chapter 4. Solar and wind availabilities in Texas for all representative seasons along the weights of the seasons are shown in Figure 4.5. It is important to point out that, Texas has a significant wind and solar potential. Texas is the nation's leading wind energy producer. Solar energy potential in TX is also extremely promising due to availability of land and consistent solar irradiation profiles. It is interesting to note from Figure 4.5, that most of the time the peak solar and wind energy in TX are asynchronous. Solar energy has a consistent presence from morning to early evening, whereas wind energy potential more often than not peaks from night to early morning. This creates a potential for synergy in integrating solar and wind, since one resource can take over the power load when the other fades.

## 5.4 Results and Discussion

### 5.4.1 Case Study I: Synthetic Fuels Production

The results of the synthetic fuels production are shown in Table 5.2 and Figure 5.3.

Table 5.2: Results for synthetic fuels production from methane autothermal reforming (ATR), methane pyrolysis (MP), electrolysis powered by solar (S), wind (W), and integrated solar-wind (SW). Case studies are done for 5 kbpd fuels production with US ratio (U) and HHV-equivalent without fuel ratio restrictions (E). Levelized cost of fuels (LCOF) is given in $/MWh and $/GJ.

| | LCOF | | Total Cost | Gasoline | Diesel | Kerosene | Net Emissions[1] |
|---|---|---|---|---|---|---|---|
| Case ID | ($/MWh) | ($/GJ) | ($ MM/a) | (kbpd) | (kbpd) | (kbpd) | (kt $CO_2$/a) |
| U-ATR | 40.9 | 11.4 | 117.18 | 3,482 | 1,207 | 324 | 0.0 |
| U-MP | 77.7 | 21.6 | 222.77 | 3,482 | 1,207 | 324 | -382.5 |
| U-S | 304.7 | 84.6 | 873.94 | 3,221 | 1,207 | 559 | -691.3 |
| U-W | 215.6 | 59.9 | 618.21 | 3,482 | 1,207 | 324 | -709.7 |
| U-SW | 168.9 | 46.9 | 484.36 | 3,482 | 1,207 | 324 | -709.7 |
| E-ATR | 32.4 | 9.0 | 92.88 | 1,314 | 3,446 | 0 | 0.0 |
| E-MP | 62.7 | 17.4 | 179.92 | 1,314 | 3,446 | 0 | -737.1 |
| E-S | 297.8 | 82.7 | 854.08 | 590 | 2,686 | 1,427 | -664.3 |
| E-W | 213.2 | 59.2 | 611.54 | 632 | 2,731 | 1,343 | -763.9 |
| E-SW | 157.6 | 43.8 | 451.88 | 1,314 | 3,446 | 0 | -797.0 |

For synthetic fuels production via GTL process, methane reforming pathway is found to be the most efficient method with at a cost of $32-$41/MWh ($9.0-$11.4/GJ), followed by methane pyrolysis pathway and direct air capture $62-$77/MWh ($17.4-$21.6/GJ). Fuels production from solar and with powered pathway to produce fuels (also called electrofuels) is much more energy intensive with fuels costs ranging between $213-$305/MWh. Integration of solar and wind energy can bring the cost down to $158-$169/MWh. Although this is a good improvement, it is still much above methane pathways.

[1]Net emissions only include $CO_2$ emissions from the processes. Emissions related to raw material acquisition, processing unit construction, installing, or end product use are not included in the values.

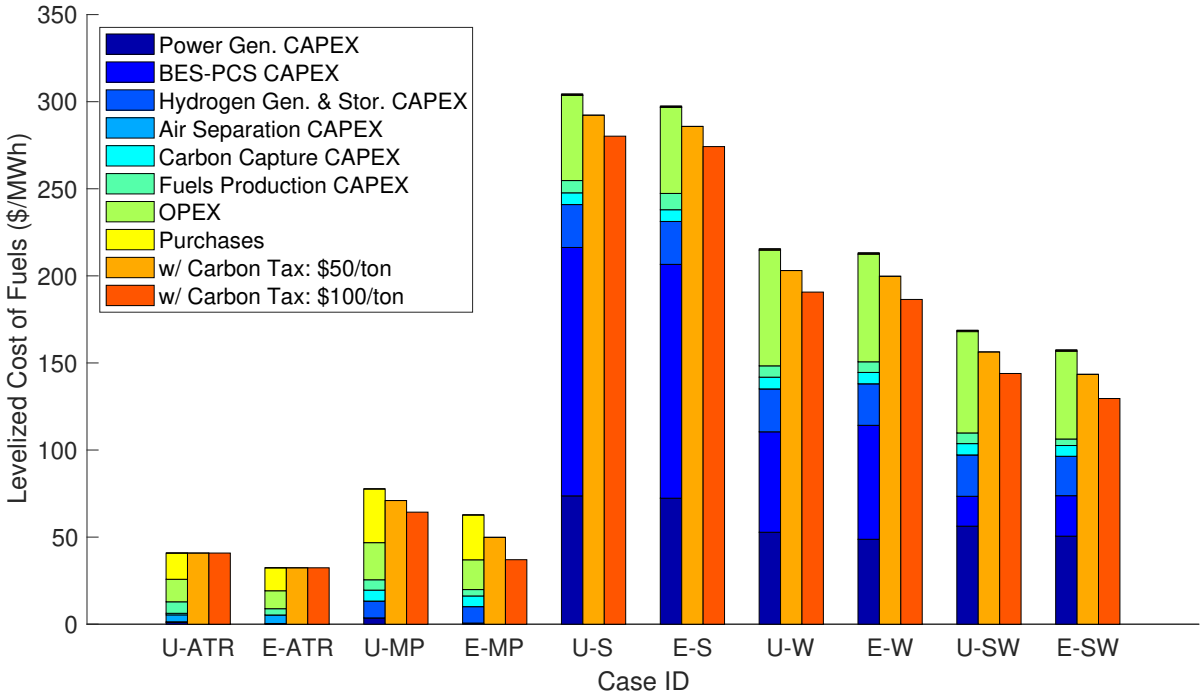


Figure 5.3: Total annual cost breakdown of synthetic fuels production results show that methane pathways (U-ATR, U-MP, E-ATR, and E-MP) are more efficient that renewable-powered electrolysis pathways (U-S, U-W, U-SW, E-S, E-W, and E-SW.). Removal of fuel production ratio restriction favor FTS over MTG/MOGD route to produce more diesel instead of kerosene.

Total annual cost breakdown of synthetic fuels production results show that methane pathways (U-ATR, U-MP, E-ATR, and E-MP) are more efficient that renewable-powered electrolysis pathways (U-S, U-W, U-SW, E-S, E-W, and E-SW.). Removal of fuel production ratio restriction favor FTS over MTG/MOGD route to produce more diesel as shown in Table 5.2. If combined with carbon credits due to using carbon dioxide captured from air, synthetic fuels production from methane pyrolysis can produce fuels at a cost of $49 and $37/MWh for carbon tax of $50 and $100/t, respectively.

### 5.4.2 Case Study II: Chemicals Production

Chemicals production cases study results are presented in Table 5.3 and Figures 5.4, 5.5, and 5.6. Results from Table 5.3 show that steady output hydrogen production via methane pyrolysis is 58-70% cheaper than renewable powered water electrolysis. Integrating solar and wind power

can bring the costs down, however, electrolysis is still highly energy intensive. High hydrogen production costs of electrolysis pathway is the reason solar and wind powered ammonia and methanol productions are more costly that the methane pathway.

Table 5.3: Results for hydrogen (H), ammonia (A), and methanol (M) production from methane pyrolysis (MP), electrolysis powered by solar (S), wind (W), and integrated solar-wind (SW) are shown. Case studies are done for 50 tpd hdyrogen production and 500 tpd ammonia or methanol production scales. Levelized cost of chemicals (LCOC) is given in $/MWh and $/GJ.

| Case ID | LCOE ($/kg or $/t) | Total Cost ($ MM/a) | NG Purc. (MSCF/a) | RE Gen. (GWh/a) | $H_2$ Prod. (kt/a) | Net Emissions (kt $CO_2$/a) |
|---|---|---|---|---|---|---|
| H-MP | $1.52/kg | 32.28 | 5.56 | 0 | 21.3 | 0.0 |
| H-S | $5.06/kg | 107.73 | 0 | 1,360 | 21.3 | 0.0 |
| H-W | $3.64/kg | 77.41 | 0 | 1,360 | 21.3 | 0.0 |
| H-SW | $3.41/kg | 72.53 | 0 | 1,360 | 21.3 | 0.0 |
| A-MP | $341/t | 72.71 | 10.95 | 0 | 37.8 | 0.0 |
| A-S | $1,426/t | 303.69 | 0 | 2,911 | 37.8 | 0.0 |
| A-W | $883/t | 188 | 0 | 2,609 | 37.8 | 0.0 |
| A-SW | $773/t | 164.49 | 0 | 2,616 | 37.8 | 0.0 |
| M-MP | $381/t | 81.09 | 11.83 | 0 | 41.3 | -113.6 |
| M-S | $1,487/t | 316.61 | 0 | 3,274 | 41.3 | -254.5 |
| M-W | $933/t | 198.61 | 0 | 2,934 | 41.3 | -254.5 |
| M-SW | $796/t | 169.56 | 0 | 2,922 | 41.3 | -254.5 |

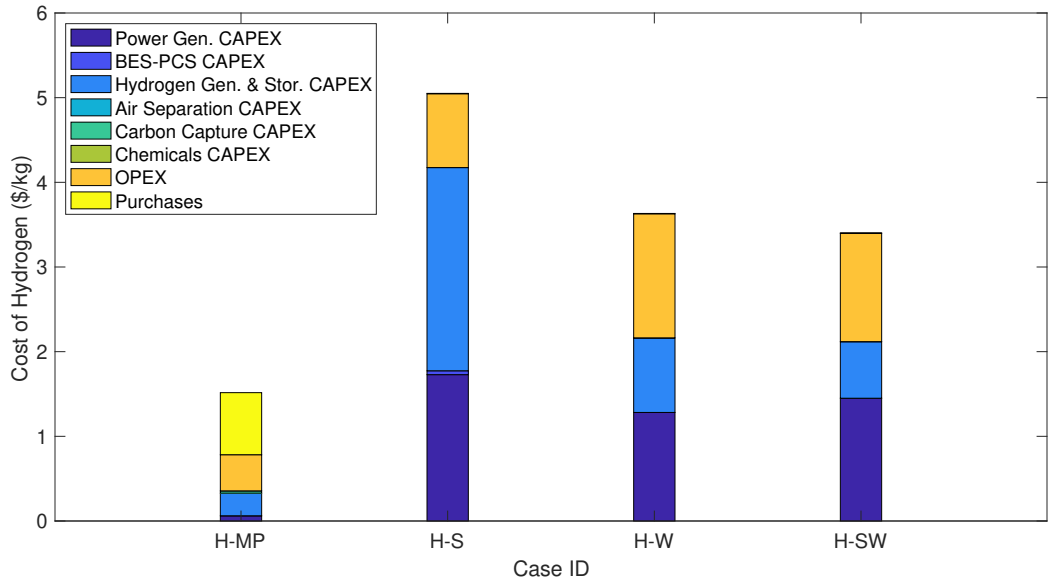


Figure 5.4: Total cost breakdown of hydrogen (H) production from methane pyrolysis (MP), solar (S), wind (W), and solar-wind (SW) powered water electrolysis.

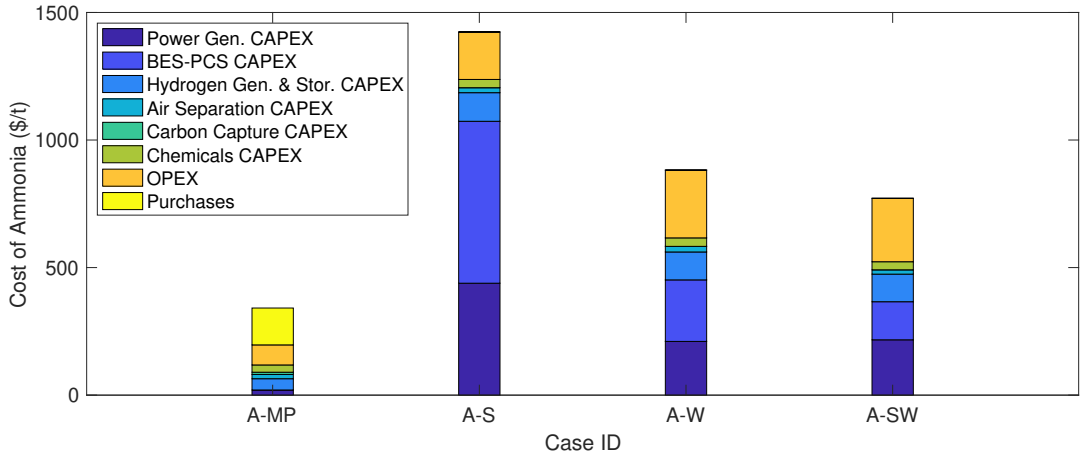


Figure 5.5: Total cost breakdown of ammonia (A) production from methane pyrolysis (MP), solar (S), wind (W), and solar-wind (SW) powered water electrolysis.

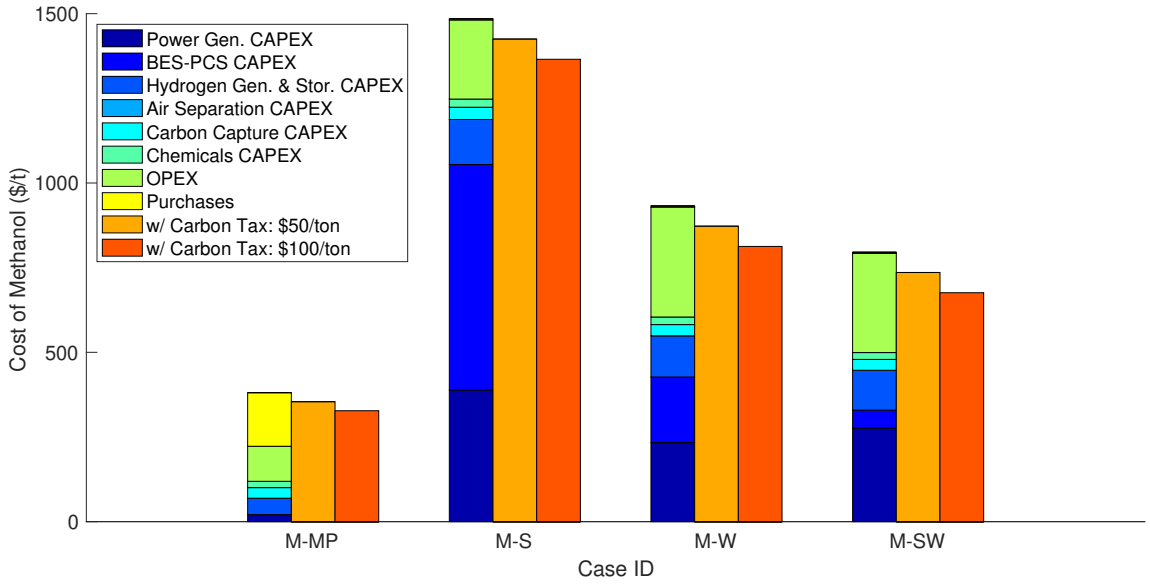


Figure 5.6: Total cost breakdown of methane (M) production from methane pyrolysis (MP), solar (S), wind (W), and solar-wind (SW) powered water electrolysis. Effect of carbon tax on methanol production is also investigated.

Figures 5.4, 5.5, and 5.6 show that production costs of hydrogen, ammonia, and methanol depend heavily on power generation, BES-PCS, and hydrogen generation & storage CAPEX. Methane pyrolysis is more cost effective pathway to produce hydrogen compared to water electrolysis powered by intermittent solar and wind. Integration of solar and wind power can bring the BES-PCS CAPEX down dramatically, due to synergistic effect of asynchronous solar and wind power availability. However, it should be noted that the strong solar and wind potential in Amarillo, Texas might not be easy to find in other parts of the world. It is highly likely that solar and wind power might not be available at the same time.

### 5.4.3 Case Study III: Power Production

Power production results are presented in Table 5.4. For steady 500 MW output, the strong solar and wind potential in Amarillo, Texas results in low cost of electricity. Integrated solar and wind powered power (P-SW) production cost is $0.054/kWh, that only 10% more than unsteady solar or wind electricity price as mentioned in the earlier chapters.

Table 5.4: Results for power (P) from solar (S), wind (W), and integrated solar-wind (SW) are shown. Case studies are done for 500 MW steady ac power output. Levelized cost of electricity (LCOE) is given in $/kWh.

| Case ID | LCOE ($/kWh) | Total Cost ($ MM/a) | RE Cap. (GW) | RE Gen. (GWh/a) | BES Storage (GWh) | DEC Prod. (kt/a) | Net Emissions (kt $CO_2$/a) |
|---|---|---|---|---|---|---|---|
| P-S | 0.116 | 592.82 | 1.74 | 6,498 | 10.50 | 28.2 | 0.0 |
| P-W | 0.077 | 394.96 | 0.86 | 6,250 | 2.22 | 74.3 | 0.0 |
| P-SW | 0.054 | 273.67 | 1.14 | 5,447 | 0.30 | 1.4 | 0.0 |

### 5.4.4 Case Study IV: Multi-product Networks

In this final case study, the combination of the results obtained from separate energy systems are compared with an integrated multi-product process network that has the same output. The best performing cases for individual fuels, hydrogen, ammonia, methanol, and power production are E-ATR, H-MP, A-MP, M-MP, and P-SW, respectively. For this comparison case study, all the five aforementioned separate facility costs are added to obtain the combined results. The details of the integrated process network and its total cost breakdown are given in Table 5.5 and Figure 5.7 in comparison with the combined process network.

Table 5.5: Results for integrated fuels, chemicals, and power process network (INT-NT) are compared with the combination of best separate fuels, chemicals, and power production facilities (Combined) that are E-ATR, H-MP, A-MP, M-MP, and P-SW.

| | Units | INT-NT | Combined |
|---|---|---|---|
| Total Production Costs | ($ MM/a) | 455.36 | 547.70 |
| Annualized CAPEX | ($ MM/a) | 213.43 | 292.68 |
| Annual OPEX (w/o Purchases) | ($ MM/a) | 134.86 | 137.10 |
| Annual Resource Purchases | ($ MM/a) | 107.07 | 117.89 |
| Natural Gas Purchase | (MSCF/a) | 38.04 | 41.81 |
| Renewable Energy Capacity | (GW) | 0.66 | 1.14 |
| Renewable Energy Production | (GWh/a) | 4,583 | 5,447 |
| Total Energy Storage Capacity | (GWh) | 0.12 | 0.30 |
| Net Emissions | (kt $CO_2$/a) | 0.00 | -113.55 |

Results from Table 5.5 show that integrated multi-product process network (INT-NT) brings

the total production cost 16.9% down compared to individual plants. Figure 5.7 shows that the INT-NT has the biggest advantage in reduced costs of power and hydrogen generation and storage sections. For hydrogen generation, INT-NT relies entirely on methane. For power generation methane gas turbine is combined with solar PV and wind farms. INT-NT requires a smaller renewable power generation and storage capacity, since methane gas turbine is used to back it up. While combined process network can give negative process emissions due to some forced pathways, INT-NT uses full advantage of the net zero emission constraint. There are scale-up synergies in methanol synthesis and air separation units. Methanol synthesis is found to play an important role in both fuels production and chemicals production. In Chapter 4, its role as a DEC is also shown.

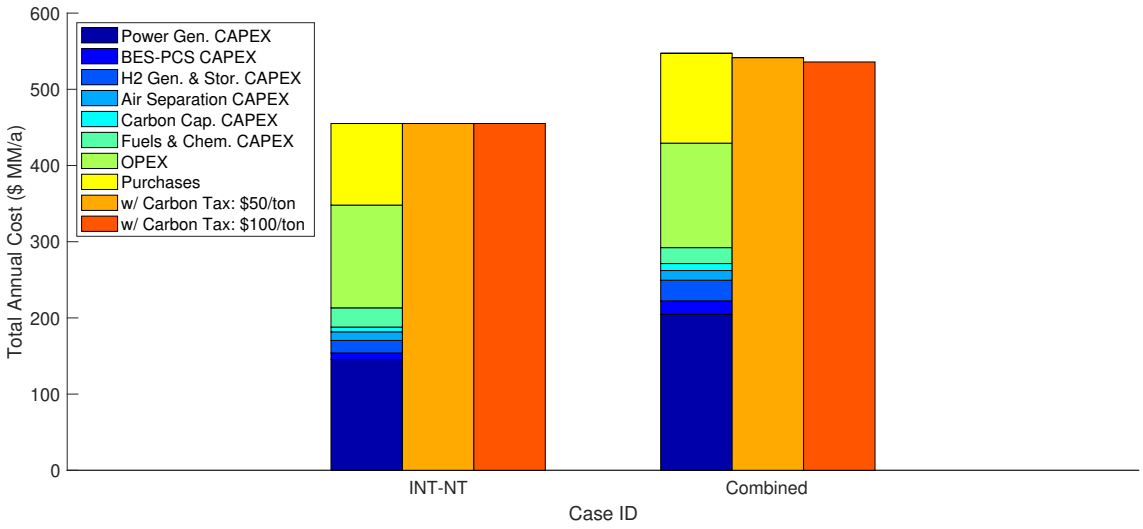


Figure 5.7: Total annual cost breakdown of selected cases for base and peak load matching.

The process network for INT-NT with the process capacities is given in Figure 5.8.

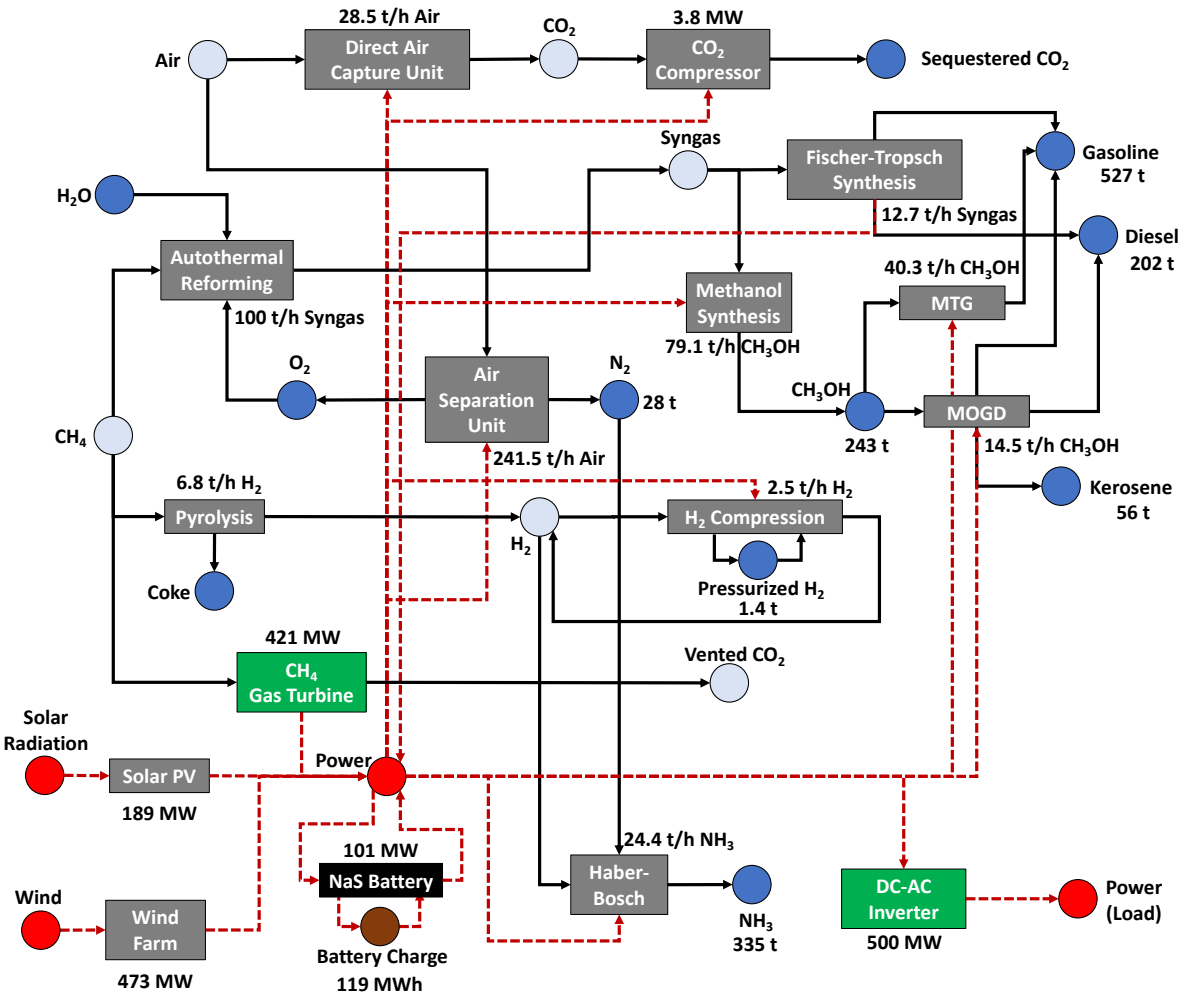


Figure 5.8: Optimal process network for integrated fuels, chemicals, and power production facility (INT-NT).

## 5.5 Conclusions

In this study, an optimization-based multi-scale design and operation strategy is used to analyze process networks of fuels, chemicals, and power production. With this method, each energy sector can be modeled separately or integrated in a multi-product process network.

This strategy is tested in synthetic transportation fuels (i.e. gasoline, diesel, kerosene), hydrogen, ammonia, methanol, and steady renewable power production using the resources in Amarillo, Texas. Case studies aimed to test various pathways ranging from methane reforming, methane pyrolysis, water electrolysis powered by solar and wind energy to generate power and

hydrogen. Carbon dioxide is either produced via methane reforming or captured from air via direct air capture method.

Integration of fuels, chemicals, and power production networks results in significant synergies in hydrogen and power generation systems. With such integrated facilities, methane conversion technologies, and methanol synthesis can play important roles, since they are versatile pathways leading to power and fuel&chemicals, respectively.

Case study results show that methane pyrolysis method can produce emission-free hydrogen at a lower cost that water electrolysis method. While still at prototype level, due to high process efficiency of the process it might offer a much stronger alternative against water electrolysis to generate low-carbon hydrogen. Intermittent solar and wind power are found to be most useful in power generation. In separate and integrated facilities, hydrogen production via water electrolysis powered by renewables is 2-3 times more expensive than methane pathways.

# 6. CONCLUSION AND FUTURE WORK

## 6.1 Concluding Remarks

The challenges related to the energy transition is multi-faceted and multi-scale. There is no silver bullet to solve all the problems, instead there are a multitude of alternatives that need to work together. To help better understand those systems while advancing the field of PSE, this dissertation develops new frameworks to optimally design and operate fossil and renewable energy systems. The studies are organized under four chapters. Below are given insightful concluding remarks on each chapter.

In Chapter 2, it is shown that given operational data, accurate nonlinear data-driven input-output models for refinery processing and mixing units can be obtained. Regularization methods are used to obtain sparse process models that can be efficiently used in large-scale multi-period NLP problems. Optimal production plans provide improvement over the actual plans by allocating the streams more efficiently between units to reduce raw material and operating costs. Multi-period planning approach provides further improvement over single-period planning.

In Chapter 3, production of ammonia is investigated for a variety of fossil and renewable pathways via a process synthesis and global optimization framework to reduce the carbon footprint of ammonia production. The effects of feedstock availabilities and prices in Texas, California, and Iowa are investigated via location-specific case studies. Biomass gasification is found to be an attractive choice over steam reforming of natural gas for bringing down the emissions of ammonia plants to 25% of the current level. Hardwood type of biomass performed better than corn stover and MSW. For all the states under investigation, wind and solar powered ammonia production costs are found to be much higher. Unless very strict GHG emission limitations or economic incentives are imposed, it is hard for these technologies to compete with natural gas and biomass pathways. Biggest reason for this is the high energy consumption of hydrogen production via water electrolysis.

In Chapter 4, an optimization-based multi-scale design and operation strategy is introduced to analyze the techno-economic feasibility of renewable power generation and storage systems that use battery electric storage and dense energy carriers. Single-location and multi-location case studies are investigated to find out that when DECs used together with local battery storage, they can offer up to 50% cost reductions. The main advantage of using DECs is providing a clean backup fuel for times when local intermittent renewable resources are scarce. In the absence of such backup fuels, local power generation and storage capacities are oversizing to make up for scarce resource period. Fully replacing the energy demand via DECs produced at a high renewable energy potential region like TX offer less promising economics due to increased transportation and storage costs. The DEC-local resource synergy is found to be more valuable to exploit. The cost of local power generation and storage, if available, is highly sensitive to renewable penetration levels. Availability of a clean backup power source helps to stabilize it. Also, integration of solar and wind power to be highly beneficial since these two resources generally peak at different times. Integration of solar and wind mitigates the intermittency effects of a single resource.

In Chapter 5, the multi-scale simultaneous design and operation strategy is extended to integrated power, fuels, and chemicals production. With this method, each energy sector can be modeled separately or in an integrated fashion for a multi-product process network. Integrated facilities successfully bring down the process costs by 17%. The key synergies in integration are observed at power and hydrogen generation and storage sections. For fuels or chemicals production via low-carbon pathways, methane pyrolysis is shown to have a promising potential. Intermittent solar and wind power are found to be most useful in power generation. In both separate and integrated facilities, hydrogen production via water electrolysis powered by renewables is 2-3 times more expensive than methane pathways. While increasing renewable penetration in power sector can have an impact on lowering the emissions, using renewable power to produce liquid products might not be the most cost effective pathway as of today's technological capability.

## 6.2 Key Contributions

The key contributions of this dissertation are summarized below:

1. Development of a framework that combines data-driven modeling with nonlinear multi-period planning formulation that is used for optimizing refinery production plans using real plant data. Nonlinear input-output models for all processing units are created using real plant data. The developed feature selection procedure allows for efficient integration of modeling and multi-period optimization. The multi-period production plan allows for inventory management to increase the degrees of freedom of the optimization problem.

2. Implementation of process synthesis and global optimization methods to synthesize sustainable ammonia production processes with significant GHG reductions. Aim of this study is to compare biomass-, wind-, and solar-based ammonia production routes with natural gas-based reference case study via having all process options in the same process superstructure. Case studies are done for different geographical locations, where feedstock and electricity prices and availability vary greatly.

3. Development a multi-scale modeling and optimization strategy relying on mixed-integer linear programming techniques to find the optimal design and operational decisions of multi-location GWh-scale energy generation and storage systems. The strategy uses multi-period formulation to address the intermittency in the resource availability. The multi-location aspect allows for the production and transportation of DECs between high- and low-potential regions to account for the supply chain problems. Hierarchical clustering techniques are used to find representative seasons to reduce the size of the problem. The overall approach is multi-scale by nature since it deals with problems of design, scheduling, and supply chain simultaneously.

4. Further extension of the multi-scale modeling and optimization strategy developed for renewable energy generation, storage, and transportation to power, fuels, and chemicals production to optimally design and operate multi-product process networks. Using multi-period formulation the intermittent renewable resources are integrated with fossil fuel technologies.

## 6.3 Future Work

This dissertation is aimed to develop novel strategies for tackling energy transition challenges by using the process systems engineering methods. The methods presented are designed to be generalizable, however, it is not possible to cover the entire landscape with this dissertation. In this section, a brief list of possible future directions is presented. Each direction aims to follow the natural extensions of the completed work, introduce the fundamental difficulties that can manifest itself as a result of such effort, and finally present a strategy.

### 6.3.1 Uncertainty as a Part of Design and Operation of Energy Systems

Uncertainty appears in any optimization work. The parameter estimates that are used in raw material costs, performance coefficient, unit capital costs, or product demands are assumed to be at nominal values, making the problems deterministic. However, in reality all parameters are uncertain with different intervals of confidence. An optimal profitable design that is made based on a certain cost of natural gas, might be unprofitable if that cost changes. All models and optimal solutions are subjected to uncertainty in Chapters 2, 3, 4, and 5.

The impacts of parameter uncertainty on the optimal solutions can be quantitatively assessed via either robust optimization or stochastic programming. One application of these methods can be assessing the effects of uncertainty of solar DNI, wind speed, and electricity prices on the renewable power generation and storage problem. In Chapters 4 and 5, the design decisions are made based on representative days, that are centroids of each data cluster they represent. However, if the best and worst cases of each cluster are also included in the data set, the optimal design can be different. It will be interesting to see the effects of uncertainty on network designs.

### 6.3.2 Life Cycle GHG Analysis as a Part of Decision-Making Processes

In Chapter 3, the GHG emissions related with process byproducts, feedstock acquisition, and end-product use are accounted and restricted. In Chapters 4 and 5, only the process emissions are acounted and restricted. For a more thorough life cycle GHG analysis, the GHG emissions related with manufacturing, installation, and maintenance of each technology need to be considered

along the aforementioned sources of emissions. For this purpose, there are published work and available software tools to estimate system level GHG emissions such as NREL's GREET or MIT's Sustainable Energy System Analysis Modelling Environment (SESAME).

The incorporation of such life cycle GHG emission analysis can change to decision-making process. By putting strict limitations on GHG emissions via policy decisions, the techno-economic performance of the process networks change. It can be interesting to see the trade-offs between competing objectives of cost minimization, profit maximization, and GHG emisison minimization. Multi-objective optimization strategies to produce Pareto curves can provide insights to the decision-makers.

### 6.3.3 Strategic Planning and Capacity Expansion of Renewable and Fossil Energy Systems

The multi-scale design and operation strategy developed for Chapters 4 and 5, assume a static investment horizon. The decision of investment is made here-and-now, and there is no recourse or capacity expansion that follows that initial decision. However, as history has shown, both process efficiencies and capital costs are functions of time. The energy transition will definitely not take place in a decade, but over a period of multiple decades. In this picture, there is a great value in analyzing long-term strategic planning and capacity expansion methods [221].

The RTN formulation that is used in Chapters 4 and 5 is well-suited for a strategic planning formulation. By including an investment period horizon to the decisions, great insights into possible future evolution of the energy systems can be investigated. With such an approach, it is important to include learning curves to all the technologies. Just to give an example, from 2009 to 2017, the cost of solar PV modules and wind turbines decreased up to 81 and 50%, respectively [74]. Such changes can significantly improve the attractiveness and the penetration of certain technologies over time. Because of the growing size of the problem, rolling horizon method can be implemented to solve the optimization model.

### 6.3.4 The Reliability and Resilience of Integrated Process Networks

As the process networks become more interconnected, they also become more interdependent. The security of the energy, fuels, and chemicals supply chains are vulnerable to natural disasters like hurricanes, earthquakes, and pandemic spreads. Integrated systems provide efficient resource utilization and distribution, however, with the current approach the reliability (i.e. if a site closes down, how does the rest of the networks work) and resilience (i.e. if a system goes on outage, how can it come back to operation) of the process networks are not considered in the design and operation optimization.

The RTN formulation used with multiple sites can be used in a network analysis to test different scenarios to investigate how the entire supply chain is affected after a partial or complete shutdown or fail takes place at a site. Through such an analysis, the importance of backup and auxiliary units can be determined.

# REFERENCES


[1] V. Smil, *Energy and Civilization: A History*. Cambridge, Massachusetts: The MIT Press, 2017.

[2] J. K. Steinberger, "Energising human development," 2016.

[3] D. M. Martínez and B. W. Ebenhack, "Understanding the role of energy consumption in human development through the use of saturation phenomena," *Energy Policy*, vol. 36, no. 4, pp. 1430 – 1435, 2008.

[4] World Bank, "Population Estimates and Projections." https://datacatalog.worldbank.org/dataset/population-estimates-and-projections, Retrieved May 25, 2018.

[5] ExxonMobil, "2019 outlook for energy: A perspective to 2040."

[6] Shell, "Shell Energy Transition Report." https://www.shell.com/energy-and-innovation/the-energy-future/shell-energy-transition-report.html, 2018.

[7] BP, "Energy Outlook 2018 Edition." https://www.bp.com/en/global/corporate/energy-economics/energy-outlook.html, 2018.

[8] A. A. Lacis, G. A. Schmidt, D. Rind, and R. A. Ruedy, "Atmospheric co2: Principal control knob governing earth's temperature," *Science*, vol. 330, no. 6002, pp. 356–359, 2010.

[9] NASA, "Carbon dioxide controls Earth's temperature." https://climate.nasa.gov/news/423/carbon-dioxide-controls-earths-temperature/, 2010.

[10] Scientific American, "$CO_2$ Emissions Will Break Another Record in 2019." https://www.scientificamerican.com/article/co2-emissions-will-break-another-record-in-2019/, 2019.

[11] IPCC, "Climate Change 2014 - Synthesis Report." https://www.ipcc.ch/site/assets/uploads/2018/02/SYR_AR5_FINAL_full.pdf, 2014.

[12] P. Liu, E. N. Pistikopoulos, and Z. Li, "Energy systems engineering: methodologies and applications," *Front. Energy Power Eng. China*, vol. 4(2), pp. 131–142, 2010.

[13] E. J. Sheu, A. Mitsos, A. A. Eter, E. M. Mokheimer, M. A. Habib, and A. Al-Qutub, "A review of hybrid solar–fossil fuel power generation systems and performance metrics," *Journal of Solar Energy Engineering*, vol. 134, no. 4, p. 041006, 2012.

[14] A. Mitsos, N. Asprion, C. A. Floudas, M. Bortz, M. Baldea, D. Bonvin, A. Caspari, and P. Schaefer, "Challenges in process optimization for new feedstocks and energy sources," *Comput. Chem. Eng.*, vol. 113, pp. 209–221, 2018.

[15] EIA, "Monthly Energy Review – March 2020." https://www.eia.gov/totalenergy/data/monthly/, 2020.

[16] "IRENA - Renewable Capacity Statistics 2019."

[17] National Renewable Energy Laboratory, "Overgeneration from Solar Energy in California: A Field Guide to the Duck Chart." USDOE contract DE-AC36-08GO28308, 2015.

[18] National Renewable Energy Laboratory, "National Solar Radiation Database (NSRDB." https://nsrdb.nrel.gov/, 2015.

[19] National Renewable Energy Laboratory, "Wind Integration National Dataset Toolkit." https://www.nrel.gov/grid/wind-toolkit.html, 2018.

[20] National Renewable Energy Laboratory, "Biomass Maps." https://www.nrel.gov/gis/biomass.html, 2015.

[21] I. E. Grossmann, "Mixed-integer programming approach for the synthesis of integrated process flowsheets," *Comput. Chem. Eng.*, vol. 9(5), pp. 463–482, 1985.

[22] M. Martin and T. A. Adams, "Future directions in process and product synthesis and design," in *Proceedings of the 13$^{th}$ International Symposium on Process Systems Engineering - PSE 2018*, (San Diego, CA), 2018.

[23] C. A. Floudas, *Nonlinear and Mixed-Integer Optimization*. New York, NY: Oxford University Press, 1995.

[24] L. T. Biegler, I. E. Grossmann, and A. W. Westerberg, *Systematic methods for chemical process design*. Old Tappan, NJ: Prentice Hall, 1997.

[25] M. C. Georgiadis, E. S. Kikkinides, and E. N. Pistikopoulos, *Energy systems engineering*, vol. 5. Weinheim, Germany: John Wiley & Sons, 2008.

[26] C. A. Floudas, A. M. Niziolek, O. Onel, and L. R. Matthews, "Multi-scale systems engineering for energy and the environment: Challenges and opportunities," *AIChE J*, vol. 62(3), pp. 602–623, 2016.

[27] L. T. Biegler, Y.-d. Lang, and W. Lin, "Multi-scale optimization for process systems engineering," *Computers & Chemical Engineering*, vol. 60, pp. 17–30, 2014.

[28] C. D. Demirhan, W. W. Tso, G. S. Ogumerem, and E. N. Pistikopoulos, "Energy systems engineering - a guided tour," *BMC Chemical Engineering*, vol. 1, no. 11, 2019.

[29] A. Subramanian, T. Gundersen, and T. Adams, "Modeling and simulation of energy systems: A review," *Processes*, vol. 6, no. 12, p. 238, 2018.

[30] D. G. Vlachos, "A review of multiscale analysis: examples from systems biology, materials engineering, and other fluid–surface interacting systems," *Advances in Chemical Engineering*, vol. 30, pp. 1–61, 2005.

[31] M. Salciccioli, M. Stamatakis, S. Caratzoulas, and D. G. Vlachos, "A review of multiscale modeling of metal-catalyzed reactions: Mechanism development for complexity and emergent behavior," *Chemical Engineering Science*, vol. 66, no. 19, pp. 4319–4355, 2011.

[32] S. J. Qin, "Survey on data-driven industrial process monitoring and diagnosis," *Annual Reviews in Control*, vol. 36, no. 2, pp. 220–234, 2012.

[33] A. Bhosekar and M. Ierapetritou, "Advances in surrogate based modeling, feasibility analysis, and optimization: A review," *Computers & Chemical Engineering*, vol. 108, pp. 250–267, 2018.

[34] J. H. Lee, J. Shin, and M. J. Realff, "Machine learning: Overview of the recent progresses and implications for the process systems engineering field," *Computers & Chemical Engineering*, vol. 114, pp. 111–121, 2018.

[35] J. Gong and F. You, "Sustainable design and synthesis of energy systems," *Current Opinion in Chemical Engineering*, vol. 10, pp. 77–86, 2015.

[36] I. E. Grossmann, J. A. Caballero, and H. Yeomans, "Mathematical programming approaches to the synthesis of chemical process systems," *Korean Journal of Chemical Engineering*, vol. 16, no. 4, pp. 407–426, 1999.

[37] S. E. Demirel, J. Li, and M. F. Hasan, "Systematic process intensification using building blocks," *Computers & Chemical Engineering*, vol. 105, pp. 2–38, 2017.

[38] Y. Tian, S. E. Demirel, M. F. Hasan, and E. N. Pistikopoulos, "An overview of process systems engineering approaches for process intensification: State of the art," *Chemical Engineering and Processing-Process Intensification*, vol. 133, pp. 278–293, 2018.

[39] M. T. Melo, S. Nickel, and F. Saldanha-Da-Gama, "Facility location and supply chain management–a review," *European Journal of Operational Research*, vol. 196, no. 2, pp. 401–412, 2009.

[40] L. G. Papageorgiou, "Supply chain optimisation for the process industries: Advances and opportunities," *Computers & Chemical Engineering*, vol. 33, no. 12, pp. 1931–1938, 2009.

[41] M. F. Hasan, F. Boukouvala, E. L. First, and C. A. Floudas, "Nationwide, regional, and statewide co2 capture, utilization, and sequestration supply chain network optimization," *Industrial & Engineering Chemistry Research*, vol. 53, no. 18, pp. 7489–7506, 2014.

[42] L. V. Kantorovich, "Mathematical methods of organizing and planning production," *Management Science*, vol. 6, no. 4, pp. 366–422, 1960.

[43] G. B. Dantzig, "Programming in a linear structure," *Econometrica*, vol. 17, pp. 73–74, 1949.

[44] E. Balas, "Disjunctive programming," *Annals of Discrete Mathematics*, vol. 5, pp. 3–51, 1979.

[45] R. C. Baliban, J. A. Elia, R. Misener, and C. A. Floudas, "Global optimization of a minlp process synthesis model for thermochemical based conversion of hybrid coal, biomass, and natural gas to liquid fuels," *Computers & Chemical Engineering*, vol. 42, pp. 64–86, 2012.

[46] C. A. Floudas, *Deterministic global optimization: theory, methods and applications*, vol. 37. Boston, MA: Springer Science & Business Media, 2000.

[47] F. Boukouvala, R. Misener, and C. A. Floudas, "Global optimization advances in mixed-integer nonlinear programming, minlp, and constrained derivative-free optimization, cdfo," *European Journal of Operational Research*, vol. 252, no. 3, pp. 701–727, 2016.

[48] S. L. Janak, C. A. Floudas, J. Kallrath, and N. Vormbrock, "Production scheduling of a large-scale industrial batch plant. i. short-term and medium-term scheduling," *Industrial & Engineering Chemistry Research*, vol. 45, no. 25, pp. 8234–8252, 2006.

[49] N. K. Shah, Z. Li, and M. G. Ierapetritou, "Petroleum refining operations: Key issues, advances, and opportunities," *Industrial & Engineering Chemistry Research*, vol. 50, no. 3, pp. 1161–1170, 2011.

[50] J. Kallrath, "Planning and scheduling in the process industry," *OR Spectrum*, vol. 24, no. 3, pp. 219–250, 2002. cited By 218.

[51] J. Kallrath, "Solving planning and design problems in the process industry using mixed integer and global optimization," *Annals of Operations Research*, vol. 140, no. 1, pp. 339–373, 2005. cited By 47.

[52] J. Li, X. Xiao, F. Boukouvala, C. A. Floudas, B. Zhao, G. Du, X. Su, and H. Liu, "Data-driven mathematical modeling and global optimization framework for entire petrochemical planning operations," *AIChE Journal*, vol. 62, no. 9, pp. 3020–3040, 2016.

[53] C. S. Khor and D. Varvarezos, "Petroleum refinery optimization," *Optimization and Engineering*, vol. 18, pp. 943–989, Dec 2017.

[54] M. Tawarmalani and N. Sahinidis, "A polyhedral branch-and-cut approach to global optimization," *Mathematical Programming*, vol. 103, no. 2, pp. 225–249, 2005. cited By 367.

[55] R. Misener and C. A. Floudas, "ANTIGONE: Algorithms for coNTinuous / Integer Global Optimization of Nonlinear Equations," *Journal of Global Optimization*, vol. 59, no. 2-3, pp. 503–526, 2014.

[56] C. Tsay, R. C. Pattison, M. R. Piana, and M. Baldea, "A survey of optimal process design capabilities and practices in the chemical and petrochemical industries," *Comput. & Chem. Eng.*, vol. 112, pp. 180 – 189, 2018.

[57] C. Cuiwen, G. Xingsheng, and X. Zhong, "A data-driven rolling-horizon online scheduling model for diesel production of a real-world refinery," *AIChE Journal*, vol. 59, no. 4, pp. 1160–1174, 2013. cited By 10.

[58] United States Geological Survey, "Nitrogen - Statistics and Information." https://minerals.usgs.gov/minerals/pubs/commodity/nitrogen/, 2018.

[59] M. Appl, *Ammonia: Principles and Industrial Practice*. Weinheim, Germany: Wiley-VCH Verlag, 1999.

[60] Food and Agriculture Organization of the United Nations, "World Agriculture Towards 2030/2050." http://www.fao.org/economic/esa, 2012.

[61] E. R. Morgan, J. F. Manwell, and J. G. McGowan, "Sustainable ammonia production from u.s. offshore wind farms: A techno-economic review," *ACS Sustainable Chemistry and Engineering*, vol. 5, no. 11, pp. 9554–9567, 2017. cited By 1.

[62] E. Morgan, J. Manwell, and J. McGowan, "Wind-powered ammonia fuel production for remote islands: A case study," *Renewable Energy*, vol. 72, pp. 51 – 61, 2014.

[63] Department of Energy, "Potential Roles of Ammonia in a Hydrogen Economy: A Study of Issues Related to the Use of Ammonia for On-Board Vehicular Hydrogen Storage." https:

//www.energy.gov/eere/fuelcells/downloads/potential-roles-ammonia-hydrogen-economy, 2006.

[64] L. Green, "An ammonia energy vector for the hydrogen economy," *International Journal of Hydrogen Energy*, vol. 7, no. 4, pp. 355 – 359, 1982.

[65] R. Lan, J. T. S. Irvine, and S. Tao, "Ammonia and related chemicals as potential indirect hydrogen storage materials," *International Journal of Hydrogen Energy*, vol. 37, no. 2, pp. 1482 – 1494, 2012.

[66] D. Miura and T. Tezuka, "A comparative study of ammonia energy systems as a future energy carrier, with particular reference to vehicle use in japan," *Energy*, vol. 68, pp. 428 – 436, 2014.

[67] P. Preuster, A. Alekseev, and P. Wasserscheid, "Hydrogen storage technologies for future energy systems," *Annual Review of Chemical and Biomolecular Engineering*, vol. 8, no. 1, pp. 445–471, 2017.

[68] G. Wang, A. Mitsos, and W. Marquardt, "Conceptual design of ammonia-based energy storage system: System design and time-invariant performance," *AIChE Journal*, vol. 63, no. 5, pp. 1620–1637, 2017. cited By 1.

[69] V. Smil, "Detonator of the population explosion," *Nature*, vol. 400, no. 6743, p. 415, 1999. cited By 134.

[70] "Ammonia production causes 1 % of total global ghg emissions."

[71] International Energy Agency, "Renewable Energy for Industry: From green energy to green materials and fuels." https://www.iea.org/publications/insights/insightpublications/, 2017.

[72] P. Arora, A. F. A. Hoadley, S. M. Mahajani, and A. Ganesh, "Small-scale ammonia production from biomass: A techno-enviro-economic perspective," *Industrial & Engineering Chemistry Research*, vol. 55, no. 22, pp. 6422–6434, 2016.

[73] BP, "BP Statistical Review of World Energy 2019." https://www.bp.com/en/global/corporate/energy-economics/statistical-review-of-world-energy.html, 2019.

[74] International Renewable Energy Agency, "Renewable Power Generation Costs in 2017." http://irena.org/publications/2018/Jan/Renewable-power-generation-costs-in-2017, 2018.

[75] O. Schmidt, A. Gambhir, I. Staffell, A. Hawkes, J. Nelson, and S. Few, "Future cost and performance of water electrolysis: An expert elicitation study," *International Journal of Hydrogen Energy*, vol. 42, no. 52, pp. 30470 – 30492, 2017.

[76] "ENEA Consulting - Energy Storage Facts & Figures."

[77] R. C. Baliban, J. A. Elia, and C. A. Floudas, "Toward novel biomass, coal, and natural gas processes for satisfying current transportation fuel demands, 1: Process alternatives, gasification modeling, process simulation, and economic analysis," *Ind. Eng. Chem. Res.*, vol. 49, no. 16, pp. 7343–7370, 2010.

[78] O. Onel, A. M. Niziolek, M. M. F. Hasan, and C. A. Floudas, "Municipal solid waste to liquid transportation fuels - Part I: Mathematical modeling of a municipal solid waste gasifier," *Comput. Chem. Eng.*, vol. 71(0), pp. 636–647, 2014.

[79] A. M. . Niziolek, O. Onel, M. M. F. Hasan, and C. A. Floudas, "Municipal solid waste to liquid transportation fuels - Part II: Process synthesis and global optimization strategies," *Comput. Chem. Eng.*, vol. 74, pp. 184 – 203, 2015.

[80] A. M. Niziolek, O. Onur, Y. Tian, C. A. Floudas, and E. N. Pistikopoulos, "Municipal solid waste to liquid transportation fuels – part iii: An optimization-based nationwide supply chain management framework," *Comput. Chem. Eng.*, vol. 116, pp. 468 – 487, 2018.

[81] G. S. Ogumerem, W. W. Tso, C. D. Demirhan, S. Y. Lee, H. E. Song, and E. N. Pistikopoulos, "Toward the optimization of hydrogen, ammonia, and methanol supply chains," *IFAC-PapersOnLine*, vol. 52, no. 1, pp. 844 – 849, 2019. 12th IFAC Symposium on Dynamics and Control of Process Systems, including Biosystems DYCOPS 2019.

[82] ExxonMobil, "Exxonmobil 2018 outlook for energy: A view to 2040."

[83] P. Liu, M. C. Georgiadis, and E. N. Pistikopoulos, "Advances in energy systems engineering," *Ind. Eng. Chem. Res*, vol. 50, pp. 4915–4925, 2011.

[84] R. J. Quann and S. B. Jaffe, "Structure-oriented lumping: describing the chemistry of complex hydrocarbon mixtures," *Industrial & Engineering Chemistry Research*, vol. 31, no. 11, pp. 2483–2497, 1992.

[85] S. B. Jaffe, H. Freund, and W. N. Olmstead, "Extension of structure-oriented lumping to vacuum residua," *Industrial & Engineering Chemistry Research*, vol. 44, no. 26, pp. 9840–9852, 2005.

[86] R. J. Quann, "Modeling the chemistry of complex petroleum mixtures.," *Environmental Health Perspectives*, vol. 106, no. suppl 6, pp. 1441–1448, 1998.

[87] J. M. Pinto, M. Joly, and L. F. L. Moro, "Planning and scheduling models for refinery operations," *Computers and Chemical Engineering*, vol. 24, no. 9-10, pp. 2259–2276, 2000.

[88] J. Li and I. A. Karimi, "Scheduling gasoline blending operations from recipe determination to shipping using unit slots," *Industrial & Engineering Chemistry Research*, vol. 50, no. 15, pp. 9156–9174, 2011.

[89] J. Li, R. Misener, and C. A. Floudas, "Continuous-time modeling and global optimization approach for scheduling of crude oil operations," *AIChE Journal*, vol. 58, no. 1, pp. 205–226, 2012.

[90] W. Li, C.-W. Hui, and A. Li, "Integrating cdu, fcc and product blending models into refinery planning," *Computers and Chemical Engineering*, vol. 29, no. 9, pp. 2010–2028, 2005. cited By 67.

[91] I. Alhajri, A. Elkamel, T. Albahri, and P. Douglas, "A nonlinear programming model for refinery planning and optimisation with rigorous process models and product quality specifications," *International Journal of Oil, Gas and Coal Technology*, vol. 1, no. 3, pp. 283–307, 2008.

[92] B. Menezes, J. Kelly, and I. Grossmann, "Improved swing-cut modeling for planning and scheduling of oil-refinery distillation units," *Industrial and Engineering Chemistry Research*, vol. 52, no. 51, pp. 18324–18333, 2013. cited By 19.

[93] S. M. S. Neiro and J. M. Pinto, "Multiperiod optimization for production planning of petroleum refineries," *Chemical Engineering Communications*, vol. 192, no. 1-3, pp. 62–88, 2005. cited By 0.

[94] L. d. P. A. Sales, F. M. T. d. Luna, and B. d. A. Prata, "An integrated optimization and simulation model for refinery planning including external loads and product evaluation," *Brazilian Journal of Chemical Engineering*, vol. 35, no. 1, pp. 199–215, 2018.

[95] Y. Yang and P. I. Barton, "Refinery optimization integrated with a nonlinear crude distillation unit model," *IFAC-PapersOnLine*, vol. 48, no. 8, pp. 205 – 210, 2015. 9th IFAC Symposium on Advanced Control of Chemical Processes ADCHEM 2015.

[96] P. Castillo Castillo, P. M. Castro, and V. Mahalec, "Global optimization algorithm for large-scale refinery planning models with bilinear terms," *Industrial & Engineering Chemistry Research*, vol. 56, no. 2, pp. 530–548, 2017.

[97] R. Baliban, J. Elia, and C. Floudas, "Toward novel hybrid biomass, coal, and natural gas processes for satisfying current transportation fuel demands, 1: Process alternatives, gasification modeling, process simulation, and economic analysis," *Industrial and Engineering Chemistry Research*, vol. 49, no. 16, pp. 7343–7370, 2010. cited By 83.

[98] O. Onel, A. Niziolek, H. Butcher, B. Wilhite, and C. Floudas, "Multi-scale approaches for gas-to-liquids process intensification: Cfd modeling, process synthesis, and global optimization," *Computers and Chemical Engineering*, 2017. cited By 0; Article in Press.

[99] B. Beykal, F. Boukouvala, C. A. Floudas, N. Sorek, H. Zalavadia, and E. Gildin, "Global optimization of grey-box computational systems using surrogate functions and application to highly constrained oil-field operations," *Computers & Chemical Engineering*, vol. 114, pp. 99 – 110, 2018. FOCAPO/CPC 2017.

[100] T. E. Swaty, "Consider over-the-fence product stream swapping to raise profitability," *Hydrocarbon Processing*, vol. 81, no. 3, pp. 37–42, 2002.

[101] K. Al-Qahtani and A. Elkamel, "Multisite refinery and petrochemical network design: Optimal integration and coordination," *Industrial & Engineering Chemistry Research*, vol. 48, no. 2, pp. 814–826, 2009.

[102] S. A. Imtiaz and S. L. Shah, "Treatment of missing values in process data analysis," *The Canadian Journal of Chemical Engineering*, vol. 86, no. 5, pp. 838–858, 2008.

[103] A. Folch-Fortuny, F. Arteaga, and A. Ferrer, "Pca model building with missing data: New proposals and a comparative study," *Chemometrics and Intelligent Laboratory Systems*, vol. 146, pp. 77 – 88, 2015.

[104] S. Xu, B. Lu, M. Baldea, T. F. Edgar, W. Wojsznis, T. Blevins, and M. Nixon, "Data cleaning in the process industries.," *Reviews in Chemical Engineering*, vol. 31, no. 5, pp. 453 – 490, 2015.

[105] K. A. Severson, M. C. Molaro, and R. D. Braatz, "Principal component analysis of process datasets with missing values," *Processes*, vol. 5, no. 3, 2017.

[106] A. Folch-Fortuny, F. Arteaga, and A. Ferrer, "Missing data imputation toolbox for matlab," *Chemometrics and Intelligent Laboratory Systems*, vol. 154, pp. 93 – 100, 2016.

[107] R. H. Myers, D. C. Montogomery, and C. M. Anderson-Cook, *Response Surface Methodology - Process and Product Optimization Using Designed Experiments*. Hoboken, NJ: John Wiley & Sons, 2012.

[108] H. Xiang, Y. Li, H. Liao, and C. Li, "An adaptive surrogate model based on support vector regression and its application to the optimization of railway wind barriers," *Struct. Multidiscip. Optim.*, vol. 55, pp. 701–713, Feb. 2017.

[109] J. Zhai and F. Boukouvala, "Nonlinear variable selection algorithms for surrogate modeling," *AIChE Journal*, vol. 65, no. 8, 2019.

[110] T. Hastie, R. Tibshirani, and M. Wainwright, *Statistical Learning with Sparsity: The Lasso and Generalizations*. Chapman & Hall/CRC, 2015.

[111] A. Alattas, I. Grossmann, and I. Palou-Rivera, "Refinery production planning: Multiperiod minlp with nonlinear cdu model," *Industrial and Engineering Chemistry Research*, vol. 51, no. 39, pp. 12852–12861, 2012. cited By 8.

[112] J. H. Merrick, "On representation of temporal variability in electricity capacity planning models," *Energy Economics*, vol. 59, pp. 261 – 274, 2016.

[113] L. Kotzur, P. Markewitz, M. Robinius, and D. Stolten, "Impact of different time series aggregation methods on optimal energy system design," *Renewable Energy*, vol. 117, pp. 474 – 487, 2018.

[114] S. Pineda and J. M. Morales, "Chronological time-period clustering for optimal capacity expansion planning with storage," *IEEE Transactions on Power Systems*, vol. 33, no. 6, pp. 7162–7170, 2018.

[115] G. Marnellos and M. Stoukides, "Ammonia synthesis at atmospheric pressure," *Science*, vol. 282, no. 5386, pp. 98–100, 1998.

[116] M. Malmali, Y. Wei, A. McCormick, and E. L. Cussler, "Ammonia synthesis at reduced pressure via reactive separation," *Industrial & Engineering Chemistry Research*, vol. 55, no. 33, pp. 8922–8932, 2016.

[117] M. Aziz, T. Oda, A. Morihara, and T. Kashiwagi, "Combined nitrogen production, ammonia synthesis, and power generation for efficient hydrogen storage," *Energy Procedia*, vol. 143, pp. 674 – 679, 2017. Leveraging Energy Technologies and Policy Options for Low Carbon Cities.

[118] Department of Energy, "Sustainable Ammonia Synthesis: DOE Roundtable Report." https://science.energy.gov/bes/community-resources/reports/, 2016.

[119] International Fertilizer Industry Association, "Fertilizers, Climate Change and Enchancing Agricultural Productivity Sustainably," 2009.

[120] Industrial Efficiency Technological Database, "Ammonia." http://ietd.iipnetwork.org/content/ammonia, Retrieved May 27, 2018.

[121] IPCC, "2006 IPCC Guidelines for National Greenhouse Gas Inventories Volume 3 Industrial Processes and Product Use." https://www.ipcc-nggip.iges.or.jp/public/2006gl/, 2006.

[122] P. Gilbert, S. Alexander, P. Thornley, and J. Brammer, "Assessing economically viable carbon reductions for the production of ammonia from biomass gasification," *Journal of Cleaner Production*, vol. 64, pp. 581 – 589, 2014.

[123] L. Tock, F. Marechal, and M. Perrenoud, "Thermo-environomic evaluation of the ammonia production," *The Canadian Journal of Chemical Engineering*, vol. 93, no. 2, pp. 356–362, 2015.

[124] J. Andersson and J. Lundgren, "Techno-economic analysis of ammonia production via integrated biomass gasification," *Applied Energy*, vol. 130, pp. 484 – 490, 2014.

[125] P. Arora, A. F. A. Hoadley, S. M. Mahajani, and A. Ganesh, "Multi-objective optimization of based ammonia production - potential and perspective in different countries," *Journal of Cleaner Production*, vol. 148, pp. 363 – 374, 2017.

[126] S. S. Randhava, S. S. Randhava, T. Harvey, and R. L. Kao, "Process for producing ammonia from biomass," Aug. 18 2008. US Patent 8,679,439 B2.

[127] A. Allman, P. Daoutidis, D. Tiffany, and S. Kelley, "A framework for ammonia supply chain optimization incorporating conventional and renewable generation," *AIChE Journal*, vol. 63, no. 10, pp. 4390–4402, 2017. cited By 1.

[128] A. Allman and P. Daoutidis, "Optimal scheduling for wind-powered ammonia generation: Effects of key design parameters," *Chemical Engineering Research and Design*, vol. 131, pp. 5 – 15, 2018. Energy Systems Engineering.

[129] Z. Du, D. Denkenberger, and J. M. Pearce, "Solar photovoltaic powered on-site ammonia production for nitrogen fertilization," *Solar Energy*, vol. 122, pp. 562 – 568, 2015.

[130] A. Sanchez and M. Martin, "Optimal renewable production of ammonia from water and air," *Journal of Cleaner Production*, vol. 178, pp. 325 – 342, 2018.

[131] J. A. Elia, R. C. Baliban, and C. A. Floudas, "Toward novel biomass, coal, and natural gas processes for satisfying current transportation fuel demands, 2: Simultaneous heat and power integration," *Ind. Eng. Chem. Res.*, vol. 49, no. 16, pp. 7371–7388, 2010.

[132] R. C. Baliban, J. A. Elia, and C. A. Floudas, "Optimization framework for the simultaneous process synthesis, heat and power integration of a thermochemical hybrid biomass, coal, and natural gas facility," *Comput. Chem. Eng.*, vol. 35(9), pp. 1647–1690, 2011.

[133] R. C. Baliban, J. A. Elia, and C. A. Floudas, "Biomass and Natural Gas to Liquid Transportation Fuels: Process Synthesis, Global Optimization, and Topology Analysis," *Ind. Eng. Chem. Res.*, vol. 52, pp. 3381–3406, 2013.

[134] S. B. Jones, Y. Zhu, and C. Valkenburg, "Municipal solid waste (msw) to liquid fuels synthesis, volume 2: A techno-economic evaluation of the production of mixed alcohols," *Richland, WA: Pacific Northwest National Laboratory*, 2009.

[135] T. H. Christensen, *Solid waste technology & management*, vol. 2. Wiley Online Library, 2011.

[136] T. G. Kreutz, E. D. Larson, G. Liu, and R. H. Williams, "Fischer-Tropsch Fuels from Coal and Biomass." Proceedings of the $25^{th}$ International Pittsburg Coal Conference, 2008.

[137] National Renewable Energy Laboratory, "Survey and Down-Selection of Acid Gas Removal Systems for the Thermochemical Conversion of Biomass to Ethanol with Detailed Analysis of an MDEA System." NREL/SR-5100-50482, 2011.

[138] J. R. LeBlanc and S. A. Knez, "Ammonia production with enriched air reforming and nitrogen injection into the synthesis loop," Oct. 25 1995. US Patent 5,736,116.

[139] A. Pinto, "Ammonia production process," May 9 1985. US Patent 4,681,745.

[140] T. A. Czuppon, "Isothermal ammonia converter," Oct. 12 1998. US Patent 6,171,570 B1.

[141] A. Pinto and J. B. H. Johnson, "Ammonia synthesis process," Feb. 3 1984. US Patent 4,695,442.

[142] A. Pinto, "Synthesis process and reactor," Nov. 19 1981. US Patent 4,778,662.

[143] A. Notman, "Synthesis reactor," Sept. 14 1979. US Patent 4,311,671.

[144] D. L. Banquy, "Process for the production of ammonia and the corresponding synthesis gas," Nov. 19 1980. US Patent 4,296,085.

[145] U. Zardi, "System for reducing energy consumption improving reactors for heterogeneous catalytic synthesis and relative reactors," May 15 1985. US Patent 4,755,362.

[146] S. Lou and R. Lou, "Method of catalytic reaction carried out near the optimal temperature and an apparatus for the method," Aug. 21 1996. US Patent 6,214,296 B1.

[147] E. A. Gam, "Apparatus and process for the synthesis of ammonia," Mar. 10 1976. US Patent 4,181,701.

[148] C. Speth, "Process for the preparation of ammonia," Oct. 30 1998. US Patent 6,955,797.

[149] R. B. Strait, "Pseudoisothermal ammonia process," July 2 2004. US Patent 2008/0161428 A1.

[150] L. D. Gaines, "Ammonia synthesis loop variables investigated by steady-state simulation," *Chemical Engineering Science*, vol. 34, no. 1, pp. 37 – 50, 1979.

[151] C. P. P. Singh and D. N. Saraf, "Simulation of ammonia synthesis reactors," *Industrial & Engineering Chemistry Process Design and Development*, vol. 18, no. 3, pp. 364–370, 1979.

[152] S. S. Elnashaie, M. E. Abashar, and A. S. Al-Ubaid, "Simulation and optimization of an industrial ammonia reactor," *Industrial & Engineering Chemistry Research*, vol. 27, no. 11, pp. 2015–2022, 1988.

[153] M. R. Panahandeh, J. Fathikaljahi, and M. Taheri, "Steady-state modeling and simulation of an axial-radial ammonia synthesis reactor," *Chemical Engineering & Technology*, vol. 26, no. 6, pp. 666–671, 2003.

[154] M. J. Azarhoosh, F. Farivar, and H. Ale Ebrahim, "Simulation and optimization of a horizontal ammonia synthesis reactor using genetic algorithm," *RSC Adv.*, vol. 4, pp. 13419–13429, 2014.

[155] F. Boukouvala, M. M. F. Hasan, and C. A. Floudas, "Global optimization of general constrained grey-box models: new method and its application to constrained pdes for pressure swing adsorption," *Journal of Global Optimization*, pp. 1–40, 2015.

[156] O. Onel, A. M. Niziolek, H. Butcher, B. A. Wilhite, and C. A. Floudas, "Multi-scale approaches for gas-to-liquids process intensification: Cfd modeling, process synthesis, and global optimization," *Computers & Chemical Engineering*, vol. 105, pp. 276 – 296, 2017. Process Intensification.

[157] Environmental Protection Agency, "Air Pollution Control Technology Fact Sheet. Document Number: EPA-452/F-03-015."

[158] E. D. Larson, H. Jin, and F. E. Celik, "Large-scale gasification-based coproduction of fuels and electricity from switchgrass," *Biofuels, Bioprod. Bioref.*, vol. 3, pp. 174–194, 2009.

[159] National Energy Technology Laboratory, "Analysis of Natural Gas-to Liquid Transportation Fuels via Fischer-Tropsch." DOE/NETL-2013/1597, 2013.

[160] Nel, "Nel hydrogen electrolyzer." http://nelhydrogen.com/product/electrolysers/, 2017.

[161] National Renewable Energy Laboratory, "Gasoline from Wood via Integrated Gasification, Synthesis, and Methanol-to-Gasoline Technologies." USDOE contract DE-AC36-08GO28308, 2011.

[162] National Energy Technology Laboratory, "Cost and Performance Baseline for Fossil Energy Plants Volume 2: Coal to Synthetic Natural Gas and ." DOE/NETL-2010/1402, 2011.

[163] National Renewable Energy Laboratory, "Process Design and Economics for Biochemical Conversion of Lignocellulosic Biomass to Ethanol." NREL/TP-5100-47764, 2011.

[164] L. T. Biegler, I. E. Grossmann, and A. W. Westerberg, *Systematic methods for chemical process design*. Prentice Hall, Old Tappan, NJ (United States), 1997.

[165] Aspen Technologies, "Aspen Process Economic Analyzer."

[166] Schendel, R. L., Mariz, C. L., Mak, J. Y., "Is permeation competitive?," 1983.

[167] National Energy Technology Laboratory, "Cost and Performance Baseline for Fossil Energy Plants. Volume 1: Bituminous Coal and Natural Gas to Electricity Final Report. Document Number: DOE/NETL-2007/1281." http://www.netl.doe.gov/energy-analyses/baseline_studies.html, 2007.

[168] P. Balmer and B. Mattsson, "Wastewater treatment plant operation costs," *Wat. Sci. Tech.*, vol. 30, no. 4, pp. 7–15, 1994.

[169] Argonne National Laboratory, "GREET 1.8b, The Greenhouse Gases, Regulated Emisssions, and Energy Use in Transportation (GREET) Model." , 2007. Released September 2008.

[170] R. Misener, J. P. Thompson, and C. A. Floudas, "APOGEE: Global optimization of standard, generalized, and extended pooling problems via linear and logarithmic partitioning schemes," *Operations Research*, vol. 35, no. 5, pp. 876–892, 2011.

[171] CPLEX, *ILOG CPLEX C++ API 12.1 Referece Manual*, 2009.

[172] A. Drud, "Conopt: A grg code for large sparse dynamic nonlinear optimization problems," *Mathematical Programming*, vol. 31, no. 2, pp. 153–191, 1985.

[173] C. A. Floudas, *Nonlinear and Mixed-Integer Optimization*. Oxford University Press, New York, 1995.

[174] C. A. Floudas, *Deterministic Global Optimization: Theory, Methods and Applications*. Kluwer Academic Publishers, Dordrecht, Netherlands, 2000.

[175] T. Brown, "Ammonia Capacity in North America." https://ammoniaindustry.com/ammonia-plants-in-north-america/, 2014.

[176] U.S. Environmental Protection Agency Office of Air and Radiation, "Technical Support Document for the Ammonia Production Sector: Proposed Rule for Mandatory Reporting of Greenhouse Gases," 2009.

[177] National Renewable Energy Laboratory, "U.S. Solar Photovoltaic System Cost Benchmark: Q1 2017." https://www.nrel.gov/research/publications.html, 2017.

[178] Department of Energy, "2016 Billion-Ton Report: Advancing Domestic Resources for a Thriving Bioeconomy." http://www1.eere.energy.gov/biomass/publications.html, 201.

[179] Department of Energy, "2016 Wind Technologies Market Report." https://www.energy.gov/eere/wind/downloads/2016-wind-technologies-market-report, 2016.

[180] A. M. Niziolek, O. Onel, Y. A. Guzman, and C. A. Floudas, "Biomass-based production of benzene, toluene, and xylenes via methanol: Process synthesis and deterministic global optimization," *Energy & Fuels*, vol. 30, no. 6, pp. 4970–4998, 2016.

[181] EIA, "Annual Electric Generator Report," 2016.

[182] Energy Information Administration, "Natural Gas Prices." https://www.eia.gov/dnav/ng/NG_PRI_SUM_A_EPG0_PIN_DMCF_A.htm, 2018.

[183] C. D. Demirhan, W. W. Tso, J. B. Powell, and E. N. Pistikopoulos, "Sustainable ammonia production through process synthesis and global optimization," *AIChE Journal*, vol. 65, no. 7, p. e16498, 2019.

[184] I. Staffell, D. Scamman, A. Velazquez Abad, P. Balcombe, P. E. Dodds, P. Ekins, N. Shah, and K. R. Ward, "The role of hydrogen and fuel cells in the global energy system," *Energy Environ. Sci.*, vol. 12, pp. 463–491, 2019.

[185] J. O. Bockris, "A hydrogen economy," *Science*, vol. 176, no. 4041, pp. 1323–1323, 1972.

[186] "Japan's hydrogen dream: game-changer or a lot of hot air?," 2019.

[187] M. Nagashima, "Japan's hydrogen strategy and its economic and geopolitical implications," 2018.

[188] W. W. Tso, C. D. Demirhan, J. B. Powell, and E. N. Pistikopoulos, "Toward optimal synthesis of renewable ammonia and methanol processes (ramp)," in *Proceedings of the 13th International Symposium on Process Systems Engineering - PSE 2018*, (San Diego, CA), 2018.

[189] W. W. Tso, C. D. Demirhan, S. Lee, H. Song, J. B. Powell, and E. N. Pistikopoulos, "Energy carrier supply chain optimization: A texas case study," in *Proceedings of the 9th International Conference on Foundations of Computer-Aided Process Design* (S. G. Muñoz, C. D. Laird, and M. J. Realff, eds.), vol. 47 of *Computer Aided Chemical Engineering*, pp. 1 – 6, Elsevier, 2019.

[190] P. Castro, I. Grossmann, and Q. Zhang, "Expanding scope and computational challenges in process scheduling," *Computers and Chemical Engineering*, vol. 114, pp. 14–42, 6 2018.

[191] N. E. Koltsaklis and M. C. Georgiadis, "A multi-period, multi-regional generation expansion planning model incorporating unit commitment constraints," *Applied Energy*, vol. 158, pp. 310 – 331, 2015.

[192] S. Sass and A. Mitsos, "Optimal operation of dynamic (energy) systems: When are quasi-steady models adequate?," *Computers & Chemical Engineering*, vol. 124, pp. 133 – 139, 2019.

[193] P. Voll, C. Klaffke, M. Hennen, and A. Bardow, "Automated superstructure-based synthesis and optimization of distributed energy supply systems," *Energy*, vol. 50, pp. 374 – 388, 2013.

[194] Q. Zhang and I. E. Grossmann, "Enterprise-wide optimization for industrial demand side management: Fundamentals, advances, and perspectives," *Chemical Engineering Research and Design*, vol. 116, pp. 114 – 131, 2016. Process Systems Engineering - A Celebration in Professor Roger Sargent's 90th Year.

[195] S. Samsatli and N. J. Samsatli, "A general spatio-temporal model of energy systems with a detailed account of transport and storage," *Computers & Chemical Engineering*, vol. 80,

pp. 155 – 176, 2015.

[196] C. F. Heuberger, P. K. Bains, and N. M. Dowell, "The ev-olution of the power system: A spatio-temporal optimisation model to investigate the impact of electric vehicle deployment," *Applied Energy*, vol. 257, p. 113715, 2020.

[197] A. Allman and P. Daoutidis, "Optimal design of synergistic distributed renewable fuel and power systems," *Renewable Energy*, vol. 100, pp. 78 – 89, 2017. Special Issue: Control and Optimization of Renewable Energy Systems.

[198] A. Allman, M. J. Palys, and P. Daoutidis, "Scheduling-informed optimal design of systems with time-varying operation: A wind-powered ammonia case study," *AIChE Journal*, 2018.

[199] A. Ghobeity and A. Mitsos, "Optimal design and operation of a solar energy receiver and storage," *Journal of solar energy engineering*, vol. 134, no. 3, 2012.

[200] E. Gençer and R. Agrawal, "Synthesis of efficient solar thermal power cycles for baseload power supply," *Energy Conversion and Management*, vol. 133, pp. 486–497, 2017.

[201] P. G. Brodrick, A. R. Brandt, and L. J. Durlofsky, "Optimal design and operation of integrated solar combined cycles under emissions intensity constraints," *Applied Energy*, vol. 226, pp. 979 – 990, 2018.

[202] P. Gabrielli, M. Gazzani, E. Martelli, and M. Mazzotti, "Optimal design of multi-energy systems with seasonal storage," *Applied Energy*, vol. 219, pp. 408–424, 2018.

[203] X. Peng, T. W. Root, and C. T. Maravelias, "Optimization-based process synthesis under seasonal and daily variability: Application to concentrating solar power," *AIChE Journal*, vol. 65, no. 7, p. e16458, 2019.

[204] Q. Zhang, M. Martín, and I. E. Grossmann, "Integrated design, planning, and scheduling of renewables-based fuels and power production networks," in *27th European Symposium on Computer Aided Process Engineering* (A. Espuña, M. Graells, and L. Puigjaner, eds.), vol. 40 of *Computer Aided Chemical Engineering*, pp. 1879 – 1884, Elsevier, 2017.

[205] Q. Zhang, M. Martín, and I. E. Grossmann, "Integrated design and operation of renewables-based fuels and power production networks," *Computers & Chemical Engineering*, vol. 122, pp. 80 – 92, 2019. 2017 Edition of the European Symposium on Computer Aided Process Engineering (ESCAPE-27).

[206] C. Pantelides, "Unitified frameworks for optimal process planning and scheduling," in *Proceedings of the Second International COnference on Foundations of Computer-Aided Process Operations (FOCAPO)*, (Austin, TX, USA), 1993.

[207] B. Bahl, J. Lützow, D. Shu, D. E. Hollermann, M. Lampe, M. Hennen, and A. Bardow, "Rigorous synthesis of energy systems by decomposition via time-series aggregation," *Computers & Chemical Engineering*, vol. 112, pp. 70–81, 2018.

[208] C. F. Heuberger, E. S. Rubin, I. Staffell, N. Shah, and N. M. Dowell, "Power capacity expansion planning considering endogenous technology cost learning," *Applied Energy*, vol. 204, pp. 831 – 845, 2017.

[209] C. L. Lara, J. D. Siirola, and I. E. Grossmann, "Electric power infrastructure planning under uncertainty: stochastic dual dynamic integer programming (sddip) and parallelization scheme," *Optimization and Engineering*, Oct 2019.

[210] W. W. Tso, C. D. Demirhan, C. F. Heuberger, J. B. Powell, and E. N. Pistikopoulos, "A hierarchical clustering decomposition algorithm for optimizing renewable power systems with storage," *Applied Energy*, vol. 270, p. 115190, 2020.

[211] National Renewable Energy Laboratory, "U.S. Renewable Energy Technical Potentials: A GIS-Based Analysis." https://www.nrel.gov/research/publications.html, 2012.

[212] ERCOT, "Texas electricity prices." http://www.ercot.com/mktinfo/prices, 2019.

[213] LCG Consulting, "New York electricity prices." http://www.energyonline.com/Data/, 2019.

[214] C. D. Demirhan, W. W. Tso, J. B. Powell, C. F. Heuberger, and E. N. Pistikopoulos, "A multiscale energy systems engineering approach for renewable power generation and

storage optimization," *Industrial & Engineering Chemistry Research*, vol. 59, no. 16, pp. 7706–7721, 2020.

[215] C. A. Floudas, J. A. Elia, and R. C. Baliban, "Hybrid and Single Feedstock Energy Processes for Liquid Transportation Fuels: A Critical Review," *Comp. Chem. Eng.*, vol. 41, pp. 24–51, 2012.

[216] A. M. Niziolek, O. Onel, J. A. Elia, R. C. Baliban, X. Xiao, and C. A. Floudas, "Coal and biomass to liquid transportation fuels: Process synthesis and global optimization strategies," *Ind Eng Chem Res*, vol. 53, no. 44, pp. 17002–17025, 2014.

[217] W. W. Tso, A. M. Niziolek, O. Onel, C. D. Demirhan, C. A. Floudas, and E. N. Pistikopoulos, "Enhancing natural gas-to-liquids (gtl) processes through chemical looping for syngas production: Process synthesis and global optimization," *Comput. Chem. Eng.*, vol. 45(23), pp. 7807–7816, 2018.

[218] EIA, "Use of energy explained." https://www.eia.gov/energyexplained/use-of-energy/transportation.php, 2019.

[219] EIA, "How much oil is consumed in the united states?." https://www.eia.gov/tools/faqs/faq.php?id=33&t=6, 2019.

[220] S. Brynolf, M. Taljegard, M. Grahn, and J. Hansson, "Electrofuels for the transport sector: A review of production costs," *Renewable and Sustainable Energy Reviews*, vol. 81, pp. 1887 – 1905, 2018.

[221] J. A. Elia, J. Li, and C. A. Floudas, "Strategic planning optimization for natural gas to liquid transportation fuel (gtl) systems," *Computers & Chemical Engineering*, vol. 72, pp. 109–125, 2015.

[222] National Renewable Energy Laboratory, "2015 Cost of Wind Energy Review." https://www.nrel.gov/docs/fy17osti/66861.pdf, 2015.

[223] D. W. Keith, G. Holmes, D. S. Angelo, and K. Heidel, "A process for capturing co2 from the atmosphere," *Joule*, vol. 2, no. 8, pp. 1573 – 1594, 2018.

[224] M. Pérez-Fortes, J. C. Schöneberger, A. Boulamanti, and E. Tzimas, "Methanol synthesis using captured co2 as raw material: Techno-economic and environmental assessment," *Applied Energy*, vol. 161, pp. 718 – 732, 2016.

[225] B. Parkinson, P. Balcombe, J. Speirs, A. Hawkes, and K. Hellgardt, "Levelized cost of co 2 mitigation from hydrogen production routes," *Energy & Environmental Science*, vol. 12, no. 1, pp. 19–40, 2019.

[226] EIA, "Capital cost estimates for utility scale electricity generating plants." https://www.eia.gov/analysis/studies/powerplants/capitalcost/pdf/capcost_assumption.pdf, 2016.

[227] U. Bossell and B. Eliasson, "Energy and the Hydrogen Economy." https://afdc.energy.gov/files/pdfs/hyd_economy_bossel_eliasson.pdf, 2015.

[228] B. Zakeri and S. Syri, "Electrical energy storage systems: A comparative life cycle cost analysis," *Renewable and Sustainable Energy Reviews*, vol. 42, pp. 569–596, 2015.

[229] Strategic Analysis Inc., "Manufacturing cost and installed price analysis of stationary fuel cell systems," 2015.

# APPENDIX A

# SUPPORTING INFORMATION FOR CHAPTER 2

The list of all the units, subscripts, superscripts, sets, variables, and parameters are given in this section.

## Sets & Indices

| | |
|---|---|
| $u$ | Unit |
| $s$ | Stream |
| $p$ | Property |
| $t$ | Period |
| $i$ | Model parameter index 1 |
| $j$ | Model parameter index 2 |

## Subsets

| | |
|---|---|
| $U^{pro}$ | Processing units |
| $U^{hyp}$ | Hypothetical units |
| $S_u^{in}$ | Inlet streams to unit u |
| $S_u^{out}$ | Outlet streams from unit u |
| $P_{s,u}^{in}$ | Inlet stream properties for stream s to unit u |
| $P_{s,u}^{out}$ | Outlet stream properties for stream s from unit u |
| $UC$ | Stream connection from stream s of unit u to stream s' of unit u' |
| $I_{yield,u}$ | Set of inputs for yield prediction models of unit u |
| $I_{prop,u}$ | Set of inputs for property prediction models of unit u |

## Subscripts

| | |
|---|---|
| $in$ | Inlet |
| $out$ | Outlet |

## Processing Units

| | |
|---|---|
| $CDU$ | Crude distillation unit |
| $GHT$ | Gasoil hydrotreating unit |
| $KMX1$ | Kerosene mercaptan oxidation unit #1 |
| $KMX2$ | Kerosene mercaptan oxidation unit #2 |
| $LMX$ | LPG mercaptan oxidation unit |
| $LER$ | Light ends recovery unit |
| $NHT$ | Naphtha hydrotreating unit |
| $PLT$ | Platforming unit |
| $HMU$ | Hydrogen manufacturing unit |
| $DCU$ | Delayed coker unit |
| $HCR$ | Hydrocracker unit |
| $LBO$ | Lube base oil unit |
| $VDU$ | Vacuum distillation unit |
| $LER\,Mixer$ | Mixer for light ends recovery unit |
| $NHT\,Mixer$ | Mixer for naphtha hydrotreating unit |
| $PLT\,Mixer$ | Mixer for platforming unit |
| $DCU\,Mixer$ | Mixer for delayed coker unit |
| $HCR\,Mixer$ | Mixer for hydrocracker unit |

## Hypothetical Units

| | |
|---|---|
| $PURC$ | Unit for all the purchased raw materials |
| $SALES$ | Unit for all the sold products |

## Properties

| | |
|---|---|
| $ACN$ | Acid number |
| $API$ | API density |
| $ARO$ | Aromatics content |
| $BENZ$ | Benzene content |
| $C1$ | C1 content |
| $C2$ | C2 content |

| | |
|---|---|
| $CEN$ | Cetane number |
| $D05$ | Temperature at which 5% of the mixture boils |
| $D10$ | Temperature at which 10% of the mixture boils |
| $D95$ | Temperature at which 95% of the mixture boils |
| $Fe$ | Fe content |
| $FP$ | Flash point |
| $H2S$ | $H_2S$ content |
| $NAPH$ | Naphthenes content |
| $PP$ | Pour point |
| $RON$ | Research octane number |
| $PAR$ | Paraffins content |
| $RVP$ | Reed vapor pressure |
| $SALT$ | Salt content |
| $SUL$ | Sulfur content |
| $V60$ | Viscosity at 60 °C |
| $V100$ | Viscosity at 100 °C |

## Continuous Variables

| | |
|---|---|
| $F(s, u, s', u', t)$ | Mass flow rate of stream s from unit u to unit u' as stream s' at period t |
| $F_{in}(s, u, t)$ | Inlet mass flow rate of stream s to unit u at period t |
| $F_{out}(s, u, t)$ | Outlet mass flow rate of stream s from unit u at period t |
| $Yield(s, u, t)$ | Percent yield of outlet stream s from unit u at period t |
| $P_{in}(p, s, u, t)$ | Property p of inlet stream s to unit u at period t |
| $P_{out}(p, s, u, t)$ | Property p of outlet stream s from unit u at period t |
| $Profit$ | Total profit ($\$/day$) |
| $LossYield(u, t)$ | Percent loss yield of unit u at period t |
| $UnitSlacks(u, t)$ | Slacks for sum of yields for unit u at period t |
| $YieldSlacks(s, u, t)$ | Slacks for yield prediction of stream s from unit u at period t |
| $PropSlacks(p, s, u, t)$ | Slacks for property prediction of property p of stream s from unit u at period t |
| $Inv(s, t)$ | Initial inventory level for product s at the beginning of time period t |
| $Inv^0(s, t)$ | Inventory level for product s at time period t after demands are satisfied |
| $W(s, t)$ | Mass flow rate of the waste stream s at period t |

## Parameters

| | |
|---|---|
| $\gamma$ | Weight parameter for the sum of slack variables in the objective function |
| $\beta_{yield,0}(s,u)$ | Parameter for constant term in yield prediction equation of stream s from unit u |
| $\beta_{yield,i}(s,u)$ | Parameter for linear terms in yield prediction equation of stream s from unit u |
| $\beta_{yield,i,j}(s,u)$ | Parameter for bilinear and quadratic term in yield prediction equation of stream s from unit u |
| $\beta_{prop,0}(p,s,u)$ | Parameter for constant term in yield prediction equation of property p stream s from unit u |
| $\beta_{prop,i}(p,s,u)$ | Parameter for linear terms in yield prediction equation of property p of stream s from unit u |
| $\beta_{prop,i,j}(p,s,u)$ | Parameter for bilinear and quadratic term in yield prediction equation of property p of stream s from unit u |
| $F_{in}^{up}(s,u)$ | Upper bound on inlet mass flow rate of stream s to unit u |
| $F_{in}^{low}(s,u)$ | Lower bound on inlet mass flow rate of stream s to unit u |
| $F_{out}^{up}(s,u)$ | Upper bound on inlet mass flow rate of stream s to unit u |
| $F_{out}^{low}(s,u)$ | Lower bound on outlet mass flow rate of stream s from unit u |
| $Yield^{up}(s,u)$ | Upper bound on percent yield of outlet stream s from unit u |
| $Yield^{low}(s,u)$ | Lower bound on percent yield of outlet stream s from unit u |
| $P_{in}^{up}(p,s,u)$ | Upper bound on property p of inlet stream s to unit u |
| $P_{in}^{low}(p,s,u)$ | Lower bound on property p of inlet stream s to unit u |
| $P_{out}^{up}(p,s,u)$ | Upper bound on property p of outlet stream s from unit u |
| $P_{out}^{low}(p,s,u)$ | Lower bound on property p of outlet stream s from unit u |
| $OperatingCost(u)$ | Operational cost of unit u as a function of unit throughput ($\$/ton$) |
| $Price(s,t)$ | Price of product stream s ($\$/ton$) at period t |
| $Cost(s,t)$ | Cost of raw material stream s ($\$/ton$) at period t |
| $InvCost(s,t)$ | Inventory cost of storing product s ($\$/ton$) at period t |
| $CAPmin(u)$ | Minimum capacity for unit u |
| $CAPmax(u)$ | Maximum capacity for unit u |
| $MinDemand(s,t)$ | Minimum demand requirement for product s at period t |
| $MaxDemand(s,t)$ | Maximum demand requirement for product s at period t |

APPENDIX B

SUPPORTING INFORMATION FOR CHAPTER 3

## B.1 Nomenclature for the MINLP Process Synthesis Model

### Process Units

The set of process units in the ammonia plant is outlined in Table B.1. Equation B.1 defines these units formally. Multiple realizations of the same unit may occur within the process synthesis framework. Such units operate with their own distinct set of operating conditions and are defined as $u_n$, where $n$ represents the $n$-th realization of a given unit. These units are modeled using binary variables.

$$u \in U = \{\text{Complete set of process units listed in Table B.1}\} \tag{B.1}$$

Table B.1: Process units describing the ammonia plant are listed below. Multiple realizations of the same unit may exist and are denoted with the subscript $n$.

| Unit Name | Unit Index | Unit Name | Unit Index |
|---|---|---|---|
| *Process Inlets* | | | |
| Inlet Air | IN-AIR | Inlet Water | IN-H2O |
| Inlet Natural Gas | IN-NG | Inlet Biomass | IN-BIO |
| *Process Outlets* | | | |
| Outlet Sequestered $CO_2$ | OUT-$CO_2$ | Outlet Wastewater | OUT-WW |
| Outlet Vent | OUT-V | Outlet Ammonia | OUT-$NH_3$ |
| *Natural Gas Conversion* | | | |
| Autothermal Reformer | $ATR_n$ | Steam Methane Reformer | $SMR_n$ |
| Primary Reformer | AM-PR | Secondary Reformer | AM-SR |
| *Biomass Gasification* | | | |
| Biomass Dryer | BDR | Biomass Dryer Air Heater | X-BDR |
| Biomass Lockhopper | BLK | Biomass Gasifier | $BGS_n$ |
| First Biomass Vapor Cyclone | $BC_1$ | Second Biomass Vapor Cyclone | $BC_2$ |
| Tar Cracker | TCK | Tar Cracker Splitter | SP-TC |
| Tar Cracker Cooler | X-TCK | | |
| *Syngas Cleanup* | | | |
| Dedicated Reverse Water-Gas Shift Unit | $RGS_n$ | RGS Effluent Cooler | X-RGS |
| HT Forward Water-Gas Shift Unit | HT-WGS | Raw Syngas Splitter | SP-RS |
| High Temperature Shift | AM-HTS | Low Temperature Shift | LTS |
| COS-HCN Hydrolyzer | CHH | $NH_3$-HCl Stripper | NHS |
| Acid Gas Flash Vapor Cooler | X-AGF | Acid Gas Flash 2-Phase Cooler | X-$AGF_n$ |
| Acid Gas Flash Unit | AGF | Acid Gas Thermal Analyzer | X-AGR |
| Rectisol Unit | AGR-CREC | aMDEA unit | AM-CO2SEP |
| First $CO_2$ Compressor | $CO_2$C | $CO_2$ Recycle Compressor | $CO_2$RC |
| $CO_2$ Sequestration Compressor | $CO_2$SC | Acid Gas Compressor | AGC |
| LT Water-Gas Shift Unit | LT-WGS | Pressure Swing Adsorption Unit | PSA |
| PSA Effluent Splitter | SP-PSA | PSA Hydrogen Preheater | X-$H_2$P |
| PSA Hydrogen Splitter | SP-$H_2$P | PSA Hydrogen Compressor for ASL | CMP-AM-H2 |
| Liquid Nitrogen Was Unit | AM-N2WASH | Clean Acid Gas Splitter | SP-AGR |
| Methanator | AM-METH | Dryer | AM-DRYER1 |

Table B.1: (continued)

| Unit Name | Unit Index | Unit Name | Unit Index |
|---|---|---|---|
| *Water Electrolysis* | | | |
| Alkaline Electrolyzer | AL-EYZ | PEM Electrolyzer | PEM-EYZ |
| Deionizer | DEION | Oxygen Compressor for AL-EYZ | CMP-EYZ-O2 |
| First Compressor for AL-EYZ | CMP1-EYZ | Second Compressor for AL-EYZ | CMP12-EYZ |
| Electrolyzer Hydrogen Splitter | SP-H2E | | |
| *Air Separation* | | | |
| Air Compressor | AC | Air Separation Unit | ASU |
| Oxygen Compressor | OC | Nitrogen Compressor | CMP-N2 |
| ASU Oxygen Preheater | X-$O_2$A | OC Oxygen Splitter | SP-$O_2$C |
| OC Oxygen Preheater | X-$O_2$C | | |
| *Ammonia Synthesis Loop* | | | |
| First Loop Compressor | CMP-AM-HBR1 | Second Loop Compressor | CMP-AM-HBR$_n$ |
| Haber-Bosch Reactor | HBR$_n$ | Letdown Vessel | AM-LETDOWN |
| Letdown Vapor Splitter | SP-LV | $NH_3$-$H_2O$ Scrubber | AM-SCRUB |
| $NH_3$-$H_2O$ Distillation | AM-DIST | Dryer | AM-DRYER2 |
| Second Recycle Splitter | SP-HB-O | Membrane Separator | AM-MEMBRANE |
| Haber-Bosch Reactor | HBR$_n$ | Letdown Vessel | AM-LETDOWN |
| First Recycle Compressor | CMP-LET-REC | Second Recycle Compressor | CMP-AM-REC |
| *Recycle Gas Treatment* | | | |
| Light Gas Compressor | LGC | Light Gas Splitter | SP-LG |
| Fuel Combustor | FCM | Fuel Combuster Effluent Cooler | X-FCM |
| Fuel Combustor Flash Unit | FCF | First Gas Turbine Air Compressor | GTAC$_1$ |
| Second Gas Turbine Air Compressor | GTAC$_2$ | Gas Turbine Combustor | GTC |
| First Gas Turbine | GT$_1$ | Second Gas Turbine | GT$_2$ |
| Gas Turbine Effluent Cooler | X-GT | Gas Turbine Flash Unit | GTF |
| Gas Turbine Effluent Compressor | GTEC | $CO_2$ Recovery Unit | $CO_2$R |
| *Water Treatment* | | | |
| Biological Digestor | BD | Reverse Osmosis | RO |
| Cooling Tower | CLTR | Process Cooling | COOL-P |
| Heat & Power System | HEP | Heat & Power Utilities | HEAT-P |
| Deaerator | DEA | Process Water Economizer | X-WPR |
| Process Water Boiler | X-WBL | | |

### Process Species

All the species that exist in the ammonia plant are included in Table B.2. Equation B.2 defines these species formally.

$$s \in S = \{\text{Complete set of species listed in Table B.2}\} \tag{B.2}$$

Table B.2: Species present in the ammonia plant

| Species Name | Species Index | Species Name | Species Index | Species Name | Species Index |
|---|---|---|---|---|---|
| *Light Non-Hydrocarbon Gases* | | | | | |
| Oxygen | $O_2$ | Nitrogen | $N_2$ | Argon | Ar |
| Nitric Oxide | NO | Nitrous Oxide | $N_2O$ | Water | $H_2O$ |
| Carbon Monoxide | CO | Hydrogen | $H_2$ | Carbon Dioxide | $CO_2$ |
| *Hydrocarbons* | | | | | |
| Methane | $CH_4$ | Acetylene | $C_2H_2$ | Ethylene | $C_2H_4$ |
| Ethane | $C_2H_6$ | Propylene | $C_3H_6$ | Propane | $C_3H_8$ |
| Isobutylene | $iC_4H_8$ | 1-Butene | $nC_4H_8$ | Isobutane | $iC_4H_{10}$ |
| Methanol | $CH_3OH$ | | | | |
| *Products* | | | | | |
| Ammonia | NH3 | | | | |

**Indices/Sets**

The indices used in the process synthesis mathematical model are the following.

$$
\begin{aligned}
u &: \text{Process unit index} \\
s &: \text{Species index} \\
a &: \text{Atom index} \\
p &: \text{Proximate analysis index} \\
r &: \text{Reaction index} \\
pr &: \text{Set of products} \\
i &: \text{General counting index}
\end{aligned}
$$

As mentioned earlier, the complete set of process units is defined as $U$. Several subsets of units are defined for specific sections of the GTL refinery. Examples of these subsets are shown below.

$$
\begin{aligned}
U_{ATR} &= \{u : u = \text{ATR}_n\} \\
U_{SMR} &= \{u : u = \text{SMR}_n\} \\
U_{HBR} &= \{u : u = \text{HBR}_n\} \\
U_{CMP-AM-HBR} &= \{u : u = \text{CMP-AM-HBR}_n\} \\
u \in U_{Fl} &= \{\text{Set of flash units}\} \\
u \in U_{Sp} &= \{\text{Set of splitter units}\}
\end{aligned}
$$

The set of all atoms, $A$, includes C, H, O, N, S, Cl, and Ar as illustrated below.

$$a \in A = \{\text{C, H, O, N, S, Cl, Ar}\}$$

The list of all unit connections, $UC$, is presented below.

$$UC \quad = \quad \{(u, u') : \exists \text{ a connection between unit } u \text{ and unit } u' \text{ in the superstructure}\}$$

Using *a priori* knowledge about each unit in the ammonia plant, the set of species that can exist in a stream from unit $u$ to unit $u'$ is known and defined as $S^{UC}_{u,u'}$. The set $(u, u', s) \in S^{UF}$ is then constructed from all streams in $UC$. Likewise, the set of all species $s$ that exist within a given unit $u$ is also delineated as $S^{U}$.

$$\begin{aligned} S^{UF} &= \{(u, u', s) : \exists s \in S^{UC}_{u,u'}\} \\ S^{U} &= \{(s, u) : \exists (u, u', s) \in S^{UF} \text{ or } \exists (u', u, s) \in S^{UF}\} \end{aligned}$$

**Parameters**

The atomic weight of atoms $a$ ($AW_a$) and $AR_{s,a}$ are then used to calculate the molecular weight of species $s$ ($MW_s$) from Equation B.3.

$$\begin{aligned} AW_a &: \text{ Atomic weight of atom } a \\ MW_s &= \sum_a AW_a \cdot AR_{s,a} \end{aligned} \tag{B.3}$$

For flash separation units equilibrium split fraction of stream $s$ leaving unit $u$, $K^{VLE}_{u,s}$, is taken from Aspen Plus simulations and shown as:

$$K^{VLE}_{u,s} \quad : \quad \text{Vapor-liquid equilibrium split fraction of stream } s \text{ leaving unit } u$$

For equilibrium limited reactions, reaction equilibrium constant for reaction $r$ taking place in unit $u$,$K^{r}_{u}$, is taken from Aspen Plus and shown as:

$$K^{r}_{u} \quad : \quad \text{Reaction equilibrium constant for reaction } r \text{ taking place in unit } u$$

The coefficients of reactions are taken from reaction stoichiometry and entered as:

$$\nu_{r,s} \quad : \quad \text{Coefficient of species } s \text{ in reaction } r$$

**Variables**

Continuous variables are used to model the species molar flow rates ($N^S_{u,u',s}$), the total molar flow rates ($N^T_{u,u'}$), the extent of reaction in a process unit ($\xi^u_r$), the molar composition of a stream ($x^S_{u,u',s}$), the split fraction of a stream between two units ($sp_{u,u'}$), the total stream enthalpy flow rate ($H^T_{u,u'}$), the heat lost from a unit ($Q^L_u$), the heat transferred to or absorbed from a unit ($Q_u$), the delivered cost of feedstock ($Cost_f$), the cost of $CO_2$ sequestration ($Cost^{Seq}$), the cost of electricity ($Cost^{El}$), and the levelized unit investment cost ($Cost^U_u$). The subscripts $u$ and $u'$ are both denote an element of the set $U$ and can be used interchangeably in the stream flow indices.

$$\begin{aligned}
N^S_{u,u',s} &: \text{Molar flow of species } s \text{ from unit } u \text{ to unit } u' \\
N^T_{u,u'} &: \text{Total molar flow from unit } u \text{ to unit } u' \\
\xi^u_r &: \text{Extent of reaction } r \text{ in unit } u \\
x^S_{u,u',s} &: \text{Molar composition of species } s \text{ from unit } u \text{ to unit } u' \\
sp_{u,u'} &: \text{Split fraction of stream going from unit } u \text{ to unit } u' \\
H^T_{u,u'} &: \text{Total enthalpy flow from unit } u \text{ to unit } u' \\
Q^L_u &: \text{Heat lost from unit } u \\
Q_u &: \text{Heat transferred to or absorbed from from unit } u \\
Cost_f &: \text{Total delivered cost of feedstocks} \\
Cost^{Seq} &: \text{Total sequestration cost of } CO_2 \\
Cost^{El} &: \text{Total cost of electricity} \\
Cost^U_u &: \text{Total levelized cost of unit } u
\end{aligned}$$

Binary variables ($y_u$) are used to represent the logical existence of a process unit in the mathematical model. Only a few specific process units require binary variables as many of the units in the ammonia plant are always required.

$y_u$ : Logical existence of process unit $u$ (i.e., it takes the value of one if unit $u$ is selected and zero otherwise)

## B.2 The Mathematical Model

***General Constraints***

*Material Balances*

Species Balances

$$\sum_{(u',u)\in UC} N^S_{u',u,s} - \sum_{(u,r,s')\in R^U} \frac{\nu_{r,s}}{\nu_{r,s'}} \cdot \xi^u_r - \sum_{(u,u')\in UC} N^S_{u,u',s} \quad = 0 \quad \forall s \in S^U_u, u \in U^{Bal}_{Sp} \tag{B.4}$$

Extent of Reaction

$$\xi^u_r - fc^u_r \cdot \sum_{(u',u,s)\in S^{UF}} N^S_{u',u,s} \quad = 0 \quad \forall (u,r,s) \in R^U \tag{B.5}$$

Atom Balances

$$\sum_{(u',u,s)\in S^{UF}} AR_{s,a} \cdot N^S_{u',u,s} - \sum_{(u,u',s)\in S^{UF}} AR_{s,a} \cdot N^S_{u,u',s} \quad = 0 \quad \forall a \in A^U_u, u \in U^{Bal}_{At} \tag{B.6}$$

Total Mole Balance

$$N^T_{u',u} - \sum_{(u,u',s)\in S^{UF}} N^S_{u',u,s} \quad = 0 \quad \forall (u,u') \in UC \tag{B.7}$$

*Process Splitters*

Set Unit Split Fractions

$$N^S_{u,u',s} - \sum_{(u',u'')\in UC} sp_{u',u''} \cdot N^S_{u',u'',s} \quad = 0 \quad \forall (u,u',s) \in S^{UF}, u \in U_{Sp} \tag{B.8}$$

Split Fractions Sum to 1

$$\sum_{(u,u',s)\in S^{UF}} x^{S}_{u,u',s} - 1 \quad = 0 \quad \forall (u,u') \in UC_{Comp} \tag{B.9}$$

*Flash Units*

Upper Bound of Liquid Phase Split Fraction

$$x^{S}_{u,u_L,s} - min\{1, \frac{1}{K^{VLE}_{u,s}}\} \quad \leq 0 \quad \forall (u,u_L,s) \in S^{UF}, u \in U_{Fl} \tag{B.10}$$

Upper Bound of Vapor Phase Split Fraction

$$x^{S}_{u,u_V,s} - min\{1, K^{VLE}_{u,s}\} \quad \leq 0 \quad \forall (u,u_V,s) \in S^{UF}, u \in U_{Fl} \tag{B.11}$$

Set Liquid Phase Split Fraction

$$x^{S}_{u,u_L,s} \cdot N^{T}_{u,u_L} - N^{S}_{u,u_L,s} \quad = 0 \quad \forall u \in U_{Fl} \tag{B.12}$$

Set Vapor Phase Split Fraction

$$x^{S}_{u,u_V,s} \cdot N^{T}_{u,u_V} - N^{S}_{u,u_V,s} \quad = 0 \quad \forall u \in U_{Fl} \tag{B.13}$$

Set Phase Equilibrium

$$x^{S}_{u,u_V,s} - K^{VLE}_{u,s} \cdot x^{S}_{u,u_L,s} \quad = 0 \quad \forall u \in U_{Fl} \tag{B.14}$$

*Heat Balances*

Conservation of Energy

$$\sum_{(u,u')\in UC} H^T_{u,u'} - \sum_{(u',u)\in UC} H^T_{u',u} - Q_u - Q^L_u - Wu \quad = 0 \quad \forall u \in U/U_{Agg} \tag{B.15}$$

Total Heat Balance

$$H^T_{u,u'} - \sum_{(u,u',s)\in S^{UF}} H^S_{u,u',s} \quad = 0 \quad \forall (u,u') \in UC \tag{B.16}$$

*Logical Unit Existence*

Bound on Molar Flows

$$\sum_{(u',u)\in UC} N^T_{u',u} - UB^N_u \cdot y_u \quad \leq 0 \quad \forall u \in U^{Ex} \tag{B.17}$$

Upper Bound on Inlet Enthalpy Flow

$$H^T_{u',u} - UB^H_{u',u} \cdot y_u \quad \leq 0 \quad \forall (u',u) \in UC, u \in U^{Ex} \tag{B.18}$$

Lower Bound on Inlet Enthalpy Flow

$$LB^H_{u',u} \cdot y_u - H^T_{u',u} \quad \leq 0 \quad \forall (u',u) \in UC, u \in U^{Ex} \tag{B.19}$$

Upper Bound on Outlet Enthalpy Flow

$$H^T_{u,u'} - UB^H_{u',u} \cdot y_u \quad \leq 0 \quad \forall (u,u') \in UC, u \in U^{Ex} \tag{B.20}$$

Lower Bound on Outlet Enthalpy Flow

$$LB^{H}_{u,u'} \cdot y_u - H^{T}_{u,u'} \quad \leq 0 \quad \forall (u,u') \in UC, u \in U^{Ex} \tag{B.21}$$

***Process Inlets***

*Known Stream Compositions*

Set Stream Compositions for Inlet Streams

$$N^{S}_{u,u',s} - x^{K}_{u,s} \cdot N^{T}_{u,u'} \quad = 0 \quad \forall (u,u',s) \in S^{UF}, u = \{\text{IN}_{\text{AIR}}, \text{IN}_{\text{NG}}\} \tag{B.22}$$

*Greenhouse Gas Emissions Reduction*

Set Reduction from Petroleum Based Processes

$$GHG_{GTO} - GHG_{Red} \cdot (GHG_{Pet} + GHG_{Elec} + GHG_{Chem}) \quad = 0 \tag{B.23}$$

Sum Emissions from GTO Components

$$GHG_{GTO} - GHG^{Seq} - GHG^{Proc} - GHG^{Feed} \quad = 0 \tag{B.24}$$

Set Emissions from Feedstock Acquisition

$$GHG^{Feed} - \sum_{u \in U_{In}} \sum_{(u,u',s) \in S^{UF}} GHG^{T}_{s} \cdot MW_s \cdot N^{S}_{u,u',s} \quad = 0 \tag{B.25}$$

Set Emissions from $CO_2$ Sequestration

$$GHG^{Seq} - GHG^{T}_{\text{CO2}} \cdot MW - CO2 \cdot N^{S}_{\text{CO2SC,OUTCO2,CO2}} \quad = 0 \tag{B.26}$$

Set Emissions from $CO_2$ Venting

$$GHG^{Proc} - MW_{CO2} \cdot N^{S}_{\text{CO2R,OUTV,CO2}} \quad = 0 \tag{B.27}$$

***Natural Gas Conversion***

*Steam Methane Reformer and Primary Reformer*

SMR and AM-PR units are modeled with the same equations. Here the modeling equations are shown for SMR unit.

Logical Use of One Temperature

$$\sum_{u \in U_{SMR}} y_u - 1 \quad = 0 \tag{B.28}$$

Water-Gas-Shift Equilibrium

$$N^{S}_{u,u',\text{CO}_2} \cdot N^{S}_{u,u',\text{H}_2} - K^{RGS}_{u} \cdot N^{S}_{u,u',\text{CO}} \cdot N^{S}_{u,u',\text{H}_2\text{O}} \quad = 0 \quad \forall (u,u') \in UC, u \in U_{SMR} \tag{B.29}$$

$CH_4$ Steam Reforming Equilibrium

$$x^{S}_{u,u',\text{CO}} \cdot {x^{S}_{u,u',\text{H}_2}}^{3} - K^{SR}_{u,\text{CH}_4} \cdot x^{S}_{u,u',\text{CH}_4} \cdot x^{S}_{u,u',\text{H}_2\text{O}} \quad = 0 \quad \forall (u,u') \in UC, u \in U_{SMR} \tag{B.30}$$

Bypass of Inert Species

$$\sum_{(u',u,s) \in S^{UF}} N^{S}_{u',u,s} - \sum_{(u,u',s) \in S^{UF}} N^{S}_{u,u',s} \quad = 0 \quad \forall u \in U\_SMR, s \in S^{In}_{SMR} \tag{B.31}$$

*Autothermal Reformer and Secondary Reformer*

Both ATR and AM-SR units are modeled with the same equations. Here the modeling equations are shown for ATR unit.

Logical Use of One Temperature

$$\sum_{u \in U\_ATR} y_u - 1 \quad = 0 \tag{B.32}$$

Water-Gas-Shift Equilibrium

$$N^S_{u,u',\mathrm{CO_2}} \cdot N^S_{u,u',\mathrm{H_2}} - K^{RGS}_u \cdot N^S_{u,u',\mathrm{CO}} \cdot N^S_{u,u',\mathrm{H_2O}} \quad = 0 \quad \forall (u,u') \in UC, u \in U_{ATR} \tag{B.33}$$

$CH_4$ Steam Reforming Equilibrium

$$x^S_{u,u',\mathrm{CO}} \cdot {x^S_{u,u',\mathrm{H_2}}}^3 - K^{SR}_{u,\mathrm{CH_4}} \cdot x^S_{u,u',\mathrm{CH_4}} \cdot x^S_{u,u',\mathrm{H_2O}} \quad = 0 \quad \forall (u,u') \in UC, u \in U_{ATR} \tag{B.34}$$

Bypass of Inert Species

$$\sum_{(u',u,s) \in S^{UF}} N^S_{u',u,s} - \sum_{(u,u',s) \in S^{UF}} N^S_{u,u',s} \quad = 0 \quad \forall u \in U\_ATR, s \in S^{In}_{ATR} \tag{B.35}$$

**Biomass Conversion**

*Biomass Drier*

Upper Bound for Biomass Drier Activation

$$\begin{aligned} & MW_{\mathrm{H_2O}} \cdot N^S_{u,u',\mathrm{H_2O}} - \\ & MT\_Bio \cdot \sum_{(u,u',s) \in S^{UF}} MW_s \cdot N^S_{u,u',s} \quad \leq 0 \quad (u,u') = (IN_{BIO}, BDR) \\ & -UB \cdot y_u \end{aligned} \tag{B.36}$$

Lower Bound for Biomass Drier Activation

$$\begin{aligned} &MT\_Bio \cdot \sum_{(u,u',s)\in S^{UF}} MW_s \cdot N^S_{u,u',s} - \\ &MW_{\mathrm{H_2O}} \cdot N^S_{u,u',\mathrm{H_2O}} - UB \cdot (1 - y_u) \end{aligned} \quad \leq 0 \quad (u,u') = IN_{BIO}, BDR \tag{B.37}$$

Upper Bound for Biomass Drier Moisture Evaporation

$$\begin{aligned} &MT\_Bio \cdot \sum_{(u,u',s)\in S^{UF}} MW_s \cdot N^S_{u,u',s} - \\ &MW_{\mathrm{H_2O}} \cdot N^S_{u,u',\mathrm{H_2O}} - UB \cdot (1 - y_u) \end{aligned} \quad \leq 0 \quad (u,u') = (BDR, BLK) \tag{B.38}$$

Lower Bound for Biomass Drier Moisture Evaporation

$$\begin{aligned} &MW_{\mathrm{H_2O}} \cdot N^S_{u,u',\mathrm{H_2O}} - \\ &MT\_Bio \cdot \sum_{(u,u',s)\in S^{UF}} MW_s \cdot N^S_{u,u',s} \\ &-UB \cdot (1 - y_u) \end{aligned} \quad \leq 0 \quad (u,u') = (BDR, BLK) \tag{B.39}$$

*Gasifier Lockhopper*

Set $CO_2$ Lockhopper Flow Rate

$$MW_{\mathrm{CO_2}} \cdot N^S_{\mathrm{CO_2C_2,BLK,CO_2}} - mf_u \cdot \sum_{s\in S_{Bio}} MW_s \cdot N^S_{\mathrm{BDR,BLK},s} \quad = 0 \tag{B.40}$$

*Biomass Gasifier*

Water-Gas-Shift Equilibrium

$$N_{u,\mathrm{BC1,CO}} \cdot N_{u,\mathrm{BC1,H_2O}} - K^{RGS}_u \cdot N_{u,\mathrm{BC1,CO_2}} \cdot N_{u,\mathrm{BC1,H_2}} \quad = 0 \quad \forall u \in U_{BGS} \tag{B.41}$$

Hydrocarbon Conversion Fraction

$$MW_s \cdot N_{u,\text{BC1},s} - \sum_{(u',u,s)\in S^{UF}} cf_{u,s}^{HC} \cdot M_s^{S,Calc} \quad = 0 \quad \forall s \in S_{HC}, u \in U_{BGS} \tag{B.42}$$

Hydrocarbon Generation from Pyrolysis

$$\begin{gathered} {}^{\text{S,Calc}}_{s} - \sum_{s'\in S_{Bio}} \sum_{(u',u,s')\in S^{UF}} Pyr_{s,s'}^{HC} \cdot MW_s \cdot N_{u',u,s'}^{S} - \sum_{(u',u)\in UC} MW_s \cdot N_{u',u,s}^{S} \\ = 0 \\ u \in U_{BGS} \end{gathered} \tag{B.43}$$

Set Ratio of NO to $N_2O$

$$N_{u,\text{BC1,NO}} - sr_{u,\frac{\text{NO}}{\text{N}_2\text{O}}} \cdot N_{u,\text{BC1,N}_2\text{O}} \quad = 0 \quad \forall u \in U_{BGS} \tag{B.44}$$

Set Ratio of HCN to $NH_3$

$$N_{u,\text{BC1,HCN}} - sr_{u,\frac{\text{HCN}}{\text{NH}_3}} \cdot N_{u,\text{BC1,NH}_3} \quad = 0 \quad \forall u \in U_{BGS} \tag{B.45}$$

Set Amount Input Nitrogen to $NH_3$ and $N_2$

$$N_{u,\text{BC1,NH}_3} + 2 \cdot N_{u,\text{BC1,N}_2} - nf_u \cdot \sum_{(u,\text{BC1},s)\in S^{UF}} N_{u,\text{BC1},s}^{S} \cdot AR_{s,\text{N}} \quad = 0 \quad \forall u \in U_{BGS} \tag{B.46}$$

Set Ratio of $NH_3$ to $N_2$

$$N_{u,\text{BC1,NH}_3} - (a_{u,\text{N}_2}^1 + a_{u,\text{N}_2}^2 \cdot T_u) \cdot (N_{u,\text{BC1,NH}_3} + 2 \cdot N_{u,\text{BC1,N}_2}) \quad = 0 \quad \forall u \in U_{BGS} \tag{B.47}$$

Set Ratio of COS to $H_2S$

$$N_{u,\text{BC1,COS}} - sr_{u,\frac{\text{COS}}{\text{H}_2\text{S}}} \cdot N_{u,\text{BC1,H}_2\text{S}} \quad = 0 \quad \forall u \in U_{BGS} \tag{B.48}$$

Amount of Char Production

$$W_{\text{Char}} \cdot N^{S}_{u,\text{BC1,Char}} - (a^{1}_{u,\text{Char}} + a^{2}_{u,\text{Char}} \cdot T_u) \cdot \sum_{s \in S_{Bio}} MW_s \cdot N^{S}_{\text{BLK},u,s} = 0 \quad \forall u \in U_{BGS} \tag{B.49}$$

Rate of Ash Removal

$$N^{S}_{u,\text{OUT\_ASH,Ash}} - sf_{u,\text{Ash}} \cdot \sum_{(u',u) \in UC} N^{S}_{u',u,\text{Ash}} \quad = 0 \quad \forall u \in U_{BGS} \tag{B.50}$$

Gasifier Heat Loss

$$Q^{L}_{u} + hl_u \cdot \sum_{s \in S_{Bio}} MW_s \cdot N^{S}_{\text{BLK},u,s} \cdot LHV_s \quad = 0 \quad \forall u \in U_{BGS} \tag{B.51}$$

Logical Use of One Gasifier Temperature

$$\sum_{u \in U_{BGS}} y_u - 1 \quad = 0 \tag{B.52}$$

*Biomass Gasifier Solids*

Removal of Solids from First Cyclone

$$rf_{BC1} \cdot N^{T}_{\text{BGS,BC1}} - N^{T}_{\text{BC1,BGS}} \quad = 0 \tag{B.53}$$

Removal of Solids from Second Cyclone

$$rf_{BC2} \cdot N^{T}_{\text{BC1,BC2}} - N^{T}_{\text{BC2,BGS}} \quad = 0 \tag{B.54}$$

***Water Electrolysis***

Set Alkaline Electrolyzer Hydrogen Production

$$N^{S}_{\text{DEION,AL-EYZ,H}_2\text{O}} \cdot conv_{\text{AL-EYZ}\cdot} \quad = N^{S}_{\text{AL-EYZ,CMP-EYZ,H}_2} \tag{B.55}$$

Set PEM Electrolyzer Hydrogen Production

$$N^{S}_{\text{DEION,AL-PEM,H}_2\text{O}} \cdot conv_{\text{PEM-EYZ}\cdot} \quad = N^{S}_{\text{AL-EYZ,MX-H2E,H}_2} \tag{B.56}$$

Select Only One Type of Electrolyzer

$$y_{\text{AL-PEM}} + y_{\text{PEM-PEM}} \quad = 1 \tag{B.57}$$

***Rectisol Unit***

Set $CO_2$ Molar Fraction in Clean Output

$$N^{S}_{\text{AGR-CREC,SP\_AGR-CREC,CO}_2} - rf_{\text{AGR-CREC}} \cdot N^{T}_{\text{AGR-CREC,SP\_CG}} \quad = 0 \tag{B.58}$$

Set $CO_2$ Output Flow Rates

$$N^{T}_{\text{AGR-CREC,CO}_2\text{C}} - sf_{\text{AGR}} \cdot (N^{T}_{\text{AGR-CREC,CO}_2\text{C}} + N^{T}_{\text{AGR-CREC,MX\_CO2RC}}) \quad = 0 \tag{B.59}$$

***aMDEA Unit***

Set $CO_2$ Molar Fraction in Clean Output

$$N^{S}_{\text{AM-CO2SEP,SP\_AM-CO2SEP,CO}_2} - rf_{\text{AM-CO2SEP}} \cdot N^{T}_{\text{AM-CO2SEP,SP\_CG}} \quad = 0 \tag{B.60}$$

Set $CO_2$ Output Flow Rates

$$N^{T}_{\text{AM-CO2SEP,CO}_2\text{C}} - sf_{\text{AGR}} \cdot (N^{T}_{\text{AM-CO2SEP,CO}_2\text{C}} + N^{T}_{\text{AM-CO2SEP,MX\_CO2RC}}) \quad = 0 \tag{B.61}$$

*Pressure-Swing Adsorption*

Set Recovery Fraction of $H_2$ from Inlet

$$N^{S}_{\text{PSA,SP\_H}_2\text{P,H}_2} - Rev^{\text{H}_2}_{\text{PSA}} \cdot \sum_{(u,\text{PSA}) \in UC} N^{S}_{u,\text{PSA,H}_2} \quad = 0 \tag{B.62}$$

Set Inlet Mole Fraction of $H_2$

$$\sum_{(u,\text{PSA}) \in UC} N^{S}_{u,\text{PSA,H}_2} - In^{\text{H}_2}_{\text{PSA}} \cdot \sum_{(u,\text{PSA}) \in UC} N^{T}_{u,\text{PSA}} \quad = 0 \tag{B.63}$$

*Haber-Bosch Reactor*

Calculate Extent of Reaction

$$HBR^{Conv} = A + B \cdot T + C \cdot P + D \cdot x^{s}_{uc,H_2} + E \cdot x^{s}_{uc,N_2} + F \cdot x^{s}_{uc,NH_3} + G \cdot x^{s}_{uc,s_{inert}} \tag{B.64}$$

Calculate Outlet Flow Rate of Hydrogen for Hydrogen as the Limiting Reactant

$$N^{S}_{uc2,H_2} = N^{S}_{uc,H_2} \cdot (1 - HBR^{Conv}) \tag{B.65}$$

Calculate Outlet Flow Rate of Nitrogen for Hydrogen as the Limiting Reactant

$$N^{S}_{uc2,N_2} = N^{S}_{uc,N_2} - (1/3) \cdot (N^{S}_{uc,H_2} - N^{S}_{uc2,H_2}) \tag{B.66}$$

Calculate Outlet Flow Rate of Ammonia for Hydrogen as the Limiting Reactant

$$N^S_{uc2,NH_3} = N^S_{uc,NH_3} + (2/3) \cdot (N^S_{uc,H_2} - N^S_{uc2,H_2}) \tag{B.67}$$

Calculate Outlet Flow Rate of Hydrogen for Nitrogen as the Limiting Reactant

$$N^S_{uc2,H_2} = N^S_{uc,H_2} - 3 \cdot (N^S_{uc,N_2} - N^S_{uc2,N_2}) \tag{B.68}$$

Calculate Outlet Flow Rate of Nitrogen for Nitrogen as the Limiting Reactant

$$N^S_{uc2,N_2} = N^S_{uc,N_2} \cdot (1 - HBR^{Conv}) \tag{B.69}$$

Calculate Outlet Flow Rate of Ammonia for Nitrogen as the Limiting Reactant

$$N^S_{uc2,NH_3} = N^S_{uc,NH_3} + 2 \cdot (N^S_{uc,N_2} - N^S_{uc2,N_2}) \tag{B.70}$$

***Recycle Gas Treatment***

*Fuel Combustor*

Set Inlet Combustor Oxygen Level

$$\sum_{(u,\text{FCM}) \in UC} N^S_{u,\text{FCM},O_2} - er_{\text{FCM}} \cdot \sum_{(\text{SP\_LG,FCM},s) \in S^{UF}} N^S_{\text{SP\_LG,FCM},s} \cdot sor_s \quad = 0 \tag{B.71}$$

*Gas Turbine*

Set Air Leakage From First Compressor

$$N^S_{\text{GTAC1,OUT\_V},s} - lk\_GTAC1 \cdot N^S_{\text{IN\_AIR,GTAC1},s} \quad = 0 \quad \forall(\text{GTAC1}, s) \in S^U \tag{B.72}$$

Set Air Bypass From First Compressor

$$N^{S}_{\text{GTAC1,GT2},s} - by\_GTAC1 \cdot N^{S}_{\text{IN\_AIR,GTAC1},s} \quad = 0 \quad \forall(\textbf{GTAC2}, s) \in S^{U} \tag{B.73}$$

Set Inlet Oxygen Flow Rate in Combustor

$$er_{\text{GTC}} \cdot \sum_{(u,\text{GTC},s)\in S^{UF}} sor_{s} \cdot N^{S}_{u,\text{GTC},s} - \sum_{(u,\text{GTC},s)\in S^{UF}} N^{S}_{u,\text{GTC,O2}} \quad = 0 \tag{B.74}$$

Set Heat Loss in Combustor

$$Q^{L}_{\text{GTC}} - hl\_GTC \cdot (H^{T}_{\text{SP\_LG,GTC}} - H^{T}_{\text{X\_GTF,GTF}}) \quad = 0 \tag{B.75}$$

***Wastewater Treatment***

*Biological Digestor*

Set Biogas Ratio of $CH_4$ to $CO_2$

$$N^{S}_{\text{BD,CC,CH}_4} - cr_{\text{BD}} \cdot N^{S}_{\text{BD,CC,CO}_2} \quad = 0 \tag{B.76}$$

*Reverse Osmosis*

Set Removal Fraction of Solids

$$N^{S}_{\text{RO,SP\_RO},s} - rf_{\text{RO}} \cdot N^{S}_{\text{MX\_RO,RO},s} \quad = 0 \quad \forall s \in S_{Sol} \tag{B.77}$$

*Cooling Cycle*

Cooling Tower Flow Rate from Energy Requirement

$$Q_{C} - hr_{\text{COOL-P}} \cdot N^{S}_{\text{CLTR,COOL-P,H}_2\text{O}} \quad = 0 \tag{B.78}$$

Cooling Tower Evaporation Loss

$$N^{Evap}_{\text{CLTR}} - 0.00085 \cdot \Delta T_{\text{CLTR}} \cdot N^{S}_{\text{CLTR,COOL-P,H}_2\text{O}} \quad = 0 \tag{B.79}$$

Cooling Tower Drift Loss

$$N^{Drift}_{\text{CLTR}} - 0.001 \cdot N^{S}_{\text{MX\_CLTR,CLTR,H}_2\text{O}} \quad = 0 \tag{B.80}$$

Sum Total Cooling Tower Losses

$$N^{Evap}_{\text{CLTR}} + N^{Drift}_{\text{CLTR}} - N^{S}_{\text{CLTR,OUT\_V,H}_2\text{O}} \quad = 0 \tag{B.81}$$

Set Known Cooling Tower Output Solid Concentrations

$$x^{Kn}_{\text{CLTR,SP\_CLTR},s} \cdot N^{T}_{\text{CLTR,SP\_CLTR}} - N^{S}_{\text{CLTR,SP\_CLTR},s} \quad = 0 \quad \forall s \in S_{Sol} \tag{B.82}$$

*Steam Cycle*

Set Known Process Steam Boiler Output Solid Concentrations

$$x^{Kn}_{\text{X\_PWB,MX\_BLR},s} \cdot N^{T}_{\text{X\_PWB,MX\_BLR}} - N^{S}_{\text{X\_PWB,MX\_BLR},s} \quad = 0 \quad \forall s \in S_{Sol} \tag{B.83}$$

Set Known Heat Engine Boiler Output Solid Concentrations

$$x^{Kn}_{\text{HEP,MX\_BLR},s} \cdot N^{T}_{\text{HEP,MX\_BLR}} - N^{S}_{\text{HEP,MX\_BLR},s} \quad = 0 \quad \forall s \in S_{Sol} \tag{B.84}$$

*Outlet Wastewater*

Upper Bound on Output Wastewater Concentrations

$$N^{S}_{\text{MX\_WW,OUT\_V},s} - x^{Max}_{\text{MX\_WW,OUT\_V},s} \cdot N^{T}_{\text{MX\_WW,OUT\_V}} \quad \leq 0 \quad \forall s \in S_{WW} \tag{B.85}$$

***Air Separation***

*Air Separation Unit*

Recovery Fraction of $O_2$

$$N^{S}_{\text{ASU,OUT\_V},s} - (1 - sf_{\text{ASU}}) \cdot N^{S}_{\text{AC,ASU},s} \quad = 0 \quad \forall s \in S^{U}_{ASU} \tag{B.86}$$

***Process Hot/Cold/Power Utility Requirements***

Set Electricity Needed for Process Units

$$Q^{El}_{P} - \sum_{u \in U_{Util}} S_u \cdot El^{Base}_{u} \quad = 0 \tag{B.87}$$

Set Cooling Water Needed for Process Units

$$Q^{CW}_{P} - \sum_{u \in U_{Util}} S_u \cdot CW^{Base}_{u} \quad = 0 \tag{B.88}$$

Set Heating Fuel Needed for Process Units

$$Q_{\text{FCM}} - \sum_{u \in U_{Util}} S_u \cdot F^{Base}_{u} \quad = 0 \tag{B.89}$$

Set Utilities Needed for Process Units

$$Q^{HU}_{u,ut} - S_u \cdot U^{Base}_{u,ut} \quad = 0 \quad \forall ut, u \in U_{Util} \tag{B.90}$$

***Process Costs***

*Feedstock Costs*

Levelized Cost of Natural Gas Feedstock

$$Cost_{NG} = \sum_{(\text{IN\_NG},u)\in UC} \frac{(\sum_{s\in S_{NG}} MW_s \cdot N^S_{\text{IN\_NG},u,s}) \cdot C^F_{NG}}{Prod} \tag{B.91}$$

Levelized Cost of Freshwater Feedstock

$$Cost_{\text{H2O}} = \frac{MW\_H2O \cdot N^S_{\text{IN\_H2O,SP\_WRI,H2O}} \cdot C^F_{\text{H2O}}}{Prod} \tag{B.92}$$

Levelized Cost of Ammonia

$$Cost_{NH3} = \sum_{(u,\text{OUT\_NH3})\in UC} \frac{(\sum_{s\in S_{NH3}} MW_s \cdot N^S_{\text{u,OUT\_NH3},s}) \cdot C^P_{NH3}}{Prod} \tag{B.93}$$

*Electricity Costs*

Levelized Cost of Electricity

$$Cost^{El} = \frac{F^{El}_{In} \cdot C^{El}_{In} - F^{El}_{Out} \cdot C^{El}_{Out}}{Prod \cdot LHV_{Prod}} \tag{B.94}$$

*$CO_2$ Sequestration Costs*

Levelized Cost of $CO_2$ Sequestration

$$Cost^{Seq} = \frac{MW\_CO2 \cdot N^S_{\text{CO2SC,OUT\_CO2,CO2}} \cdot C^{Seq}}{Prod \cdot LHV_{Prod}} \tag{B.95}$$

*Levelized Investment Costs*

Total Overnight Cost of Process Units

$$TOC_u = (1 + IC_u) \cdot (1 + BOP_u) \cdot C_{o,u} \cdot (\frac{S_u}{S_{o,u}})^{sf_u} \tag{B.96}$$

Variable Capital Costs of Process Units

$$CC_u = LCCR \cdot IDCF \cdot TOC_u \tag{B.97}$$

Levelized Cost of Process Units

$$Cost_u^U = \frac{CC_u \cdot (1 + OM)}{CAP \cdot Prod\cdot} \tag{B.98}$$

***Objective Function***

Levelized Cost of Fuels Production

$$\text{MIN} \quad \sum_{f \in Feed} Cost_f + Cost^{El} + Cost^{Seq} + \sum_{u \in U_{Inv}} Cost_u^U - Sales_{LPG} \tag{B.99}$$

***Simultaneous Heat, Power, and Water Integration***

*Pinch Points*

Set Pinch Points Based on Inlet Temperatures

$$\left\{\begin{array}{l} T_{pi} = T_{u,u'}^{HP-in} \ \forall (u,u') \in HP;\ T_{pi} = T_u \ \forall u \in HPt^{HB}; \\ T_{pi} = T_{ut} \ \forall (ut,pi) \in HPt - PI^{Ut}; \\ T_{pi} = T_{b,c,t}^{PC-in} \ \forall (b,c,t) \in HEP;\ T_{pi} = T_c \\ T_{pi} = T_{u,u'}^{CP-in} + \Delta T \ \forall (u,u') \in CP;\ T_{pi} = T_{b,c}^{EC-in} + \Delta T \ \forall (b,c) \in CP^{EC}; \\ T_{pi} = T_{b,t}^{SH-in} + \Delta T \ \forall (b,t) \in CP^{SH}; \\ T_{pi} = T_{ut} + \Delta T \ \forall (ut,pi) \in CPt - PI^{Ut}; \\ T_{pi} = T_b + \Delta T \end{array}\right\} \quad \text{(B.100)}$$

*Temperature Differences*

Process Unit Hot Stream Inlets

$$\Delta T_{u,u',pi}^{HP-in} = \max\{0, T_{u,u'}^{HP-in} - T_{pi}\} \quad \text{(B.101)}$$

Process Unit Hot Stream Outlets

$$\Delta T_{u,u',pi}^{HP-out} = \max\{0, T_{u,u'}^{HP-out} - T_{pi}\} \quad \text{(B.102)}$$

Process Unit Cold Stream Inlets

$$\Delta T_{u,u',pi}^{CP-in} = \max\{0, T_{u,u'}^{CP-in} - (T_{pi} - \Delta T)\} \quad \text{(B.103)}$$

Process Unit Cold Stream Outlets

$$\Delta T_{u,u',pi}^{CP-out} = \max\{0, T_{u,u'}^{CP-out} - (T_{pi} - \Delta T)\} \quad \text{(B.104)}$$

Heat Engine Precooler Inlets

$$\Delta T_{b,c,t,pi}^{PC-in} = \max\{0, T_{b,c,t}^{PC-in} - T_{pi}\} \quad \text{(B.105)}$$

Heat Engine Precooler Outlets

$$\Delta T_{b,c,t,pi}^{PC-out} = \max\{0, T_{b,c,t}^{PC-out} - T_{pi}\} \quad \text{(B.106)}$$

Heat Engine Economizer Inlets

$$\Delta T_{b,c,pi}^{EC-in} = \max\{0, T_{b,c}^{EC-in} - (T_{pi} - \Delta T)\} \quad \text{(B.107)}$$

Heat Engine Economizer Outlets

$$\Delta T_{b,c,pi}^{EC-out} = \max\{0, T_{b,c}^{EC-out} - (T_{pi} - \Delta T)\} \quad \text{(B.108)}$$

Heat Engine Superheater Inlets

$$\Delta T_{b,t,pi}^{SH-in} = \max\{0, T_{b,t}^{SH-in} - (T_{pi} - \Delta T)\} \quad \text{(B.109)}$$

Heat Engine Superheater Outlets

$$\Delta T_{b,t,pi}^{SH-out} = \max\{0, T_{b,t}^{SH-out} - (T_{pi} - \Delta T)\} \quad \text{(B.110)}$$

*Heat Engine Logical Existence*

Bound on Heat Engine Flow Rate

$$F_{b,c,t}^{Up} \cdot y_{b,c,t}^{En} \geq F_{b,c,t}^{En} \quad \forall (b,c,t) \in HEP \quad \text{(B.111)}$$

Bound on Total Amount of Heat Engines

$$\sum_{(b,c,t)\in HEP} y^{En}_{b,c,t} \quad \leq EnMax \tag{B.112}$$

*Heat Balances*

Heat Engine Electricity Balance

$$\sum_{(b,c,t)\in HEP} (w^{Tur}_{b,c,t} - w^{Pum}_{b,c,t}) \cdot F^{En}_{b,c,t} \quad = F_{El} \tag{B.113}$$

Upper Heat Balance for Pinch Points

$$\begin{aligned} Q^H_{pi} = \quad & \sum_{(u,u')\in HP} \sum_{s} N^s_{u,u',s} \cdot Cp^P_{u,u',s} \cdot (\Delta T^{HP-in}_{u,u',pi} - \Delta T^{HP-out}_{u,u',pi}) \\ & + \sum_{(b,c,t)\in HEP} F^{En}_{b,c,t} \cdot Cp^{HE-P} \cdot (\Delta T^{PC-in}_{b,c,t,pi} - \Delta T^{PC-out}_{b,c,t,pi}) \\ & + \sum_{(ut,pi)\in HPt-PI^{Ut}} \sum_{(u,ut)\in HPt} Q^{HU}_{u,ut} + \\ & + \sum_{(u,pi)\in HPt-PI^{HB}} Q_u + \sum_{b} \sum_{(c,pi)\in HPt-PI^{C}} \sum_{t} F^{En}_{b,c,t} \cdot dH^C_c \end{aligned} \tag{B.114}$$

Lower Heat Balance for Pinch Points

$$\begin{aligned} Q^C_{pi} = \quad & \sum_{(u,u')\in CP} \sum_{s} N^s_{u,u',s} \cdot Cp^P_{u,u',s} \cdot (\Delta T^{CP-out}_{u,u',pi} - \Delta T^{CP-in}_{u,u',pi}) \\ & + \sum_{(b,c,t)\in HEP} F^{En}_{b,c,t} \cdot Cp^{HE-E} \cdot (\Delta T^{EC-out}_{b,c,pi} - \Delta T^{EC-in}_{b,c,pi}) \\ & + \sum_{(b,c,t)\in HEP} F^{En}_{b,c,t} \cdot Cp^{HE-S} \cdot (\Delta T^{SH-out}_{b,t,pi} - \Delta T^{SH-in}_{b,t,pi}) \\ & + \sum_{(ut,pi)\in CPt-PI^{Ut}} \sum_{(u,ut)\in CPt} Q^{HU}_{u,ut} + \sum_{(b,pi)\in CPt-PI^{B}} \sum_{c} \sum_{t} F^{En}_{b,c,t} \cdot dH^B_b \end{aligned} \tag{B.115}$$

Pinch Point Heating Deficit

$$z_{pi} = Q^C_{pi} - Q^H_{pi} \tag{B.116}$$

Negativity of Pinch Deficits

$$z_{pi} \leq 0 \tag{B.117}$$

Total Heating Deficit

$$\Omega - Q_c = 0 \tag{B.118}$$

Total Heat Balance

$$\begin{aligned}
\Omega = & \sum_{(u,u') \in HP} \sum_{s} N^{s}_{u,u',s} \cdot Cp^{P}_{u,u',s} \cdot (T^{HP-in}_{u,u'} - T^{HP-out}_{u,u'}) \\
& + \sum_{(b,c,t) \in HEP} F^{En}_{b,c,t} \cdot Cp^{HE-P} \cdot (T^{PC-in}_{b,c,t} - T^{PC-out}_{b,c,t}) \\
& + \sum_{(u,ut) \in HPt} Q^{HU}_{u,ut} + \sum_{u \in HPt^{HB}} Q_u + \sum_{(b,c,t) \in HEP} F^{En}_{b,c,t} \cdot dH^{C}_{c} \\
& - \sum_{(u,u') \in CP} \sum_{s} N^{s}_{u,u',s} \cdot Cp^{P}_{u,u',s} \cdot (T^{CP-out}_{u,u'} - T^{CP-in}_{u,u'}) \\
& - \sum_{(b,c,t) \in HEP} F^{En}_{b,c,t} \cdot Cp^{HE-E} \cdot (T^{EC-out}_{b,c} - T^{EC-in}_{b,c}) \\
& - \sum_{(b,c,t) \in HEP} F^{En}_{b,c,t} \cdot Cp^{HE-S} \cdot (T^{SH-out}_{b,t} - T^{SH-in}_{b,t}) \\
& - \sum_{(u,ut) \in CPt} Q^{HU}_{u,ut} - \sum_{(b,c,t) \in HEP} F^{En}_{b,c,t} \cdot dH^{B}_{b}
\end{aligned} \tag{B.119}$$

## B.3 The Process Superstructure

### *Light Gas Handling*

The light gases ($C_1$/$C_2$ hydrocarbons, unreacted syngas, and inert species) are handled in two different ways. An internal loop design recycles the light gases back to process units such as the reformers, chemical looping FRs, MEOHS, FT units, and pressure swing absorption to increase the overall conversion to desired products. To avoid a build-up of inert species, not all the light gases can be recycled. As such, a split of the light gases is purged through an external loop configuration. In this loop, the purged gases are sent to either a fuel combustor or gas turbine to provide heat or electricity for the process, respectively. Based on GHG emissions constraints, the effluent from these units is either vented or sent to a $CO_2$ recovery unit.

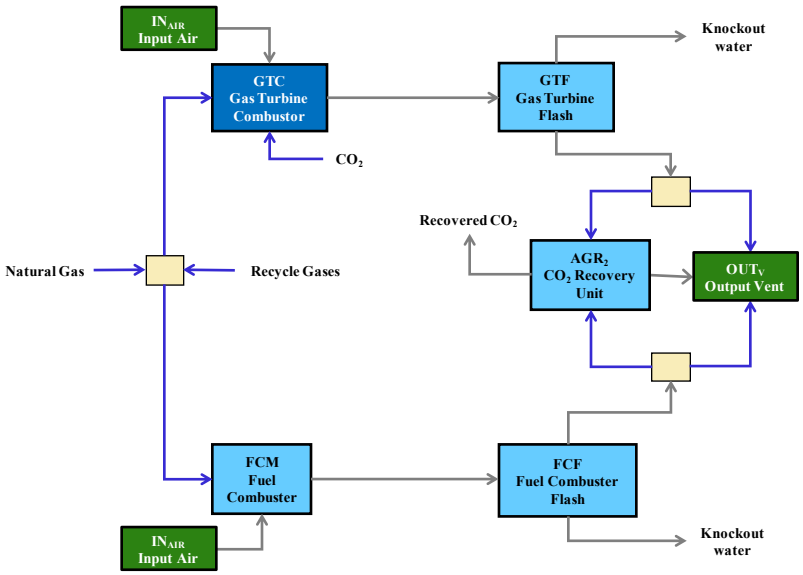


Figure B.1: Light gas handling section.

### *Air Separation*

Pressure swing absorption (PSA) or EYZ can deliver high purity $H_2$ (>90%) to any process unit that requires it. Similarly, high purity $O_2$ (>99%) can be supplied through an ASU or EYZ.

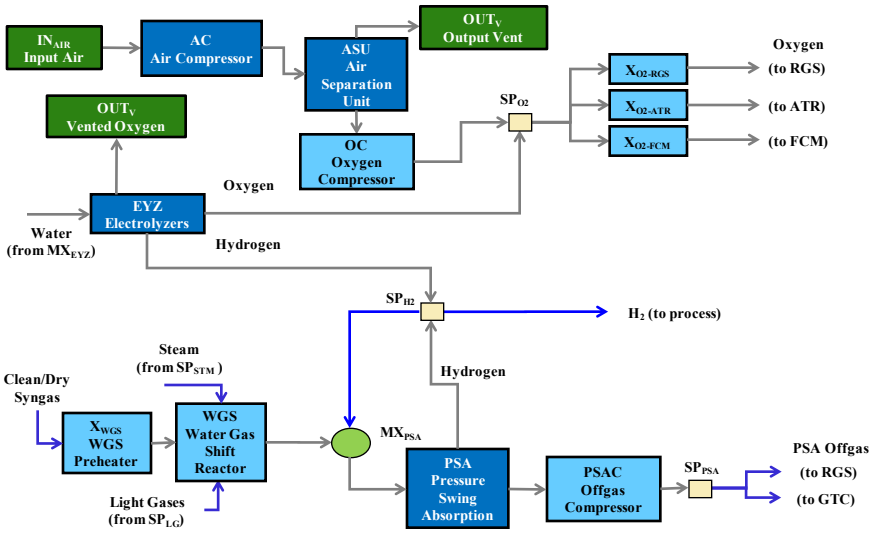


Figure B.2: Air separation section.

### *Wastewater Treatment*

The wastewater from various process units is treated with a sour stripper and a biological digestor. A reverse osmosis unit and a cooling tower further purifies the treated water. Along with any necessary fresh water input, the treated water is heated in boilers to generate steam for the process. Excess purified water is discharged.

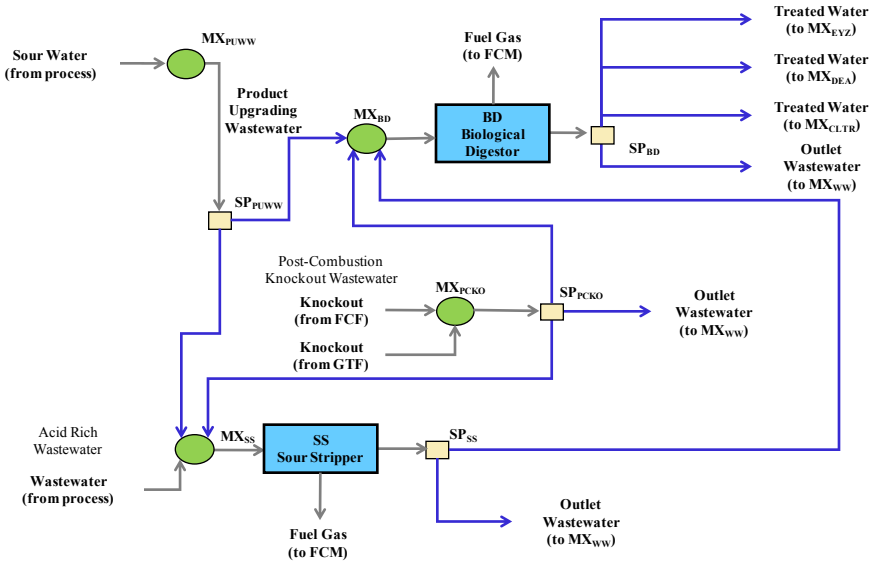


Figure B.3: Process wastewater treatment section.

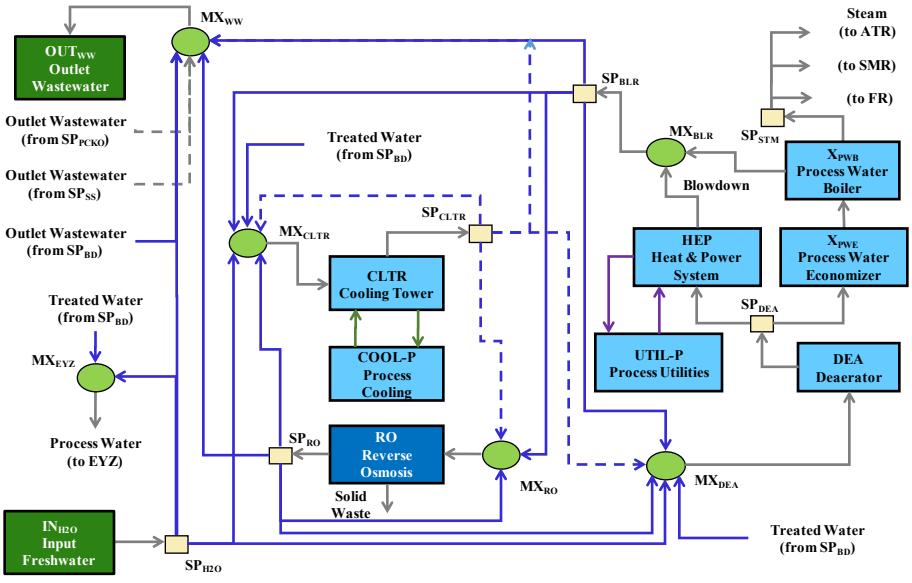


Figure B.4: Utility wastewater treatment section.

## B.4 Data-driven Modeling of the Haber-Bosch Reactor

We did not use an equilibrium model for the ammonia synthesis reactors because the conversion does not reach the equilibrium value. Instead, the reactors are modeled through a data-driven approach using a data set of 25 industrial (Imperical Chemical Industries, Kellogg Brown & Root, Haldor Topsøe, Uhde GmbH, Casale) and experimental values. We employ a bootstrapping technique to create random samples of size 55. Regression models with different linear and nonlinear terms are then fitted and best model is selected based on 5-fold cross-validation. In the selected model, we allowed the conversion $X_r$, based on the limiting reactant of either $H_2$ or $N_2$, to be linearly dependent on inlet composition, temperature, and pressure (Eq. B.121).

$$N_2 + 3H_2 \rightarrow 2NH_3 \tag{B.120}$$

$$\begin{aligned} X_r(T, P, y_i) = (-3.8404 \times 10^{-1}) + (-6.7630 \times 10^{-1}) \cdot T + (9.4042 \times 10^{-2}) \cdot P \\ +(3.4163 \times 10^{-1}) \cdot y_{H_2} + (2.1362 \times 10^{-1}) \cdot y_{N_2} + (9.4756 \times 10^{-2}) \cdot y_{Inert} \end{aligned} \tag{B.121}$$

The fitted parameters are determined from the data-driven approach. We separate our dataset into training, validation, and testing subsets. After performing 5-fold cross-validation with the training and validation sets, we test the fitted parameters on the testing data not included in training and validation. The data set is shown in Table B.3.

Statistics of the cross validated linear models are shown in Table B.4.

We observe that the linear model closely approximates the actual conversion values. After calculating the conversion, amount of ammonia produced in the reactor is determined using reaction stoichiometry. For example, if $N_2$ is the limiting reactant, the following equations are used:

$$N_2^{out} = N_2^{in}(1 - X_r) \tag{B.122}$$

$$H_2^{out} = H_2^{in} - 3(N_2^{in} - N_2^{out}) \tag{B.123}$$

Table B.3: Data set for data-driven modeling of Haber-Bosch Reactor.

| # | $T_{out}$ (°C) | P (bar) | $y_{H_2}$ | $y_{N_2}$ | $y_{NH_3}$ | Inert | $H_2/N_2$ | Conversion | References |
|---|---|---|---|---|---|---|---|---|---|
| 1 | 354 | 171.0 | 0.659 | 0.210 | 0.018 | 0.113 | 3.14 | 0.313 | US 5,736,116 |
| 2 | 401 | 171.0 | 0.650 | 0.240 | 0.020 | 0.090 | 2.71 | 0.368 | US 5,736,116 |
| 3 | 395 | 85.6 | 0.660 | 0.220 | 0.040 | 0.080 | 3.00 | 0.201 | US 4,681,745 |
| 4 | 438 | 93.0 | 0.620 | 0.280 | 0.050 | 0.050 | 2.21 | 0.197 | US 4,681,745 |
| 5 | 370 | 199.0 | 0.653 | 0.217 | 0.010 | 0.120 | 3.01 | 0.287 | US 6,171,570 |
| 6 | 432 | 104.0 | 0.650 | 0.216 | 0.037 | 0.097 | 3.01 | 0.219 | US 4,695,442 |
| 7 | 402 | 85.5 | 0.605 | 0.275 | 0.038 | 0.082 | 2.20 | 0.143 | US 4.778.662 |
| 8 | 473 | 128.0 | 0.625 | 0.215 | 0.023 | 0.137 | 2.91 | 0.214 | Gaines |
| 9 | 450 | 127.0 | 0.667 | 0.230 | 0.022 | 0.081 | 2.90 | 0.207 | Azarhoosh |
| 10 | 480 | 200.0 | 0.639 | 0.213 | 0.013 | 0.135 | 3.00 | 0.212 | Azarhoosh |
| 11 | 455 | 229.0 | 0.670 | 0.222 | 0.028 | 0.081 | 3.02 | 0.305 | Singh |
| 12 | 440 | 179.0 | 0.651 | 0.196 | 0.032 | 0.121 | 3.32 | 0.295 | Singh |
| 13 | 440 | 210.0 | 0.621 | 0.206 | 0.032 | 0.141 | 3.01 | 0.311 | Singh |
| 14 | 438 | 283.0 | 0.650 | 0.219 | 0.052 | 0.079 | 2.97 | 0.287 | Singh |
| 15 | 460 | 272.0 | 0.658 | 0.212 | 0.030 | 0.100 | 3.10 | 0.317 | Singh |
| 16 | 443 | 362.0 | 0.595 | 0.188 | 0.030 | 0.187 | 3.16 | 0.370 | Singh |
| 17 | 469 | 185.0 | 0.612 | 0.235 | 0.042 | 0.111 | 2.60 | 0.269 | Appl |
| 18 | 460 | 177.0 | 0.682 | 0.227 | 0.043 | 0.048 | 3.00 | 0.246 | US 4,296,085 |
| 19 | 460.3 | 144.0 | 0.672 | 0.224 | 0.020 | 0.084 | 3.00 | 0.210 | US 4,755,362 |
| 20 | 459.5 | 146.0 | 0.672 | 0.224 | 0.020 | 0.084 | 3.00 | 0.246 | US 4,755,362 |
| 21 | 448 | 240.0 | 0.658 | 0.219 | 0.018 | 0.105 | 3.00 | 0.338 | US 6,214,296 B1 |
| 22 | 350 | 134.0 | 0.736 | 0.254 | 0.000 | 0.010 | 2.90 | 0.430 | US 6,955,797 |
| 23 | 453 | 88.6 | 0.622 | 0.309 | 0.020 | 0.050 | 2.01 | 0.331 | US 20080161428 A1 |
| 24 | 455 | 88.6 | 0.627 | 0.309 | 0.019 | 0.045 | 2.03 | 0.332 | US 20080161428 A1 |
| 25 | 472 | 265.8 | 0.634 | 0.211 | 0.035 | 0.120 | 3.00 | 0.338 | US 4,181,701 |
| 26 | 419 | 105.0 | 0.656 | 0.222 | 0.038 | 0.084 | 2.96 | 0.224 | US 4,311,671 |
| 27 | 445 | 223.0 | 0.628 | 0.209 | 0.035 | 0.128 | 3.00 | 0.333 | Panahandeh |
| 28 | 455 | 229.0 | 0.670 | 0.222 | 0.028 | 0.080 | 3.02 | 0.305 | Elnashaie |

$$NH_3^{out} = NH_3^{in} + 2(N_2^{in} - N_2^{out}) \tag{B.124}$$

Table B.4: Model predictions of testing data using the fitted parameters from cross-validation. Error is reported for each prediction.

| Testing Set | Model 1 | Model 2 | Model 3 | Model 4 | Model 5 | Actual |
|---|---|---|---|---|---|---|
| Test 1 | 0.327 | 0.329 | 0.332 | 0.324 | 0.327 | 0.338 |
| Test 2 | 0.303 | 0.299 | 0.300 | 0.297 | 0.301 | 0.305 |
| Test 3 | 0.315 | 0.316 | 0.284 | 0.329 | 0.318 | 0.331 |
| Test 4 | 0.213 | 0.209 | 0.209 | 0.211 | 0.209 | 0.224 |
| Test 5 | 0.209 | 0.238 | 0.220 | 0.214 | 0.220 | 0.214 |
| Test RMSE | 0.061 | 0.089 | 0.130 | 0.056 | 0.062 | - |

## B.5 Material and Energy Balance Results

### Material Balances

Table B.5: Overall material balances for the case studies.

| | TX-N-250 | TX-N-500 | TX-N-1000 | CA-N-250 | CA-N-500 | CA-N-1000 | IA-N-250 | IA-N-500 | IA-N-1000 |
|---|---|---|---|---|---|---|---|---|---|
| Biomass (dt/h) | 0.000 | 0.000 | 0.000 | 0.000 | 0.000 | 0.000 | 0.000 | 0.000 | 0.000 |
| Natural gas (MSCF/h) | 0.251 | 0.542 | 1.080 | 0.326 | 0.618 | 1.386 | 0.244 | 0.536 | 1.085 |
| Fresh water (kBD) | 2.248 | 4.352 | 8.309 | 3.210 | 5.754 | 13.940 | 3.012 | 4.160 | 11.179 |
| Seq. CO2 (MT/h) | 14.132 | 30.279 | 59.828 | 17.956 | 33.831 | 76.640 | 13.803 | 29.867 | 60.022 |
| Vented CO2 (MT/h) | 0.349 | 0.994 | 2.467 | 0.866 | 1.824 | 3.387 | 0.272 | 1.060 | 2.562 |
| Ammonia (MT/h) | 10.416 | 20.832 | 41.664 | 10.416 | 20.832 | 41.664 | 10.416 | 20.832 | 41.664 |
| | TX-H-250 | TX-H-500 | TX-H-1000 | CA-H-250 | CA-H-500 | CA-H-1000 | IA-C-250 | IA-C-500 | IA-C-1000 |
| Biomass (dt/h) | 17.004 | 35.776 | 82.192 | 21.430 | 42.874 | 85.747 | 18.001 | 36.002 | 72.005 |
| Natural gas (MSCF/h) | 0.000 | 0.000 | 0.000 | 0.000 | 0.000 | 0.000 | 0.000 | 0.000 | 0.000 |
| Fresh water (kBD) | 3.019 | 6.244 | 14.862 | 4.045 | 8.097 | 16.194 | 3.925 | 7.850 | 15.700 |
| Seq. CO2 (MT/h) | 0.801 | 0.322 | 0.204 | 0.097 | 0.196 | 0.392 | 0.000 | 0.000 | 0.000 |
| Vented CO2 (MT/h) | 30.594 | 65.540 | 151.145 | 39.357 | 78.736 | 157.473 | 30.900 | 61.801 | 123.602 |
| Ammonia (MT/h) | 10.416 | 20.832 | 41.664 | 10.416 | 20.832 | 41.664 | 10.416 | 20.832 | 41.664 |
| | TX-M-250 | TX-M-500 | TX-M-1000 | CA-M-250 | CA-M-500 | CA-M-1000 | IA-M-250 | IA-M-500 | IA-M-1000 |
| Biomass (dt/h) | 15.996 | 32.949 | 58.137 | 21.315 | 42.577 | 73.946 | 16.492 | 32.920 | 57.573 |
| Natural gas (MSCF/h) | 0.000 | 0.000 | 0.000 | 0.000 | 0.000 | 0.000 | 0.000 | 0.000 | 0.000 |
| Fresh water (kBD) | 3.226 | 6.278 | 10.997 | 4.397 | 8.802 | 15.197 | 3.115 | 6.228 | 10.953 |
| Seq. CO2 (MT/h) | 0.000 | 0.000 | 0.000 | 0.000 | 0.000 | 0.000 | 0.000 | 0.000 | 0.000 |
| Vented CO2 (MT/h) | 30.420 | 62.601 | 110.475 | 40.528 | 80.938 | 140.575 | 31.341 | 62.558 | 109.386 |
| Ammonia (MT/h) | 10.416 | 20.832 | 41.664 | 10.416 | 20.832 | 41.664 | 10.416 | 20.832 | 41.664 |
| | TX-W-250 | TX-W-500 | TX-W-1000 | CA-W-250 | CA-W-500 | CA-W-1000 | IA-W-250 | IA-W-500 | IA-W-1000 |
| Biomass (dt/h) | 0.000 | 0.000 | 0.000 | 0.000 | 0.000 | 0.000 | 0.000 | 0.000 | 0.000 |
| Natural gas (MSCF/h) | 0.000 | 0.000 | 0.000 | 0.000 | 0.000 | 0.000 | 0.000 | 0.000 | 0.000 |
| Fresh water (kBD) | 7.587 | 15.174 | 29.911 | 7.478 | 14.955 | 29.922 | 7.587 | 15.174 | 29.911 |
| Seq. CO2 (MT/h) | 0.000 | 0.000 | 0.000 | 0.000 | 0.000 | 0.000 | 0.000 | 0.000 | 0.000 |
| Vented CO2 (MT/h) | 0.007 | 0.013 | 0.026 | 0.007 | 0.013 | 0.026 | 0.007 | 0.013 | 0.026 |
| Ammonia (MT/h) | 10.416 | 20.832 | 41.664 | 10.416 | 20.832 | 41.664 | 10.416 | 20.832 | 41.664 |
| | TX-S-250 | TX-S-500 | TX-S-1000 | CA-S-250 | CA-S-500 | CA-S-1000 | - | - | - |
| Biomass (dt/h) | 0.000 | 0.000 | 0.000 | 0.000 | 0.000 | 0.000 | - | - | - |
| Natural gas (MSCF/h) | 0.000 | 0.000 | 0.000 | 0.000 | 0.000 | 0.000 | - | - | - |
| Fresh water (kBD) | 7.587 | 14.955 | 29.921 | 7.587 | 15.174 | 29.911 | - | - | - |
| Seq. CO2 (MT/h) | 0.000 | 0.000 | 0.000 | 0.000 | 0.000 | 0.000 | - | - | - |
| Vented CO2 (MT/h) | 0.007 | 0.013 | 0.026 | 0.007 | 0.013 | 0.026 | - | - | - |
| Ammonia (MT/h) | 10.416 | 20.832 | 41.664 | 10.416 | 20.832 | 41.664 | - | - | - |

## Energy Balances

Table B.6: Overall energy balances for the case studies.

| Energy bal. (MW) | TX-N-250 | TX-N-500 | TX-N-1000 | CA-N-250 | CA-N-500 | CA-N-1000 | IA-N-250 | IA-N-500 | IA-N-1000 |
|---|---|---|---|---|---|---|---|---|---|
| Biomass | 0.00 | 0.00 | 0.00 | 0.00 | 0.00 | 0.00 | 0.00 | 0.00 | 0.00 |
| Natural Gas | 68.54 | 148.00 | 294.81 | 89.04 | 168.66 | 378.51 | 66.63 | 137.09 | 296.18 |
| Electricity | 20.83 | 34.65 | 64.46 | 8.07 | 18.40 | 25.40 | 22.34 | 41.66 | 62.95 |
| Total | 89.37 | 182.65 | 359.27 | 97.11 | 187.06 | 403.91 | 88.96 | 178.75 | 359.12 |
| Energy bal. (MW) | TX-H-250 | TX-H-500 | TX-H-1000 | CA-H-250 | CA-H-500 | CA-H-1000 | IA-C-250 | IA-C-500 | IA-C-1000 |
| Biomass | 84.28 | 177.31 | 407.35 | 106.21 | 212.49 | 424.97 | 84.25 | 168.50 | 337.00 |
| Natural Gas | 0.00 | 0.00 | 0.00 | 0.00 | 0.00 | 0.00 | 0.00 | 0.00 | 0.00 |
| Electricity | 16.94 | 17.80 | 5.82 | 0.00 | 0.00 | 0.00 | 10.91 | 21.83 | 43.66 |
| Total | 101.22 | 195.11 | 413.17 | 106.21 | 212.49 | 424.97 | 95.16 | 190.33 | 380.66 |
| Energy bal. (MW) | TX-M-250 | TX-M-500 | TX-M-1000 | CA-M-250 | CA-M-500 | CA-M-1000 | IA-M-250 | IA-M-500 | IA-M-1000 |
| Biomass | 94.67 | 195.00 | 344.08 | 126.15 | 251.98 | 437.64 | 97.61 | 194.83 | 340.74 |
| Natural Gas | 0.00 | 0.00 | 0.00 | 0.00 | 0.00 | 0.00 | 0.00 | 0.00 | 0.00 |
| Electricity | 16.59 | 22.18 | 35.88 | 0.00 | 0.00 | 0.00 | 10.72 | 21.47 | 38.75 |
| Total | 111.26 | 217.18 | 379.95 | 126.15 | 251.98 | 437.64 | 108.33 | 216.30 | 379.49 |
| Energy bal. (MW) | TX-W-250 | TX-W-500 | TX-W-1000 | CA-W-250 | CA-W-500 | CA-W-1000 | IA-W-250 | IA-W-500 | IA-W-1000 |
| Biomass | 0.00 | 0.00 | 0.00 | 0.00 | 0.00 | 0.00 | 0.00 | 0.00 | 0.00 |
| Natural Gas | 0.00 | 0.00 | 0.00 | 0.00 | 0.00 | 0.00 | 0.00 | 0.00 | 0.00 |
| Electricity | 126.05 | 252.10 | 496.81 | 124.20 | 248.41 | 496.93 | 126.05 | 252.10 | 496.81 |
| Total | 126.05 | 252.10 | 496.81 | 124.20 | 248.41 | 496.93 | 126.05 | 252.10 | 496.81 |
| Energy bal. (MW) | TX-S-250 | TX-S-500 | TX-S-1000 | CA-S-250 | CA-S-500 | CA-S-1000 | - | - | - |
| Biomass | 0.00 | 0.00 | 0.00 | 0.00 | 0.00 | 0.00 | - | - | - |
| Natural Gas | 0.00 | 0.00 | 0.00 | 0.00 | 0.00 | 0.00 | - | - | - |
| Electricity | 126.05 | 248.41 | 497.00 | 126.05 | 252.10 | 496.81 | - | - | - |
| Total | 126.05 | 248.41 | 497.00 | 126.05 | 252.10 | 496.81 | - | - | - |

## Carbon balance

Table B.7: Overall Carbon balance for the case studies.

| C bal. (kg/s) | TX-N-250 | TX-N-500 | TX-N-1000 | CA-N-250 | CA-N-500 | CA-N-1000 | IA-N-250 | IA-N-500 | IA-N-1000 |
|---|---|---|---|---|---|---|---|---|---|
| Biomass | 0.0000 | 0.0000 | 0.0000 | 0.0000 | 0.0000 | 0.0000 | 0.0000 | 0.0000 | 0.0000 |
| Natural Gas | 1.0966 | 2.3678 | 4.7167 | 1.4245 | 2.6984 | 6.0559 | 1.0660 | 2.1933 | 4.7386 |
| Vented CO2 | 0.0265 | 0.0753 | 0.1870 | 0.0656 | 0.1382 | 0.2567 | 0.0206 | 0.0529 | 0.1942 |
| Seq CO2 | 1.0713 | 2.2954 | 4.5355 | 1.3612 | 2.5647 | 5.8100 | 1.0464 | 2.1426 | 4.5502 |
| C bal. (kg/s) | TX-H-250 | TX-H-500 | TX-H-1000 | CA-H-250 | CA-H-500 | CA-H-1000 | IA-C-250 | IA-C-500 | IA-C-1000 |
| Biomass | 2.3708 | 4.9879 | 11.4592 | 2.9878 | 5.9775 | 11.9549 | 2.3407 | 4.6814 | 9.3628 |
| Natural Gas | 0.0000 | 0.0000 | 0.0000 | 0.0000 | 0.0000 | 0.0000 | 0.0000 | 0.0000 | 0.0000 |
| Vented CO2 | 2.3193 | 4.9685 | 11.4581 | 2.9836 | 5.9689 | 11.9378 | 2.3425 | 4.6850 | 9.3701 |
| Seq CO2 | 0.0607 | 0.0244 | 0.0155 | 0.0073 | 0.0149 | 0.0298 | 0.0000 | 0.0000 | 0.0000 |
| C bal. (kg/s) | TX-M-250 | TX-M-500 | TX-M-1000 | CA-M-250 | CA-M-500 | CA-M-1000 | IA-M-250 | IA-M-500 | IA-M-1000 |
| Biomass | 2.3021 | 4.7418 | 8.3668 | 3.0675 | 6.1274 | 10.6419 | 2.3735 | 4.7376 | 8.2856 |
| Natural Gas | 0.0000 | 0.0000 | 0.0000 | 0.0000 | 0.0000 | 0.0000 | 0.0000 | 0.0000 | 0.0000 |
| Vented CO2 | 2.3061 | 4.7457 | 8.3750 | 3.0723 | 6.1358 | 10.6568 | 2.3759 | 4.7424 | 8.2924 |
| Seq CO2 | 0.0000 | 0.0000 | 0.0000 | 0.0000 | 0.0000 | 0.0000 | 0.0000 | 0.0000 | 0.0000 |
| C bal. (kg/s) | TX-W-250 | TX-W-500 | TX-W-1000 | CA-W-250 | CA-W-500 | CA-W-1000 | IA-W-250 | IA-W-500 | IA-W-1000 |
| Biomass | 0.0000 | 0.0000 | 0.0000 | 0.0000 | 0.0000 | 0.0000 | 0.0000 | 0.0000 | 0.0000 |
| Natural Gas | 0.0000 | 0.0000 | 0.0000 | 0.0000 | 0.0000 | 0.0000 | 0.0000 | 0.0000 | 0.0000 |
| Vented CO2 | 0.0005 | 0.0010 | 0.0020 | 0.0005 | 0.0010 | 0.0020 | 0.0005 | 0.0010 | 0.0020 |
| Seq CO2 | 0.0000 | 0.0000 | 0.0000 | 0.0000 | 0.0000 | 0.0000 | 0.0000 | 0.0000 | 0.0000 |
| C bal. (kg/s) | TX-S-250 | TX-S-500 | TX-S-1000 | CA-S-250 | CA-S-500 | CA-S-1000 | - | - | - |
| Biomass | 0.0000 | 0.0000 | 0.0000 | 0.0000 | 0.0000 | 0.0000 | - | - | - |
| Natural Gas | 0.0000 | 0.0000 | 0.0000 | 0.0000 | 0.0000 | 0.0000 | - | - | - |
| Vented CO2 | 0.0005 | 0.0010 | 0.0020 | 0.0005 | 0.0010 | 0.0020 | - | - | - |
| Seq CO2 | 0.0000 | 0.0000 | 0.0000 | 0.0000 | 0.0000 | 0.0000 | - | - | - |

## Sample Flowsheet

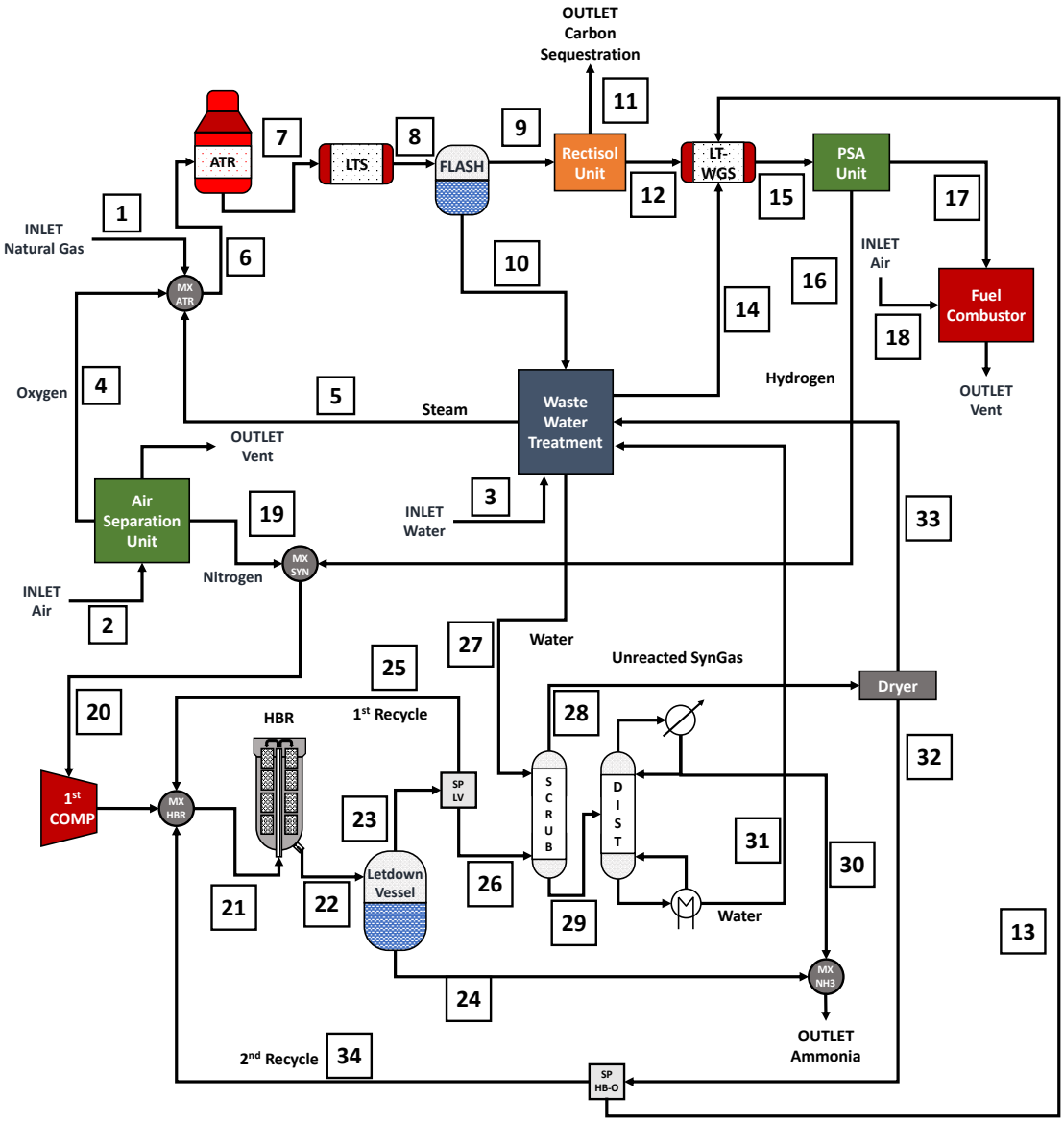


Figure B.5: Sample flowsheet for CA-N-1000 case.

Table B.8: Stream conditions and flow rates for the sample flowsheet of CA-N-1000 case.

| Stream ID | 1 | 2 | 3 | 4 | 5 | 6 | 7 | 8 | 9 | 10 |
|---|---|---|---|---|---|---|---|---|---|---|
| Temperature (°C) | 25 | 25 | 25 | 400 | 600 | 900 | 900 | 250 | 35 | 35 |
| Pressure (bar) | 31 | 1.01 | 1.01 | 32 | 32 | 30 | 30 | 28.5 | 24.5 | 24.5 |
| Vapor fraction | 1 | 1 | 0 | 1 | 1 | 1 | 1 | 1 | 1 | 0 |
| Flow rates (mol/s) | | | | | | | | | | |
| $O_2$ | 0.00 | 213.28 | 0.00 | 213.28 | 0.00 | 213.28 | 0.00 | 0.00 | 0.00 | 0.00 |
| CO | 0.00 | 0.00 | 0.00 | 0.00 | 0.00 | 0.00 | 351.44 | 53.11 | 53.11 | 0.00 |
| $CO_2$ | 4.84 | 0.37 | 0.00 | 0.00 | 0.00 | 4.84 | 99.49 | 397.82 | 397.81 | 0.01 |
| $H_2$ | 0.00 | 0.00 | 0.00 | 0.00 | 0.00 | 0.00 | 978.32 | 1276.64 | 1276.64 | 0.00 |
| $N_2$ | 7.74 | 795.08 | 0.00 | 1.06 | 0.00 | 8.80 | 8.80 | 8.80 | 8.80 | 0.00 |
| $H_20$ | 0.00 | 0.00 | 1423.82 | 0.00 | 519.11 | 519.11 | 404.92 | 106.59 | 4.02 | 102.57 |
| Ar | 0.00 | 9.51 | 0.00 | 0.01 | 0.00 | 0.01 | 0.01 | 0.01 | 0.01 | 0.00 |
| $CH_4$ | 450.50 | 0.00 | 0.00 | 0.00 | 0.00 | 450.50 | 53.27 | 53.27 | 53.27 | 0.00 |
| $C_2H_6$ | 15.48 | 0.00 | 0.00 | 0.00 | 0.00 | 15.48 | 0.00 | 0.00 | 0.00 | 0.00 |
| $C_3H_8$ | 3.39 | 0.00 | 0.00 | 0.00 | 0.00 | 3.39 | 0.00 | 0.00 | 0.00 | 0.00 |
| $nC_4H_{10}$ | 1.94 | 0.00 | 0.00 | 0.00 | 0.00 | 1.94 | 0.00 | 0.00 | 0.00 | 0.00 |
| Stream ID | 11 | 12 | 13 | 14 | 15 | 16 | 17 | 18 | 19 | 20 |
| Temperature (°C) | 25 | 25 | 60 | 237.4 | 35 | 28.6 | 28.6 | 25 | 30 | 30 |
| Pressure (bar) | 3 | 20.1 | 25 | 32 | 31 | 31 | 31 | 1.01 | 32 | 31 |
| Vapor fraction | 1 | 1 | 1 | 0 | 1 | 1 | 1 | 1 | 1 | 1 |
| Flow rates (mol/s) | | | | | | | | | | |
| $O_2$ | 0.00 | 0.00 | 0.00 | 0.00 | 0.00 | 0.00 | 0.00 | 313.74 | 0.00 | 0.00 |
| CO | 0.00 | 53.11 | 0.00 | 0.00 | 0.01 | 0.00 | 0.01 | 0.00 | 0.00 | 0.00 |
| $CO_2$ | 358.03 | 39.78 | 0.00 | 0.00 | 92.89 | 0.00 | 92.89 | 0.54 | 0.00 | 0.00 |
| $H_2$ | 0.00 | 1276.64 | 1051.06 | 0.00 | 2380.81 | 2071.31 | 309.51 | 0.00 | 0.00 | 2071.31 |
| $N_2$ | 0.00 | 8.80 | 439.12 | 0.00 | 447.92 | 0.00 | 447.92 | 1169.58 | 779.18 | 779.18 |
| $NH_3$ | 0.00 | 0.00 | 0.15 | 0.00 | 0.15 | 0.00 | 0.15 | 0.00 | 0.00 | 0.00 |
| $H_20$ | 0.00 | 4.02 | 0.00 | 49.09 | 0.00 | 0.00 | 0.00 | 0.00 | 0.00 | 0.00 |
| Ar | 0.00 | 0.01 | 0.00 | 0.00 | 0.01 | 0.00 | 0.01 | 13.99 | 0.00 | 0.00 |
| $CH_4$ | 0.00 | 53.27 | 0.00 | 0.00 | 53.27 | 0.00 | 53.27 | 0.00 | 0.00 | 0.00 |
| Stream ID | 21 | 22 | 23 | 24 | 25 | 26 | 27 | 28 | 29 | 30 |
| Temperature (°C) | 400 | 440 | -20 | -20 | 60 | 60 | 150 | 105.9 | 105.9 | 58.3 |
| Pressure (bar) | 85.5 | 85.5 | 25 | 25 | 25 | 25 | 25 | 25 | 25 | 25 |
| Vapor fraction | 1 | 1 | 1 | 0 | 1 | 1 | 0 | 1 | 0 | 0 |
| Flow rates (mol/s) | | | | | | | | | | |
| $H_2$ | 4845.60 | 3825.86 | 3825.36 | 0.50 | 2613.23 | 1212.12 | 0.00 | 1212.12 | 0.00 | 0.00 |
| $N_2$ | 1938.24 | 1598.33 | 1598.18 | 0.14 | 1091.77 | 506.41 | 0.00 | 506.41 | 0.00 | 0.00 |
| $NH_3$ | 357.04 | 1036.87 | 522.62 | 514.25 | 357.02 | 165.60 | 0.00 | 0.17 | 165.43 | 165.38 |
| $H_20$ | 0.00 | 0.00 | 0.00 | 0.00 | 0.00 | 0.00 | 231.60 | 2.87 | 228.73 | 0.05 |
| Stream ID | 31 | 32 | 33 | 34 | - | - | - | - | - | - |
| Temperature (°C) | 222.5 | 60 | 60 | 60 | - | - | - | - | - | - |
| Pressure (bar) | 25 | 25 | 25 | 25 | - | - | - | - | - | - |
| Vapor fraction | 0 | 1 | 0 | 1 | - | - | - | - | - | - |
| Flow rates (mol/s) | | | | | - | - | - | - | - | - |
| $H_2$ | 0.00 | 1212.12 | 0.00 | 161.06 | - | - | - | - | - | - |
| $N_2$ | 0.00 | 506.41 | 0.00 | 67.29 | - | - | - | - | - | - |
| $NH_3$ | 0.05 | 0.17 | 0.00 | 0.02 | - | - | - | - | - | - |
| $H_20$ | 228.68 | 0.00 | 2.87 | 0.00 | - | - | - | - | - | - |

APPENDIX C

SUPPORTING INFORMATION FOR CHAPTERS 4 AND 5

## C.1 Nomenclature for MILP Design and Operation Model

### Sets

| | |
|---|---|
| $t$ | Time periods in hours |
| $h$ | Representative seasons |
| $a$ | Location |
| $i$ | Processes |
| $j$ | Resources |
| $m$ | Operating modes |
| $q$ | Transportation modes |
| $l$ | Piecewise cost function segments |

### Subsets

| | |
|---|---|
| $Time_{h,t}$ | Time periods t in season h |
| $Season_h$ | Set of seasons considered |
| $Modes_{i,m}$ | Operating modes m in process i |
| $TransModes_{i,m,m'}$ | Possible mode transitions from m to m' in process i |
| $Seq_{i,m,m',m''}$ | Predefined sequences of mode transitions for process i |
| $Demand_j$ | Resources j for which demand exists |
| $LiquidFuels_j$ | Resources j that are to liquid transportation fuels |
| $TPModes_{j,q}$ | Allowed transportation modes q for resource j |
| $PLSegments_{i,l}$ | Segments l in piecewise linear approximations for process i |

### Variables

| | |
|---|---|
| $TotalCost$ | Total annualized cost |
| $Inv^{excess}_{a,j,h}$ | Excess inventor for resource j in season h at location a |
| $LocalGHG_a$ | Net GHG emissions the process network at location a |
| $TotalGHG$ | Total emitted $CO_2$ |

## Positive Variables

| | |
|---|---|
| $B_{a,j,h,t}$ | Amount of resource j purchased in time t of season h at location a |
| $Cap^{P}_{a,i}$ | Production capacity for process i at location a based on reference resource |
| $Cap^{S}_{a,j}$ | Storage capacity for resource j at location a |
| $Capex_{a,i}$ | Overnight capital cost for process i at location a |
| $Capex^{total}_{a}$ | Total overnight capital expenses at location a |
| $Inv_{a,j,h,t}$ | Inventory level of resource j in time t of season h at location a |
| $\lambda_{a,i,l}$ | Coefficient for segment l in piecewise linear approximation for process i at location a |
| $Opex_{a}$ | Total annual operation cost at location a |
| $P_{a,i,h,t}$ | Amount of reference resource consumed or produced by process i in time t of season h at location a |
| $P^{m}_{a,i,m,h,t}$ | Amount of reference resource consumed or produced by process i in mode m in time t of season h at location a |
| $S_{a,j,h,t}$ | Amount of resource j sold in time t of season h at location a |
| $Trans_{a,a',j,q,h,t}$ | Amount of resource j transported from location a to a' using transportation mode q in time t of season h |
| $Trans^{cost}_{j,q}$ | The transportation cost for resource j using transportation mode q |
| $Trans^{total}_{j,q}$ | The total transportation cost for resource j using transportation mode q |

## Binary Variables

| | |
|---|---|
| $w_{a,i,l}$ | Equals 1 if the capacity for process i at location a is in the range of line segment l |
| $x^{P}_{a,i}$ | Equals 1 if process i at location a is built |
| $x^{S}_{a,j}$ | Equals 1 if storage facility for resource j is built at location a |
| $y_{a,i,m,h,t}$ | Equals 1 if process i at location a operates in mode m in time t of season h |
| $z_{a,i,m,m',h,t}$ | Equals 1 if process i at location a in mode m changes to mode m' in time t of season h |

## Parameters

| | |
|---|---|
| $B^{max}_{a,j,h,t}$ | Maximum amount of resource j that can be consumed in time t of season h at location a |
| $BigM$ | Big M parameter |
| $CAP^{P-max}_{i}$ | Maximum production capacity for process i |
| $CAP^{S-max}_{j}$ | Maximum storage capacity for resource j |
| $CAP^{segment}_{i,l}$ | Capacity of process i at the right end point of segment l |
| $CAP^{util-min}_{i,m}$ | Minimum capacity utilization fraction for mode m of process i |
| $CAP^{util-max}_{i,m}$ | Maximum capacity utilization fraction for mode m of process i |
| $CAP^{mode-min}_{i,m}$ | Minimum production capacity for mode m of process i |
| $CAP^{mode-max}_{i,m}$ | Maximum production capacity for mode m of process i |

| | |
|---|---|
| $CAP_{i,m}^{\Delta rate}$ | Maximum rate of change of production for mode m of process i |
| $CAPEX_{i,l}^{segment}$ | Capital cost for process i at the right hand side of segment l |
| $CarbonTax$ | Carbon tax paid per amount of carbon dioxide emitted |
| $Conversion_{i,m,j,h}$ | Conversion factor for resource j with respect to the reference resource in mode m of process i in season h |
| $Cost_{a,j,h,t}^{discharge}$ | Cost of discharging resource j in time t of season h at location a |
| $Cost_{a,i}^{land}$ | Land cost for process i at location a |
| $Cost_{i,m,h}^{P-fix}$ | Fixed operational cost for process i operating in process i in mode m of season h |
| $Cost_{i,m,h}^{P-var}$ | Variable operational cost for process i operating in process i in mode m of season h |
| $Cost_{a,j,h,t}^{purchase}$ | Cost of purchasing resource j in time t of season h at location a |
| $Cost_{j}^{S-fix}$ | Fixed capital cost for storage of resource j |
| $Cost_{j}^{S-var}$ | Variable capital cost for storage of resource j |
| $Cost_{j,q}^{trans-fix}$ | Fixed transportation cost of resource j using mode q |
| $Cost_{j,q}^{trans-var}$ | Variable transportation cost of resource j using mode q |
| $D_{a,j,h,t}$ | Demand for resource j in time t of season h at location a |
| $D_{a,j,h}^{season}$ | Seasonla demand for resource j for season h at location a |
| $D_{a,j}^{total}$ | Aggregated demand for resource j of the annual operation |
| $D_{Fuels}^{total}$ | Total fuels demand for annual operation given in thousand barrels |
| $Distance_{a,a'}$ | Distance between locations a and a' |
| $FuelsRatio_{j}^{US}$ | United States fuel ratio given in fractions for resources j |
| $HHV_j$ | Higher heating value (HHV) of resource j |
| $Land_{a,j}^{max}$ | Maximum land availability for resource j at location a |
| $Loss_{a,j}^{S}$ | Fractional loss from storing resource j in season h |
| $Loss_{a,a',j,q}^{trans}$ | Fractional loss from of transportation between locations a and a' |
| $n_h$ | The weight of the representative season h in annual operation |
| $\rho_j$ | Density parameter to convert standard material flow unit (kg/h) of resource j to a different unit |

## C.2 Modeling Parameters

### Resource Data

Table C.1: Set of resources and the design and operational parameters for their storage.

| Resource | Description | $CAP_j^{S-max}$ | $Cost_j^{S-fix}$ | $Cost_j^{S-var}$ | $HHV_j$ |
|---|---|---|---|---|---|
| $Solar$ | Direct normal irradiation (DNI) potential in W/m$^2$ | - | - | - | - |
| $Wind$ | Wind power potential in m/s | - | - | - | - |
| $Power$ | Electrical power | - | - | - | - |
| $PowerLoad$ | Local electrical power demand | - | - | - | - |
| $GridPower$ | Power provided by the local electricity grid | - | - | - | - |
| $H_2O$ | Water | - | - | - | - |
| $Air$ | Air comprised of nitrogen and oxygen | - | - | - | - |
| $O_2$ | Oxygen | 1e9 | 0 | 0.9 | - |
| $N_2$ | Nitrogen | 1e9 | 0 | 1.2 | - |
| $H_2$ | Gaseous hydrogen | - | - | - | - |
| $CompressedH_2$ | Compressed hydrogen at 700 bar | 1e9 | 0 | 1400 | 0.0394 |
| $CryogenicH_2$ | Cryogenically liquefied hydrogen | 1e9 | 0 | 14 | 0.0394 |
| $NH_3$ | Ammonia | 6e7 | 0 | 1.5 | 0.00625 |
| $CH_3OH$ | Methanol | 6e7 | 0 | 0.9625 | 0.00639 |
| $CO_2$ | Carbon dioxide consumed or produced by processes | - | - | - | - |
| $CH_4$ | Methane | - | - | - | 0.0154 |
| $Coke$ | Elemental carbon product of the methane pyrolysis | - | - | - | - |
| $VentedCO_2$ | Vented carbon dioxide to the atmosphere | - | - | - | - |
| $SeqCO_2$ | Sequestered carbon dioxide | - | - | - | - |
| $Syngas$ | Synthesis gas with $H_2$:CO ratio of 2.2 | - | - | - | - |
| $FuelGas$ | Fuel gas that can be combusted for heat and power | - | - | - | - |
| $Gasoline$ | Synthetic gasoline fuel | 1e11 | - | - | 0.01289 |
| $Diesel$ | Synthetic diesel fuel | 1e11 | - | - | 0.01267 |
| $Kerosene$ | Synthetic kerosene fuel | 1e11 | - | - | 0.01283 |
| $WasteWater$ | Waste water | 1e11 | - | - | - |
| $BatteryCharge$ | NaS battery charge for power storage BES | 1e8 | 0 | 340,000 | - |
| $ElevatedWater$ | Elevated water for power storage in PCS | 2.5e5 | 0 | 80,000 | - |
| $CompressedAir$ | Compressed air for power storage in CAES | 2e6 | 0 | 50,000 | - |

**Transportation Data**

Table C.2: Transportation parameters.

| Resource | Transportation Mode | $Cost_{j,q}^{trans-fix}$ | $Cost_{j,q}^{trans-fix}$ |
|---|---|---|---|
| $CompressedH_2$ | Rail road | 0 | 1.667e-3 |
| $CryogenicH_2$ | Rail road | 0.5935 | 1.01e-4 |
| $NH_3$ | Rail road | 1.0674e-2 | 3.5e-5 |
| $CH_3OH$ | Rail road | 1.1746e-2 | 2.9478e-5 |

## Process Data

Table C.3: Set of processes.

| Process | Description |
|---|---|
| $WindFarm$ | Farm of wind turbines that generate $Power$ from wind |
| $SolarPV$ | Solar photovoltaic (PV) cells that produce $Power$ from solar irradiation |
| $Electrolyzer$ | Electrolysis process to produce $H_2$ and $O_2$ from water |
| $ASU$ | Air separation unit to produce nitrogen and oxygen |
| $DAC$ | Direct air capture process to capture $CO_2$ from $Air$ |
| $CO_2Sequestration$ | Process to sequester process $CO_2$ |
| $Haber-Bosch$ | Haber-Bosch process to produce ammonia from nitrogen and hydrogen |
| $MethanolSynthesis$ | Methanol synthesis process to produce methanol from $Syngas$ |
| $ATR$ | Autothermal reforming of methane to produce $Syngas$ |
| $MethanePyrolysis$ | Methane pyrolysis to produce $H_2$ |
| $CH_4GasTurbine$ | Methane gas turbine to produce $Power$ |
| $MTG$ | Methanol-to-Gasoline process to produce $Gasoline$ |
| $MOGD$ | Metanol-to-Olefins-Gasoline-Distillate to produce $Gasoline$, $Diesel$, and $Kerosene$ |
| $FTS$ | Fischer-Tropsch Synthesis to produce $Gasoline$ and $Diesel$ |
| $R-WGS$ | Reverse water-gas shift process to produce $Syngas$ from $CO_2$ and $H_2$ |
| $H_2Compression$ | $H_2$ is converted to $CompressedH_2$ |
| $H_2Liquefaction$ | $H_2$ is converted to $CryogenicH_2$ |
| $DC/AC-Inverter$ | DC/AC inverter to convert $Power$ (DC) to $PowerLoad$ (AC) |
| $NaS-Storage$ | Sodium-sulfur battery storage to produce $Power$ from $BatteryCharge$ |
| $NaS-PCS$ | Sodium-sulfur BES PCS to produce $Power$ from $BatteryCharge$ |
| $PSH-Storage$ | Pumped storage hydro storage process to store $Power$ in $ElevatedWater$ |
| $PSH-PCS$ | Pumped storage hydro PCS to produce $Power$ from $ElevatedWater$ |
| $CAES-Storage$ | Compressed air energy storage process to store $Power$ in $CompressedAir$ |
| $CAES-PCS$ | CAES PCS to produce $Power$ from $CompressedAir$ |
| $H_2FuelCell$ | Hydrogen fuel cell to produce $PowerLoad$ |
| $NH_3GasTurbine$ | Methanol gas turbine to produce $PowerLoad$ |
| $CH_3OHGasTurbine$ | Methanol gas turbine to produce $PowerLoad$ |

Table C.4: Operational cost and rate change parameters for Processes.

| Process | Basis | $CAP_{i,m}^{\Delta rate}$ | $CAP_{i,m}^{util-min}$ | $CAP_{i,m}^{util-max}$ | $Cost_{i,m,h}^{P-fix}$ | $Cost_{i,m,h}^{P-var}$ |
|---|---|---|---|---|---|---|
| $WindFarm$ [222] | MW | 1 | 0 | 1 | 0 | 14.6 |
| $SolarPV$ [177] | MW | 1 | 0 | 1 | 0 | 5.3 |
| $Electrolyzer$ [75, 183] | MW | 0.95 | 0 | 1 | 0 | 5.625 |
| $ASU$ [183] | kg/h | 0.1 | 0 | 1 | 0 | 8.32e-3 |
| $DAC$ [223] | kg/h | 0.95 | 0.5 | 1 | 0 | 0.03 |
| $CO_2Sequestration$ [183] | MW | 0.95 | 0 | 1 | 0 | 0 |
| $Haber-Bosch$ [183] | kg/h | 0.05 | 0.7 | 1 | 0 | 1.54e-2 |
| $MethanolSynthesis$ [224] | kg/h | 0.05 | 0.5 | 1 | 0 | 1.08e-2 |
| $ATR$ [183] | kg/h | 0.05 | 0.5 | 1 | 0 | 0.01538 |
| $MethanePyrolysis$ [225] | kg/h | 0.05 | 0 | 1 | 0 | 0.13995 |
| $CH_4GasTurbine$ [226] | MW | 0.2 | 0 | 1 | 0 | 9 |
| $MTG$ [217] | kg/h | 0.01 | 0.8 | 1 | 0 | 1.8473e-3 |
| $MOGD$ [217] | kg/h | 0.01 | 0.8 | 1 | 0 | 1.9564e-2 |
| $FTS$ [217] | kg/h | 0.05 | 0.8 | 1 | 0 | 0.0108 |
| $R-WGS$ [183] | kg/h | 0.1 | 0.4 | 1 | 0 | 2.732e-3 |
| $H_2Compression$ [227] | kg/h | 0.5 | 0 | 1 | 0 | 0.2 |
| $H_2Liquefaction$ [227] | kg/h | 0.5 | 0 | 1 | 0 | 0.4 |
| $DC/AC-Inverter$ | MW | 1 | 0 | 1 | 0 | 0 |
| $NaS-Storage$ [228] | MW | 1 | 0 | 1 | 0 | 2.2 |
| $NaS-PCS$ [228] | MW | 1 | 0 | 1 | 0 | 2.2 |
| $PSH-Storage$ [228] | MW | 0.95 | 0 | 1 | 0 | 0.9 |
| $PSH-PCS$ [228] | MW | 0.95 | 0 | 1 | 0 | 0.9 |
| $CAES-Storage$ [228] | MW | 1 | 0 | 1 | 0 | 0.7 |
| $CAES-PCS$ [228] | MW | 1 | 0 | 1 | 0 | 0.7 |
| $H_2FuelCell$ [229] | MW | 0.95 | 0 | 1 | 0 | 3.5 |
| $NH_3GasTurbine$ [226] | MW | 0.5 | 0 | 1 | 0 | 2.28 |
| $CH_3OHGasTurbine$ [226] | MW | 0.2 | 0 | 1 | 0 | 2.28 |

Table C.5: Conversion and capacity parameters for processes.

| Process | Basis [1] | $CAP_i^{P-max}$ | Inputs | Outputs |
|---|---|---|---|---|
| $WindFarm$ [222] | MW | 200,000 | $Wind$ = -2.5 | **Power = 1** |
| $SolarPV$ [177] | MW | 200,000 | $Solar$ = -4.44 | **Power = 1** |
| $Electrolyzer$ [183] | MW | 100,000 | **Power = -1**, $H_2O$ = -169.92 | $H_2$ = 16.98, $O_2$ = 139 |
| $ASU$ [183] | kg/h | 500,000 | **Air = -1**, $Power$ = -1.52e-4 | $N_2$ = 0.74, $O_2$ = 0.232 |
| $DAC$ [223] | kg/h | 100,000 | $Power$ = -1.4e-3, $Air$ = -2,276, $H_2$ = -4.82 | **$CO_2$ = 1** |
| $CO_2Sequestration$ [183] | MW | 10,000 | **Power = -1**, $CO_2$ = -7,549 | $SeqCO_2$ = 7,549 |
| $Haber-Bosch$ [183] | kg/h | 500,000 | $H_2$ = -0.178, $N_2$ = -0.822, $Power$ = -1.476e-3 | **$NH_3$ = 1** |
| $MethanolSynthesis$ [224] | kg/h | 250,000 | $Syngas$ = -1.063, $Power$ = -1.69e-4 | **$CH_3OH$ = 1**, $H_2$ = 0.124, $VentedCO_2$ = 0.226 |
| $ATR$ [183] | kg/h | 500,000 | $H_2O$ = -0.325, $CH_4$ = -0.481, $O_2$ = -0.578 | **Syngas = 1**, $WasteWater$ = 0.38 |
| $MethanePyrolysis$ [225] | kg/h | 100,000 | $CH_4$ = -4.86 | **$H_2$ = 1**, $Coke$ = 3.645 |
| $CH_4GasTurbine$ [226] | MW | 10,000 | $CH_4$ = -108 | **Power = 1**, $VentedCO_2$ = 297 |
| $MTG$ [217] | kg/h | 160,000 | $H_2O$ = -0.123, **$CH_3OH$ = -1**, $Power$ = -0.145e-6 | $Gasoline$ = 0.38, $WasteWater$ = 0.686, $FuelGas$ = 0.035 |
| $MOGD$ [217] | kg/h | 160,000 | $H_2O$ = -0.123, **$CH_3OH$ = -1**, $Power$ = -2.87e-6 | $Gasoline$ = 0.0454, $Diesel$ = 0.237, $Kerosene$ = 0.122, $WasteWater$ = 0.685, $FuelGas$ = 0.092 |
| $FTS$ [217] | kg/h | 500,000 | **Syngas = -1**, $H_2O$ = -0.071 | $Gasoline$ = 0.094, $Diesel$ = 0.284, $Power$ = 1.598 |
| $R-WGS$ [183] | kg/h | 500,000 | $H_2$ = -0.182, $CO_2$ = -1.337, $Power$ = -6e-5 | **Syngas = 1** |
| $H_2Compression$ [227] | kg/h | 100,000 | **$H_2$ = -1**, $Power$ = -5e-3 | $CompressedH_2$ = 1 |
| $H_2Liquefaction$ [227] | kg/h | 100,000 | **$H_2$ = -1**, $Power$ = -1.11e-2 | $CryoH_2$ = 1 |
| $DC/AC-Inverter$ | MW | 10,000 | $Power$ = -1.053 | **PowerLoad = 1** |
| $NaS-Storage$ [228] | MW | 100,000 | **Power = -1** | $BatteryCharge$ = 1 |
| $NaS-PCS$ [228] | MW | 100,000 | $BatteryCharge$ = -1.176 | **Power = 1** |
| $PSH-Storage$ [228] | MW | 10,000 | **Power = -1** | $ElevatedWater$ = 1 |
| $PSH-PCS$ [228] | MW | 10,000 | $ElevatedWater$ = -1.25 | **Power = 1** |
| $CAES-Storage$ [228] | MW | 10,000 | **Power = -1** | $CompressedAir$ = 1 |
| $CAES-PCS$ [228] | MW | 10,000 | $CompressedAir$ = -2 | **Power = 1** |
| $H_2FuelCell$ [229] | MW | 10,000 | $H_2$ = -50 | **PowerLoad = 1** |
| $NH_3GasTurbine$ [226] | MW | 10,000 | $CH_3OH$ = -303.03 | **PowerLoad = 1**, $VentedCO_2$ = 416.7 |
| $CH_3OHGasTurbine$ [226] | MW | 10,000 | $NH_3$ = -483.871 | **PowerLoad = 1** |

[1] The reference resource for each process is shown in bold in Table C.5.

Table C.6: Capital investments cost parameters for Processes with two pieces.

| | | $CAP_{i,l}^{segment}$ | | | | | | | | $CAPEX_{i,l}^{segment}$ ($ MM) | | | | | | | |
|---|---|---|---|---|---|---|---|---|---|---|---|---|---|---|---|---|---|
| | Basis | 1 | 2 | 3 | 4 | 5 | 6 | 7 | 8 | 1 | 2 | 3 | 4 | 5 | 6 | 7 | 8 |
| $WindFarm$ [222] | MW | 100 | 200,000 | - | - | - | - | - | - | 169 | 388,000 | - | - | - | - | - | - |
| $SolarPV$ [177] | MW | 100 | 200,000 | - | - | - | - | - | - | 111 | 222,000 | - | - | - | - | - | - |
| $Electrolyzer$ [75, 183] | MW | 100 | 100,000 | - | - | - | - | - | - | 1,100 | 1,100,000 | - | - | - | - | - | - |
| $ASU$ [183] | kg/h | 11,583 | 23,167 | 46,333 | 92,667 | 125,000 | 250,000 | 375,000 | 500,000 | 28.9 | 41.4 | 58.2 | 84.9 | 99.1 | 142 | 175 | 203 |
| $DAC$ [223] | kg/h | 100 | 100,000 | - | - | - | - | - | - | 0.24 | 241.18 | - | - | - | - | - | - |
| $CO_2Sequestration$ [183] | MW | 1 | 5 | 10 | 20 | 30 | 50 | 100 | 200 | 4.4 | 11.4 | 17.3 | 26.2 | 33.5 | 463 | 593 | 737 |
| $Haber-Bosch$ [183] | kg/h | 10,417 | 20,833 | 41,667 | 83,333 | 125,000 | 250,000 | 375,000 | 500,000 | 38.9 | 69.0 | 110 | 191 | 258 | 463 | 593 | 737 |
| $MethanolSynthesis$ [224] | kg/h | 40,000 | 80,000 | 120,000 | 160,000 | 200,000 | 250,000 | 300,000 | 400,000 | 79.8 | 123 | 164 | 197 | 228 | 264 | 298 | 359 |
| $ATR$ [183] | kg/h | 50,000 | 100,000 | 150,000 | 225,000 | 350,000 | 500,000 | - | - | 4.375 | 14.88 | 91.32 | 119.83 | 161.12 | 204.61 | - | - |
| $MethanePyrolysis$ [225] | kg/h | 1,000 | 100,000 | - | - | - | - | - | - | 27.24 | 2724.4 | - | - | - | - | - | - |
| $CH_4GasTurbine$ [226] | MW | 1 | 10,000 | - | - | - | - | - | - | 1.032 | 1032 | - | - | - | - | - | - |
| $MTG$ [217] | kg/h | 10,000 | 20,000 | 40,000 | 80,000 | 120,000 | 160,000 | - | - | 5.861 | 9.187 | 14.43 | 22.65 | 29.48 | 35.34 | - | - |
| $MOGD$ [217] | kg/h | 10,000 | 20,000 | 40,000 | 80,000 | 120,000 | 160,000 | - | - | 62.08 | 97.41 | 152.85 | 239.85 | 312.17 | 376.36 | - | - |
| $FTS$ [217] | kg/h | 1,000 | 500,000 | - | - | - | - | - | - | 1.89 | 945 | - | - | - | - | - | - |
| $R-WGS$ [183] | kg/h | 40,000 | 80,000 | 120,000 | 160,000 | 200,000 | 400,000 | - | - | 1.48 | 5.03 | 3.08 | 4.05 | 5.44 | 6.91 | - | - |
| $H_2Compression$ [227] | kg/h | 1 | 100,000 | - | - | - | - | - | - | 0.043 | 202.8 | - | - | - | - | - | - |
| $H_2Liquefaction$ [227] | kg/h | 1 | 100,000 | - | - | - | - | - | - | 0.076 | 600 | - | - | - | - | - | - |
| $DC/AC-Inverter$ | MW | 1 | 10,000 | - | - | - | - | - | - | 0.75 | 7,500 | - | - | - | - | - | - |
| $NaS-Storage$ [228] | MW | - | - | - | - | - | - | - | - | - | - | - | - | - | - | - | - |
| $NaS-PCS$ [228] | MW | 1 | 100,000 | - | - | - | - | - | - | 0.65 | 65,000 | - | - | - | - | - | - |
| $PSH-Storage$ [228] | MW | - | - | - | - | - | - | - | - | - | - | - | - | - | - | - | - |
| $PSH-PCS$ [228] | MW | 10 | 30,000 | - | - | - | - | - | - | 5.9 | 17,700 | - | - | - | - | - | - |
| $CAES-Storage$ [228] | MW | - | - | - | - | - | - | - | - | - | - | - | - | - | - | - | - |
| $CAES-PCS$ [228] | MW | 10 | 32,000 | - | - | - | - | - | - | 9.7 | 31,040 | - | - | - | - | - | - |
| $H_2FuelCell$ [229] | MW | 1 | 10,000 | - | - | - | - | - | - | 1.6 | 16,000 | - | - | - | - | - | - |
| $NH_3GasTurbine$ [226] | MW | 1 | 10,000 | - | - | - | - | - | - | 1.024 | 10,240 | - | - | - | - | - | - |
| $CH_3OHGasTurbine$ [226] | MW | 1 | 10,000 | - | - | - | - | - | - | 1.024 | 10,240 | - | - | - | - | - | - |

The reference resource for each process is shown in bold in Table C.5.

# APPENDIX D

# ADDITIONAL RESULTS FOR CHAPTER 4

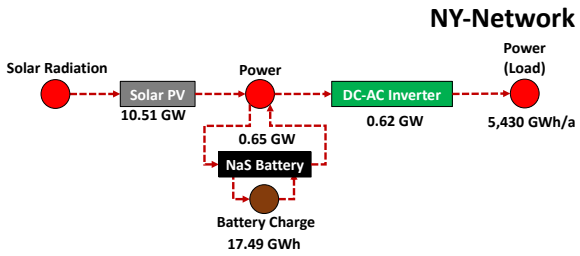


Figure D.1: Process network for BL-1-x-S.

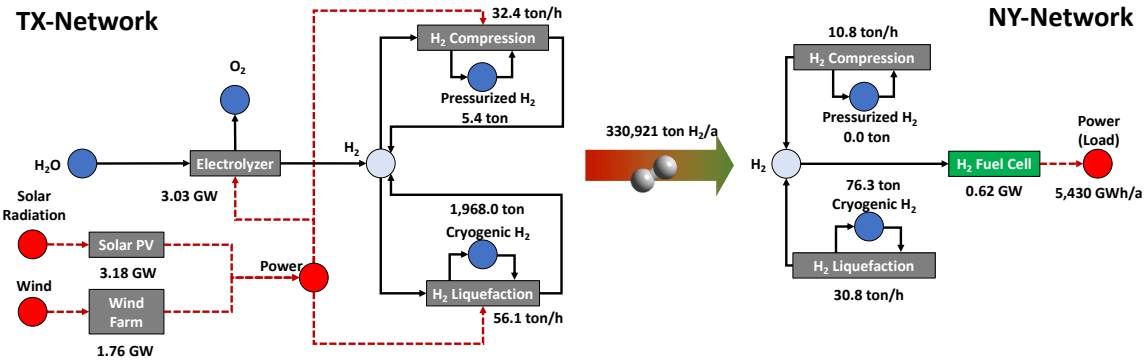


Figure D.2: Process network for BL-2-H-x.

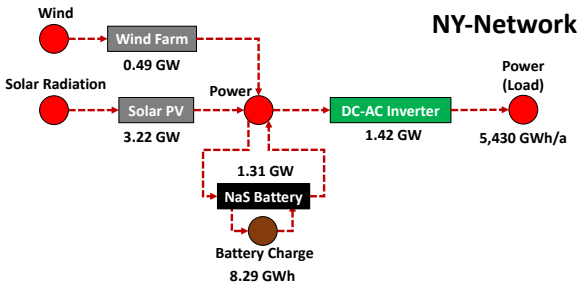


Figure D.3: Process network for PM-1-x-SW.

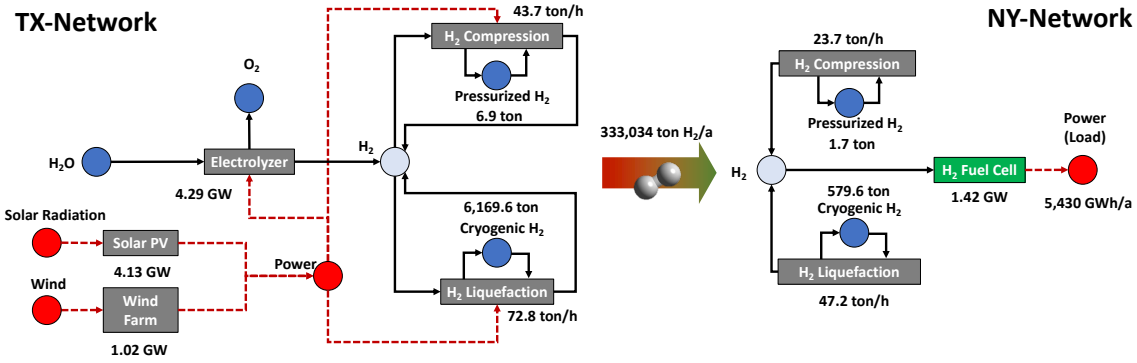


Figure D.4: Process network for PM-2-H-x.

Table D.1: Renewable energy generation and storage capacity and DEC production targets for base load matching.

| Case ID | LCOE ($/kWh) | Total Cost ($ MM/a) | TX-S (GW) | TX-W (GW) | TX-NaS (GWh) | TX Gen. (GWh/a) | NY-S (GW) | NY-W (GW) | NY-NaS (GWh) | NY Gen. (GWh/a) | Process Emission (ton $CO_2$/a) | $H_2$ (ton/a) | $NH_3$ (ton/a) | $CH_3OH$ (ton/a) |
|---|---|---|---|---|---|---|---|---|---|---|---|---|---|---|
| BL-1-x-S | 0.284 | 1,533.21 | 0.00 | 0.00 | 0.00 | 0 | 10.51 | 0.00 | 17.42 | 6,493 | 0 | 0 | 0 | 0 |
| BL-1-x-SW | 0.147 | 796.12 | 0.00 | 0.00 | 0.00 | 0 | 4.00 | 0.50 | 9.17 | 6,364 | 0 | 0 | 0 | 0 |
| BL-2-H-x | 0.341 | 1,839.96 | 3.18 | 1.76 | 0.00 | 22,962 | 0.00 | 0.00 | 0.00 | 0 | 0 | 330,921 | 0 | 0 |
| BL-2-HA-x | 0.341 | 1,839.90 | 3.11 | 1.76 | 0.00 | 22,869 | 0.00 | 0.00 | 0.00 | 0 | 0 | 329,943 | 0 | 0 |
| BL-2-HM-x | 0.321 | 1,733.30 | 3.25 | 1.59 | 0.91 | 23,131 | 0.00 | 0.00 | 0.00 | 0 | 109,756 | 329,055 | 0 | 611,030 |
| BL-3-H-S | 0.157 | 848.55 | 0.03 | 0.35 | 0.00 | 1,796 | 2.43 | 0.00 | 10.49 | 6,164 | 0 | 26,199 | 0 | 0 |
| BL-3-HA-S | 0.151 | 817.69 | 0.10 | 0.12 | 0.05 | 1,106 | 2.80 | 0.00 | 12.49 | 6,307 | 0 | 16,181 | 91,121 | 0 |
| BL-3-HM-S | 0.135 | 726.38 | 0.11 | 0.27 | 0.38 | 2,249 | 1.89 | 0.00 | 9.64 | 5,856 | 29,567 | 31,941 | 0 | 164,605 |
| BL-3-H-SW | 0.116 | 624.47 | 0.02 | 0.18 | 0.00 | 922 | 1.59 | 0.45 | 6.81 | 6,028 | 0 | 13,483 | 0 | 0 |
| BL-3-HA-SW | 0.111 | 598.43 | 0.08 | 0.19 | 0.00 | 1,612 | 1.45 | 0.43 | 6.01 | 5,891 | 0 | 23,743 | 125,175 | 0 |
| BL-3-HM-SW | 0.104 | 560.61 | 0.07 | 0.19 | 0.00 | 1,602 | 1.28 | 0.41 | 5.67 | 5,747 | 21,058 | 22,749 | 0 | 117,232 |

Table D.2: CAPEX and OPEX for base load matching.

| Case ID | LCOE ($/kWh) | Total Cost ($ MM/a) | CAPEX ($ MM) | TX-CAPEX ($ MM) | TX-CAPEX/a ($ MM/a) | TX-OPEX/a ($ MM/a) | NY-CAPEX ($ MM) | NY-CAPEX/a ($ MM/a) | NY-OPEX/a ($ MM/a) | Transportation ($ MM/a) |
|---|---|---|---|---|---|---|---|---|---|---|
| BL-1-x-S | 0.284 | 1,533.21 | 18,535.07 | 0.00 | 0.00 | 0.00 | 18,535.07 | 1,482.81 | 50.41 | 0.00 |
| BL-1-x-SW | 0.147 | 796.12 | 9,300.99 | 0.00 | 0.00 | 0.00 | 9,300.99 | 744.08 | 52.04 | 0.00 |
| BL-2-H-x | 0.341 | 1,839.96 | 11,795.20 | 10,600.62 | 848.05 | 448.66 | 1,194.58 | 95.57 | 120.48 | 327.20 |
| BL-2-HA-x | 0.341 | 1,839.90 | 11,707.30 | 10,506.98 | 840.56 | 448.54 | 1,200.32 | 96.03 | 119.71 | 327.20 |
| BL-2-HM-x | 0.321 | 1,733.30 | 12,410.77 | 11,256.58 | 900.53 | 443.31 | 1,154.19 | 92.34 | 83.12 | 214.01 |
| BL-3-H-S | 0.157 | 848.55 | 9,070.79 | 1,191.63 | 95.33 | 42.96 | 7,879.16 | 630.33 | 53.02 | 26.91 |
| BL-3-HA-S | 0.151 | 817.69 | 9,273.95 | 569.12 | 45.53 | 20.01 | 8,704.83 | 696.39 | 49.05 | 6.72 |
| BL-3-HM-S | 0.135 | 726.38 | 7,755.16 | 991.72 | 79.34 | 49.05 | 6,763.44 | 541.08 | 45.76 | 11.16 |
| BL-3-H-SW | 0.116 | 624.47 | 6,619.41 | 552.05 | 44.16 | 22.03 | 6,067.36 | 485.39 | 56.13 | 16.75 |
| BL-3-HA-SW | 0.111 | 598.43 | 6,241.94 | 689.63 | 55.17 | 32.08 | 5,552.31 | 444.18 | 52.64 | 14.37 |
| BL-3-HM-SW | 0.104 | 560.61 | 5,820.77 | 693.21 | 55.46 | 35.42 | 5,127.56 | 410.20 | 51.57 | 7.96 |

Table D.3: Renewable energy generation and storage capacity and DEC production targets for peak load matching.

| Case ID | LCOE ($/kWh) | Total Cost ($ MM/a) | TX-S (GW) | TX-W (GW) | TX-NaS (GWh) | TX Gen. (GWh/a) | NY-S (GW) | NY-W (GW) | NY-NaS (GWh) | NY Gen. (GWh/a) | Process Emission (ton $CO_2$/a) | $H_2$ (ton/a) | $NH_3$ (ton/a) | $CH_3OH$ (ton/a) |
|---|---|---|---|---|---|---|---|---|---|---|---|---|---|---|
| PM-1-x-S | 0.247 | 1,348.33 | 0.00 | 0.00 | 0.00 | 0 | 8.41 | 0.00 | 14.64 | 6,252 | 0 | 0 | 0 | 0 |
| PM-1-x-SW | 0.142 | 777.58 | 0.00 | 0.00 | 0.00 | 0 | 3.22 | 0.49 | 8.29 | 6,255 | 0 | 0 | 0 | 0 |
| PM-2-H-x | 0.371 | 2,026.97 | 4.13 | 1.02 | 0.00 | 23,048 | 0.00 | 0.00 | 0.00 | 0 | 0 | 333,034 | 0 | 0 |
| PM-2-HA-x | 0.370 | 2,021.06 | 4.20 | 1.02 | 0.05 | 23,415 | 0.00 | 0.00 | 0.00 | 0 | 0 | 337,909 | 79,621 | 0 |
| PM-2-HM-x | 0.335 | 1,827.29 | 3.10 | 1.53 | 0.91 | 23,346 | 0.00 | 0.00 | 0.00 | 0 | 110,141 | 332,308 | 0 | 613,179 |
| PM-3-H-S | 0.134 | 728.90 | 0.02 | 0.24 | 0.00 | 1,338 | 1.81 | 0.00 | 7.11 | 6,029 | 0 | 19,430 | 0 | 0 |
| PM-3-HA-S | 0.122 | 665.26 | 0.03 | 0.15 | 0.00 | 1,261 | 1.81 | 0.00 | 7.11 | 6,065 | 0 | 18,462 | 98,603 | 0 |
| PM-3-HM-S | 0.117 | 638.38 | 0.01 | 0.11 | 0.00 | 981 | 1.81 | 0.00 | 7.08 | 6,040 | 12,877 | 13,925 | 0 | 71,687 |
| PM-3-H-SW | 0.109 | 594.79 | 0.00 | 0.09 | 0.00 | 640 | 1.64 | 0.31 | 5.19 | 6,025 | 0 | 9,166 | 0 | 0 |
| PM-3-HA-SW | 0.106 | 575.82 | 0.01 | 0.07 | 0.00 | 585 | 1.68 | 0.28 | 5.40 | 6,071 | 0 | 8,565 | 46,989 | 0 |
| PM-3-HM-SW | 0.103 | 559.50 | 0.02 | 0.13 | 0.00 | 1,085 | 1.54 | 0.26 | 4.49 | 5,830 | 14,240 | 15,395 | 0 | 79,275 |

Table D.4: CAPEX and OPEX for peak load matching.

| Case ID | LCOE ($/kWh) | Total Cost ($ MM/a) | CAPEX ($ MM) | TX-CAPEX ($ MM) | TX-CAPEX/a ($ MM/a) | TX-OPEX/a ($ MM/a) | NY-CAPEX ($ MM) | NY-CAPEX/a ($ MM/a) | NY-OPEX/a ($ MM/a) | Transportation ($ MM/a) |
|---|---|---|---|---|---|---|---|---|---|---|
| PM-1-x-S | 0.247 | 1,348.33 | 16,300.36 | 0.00 | 0.00 | 0.00 | 16,300.36 | 1,304.03 | 44.30 | 0.00 |
| PM-1-x-SW | 0.142 | 777.58 | 9,158.34 | 0.00 | 0.00 | 0.00 | 9,158.34 | 732.67 | 44.91 | 0.00 |
| PM-2-H-x | 0.371 | 2,026.97 | 17,129.99 | 11,671.46 | 933.72 | 413.88 | 5,458.53 | 208.98 | 119.80 | 350.59 |
| PM-2-HA-x | 0.370 | 2,021.06 | 14,392.00 | 11,956.26 | 956.50 | 417.91 | 2,435.74 | 194.86 | 117.88 | 333.91 |
| PM-2-HM-x | 0.335 | 1,827.29 | 13,364.55 | 11,286.99 | 902.96 | 454.19 | 2,077.56 | 166.20 | 83.99 | 219.96 |
| PM-3-H-S | 0.134 | 728.90 | 7,881.46 | 794.65 | 63.57 | 32.23 | 7,086.81 | 566.94 | 47.11 | 19.04 |
| PM-3-HA-S | 0.122 | 665.26 | 7,345.01 | 527.12 | 42.17 | 25.77 | 6,817.89 | 545.43 | 43.36 | 8.52 |
| PM-3-HM-S | 0.117 | 638.38 | 7,092.70 | 405.63 | 32.45 | 22.95 | 6,687.07 | 534.97 | 42.92 | 5.09 |
| PM-3-H-SW | 0.109 | 594.79 | 6,540.24 | 257.19 | 20.58 | 16.03 | 6,283.05 | 502.64 | 48.56 | 6.98 |
| PM-3-HA-SW | 0.106 | 575.82 | 6,417.58 | 226.35 | 18.11 | 12.48 | 6,191.23 | 495.30 | 46.06 | 3.87 |
| PM-3-HM-SW | 0.103 | 559.50 | 6,047.32 | 427.38 | 34.19 | 25.01 | 5,619.94 | 449.60 | 45.14 | 5.56 |

# APPENDIX E

# LIST OF PUBLICATIONS AND PRESENTATIONS

## E.1 Journal Publications

**Demirhan, C. D.**; Tso, W. W.; Powell, J. B.; Pistikopoulos, E. N. "Sustainable Ammonia Production Through Process Synthesis and Global Optimization", *AIChE Journal*, 2019, 65, 1-23.

**Demirhan, C. D.**; Tso, W. W.; Ogumerem, G. S.; Pistikopoulos, E. N. "Energy systems engineering - a guided tour", *BMC Chemical Engineering*, 2019, 1, 11.

**Demirhan, C. D.**; Tso, W. W.; Powell, J. B.; Heuberger, C. F.; Pistikopoulos, E. N. "A Multiscale Energy Systems Engineering Approach for Renewable Power Generation and Storage Optimization", *Industrial & Engineering Chemistry Research*, 2020, Available online.

**Demirhan, C. D.**; Boukouvala, F.; Kyungwon, K.; Song, H.; Tso, W. W.; Floudas, C. A.; Pistikopoulos, E. N. "An Integrated Data-Driven Modeling & Global Optimization Approach for Multi-Period Nonlinear Production Planning", *Computers & Chemical Engineering*, In revision.

**Demirhan, C. D.**; Tso, W. W.; Pistikopoulos, E. N. "Toward Integrated Multi-product Process Network Optimization via Multi-scale Energy Systems Engineering", *Applied Energy*, In review.

Tso, W. W.; Niziolek, A. M.; Onel, O.; **Demirhan, C. D.**; Floudas, C. A.; Pistikopoulos, E. N. "Enhancing Natural Gas-to-Liquids (GTL) Processes Through Chemical Looping for Syngas Production: Process Synthesis and Global Optimization", *Computers & Chemical Engineering*, 2018, 113, 222-239.

Tso, W. W.; **Demirhan, C. D.**; Powell, J. B.; Pistikopoulos, E. N. "Toward Optimal Synthesis of Renewable Ammonia and Methanol Processes (RAMP)", 13th International Symposium on Process Systems Engineering (PSE 2018), Elsevier, 2018, 1705-1710.

Tso, W. W.; **Demirhan, C. D.**; Lee, S. Y.; Song, H.; Powell, J. B.; Pistikopoulos, E. N. "Energy Carrier Supply Chain Optimization: A Texas Case Study", Foundations of Computer-Aided Process Design (FOCAPD 2019), 2019, Accepted manuscript.

Ogumerem, G. S.; Tso, W. W.; **Demirhan, C. D.**; Lee, S. Y.; Song, H.; Pistikopoulos, E. N. "Toward the Optimization of Hydrogen, Ammonia, and Methanol Supply Chains", 12th IFAC Symposium on Dynamics and Control of Process Systems, including Biosystems (DYCOPS 2019), 2019, IFAC-PapersOnLine, 52, 844-849.

Tso, W. W.; **Demirhan, C. D.**; Floudas, C. A.; Pistikopoulos, E. N. "Multi-Scale Energy Systems Engineering for Optimal Natural Gas Utilization", *Catalysis Today*, 2019, Accepted Manuscript.

Tso, W. W.; **Demirhan, C. D.**; Heuberger, C. F.; Powell, J. B.; Pistikopoulos, E. N. "A Hierarchical Clustering Decomposition Algorithm for Optimizing Renewable Power Systems with Storage", *Applied Energy*, In revision.

## E.2 Conference Presentations

Process Synthesis and Global Optimization of Novel Ammonia Production Processes

- *2017 AIChE Annual Meeting*, *2017 Chegsa Symposium*

Sustainable Ammonia Production Through Process Synthesis and Global Optimization

- *2018 AIChE Annual Meeting*, *2018 Texas A&M Conference on Energy*

An Integrated Data-Driven Modeling & Global Optimization Approach for Production Planning

- *2018 AIChE Annual Meeting*

Toward the Optimization of Hydrogen, Ammonia, and Methanol Supply Chains

- *DYCOPS 2019*

Simultaneous Design and Operation of Renewable Energy Carrier Production

- *2019 AIChE Annual Meeting*, *2019 Texas A&M Conference on Energy*

Design and Operation of Synthetic Fuels Production from Fossil and Renewable Resources

- *2019 AIChE Annual Meeting*